In-Situ Spectroscopic Ellipsometry for Studies of Thin Films and Membranes

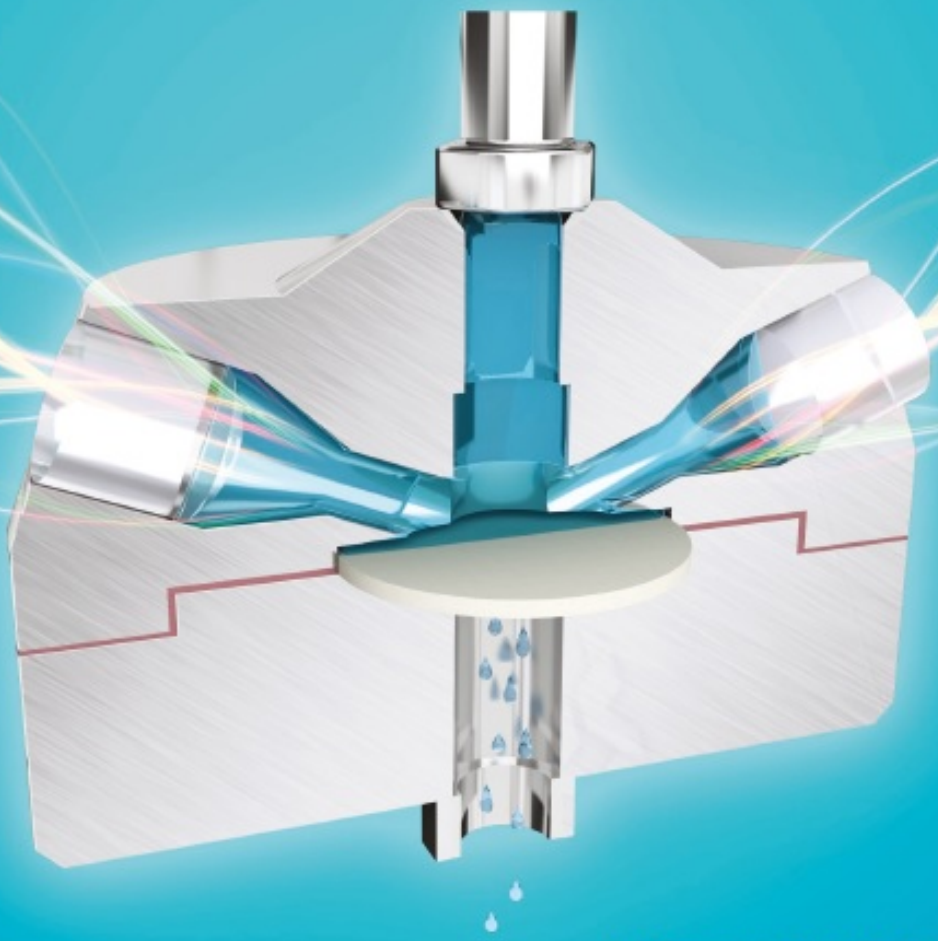

Wojciech Ogieglo

IN-SITU SPECTROSCOPIC ELLIPSOMETRY FOR STUDIES OF THIN FILMS AND MEMBRANES

Promotion committee:

Prof. Dr. Ir. Guus Rijnders (Chairman)	University of Twente
Prof. Dr.-Ing. Matthias Wessling (Promotor)	RWTH Aachen University
Dr. Ir. Nieck E. Benes (Assistant Promotor)	University of Twente
Dr. Ir. Herbert Wormeester	University of Twente
Prof. Dr. Guido Mul	University of Twente
Prof. Dr. Ir. Nico van der Vegt	Technical University of Darmstadt
Prof. Julius Vancso	University of Twente
Dr. rer. nat. Klaus-Jochen Eichhorn	Leibniz Institute of Polymer Research in Dresden

Cover design by Jonathan Bennink – www.tingle.nl
Light lines image used from www.creativity103.com

In-situ spectroscopic ellipsometry for studies of thin films and membranes
ISBN: 978-90-365-3631-8
DOI: 10.3990/1.9789036536318
URL: http://dx.doi.org/10.3990/1.9789036536318
Printed by: Ipskamp Drukkers, Enschede
© Copyright 2014 Wojciech Ogieglo

IN-SITU SPECTROSCOPIC ELLIPSOMETRY FOR STUDIES OF THIN FILMS AND MEMBRANES

DISSERTATION

to obtain

the degree of doctor at the University of Twente,
on the authority of the rector magnificus,
prof. dr. H. Brinksma,
on account of the decision of the graduation committee,
to be publicly defended
on Friday 21st of March 2014 at 16:45

by

Wojciech Ogieglo
born on 25th of November 1985
in Oświęcim, Poland

This thesis has been approved by:

Prof. Dr.-Ing. Matthias Wessling (Promotor)

Dr. Ir. Nieck E. Benes (Assistant Promotor)

“An expert is a person who has made all the mistakes that can be made in a very narrow field”

Niels Bohr

Dla moich Pysiaczek

Table of contents

Chapter 1

In-situ ellipsometry studies of thin swollen polymer films, a review 9

Scope of the Thesis 114

Chapter 2

Temperature-induced transition of the diffusion mechanism of n-hexane in ultra-thin polystyrene films, resolved by *in-situ* spectroscopic ellipsometry ... 117

Chapter 3

Probing the surface swelling in ultra-thin supported polystyrene films during Case II diffusion of n-hexane 139

Chapter 4

Effective medium approximations for penetrant sorption in glassy polymers accounting for excess free volume 159

Chapter 5

Polymer relaxations in thin films in the vicinity of penetrant or temperature induced glass transition 181

Chapter 6

Relaxation-induced optical anisotropy during dynamic overshoot swelling of zwitterionic polymer films 199

Chapter 7

Swelling dynamics of zwitterionic copolymers: the effects of concentration and type of anion and cation 221

Chapter 8

Spectroscopic ellipsometry analysis of a thin film composite membrane consisting of polysulfone on a porous α-alumina support 243

Chapter 9

n-Hexane induced swelling of thin PDMS films under non-equilibrium nanofiltration permeation conditions, resolved by spectroscopic ellipsometry 267

Chapter 10

Effects of time, temperature, and pressure in the vicinity of the glass transition of a swollen polymer 293

Chapter 11

Outlook 309

Thesis summary 325

Samenvatting 329

Streszczenie 333

Acknowledgements 339

***Curriculum Vitae* of the author** 342

Chapter 1

In-situ ellipsometry studies of thin swollen polymer films, a review

This chapter is in preparation for publication, authored by:

Ogieglo W., Wormeester H., Eichhorn K-J., Wessling M., Benes N.E.

Abstract

The properties of a thin polymer film can be significantly affected by the presence of a penetrant. This can have potential implications for many technological applications, such as protective and functional coatings, sensors, microelectronics, surface modification and membrane separations. *In-situ* ellipsometry is a powerful technique for the characterization of a film in contact with a penetrant. The main advantages of ellipsometry include the very high precision and accuracy, combined with the fact that it is non-intrusive. Recent advances in the speed and automation of the technique have further expanded its application.

This chapter provides an overview of the research that has been done with *in-situ* ellipsometry on penetrant-exposed polymeric films, in the last 15-20 years. The focus is predominantly on films that are not attached covalently to a substrate. The review addresses a variety of topics, covering instrumental aspects of *in-situ* studies, approaches to data analysis and optical models, reported precision and repeatability, the polymer-penetrant systems that have been studied, the kind of information that has been extracted, and other *in-situ* techniques that have been combined with ellipsometry. Various examples are presented to illustrate different practical approaches, the consequences of the optical properties of the ambient, and the various ways that have been employed to bring polymer films in contact with a penetrant, ranging from simple *ex-situ*-like configurations (i.e. drying studies) to complex high pressure cells. The versatility of *in-situ* ellipsometry is demonstrated by examples of the distinctive phenomena studied, such as film dilation, penetrant diffusion mechanisms, film degradation, electrochemical processes, and the broad variety of polymer - penetrant systems studied (glassy and rubbery polymers, multilayer stacks, etc.). An outlook is given on possible future trends.

Table of contents of the review

1.1. Review chapter structure 16

1.2. Theory and instrumentation 17

1.2.1. Ellipsometry – theory 17

1.2.2. Ellipsometry – data interpretation and optical modeling 21

1.2.2.1. Analysis of bulk samples, substrates and ambients 21

1.2.2.2. Analysis of thin, transparent and absorbing films 22

1.2.2.3. Optical models and modeling aspects 25

1.2.3. *In-situ* configurations 31

1.2.3.1. No *in-situ* sample cell 31

1.2.3.2. Near-atmospheric pressure *in-situ* cells 32

1.2.3.3. High pressure cells 35

1.3. Types of polymeric materials studied 37

1.3.1. Simple glassy polymers 37

1.3.2. Simple rubbery polymers 38

1.3.3. Random and block copolymers 39

1.3.4. Multilayer films 41

1.3.5. Other systems 43

1.4. Types of polymer-penetrant phenomena studied 43

1.4.1. Penetrant uptake from dry state 43

1.4.1.1. Liquid water 45

1.4.1.2. Water vapor 46

1.4.1.3. Organic solvents, liquids and vapors 48

1.4.1.4. High pressure gases 50

1.4.2. Drying processes 53

1.4.3. Thermally, pH, and ionic strength induced transitions 55

1.4.4. Reactions at interfaces, depositions and formations 58

1.4.5. Dissolution or degradation 59

1.4.6. Electrochemically induced swelling changes 60

1.5. Types of information extracted with the use of *in-situ* ellipsometry 61

1.5.1. Dynamic studies 61

1.5.1.1. Simple dynamic phenomena 61

1.5.1.2. Complex dynamic phenomena 62

1.5.2. Penetrant volume fraction calculations 67

1.5.3. Thermodynamic parameters 69

1.6. Ellipsometry combined with other techniques 72

1.6.1. Ellipsometry concurrently combined with other techniques *in-situ* .. 72

1.6.2. Ellipsometry complemented with other *in-situ* techniques 73

1.6.2.1. Quartz crystal microbalance (QCM) 73

1.6.2.2. Atomic force microscopy (AFM) 75

1.6.2.3. Neutron and X-ray reflectivity 76

1.6.2.4. Electrochemical methods 77

1.6.2.5. Gravimetric methods 78

1.6.2.6. Contact angle measurements 79

1.6.2.7. UV-VIS spectroscopy 79

1.6.2.8. IR spectroscopy 80

1.6.2.9. Surface plasmon resonance (SPR) 81

1.6.2.10. Methods to determine mechanical properties 81

1.7. Concluding remarks and outlook 82

1.8. Acknowledgments 83

1.9. Appendix 84

1.10. List of abbreviations 86

1.11. References 88

1.12. Summary of the *in-situ* ellipsometry studies included in the review 98

1.13. Scope of the Thesis 114

1.1. Review chapter structure

This chapter provides a review of the research that has been done in the last 15-20 years, involving *in-situ* ellipsometry studies of thin films exposed to penetrants. The focus is predominantly on polymer films that are not attached covalently to the substrates.

In the Theory and Instrumentation paragraph the theoretical basis and experimental aspects of ellipsometry are outlined. The precision and repeatability of the analysis of typical thin film polymeric samples are illustrated with examples. The examples are based on already published, as well as on unpublished data. Practical approaches to analysis of samples in contact with various penetrants are highlighted and the accurate determination of ambient and substrate optical constants is addressed. The paragraph also provides a survey of the optical models employed in the literature, illustrated with some noteworthy examples. The various means employed to bring thin polymer films in contact with penetrants are described, ranging from simple *ex-situ*-like configurations (i.e., drying studies) to complex high-pressure cells.

Further paragraphs focus on the particular studies done in the literature. The technique has been applied for a very broad range of different polymeric systems, that can be classified as relatively simple (glassy, rubbery polymers) and more complex ones (copolymers, multilayers and composites). A wide range of investigated phenomena demonstrates the versatility of the technique. These are not limited to determination of film swelling by the penetrant, but also address complex diffusion mechanisms, polymer degradation, glass transition, and electrochemical processes. Often penetrant concentrations and thermodynamic parameters describing polymer-penetrant mixtures are extracted from the analysis. The various approaches to these calculations found in the literature are presented and their applicability is discussed.

In the majority of studies, especially in the more recent ones, ellipsometry has been combined with other *in-situ* techniques. This has been done concurrently, using the same sample and experimental cell, or non-concurrently, where the measurements are done on separate samples but yield complementary information. Examples of studies in both categories are shown with particular focus on the complementarity of information gathered with combined techniques.

All *in-situ* ellipsometry studies discussed in this chapter are summarized in a reference table containing the most important information. Finally, conclusions and outlook for the possible future trends are given.

1.2. Theory and instrumentation

1.2.1. Ellipsometry – theory

Ellipsometry is a non-destructive optical technique that allows for very precise and accurate analysis of the optical properties, including film thickness and dielectric constants, of various thin film systems. Ellipsometry relies on the changes in the polarization state of light upon reflection from, in general, multilayer systems. The roots of the technique reach as far back as the early nineteenth century, with the experiments of Sir David Brewster and later Jules Jamin on light polarization properties upon reflection and refraction. These experiments lead to formulation of the respective laws of Brewster and Jamin. Hendrik Antoon Lorentz made important contributions to the mathematical formulation of Maxwell's equations, applied to light [1]. These developments allowed quantitative physical interpretation of light reflection and transmission. The first ellipsometry measurements, based on similar principles as those of modern devices, can be ascribed to the pioneering contributions of Paul Drude [2-4]. A rapid growth of use and applicability of ellipsometry has been observed within the past 15-20 years, due to the significant progress in speed and automation of measurements and data analysis.

In a typical ellipsometry configuration, Figure 1.1, light from a light source passes through a polarizer unit that sets the incident polarization state. Typically, this incident polarization state is linear. The probing light can be monochromatic (most commonly a He-Ne laser at 632.8 nm) or spectroscopic (incandescent or arc discharge lamps). Upon reflection from a sample, at a certain angle, the polarization state is changed. In general, polarization state of the reflected light is

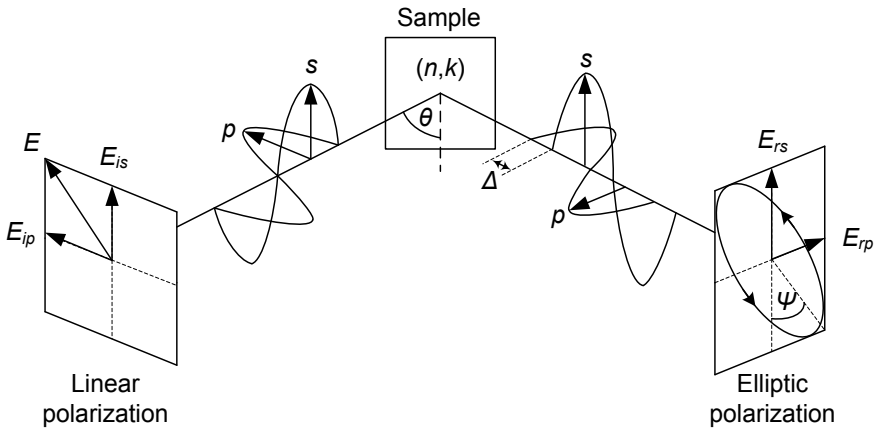

Figure 1.1 Schematics of ellipsometric measurement principle, adapted with permission from [5]. Copyright 2007 Maruzen

elliptic, evincing the name of the technique. The change in polarization state is measured by a second polarizer, the analyzer, coupled with a detector. The reflected light polarization state can be described in terms of the two angles: psi (Ψ) and delta (Δ). For a linear polarization of the incident light, that is when $E_{ip} = E_{is}$:

$$tan(\Psi) \cdot e^{i\Delta} \equiv \frac{r_p}{r_s} \equiv \frac{E_{rp}}{E_{rs}} \equiv \rho(N_0, N_1, .., N_m, h_1, .., h_{m-1}, \theta_0) \qquad (1.1)$$

The subscripts p and s refer to parallel and perpendicular (germ. senkrecht), with respect to the plane of incidence, and r_p and r_s represent the reflectivity. As such, Ψ represents the angle determined from the amplitude ratio between p- and s-polarizations, while the Δ represents the phase difference the two components. The reflectivity ratio, ρ, is a complex function of the optical structure of the sample and includes the information about its physical properties. The polarization state of the reflected light depends on the angle of incidence, θ_0, the thicknesses of the m-1 layers, h, and the complex refractive indices (N=n-ik) of all of these layers, the ambient (N_0), and the substrate N_m. This signifies the richness of information contained in the probing light.

In the early relatively simple instruments only the polarizing elements were used between the light source and the detector. The subsequent addition of a compensator allowed working with partially depolarizing samples, thereby extending the applicability of ellipsometry to samples with non-uniform thickness. This is particularly important for polymer samples that are obtained during film spin coating or dip coating. A compensator contributes to higher flexibility of the ellipsometry technique, because it allows including non-idealities in an optical model of the sample. More detailed information on the principles of optics relevant for spectroscopic ellipsometry, on the optical elements used in typical configurations, as well as on the historical record of developed instruments can be found in textbooks [5-7].

In the case of monochromatic ellipsometry, the measurable parameters include only a single pair of Ψ and Δ for the single wavelength of the light, at a single angle of incidence. This means that at maximum two parameters can be simultaneously determined from the measurement, for example the film thickness, h, and the refractive index n. This is enough information in the case of some thin film samples. In the spectroscopic ellipsometry the measurement generates a pair of Ψ and Δ for each employed wavelength. Consequently, the number of sample parameters that can be independently determined increases significantly. This opens possibilities for the characterization of complex samples, where light absorption, optical anisotropy, density gradients, roughness, and other features of the probed layers can be determined in addition to film thickness and refractive index.

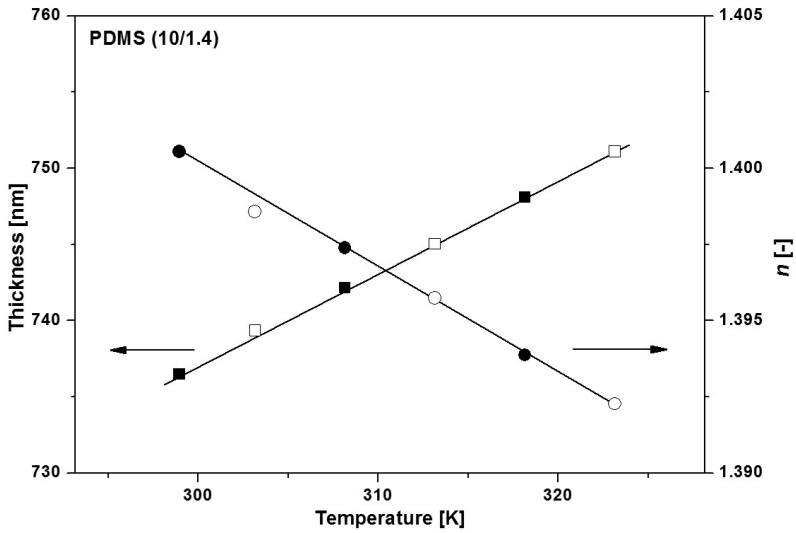

Figure 1.2 Demonstration of the ellipsometry precision for the determination of film thickness and refractive index of ~730 nm poly(dimethyl siloxane) (PDMS) film supported on a glass slide [8], closed and open symbols represent the heating and cooling modes respectively; lines are linear fits through the data. Adapted with permission from [8]. Copyright 2013 Elsevier

For ellipsometry, a clear distinction between precision and accuracy is important. Accuracy relates to the proximity of measurement results to the true value. Precision relates to the repeatability, or reproducibility of the measurement. The accuracy of ellipsometry depends very much on the validity of the assumptions related to the sample and is discussed in paragraph 1.2.2.3.The very high precision of ellipsometry originates from the fact that modern optical devices enable very precise quantification of changes in the polarization state light. This is accomplished by the measurement of *p*- and *s*- polarization light intensity *ratios*, eq. 1.1, instead of the absolute intensities. This approach is especially beneficial for *in-situ* measurements, because the introduction of a fluid ambient usually causes losses in the absolute intensity. Typically, the instrumental standard deviations in Ψ and Δ are on the order of 0.01-0.02°. For an optically uniform and transparent polymer film on a polished silicon wafer, this translates into precision in thickness determination on the order of 0.1 nm. Figure 1.2 shows an example of the precision of the ellipsometric measurements for a thin polydimethyl siloxane (PDMS) film, exposed to increasing and decreasing temperature [8]. In the temperature range studied, PDMS can be considered an equilibrium liquid polymer. For such a polymer the observed linear dependence of thickness and refractive index, and the absence of hysteresis, are expected. The experimental data agree within 10% with literature data for thermal expansion coefficient of bulk PDMS. The very small deviation from linearity, or scatter, allows estimating the thickness precision to be

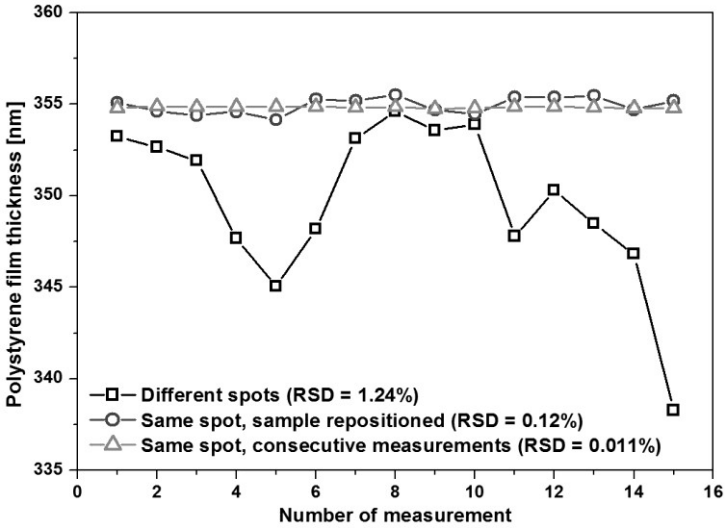

Figure 1.3 Ellipsometry repeatability and precision: squares represent measured values from 15 different spots on the same 1.5 x 1.5 cm sample; circles represent measured values when the sample is repeatedly placed on the ellipsometer stage, aligned, measured, taken off and re-positioned again on approximately the same spot as before; triangles represent consecutive measurements done on the same spot without sample repositioning. RSD indicates the relative standard deviations for the respective 15 measurement points. Data has been collected with an M-2000X spectroscopic ellipsometer of J.A. Woollam Co., Inc. at 70° angle of incidence and PS film spin-coated on a crystalline silicon wafer.

in the fraction of a nanometer. For the refractive index the precision is around ~0.0005.

As another example three data sets are shown in (Figure 1.3), which have been measured for a thin polystyrene (PS) film spin coated on a 1.5 x 1.5 cm silicon wafer. The sample has been annealed above its glass transition temperature, to relax post-preparation stresses and to remove any remaining solvent. Squares correspond to measurements of 15 different spots on the sample. Circles correspond to data measured by placing the sample on the ellipsometer stage, aligning, measuring, and taking the sample of the stage again, followed by repeating this whole procedure. The measurement spot is kept approximately the same as before. Triangles correspond to data measured on the same spot but without repositioning the sample. Scatter in the data is quantified in terms of the relative standard deviation (RSD) in 15 measurements. The RSD decreases by approximately 1 order of magnitude going from squares to circles, and another order of magnitude when going from circles to triangles. The scatter in the dataset represented by the triangles corresponds solely to the precision of the measuring device and the modeling algorithm. The extremely low RSD = 0.011% signifies the

very high precision of ellipsometry and the potential to study changes in film thickness within a fraction of a nanometer. The dataset represented by the circles, with RSD = 0.12%, corresponds roughly to the operator error, related to the repeatability of placing the sample in the same spot. The highest RSD = 1.24% for the squares corresponds to thickness non-uniformity within the sample and is related to its preparation process. The value of 1.24% is typical for a spin-coated PS film. Other polymers can be characterized by much worse thickness uniformity after preparation. This will especially be the case for high-performance polymers, with a high glass transition temperature.

1.2.2. Ellipsometry – data interpretation and optical modeling

1.2.2.1. Analysis of bulk samples, substrates and ambients

In certain cases the Ψ and Δ can be directly used to calculate the properties of simple samples (n and k) from the reflection at the sample/ambient interface, Figure 1.4. This is useful when the interest is in the characterization of a complex refractive index of a bulk material, for example: (i) a particular polymeric substance, (ii) a substrate, intended for further thin film analysis or (iii) an experimental ambient (N_0) for the *in-situ* measurements. For the latter case the optical properties of the bulk film need to be known in advance. Additionally, the influence of the experimental ambient on the optical properties of the bulk material should be negligible, as for instance, in the case of a glass slide immersed in pure water. For these types of measurements the sample is assumed to be perfectly polished (negligible roughness) and the reflection from the backside is removed. The last assumption can be fulfilled by analyzing a relatively thick sample (several mm) or by mechanically roughening its backside surface. Alternatively, adhesive tape at the backside can be used to scatter transmitted light, thereby eliminating it from the measurement. Elimination of the backside reflection has been found to be the best method of dealing with thick substrates [R. Synowicki of J.A. Woollam Co. Inc., private communication].

Quantitative information about refractive index of the ambient, N_0, in a range of experimental temperatures, is of particular importance for *in-situ* applications. Many *in-situ* ellipsometry measurements are done in liquid water, for which optical properties are very well known [9], but applications exist that involve a different ambient. These include aqueous solutions of simple and complex compounds, organic solvents, ionic liquids, compressed gasses, etc. Accurate knowledge of the optical dispersion of the particular ambient, at the experimental temperature, is an absolute prerequisite for accurate determination of the optical properties of the analyzed film. This is in particular the case for the determination of the optical dispersion of a swollen film, because in this case the experimental ambient is present not only in the experimental chamber, but also inside of the analyzed film, where it contributes to the film's optical properties.

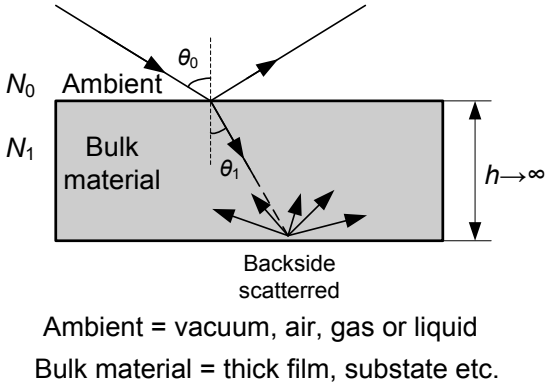

Figure 1.4 Reflection from a very thick, bulk film or a substrate with backside reflection eliminated by scattering

In the case of the single wavelength ellipsometry, the measurement of the Ψ and Δ enables determination of two parameters of the system. For example, with a known θ_0:

- If the ambient is air (n_0=1, k_0=0), then n_1 and k_1 (at the wavelength of measurement) of the sample material can be determined.
- If the substrate dispersion is known (n_1 and k_1), then the ambient properties, n_0 and k_0, can be determined. This is only valid assuming that the presence of the ambient does not alter properties of the substrate, for example by preferential adsorption of the dissolved species, etc.

In spectroscopic ellipsometry, the complete optical dispersions (n and k as a function of light wavelength) can be determined in the same way. Details of these calculations can be found in ellipsometry textbooks [5-7], and are briefly outlined in the Appendix. As an alternative method to determine the ambient dispersion a minimum deviation approach employing a prism-shaped experimental cell can be used [10].

1.2.2.2. Analysis of thin, transparent and absorbing films

In *in-situ* ellipsometry studies, the samples are in general thin polymer films on top of supporting substrates, Figure 1.5. When light enters such a sample it reflects and transmits at each of the interfaces. The rays leaving the sample interfere with each other and produce spectral oscillations in the Ψ and Δ. A more detailed mathematical description can be found in the Appendix.

Figure 1.6a and b show spectroscopic ellipsometry Ψ and Δ spectra simulated for a 1000 nm film of an optically transparent PDMS polymer supported on a polished, crystalline silicon wafer. The spectra have been generated based on realistic input

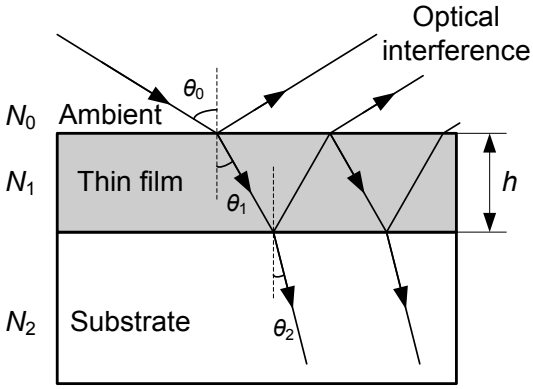

Figure 1.5 Optical structure of a typical *in-situ* ellipsometric sample, adapted with permission from [5]. Copyright 2007 Maruzen

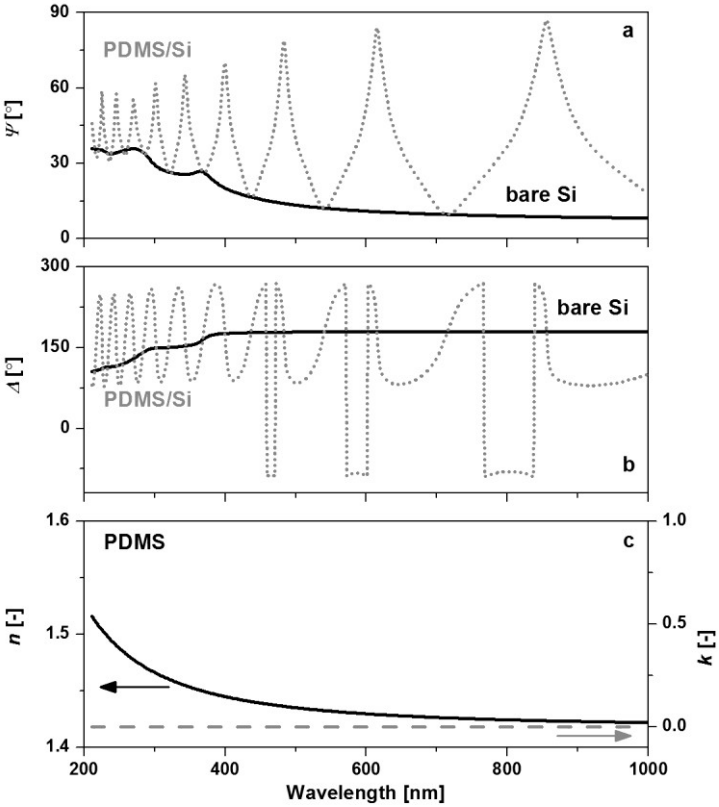

Figure 1.6 Simulated *Ψ* (a) and *Δ* (b) spectra of a 1000 nm transparent poly(dimethyl siloxane) (PDMS) film on a silicon wafer; (c) optical dispersion of PDMS

parameters regarding optical dispersion of PDMS. The bare substrate spectra are also shown.

The optical dispersion of PDMS, $n(\lambda)$, is shown in Figure 1.6c. Note that over the full wavelength range k_{PDMS}=0. The minima of the Ψ oscillating pattern coincide with the spectrum of a bare substrate that forms the so called spectral envelope. This feature of the Ψ spectrum holds for any transparent film/substrate system. The Δ spectrum oscillates around its value for the substrate. The number of oscillations in both Ψ and Δ is related to the optical thickness of the film, $n \cdot h$, and increases with increasing film thickness and refractive index. For most of the typical polymeric materials the refractive index (at 632.8 nm) varies in a relatively narrow range (n=1.4 – 1.6), therefore, the number of oscillations in a certain wavelength range (for instance 380-1000 nm) can be treated as a rough estimate of the polymer film thickness, Table 1.1.

As the film thickness increases an increasing number of oscillations need to be covered within the spectral resolution of an ellipsometer. It means that for thicker films the accuracy of the spectrum representation decreases and measurements on samples thicker than about 2000-3000 nm become much less accurate. The spectral representation of a film with a certain thickness is also worse in the lower wavelength range for the same reason: the oscillations are more densely distributed. Additionally, towards the UV region the effects of a finite spectral bandwidth may become apparent. This is because the beam is never perfectly spatially coherent but, as used in this simulation, has a finite bandwidth. The effects of this are first visible in the shorter wavelength region, where the Ψ is not exactly limited by the envelope, Figure 1.6a.

Figure 1.7 shows similar data simulated for a 1000 nm film of a sulfonated poly(ether ether ketone) (SPEEK), which is a light absorbing polymer. Its optical dispersion is plotted in Figure 1.7c. As can be seen from the figure, in a transparent region (above about 400 nm) the Ψ and Δ spectra show a similar behavior as for the PDMS, Figure 1.6, with the oscillations being limited by the substrate envelope. However, in the range where the polymer absorbs this is no longer the case.

Table 1.1 Approximate number of spectral oscillations for 4 different thicknesses and 3 different refractive indices (given at 632.8 nm) in a visible range typical for most common polymeric materials

Film thickness [nm]	n = 1.4	n = 1.5	n = 1.6
500	2	2	3
1000	4	4	4
2000	8	8	9
5000	19	20	23

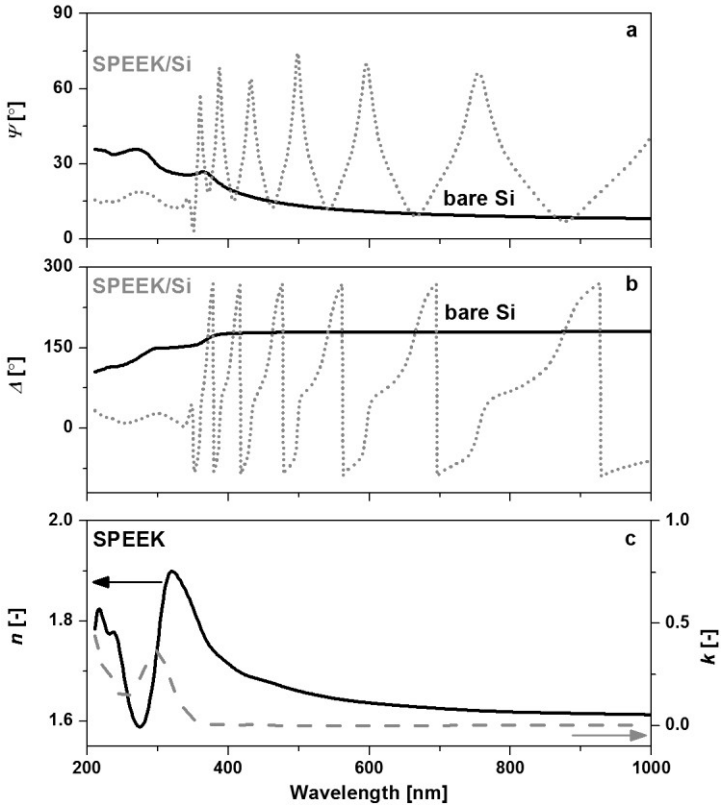

Figure 1.7 Simulated *Ψ* (a) and *Δ* (b) spectra of a 1000 nm absorbing sulfonated poly(ether ether ketone) (SPEEK) film on a silicon wafer; (c) optical dispersion of SPEEK

Because the light transmitted through the thin film is almost completely absorbed by the material, it does not interfere at the outer interface. As a consequence no oscillations are present in the near-UV region. This qualitative feature of the spectra can be often treated as a strong indication of dealing with an absorbing polymer.

It can clearly be seen that for more complex samples (multilayers, absorbing, anisotropic etc.) a simple deconvolution of the sample properties from the measured *Ψ* and *Δ* becomes very difficult. This is the reason why optical models are utilized.

1.2.2.3. Optical models and modeling aspects

1.2.2.3.1. Types of optical models used in the literature

The examples shown in paragraph 1.2.2.2 are based on the generation of *Ψ* and *Δ* spectra when the film thickness and its optical dispersion are known. However,

predominantly the ellipsometry data analysis is done in an opposite direction – the Ψ and Δ spectra for a particular sample on a known substrate are measured and the film thickness and dispersion are to be determined. This is done with a utilization of a layered optical model. Ideally, an optical model should include all of the pieces of information that are known about the sample, before the measurement is done. Most importantly, the type of a substrate (see paragraph 1.2.2.3.2) should be known. In some cases also an approximate layer thickness or refractive index of the film material are known. Figure 1.8 shows the most commonly utilized optical models that represent sample systems.

Most of the studies, about 85% of the literature included in this review, consider both dry and swollen samples as uniform films, Figure 1.8a. This Uniform model assumes little or no roughness, and that the material density is distributed evenly within the volume of the film. To limit the scope of this review, polymer brushes or grafts are not included. In these cases the Graded optical model, Figure 1.8b, is more often used. Typically, the density of the polymer material in swollen brushes is larger close to the substrates, and decays more or less exponentially towards the ambient. This mass density distribution often corresponds to refractive index distribution and can be modeled with a graded refractive index. Interested reader is referred to one of the reviews on polymer brushes [11-13], in which also the

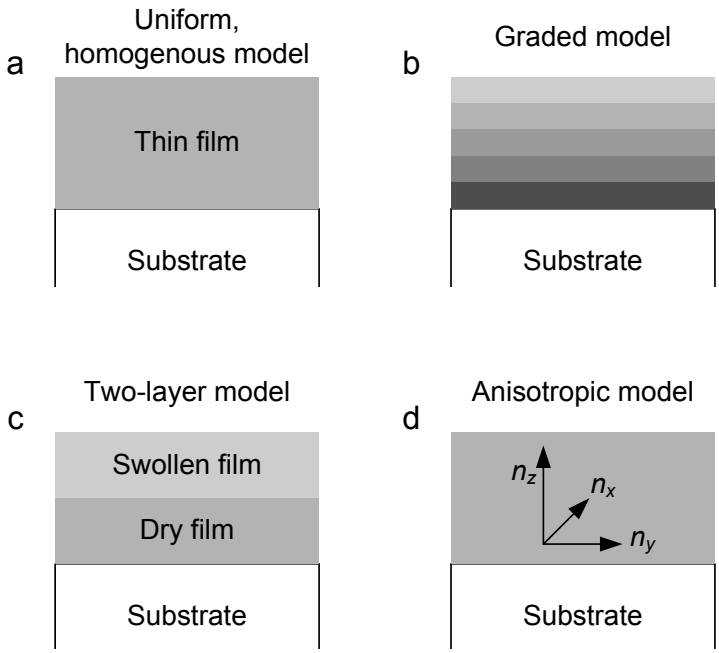

Figure 1.8 Optical models used in typical *in-situ* ellipsometry measurements of swollen polymer films

ellipsometry technique for this particular application is discussed. Density gradients within the non-covalently attached films, Figure 1.8b, have been considered during dynamic swelling measurements of zwitterionic films in water [14, 15]. In these cases however, the researchers have concluded the gradients not to be adequately captured with a Graded model. In another investigation of different zwitterionic supported films the gradients within the polymer in the process of swelling with an electrolyte solution have been found to be valid [16]. Contrary to the situation in brushes, in the polyzwitterions the formation of a gradient occurred only during the penetrant diffusion process. At equilibrium no significant gradients have been observed.

Some studies that have dealt with very particular processes consider the Two-layer model, where the top-most region of the polymer is swollen with the penetrant, while the bottom part of the film is essentially dry, Figure 1.8c. These studies describe the anomalous Case II diffusion of solvent in the swollen film where the timescale of polymer relaxation at a sharp diffusion front determines the kinetics of the process. Case II diffusion has been investigated with *in-situ* ellipsometry for poly(methyl methacrylate) (PMMA) dissolution in various organic solvents [17-22], and for the diffusion of n-hexane into PS thin and ultra thin films [23, 24]. In these studies, ellipsometry has proved to be able to resolve the temporal progress of the penetrant front within thin films and to serve as a tool to probe the surface polymer mobility of ultra thin films [24]. More complex multilayer models have also been found in the literature [25], where the problems of swelling and protein adsorption are discussed.

Ellipsometry is well capable of determination of optical anisotropy, Figure 1.8d, as has been demonstrated for dry films [26-31]. Studies where optical anisotropy is investigated in detail during swelling of polymers are very rare [16]. One interesting study uses a technique that is similar to ellipsometry, Mueller matrix polarimetry, to study swelling induced anisotropy in swollen hydrogels [32]. Optical anisotropy in dry layers of some high performance polymers, which have been subsequently swollen, is considered in [33]. However, whether the swollen layers have been modeled with a Uniform or an Anisotropic model remains unclear. Anisotropic swelling has been suggested in the investigation of Kleinfeld et al. [34], but a Uniform optical model has been used.

1.2.2.3.2. Substrates utilized for *in-situ* studies

By far the most commonly utilized substrate is a silicon wafer with a native oxide of about 1.5 – 2 nm thickness. The optical dispersion of this substrate, and its temperature dependence, are very well known [35] and do not change upon immersion in most experimental ambients. In addition, the surface roughness of a silicon wafer is very small. Therefore, it is considered an ideal substrate for *in-situ* ellipsometry. The high real part of the complex refractive index of crystalline silicon (N_{Si}=3.874-0.015i at 632.8 nm) assures very good optical contrast between

the polymer film and the substrate even when the ambient index is much larger than 1 (e.g., liquid water n_{water}=1.332). In some cases thicker, thermally grown, oxide layers are utilized. This is done predominantly to improve the accuracy of the measurements, in particular when layers below 50 nm are studied [36-38]. Other examples include studies like the one done by Kleinfeld et al, [34]. The researchers have applied variable thickness of oxide layer in a range between 1.4 nm and 216 nm and the thickness of the investigated multilayer composite film in the range 16 nm to 223 nm, while keeping the oxide plus sample thickness approximately the same, at about 230 nm. This has allowed determining the approximate depth of rapid water penetration within these potential sensor materials, and has been a way of overcoming limited temporal resolution of the used device.

If ellipsometry measurements are coupled or complemented with other techniques, in particular with the QCM or electrochemical methods, the analysis is frequently performed on gold coated quartz crystals [39-42]. Already about 50-60 nm of gold is optically non-transparent for light in the near visible range, therefore, gold coated crystals can be considered as bulk substrates for ellipsometry. The additional advantage of metal substrates is that they are compatible with total internal reflection ellipsometry (TIRE) [43]. However, the surface roughness in the case of metal substrates can be much larger and less controllable as compared with silicon wafers. Gold and other metals (Ti, Pt) are also utilized in the case of electrochemically deposited or responsive films, where they serve as electrodes [44-46]. Less frequently than silicon wafers glass slide substrates are used [8, 47-52], these however, provide much weaker optical contrast because glass refractive index is typically very close to that of the analyzed polymer (n_{glass} ~1.5).

Other, less common (including surface modified), optical substrates have been occasionally employed. Richardson et al [53], have used octyl trichlorosilane grafts on silicon wafers to study the impact of surface interactions in structural relaxation of PMMA films during solvent loss. Ogieglo et al [8], have utilized a polished, porous membrane substrate to study the behavior of 1-2 micron PDMS layers in non-equilibrium, transport conditions under high pressure of liquid n-hexane. Sirard et al [54], have studied the influence of replacing SiO_2/Si wafer with GaAs wafer on the anomalous maxima of sc-CO_2 sorption in PMMA films.

1.2.2.3.3. Optical modeling and limits of ellipsometry

After the model is constructed, the corresponding Ψ and Δ data are generated and model parameters, such as film thickness and/or refractive index, are fitted numerically to match the experimental Ψ and Δ data. This is depicted schematically in Figure 1.9. The most widely used measure of the fit quality is the (root) mean square error parameter, MSE. This parameter quantifies the error between the model-generated and measured Ψ and Δ values [55]. The iterative fitting is

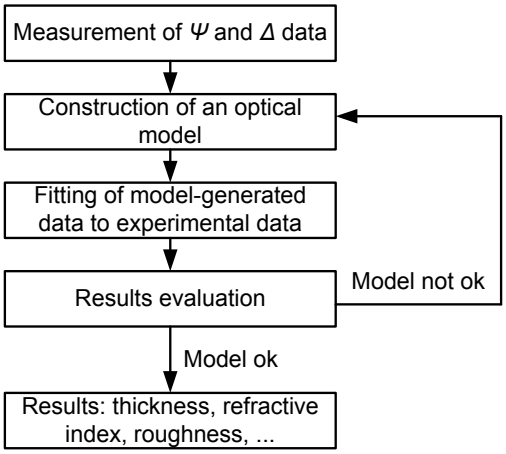

Figure 1.9 General scheme of ellipsometry data analysis and sample properties extraction

commonly done with the Marquardt-Levenberg algorithm [56]. Some authors suggest using a different measure of fit error, χ^2, which overcomes various drawbacks of the MSE [57].

Fit parameters commonly include the layer thickness, its optical dispersion and various other features of the samples. The other features may contain sample roughness, parameters describing gradients, anisotropy (Figure 1.8b-d), or sample uniformity. Because most polymeric materials are simple, transparent dielectrics, their optical dispersion can be modeled according to the Cauchy formula:

$$n(\lambda) = A + \frac{B}{\lambda^2} + \frac{C}{\lambda^4} \qquad (1.2)$$

where A, B and C can serve as adjustable fitting parameters. If the polymer is absorbing (usually in the vicinity of the UV spectral region), but the absorption spectrum is not relevant for the particular measurement problem, then the wavelength range for the modeling is often limited to the transparent part. If light absorption spectrum needs to be determined, it can be modeled with an dielectric oscillator models (for instance, Gaussian, Tauc-Lorentz, or others) [5]. Alternatively, light absorption can be represented with the B-splines [58], which also yields good results provided that it is done with appropriate assumptions accounted for.

For the majority of simple samples, for instance including thin (up to 500 nm), Cauchy-type polymer films deposited on silicon wafers the MSE values representing very good fits are in the range 1-5. For thicker films values of 10-20 are acceptable. The higher values in this case do not necessarily mean that the assumptions of a particular model are not fulfilled. Higher MSE may originate

from the limited spectral resolution of the experimental setup which is unable to represent a large number of oscillations in a spectrum, as discussed in 1.2.2.2.

If the obtained MSE value for a given optical model is not satisfactory, additional fit parameters can be included. This has to be done with care to avoid overparametrization of the sample. If the number of fitting parameters is too large significant correlations between them may be introduced. As a result the physical meaning of some parameters may become difficult to establish and the description of a sample with such a model becomes meaningless. A proper data analysis should always include parameter correlation assessment. Typically, the reduction of MSE after the introduction of an additional fitting parameter should be *significant*, that is roughly on the order of at least ~25% [59]. The significant MSE reductions may be, in a lot of cases, treated as a strong indication of meaningfulness of the extra parameters and give valuable information about the sample morphology. The examples include the large reduction of MSE with a Two-layer model over a Uniform model during Case II diffusion [23], serving as validation for the choice of the more complex model, and the more than 5-fold reduction of MSE with an Anisotropic model over a Uniform model in the study of swelling zwitterionic films [16], being a strong indication of developing anisotropy during swelling.

Parameter correlations may also become an issue when film thickness and index need to be independently determined for very thin films, in the so-called ultra-thin region much below 100 nm. This is because for typical refractive indices of polymers (n = 1.4-1.6) Ψ becomes a very weak function of the thickness below about 30 nm [5]. With state of the art ellipsometry devices, the thickness range allowing a reasonably accurate determination of the independent thickness and index is thus ~30 - 3000 nm. However, if the refractive index of the polymer is known (can either be determined independently or does not change too much from its dry value during the *in-situ* measurement) its value can be fixed and the thicknesses down to essentially fraction of a nanometer can be accurately measured.

The more complex optical models, such as those depicted in Figure 1.8b-d, usually require sufficiently thick samples to work reliably. If more complex information on density distribution within very thin films (a few nanometers) is required then ellipsometry may be supported by techniques using much shorter wavelengths, for instance neutron or X-ray reflectivity. Both of these are applicable *in-situ*. For complex optical models fit parameter correlation needs to be checked carefully. This is because these models comprise usually a large amount of fitting parameters. In some cases the validity of certain optical models over others can be assessed by additional measurements. For instance, the distinction between a graded model, Figure 1.8b, and the anisotropic model, Figure 1.8d, can be done by measuring several angles of incidence. Distinction between uniaxial and biaxial anisotropy

can be done by rotating the sample around a perpendicular axis. However, in the case of typical polymer film samples biaxial anisotropy is very unlikely.

1.2.3. *In-situ* configurations

In-situ ellipsometry often requires a means to bring the analyzed sample in contact with a penetrant. This has been realized in various ways. Some of the most frequently used configurations are briefly discussed in this paragraph.

1.2.3.1. No *in-situ* sample cell

Interactions of the penetrant with the polymeric films have been studied without confinement of the ambient within an experimental cell. The advantages of such a configuration are that the measurements can be performed at multiple angles. This may increase accuracy. The disadvantage is that the control over experimental conditions related to the ambient may not be as accurate as in the case of *in-situ* cells described in 1.2.3.2.

The no-cell configuration has been used for the observation of structural relaxations during solvent (toluene) evaporation from thin and ultra-thin PMMA films [53, 60], Figure 1.10a. The thin film samples have been simply transported from the spin coater pad onto the stage of spectroscopic ellipsometers, and measurements in relatively short time intervals (about 20 s) have been taken to dynamically observe simultaneous changes in film thickness and index. Similar methodology has been applied in the observation of drying processes in the same polymer, but with a solvent assuring relatively high optical contrast (bromobenzene) [61]. In a different configuration, Figure 1.10b, for the measurements of the contact angle hysteresis in polyimide, the film has been brought in contact with a water droplet for a certain period of time and the uptake of the penetrant has been measured with ellipsometry after the water droplet removal [62].

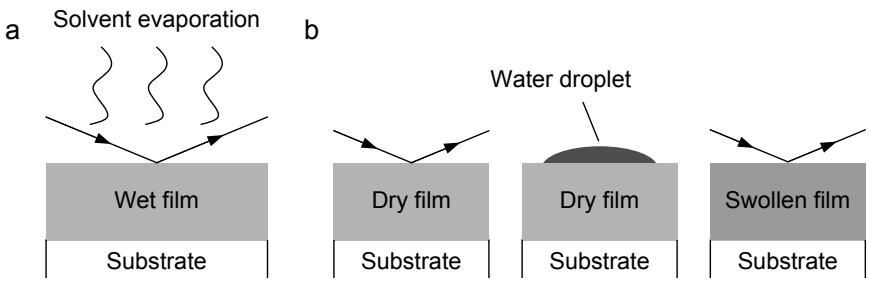

Figure 1.10 *In-situ* ellipsometry configurations without experimental cells; a [53, 60, 61], b [62]

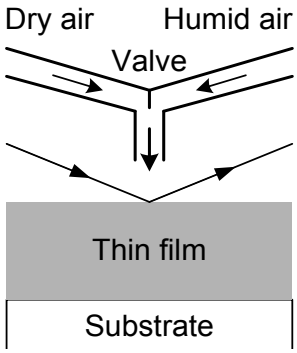

Figure 1.11 Controlled relative humidity measurements without experimental cell, with permission from [36]. Copyright 2003 American Chemical Society

The delivery of humid air for controlled relative humidity conditions can be done without the application of *in-situ* cell, as in the study of swelling of ultra-thin cellulose Langmuir – Blodgett deposited films [36]. Relative humidity measurements can also be performed in a configuration where the ellipsometer stage is placed in a relatively big container (or even a plastic bag with cut holes as windows for the light beam) in which humidity is controlled [34, 63]. An intermediate step between no sample cell, 1.2.3.1, and the utilization of such, is a trapezoidal sample cell with holes as windows. The advantage is good ambient gas or vapor flow repeatability combined with no impact of windows on the probing polarized light. However, this configuration can of course not be used with liquid or compressed fluid ambients.

1.2.3.2. Near-atmospheric pressure *in-situ* cells

Figure 1.12 shows the schematics of a typical *in-situ* ellipsometry trapezoidal flow cell equipped with a temperature control unit. Such a cell is used in most of the *in-situ* ellipsometry investigations of thin swelling films and assures excellent control over the experimental conditions. The flow of the ambient is not always employed and some investigations are done in static conditions. The body of the cell is most often made of glass or stainless steel, in some cases from high performance plastics. The windows need to be transparent in the measurement wavelength range and optically isotropic. This last condition may not always be assured. However, protocols exist that allow correcting for the birefringence of the windows (in particular for the in-plane component), which is most severe in the case of the Δ parameter determination. This can be done by running appropriate calibration procedures, for instance by measuring a sample (or pure substrate) with known optical constants inside of the cell and fitting for the Δ offsets.

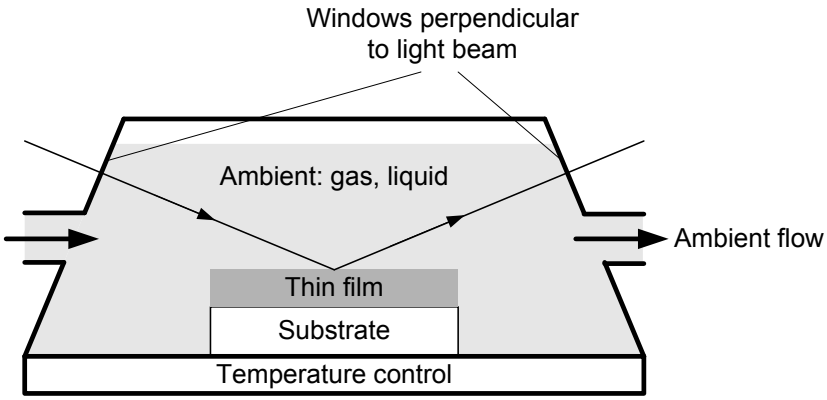

Figure 1.12 Schematics of a typical *in-situ* ellipsometry flow cell with temperature control option and windows at 70°

Out-of-plane window offsets can often be sufficiently corrected for by the design of the instrument and internal calibration methods (this is valid, for instance, for Alpha-SE, M-2000 and VASE systems of J.A. Woollam).

Windows are, in almost all cases, placed perpendicular to the light beam. This is not absolutely required when the measurements are done in vacuum, air or in fluids with index close to 1. It becomes crucial when an ambient with a refractive index significantly larger than 1 is placed inside of the measurement cell. This is because when the light enters the cell at a non-right angle, the whole cell becomes a prism in which the transmitted light travels at an angle given by the Snell's law (see Appendix, eq. A2), which is different from the incidence angle. This in turn produces a different exit angle as well. In severe cases this deviation is large enough so that the light beam might miss the sample entirely.

Typical angles of incidence found in literature are close to 70° (in a range from 65° to 75°), which is near the Brewster angle of the most commonly used crystalline silicon substrate, 73.7°. At the Brewster angle the reflectivity of *p*-polarized light as a function of incidence angle passes through a minimum [5-7]. This minimum is zero for non-absorbing substrates and close to zero for absorbing substrates. Since ellipsometry measures reflection coefficients ratio (r_p/r_s) and the difference between r_p and r_s is maximized at the Brewster angle, an increased sensitivity for a bare substrate is found at that angle. The choice of 70° angle of incidence for *in-situ* ellipsometry studies of polymers is probably made largely due to historical reasons. This is related to the extensive use of ellipsometry in semi-conductor research in the past decades. In that field crystalline silicon has been widely employed as a substrate and the analysis has been done usually on very thin films (several nm) of relatively high refractive index (metalloid elements, their oxides and alloys). In typical polymer studies the films are much thicker, from tens of nm to several microns, and have much lower refractive indices, 1.4 – 1.6. In such cases

the largest sensitivity may not necessarily be found around the Brewster angle of the substrate, but often closer to the Brewster angle of the film itself. This can be seen in Figure 1.13 where a spectroscopic ellipsometry sensitivity calculation as a function of incidence angle is shown for a 100 nm film of a polymer with a refractive index of 1.6 supported on a silicon wafer. The sensitivity is defined here as a change in the absolute MSE by changing film thickness by 1 nm and keeping the refractive index constant. It can be seen that for this particular polymer the largest sensitivity is obtained at about 550 nm wavelength for 60° angle of incidence. For this wavelength, the angle is closer to the Brewster angle of the polymer, 58.2°, than that of the wafer, 74.6°. The sensitivity at 70° is still very good and this angle of incidence should give high quality results as well. However, to obtain the best sensitivity for a particular measurement problem, similar analysis should be done to determine the most optimal incidence angle. Consequently, a custom-made optical cell adjusted for that angle may be constructed.

Depending on the type of application the ambient may be stationary or continuously flown over the thin film sample. The second case is often applied in relative humidity measurements to assure accurate control over the saturation level of water in the gas phase. Flow cells can be often used for simultaneous ellipsometry and QCM or electrochemical measurements [40, 45, 46, 64]. Such

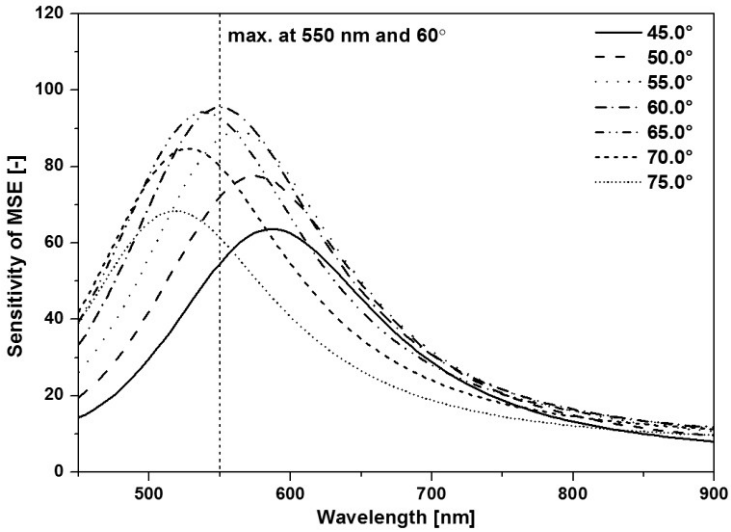

Figure 1.13 Sensitivity of MSE to thickness variation by 1 nm for a 100 nm polymer film with refractive index of 1.6 supported on a silicon wafer for various angles of incidence; maximum sensitivity observed at 550 nm for 60° incidence angle which is closer to the Brewster angle of the film itself, rather than the Brewster angle of the supporting wafer

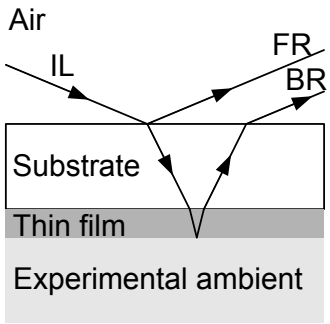

Figure 1.14 Backside *in-situ* ellipsometry configuration

applications greatly improve the amount of information that can be determined about the measured system. For example thickness/index changes within the swollen films can be observed simultaneously with viscoelastic changes within the films (QCM with dissipation, QCM-D) or redox transitions (electrochemical measurements). This is discussed in more detail in paragraph 1.6.

An alternative, but less common approach to *in-situ* liquid measurements, is the backside configuration [51, 52], Figure 1.14. It involves the measurement of the film attached to a backside of a transparent substrate (usually glass slide), where the incident light (IL) is shone from the topside of the substrate.

In this case the first reflection (FR) carries no information about the sample and the back reflection (BR) is of interest. The benefit of such a configuration is that the measurements can be performed at multiple angles of incidence because no windows perpendicular to light beam are utilized. This also reduces the complexity of the utilized cell. The disadvantage is that, in the case of liquid measurements, the cell needs to be fully filled with liquid. This may become problematic since usually the optics of the device are on the top of the sample. When the film faces the bottom direction, this may promote bubble formation at the film surface disturbing the measurements.

1.2.3.3. High pressure cells

Sirard et al. have first developed a high pressure *in-situ* ellipsometry chamber for the measurements of supported thin PDMS films exposed to carbon dioxide [65]. Due to mechanical requirements the body of the cell has been constructed from stainless steel combined with thick fused silica windows (1.5 cm diameter, 1 cm thick), Figure 1.15. High pressure can induce window birefringence, even if the windows are not birefrigent at atmospheric pressure. That is why it is usually required to calibrate for these effects by running high pressure measurements on, for instance, a calibration wafer (thermal SiO_2/Si), to determine the in-plane Δ offset. If gas refractive index shows significant dependence on pressure (like in the

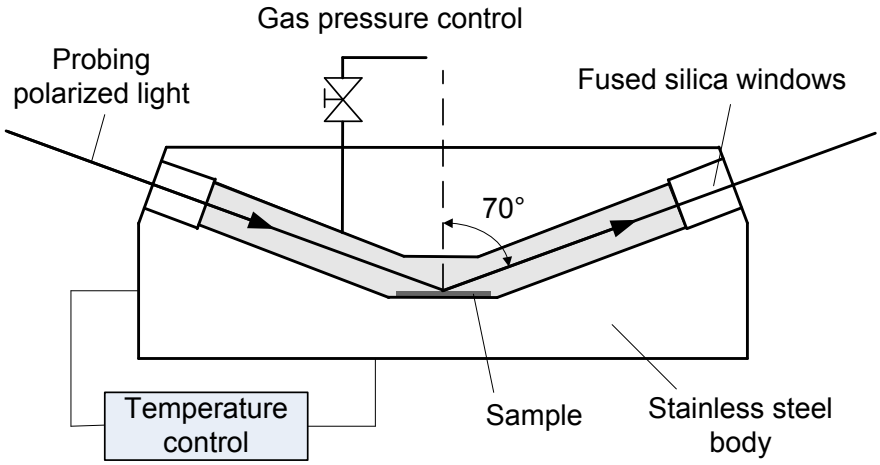

Figure 1.15 Schematics of a high pressure *in-situ* ellipsometry cell, first developed by Sirard et al [65]

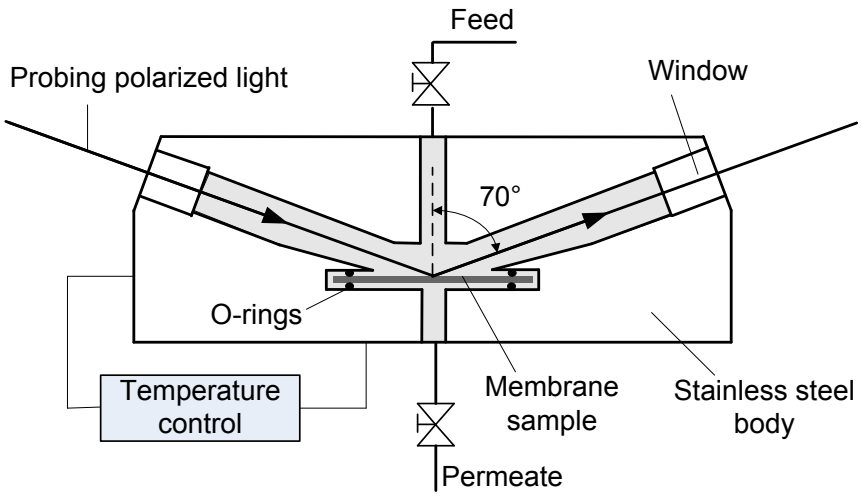

Figure 1.16 Schematics of a high pressure *in-situ* ellipsometry cell allowing for permeation experiments. With permission from [8]. Copyright 2013 Elsevier

case of CO_2) its optical properties need to be known (data for several gases including CO_2, N_2, ethylene and ethane can be found in [66-68]).

High pressure ellipsometry has also been shown to be a very powerful tool for the determination of swelling of thin and ultra-thin glassy films exposed to condensable gases, in particular CO_2, and determination of sorption induced glass transition pressure, P_g [54, 69-72]. In addition, the technique has been used to calculate concentrations of dissolved gas in thin films [48, 73, 74], investigations

of anomalous maxima in swelling near critical conditions of CO_2 [54, 75], and observations of order-disorder transitions in block copolymers in high pressure CO_2 [76].

Recently, a new type of a high pressure *in-situ* ellipsometry cell has been introduced that allows for studying the behavior of selective layers of composite membranes during permeation, Figure 1.16 [8]. The cell presented in the figure is to a large extent the same as the one from Figure 1.15. The difference is that the permeation of the species from the top to the bottom of the cell is possible. In this case different transport phenomena, important in membrane science, can be conveniently and non-invasively studied, provided that appropriate optical models for rough, porous substrates are available [77].

1.3. Types of polymeric materials studied

In this paragraph the different classes of non-covalently attached polymeric films, which have been investigated with *in-situ* ellipsometry, are briefly reviewed. The emphasis is put on the chemical structure of the material, fabrication methods, equilibrium (glassy) or non-equilibrium (rubbery) character that all influence the behavior upon exposure to various penetrants. This paragraph is intended to provide a full picture on the different types of polymeric materials investigated with *in-situ* ellipsometry.

1.3.1. Simple glassy polymers

Glassy polymers are of tremendous importance in a range of technologically important areas. This originates from their good mechanical properties, dimensional stability, and chemical resistance at room and slightly elevated temperatures. For high performance polymers the application range can be extended even further. The interaction (especially long term) with penetrants in those materials is very often determined by the non-equilibrium nature of glasses, i.e. the fact that at temperatures below T_g glassy polymers become kinetically arrested materials slowly relaxing towards equilibrium state (physical aging) [78]. In many applications, especially in coatings, barriers and membranes these long term processes are of particular importance. The slow changes in density in thin and ultra-thin films mean that often resolution on the order of sub nm is necessary, in particular when physical aging is combined with slow penetrant induced relaxations [74]. This is why ellipsometry has been demonstrated to be an ideal tool in such studies.

By far the most widely studied, with *in-situ* ellipsometry, glassy polymeric materials are PS [23, 24, 74, 75, 79-82], and PMMA [17-20, 53, 54, 60, 61, 73, 82-84]. This is because these materials constitute ideal model, amorphous, glassy polymeric systems with easily accessible T_g ($T_{g,PS}$ ~ 100 °C, $T_{g,PMMA}$ ~ 110 °C).

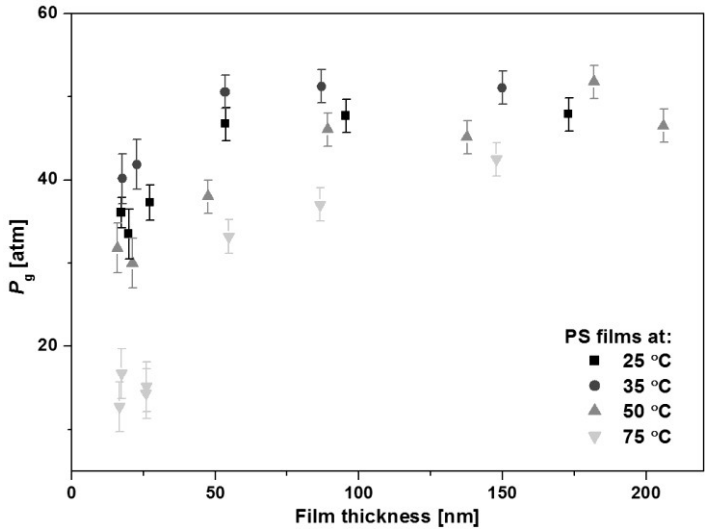

Figure 1.17 Devitrification pressure (P_g) versus film thickness; isotherms for PS (M_w = 590k) films at 25, 35, 50 and 75 °C. Adapted with permission from [81]. Copyright 2004 American Chemical Society

They are also easy to dissolve in common solvents (predominantly toluene, chloroform or acetone) and easy to tune film thicknesses during spin coating by changing solution concentration. This makes systematic investigations on the effects of dry film thickness on the interactions with penetrants possible [24, 53, 60, 61, 69, 81]. An example for such an investigation is shown in Figure 1.17, where pressure induced glass transition, P_g, is shown to vary with initial film thickness.

Other studies include investigations on the dimensional stability of high performance polymers used in microelectronics [33], water swelling in ultra-thin layers of cellulose [36, 49, 85], swelling of ion beam treated polyimide layers [86, 87], contact angle hysteresis in polyimides [62], anomalous swelling of several high performance polymers in supercritical CO_2 [75], and swelling of electrically conducting polymers [47]. In membrane science the sorption, relaxation and plasticization in high pressure CO_2 has been investigated for various high T_g materials, including polyetherimides, polyimides, polysulfone, poly(phenylene oxide) and sulfonated poly(ether ether ketone) [48, 70, 71, 74, 88]. In most cases these polymer films have been prepared by spin coating from good solvents.

1.3.2. Simple rubbery polymers

Contrary to glassy polymers, sorption in rubbers usually proceeds very fast with quick equilibration of the system (lack of long term relaxations). This made such polymers as PDMS, and its derivatives, very good candidates for volatile organic

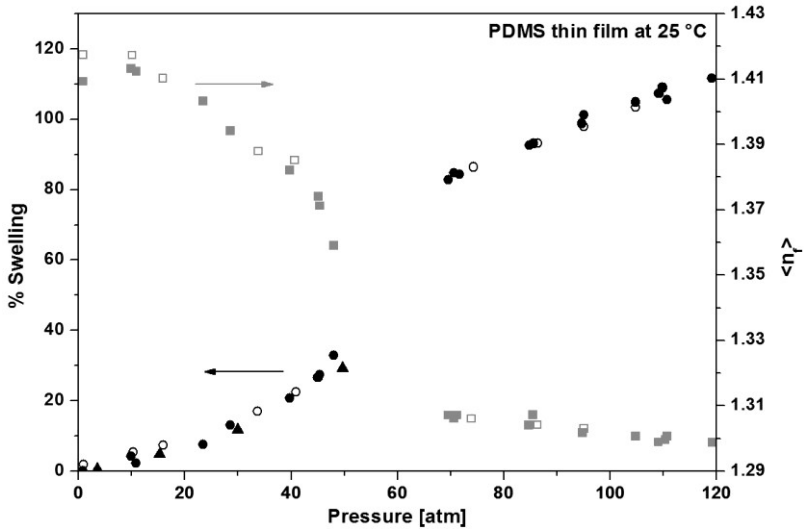

Figure 1.18 Swelling isotherms for a PDMS thin film in CO_2 at 25 °C. The circles represent the equilibrium swelling and the squares represent the refractive indices of the swollen film. Filled circles and squares correspond to sorption measurements and open circles and squares correspond to desorption measurements. Triangles are from bulk measurements [89]. Adapted with permission from [65]. Copyright 2001 American Chemical Society

compounds sensing, where the material sorption response can be conveniently studied with *in-situ* ellipsometry [90, 91]. Due to its simplicity, the same rubbery material, has been investigated as a model system in the high pressure CO_2 sorption investigation, Figure 1.18 [65], and high pressure *in-situ* liquid solvent nanofiltration experiments [8]. Other rubbery systems investigated include poly(amide-6-*b*-ethylene oxide) (PEBAX) [48] and pH-responsive poly(methylcarboxypropyl siloxane) (Posimca50) [92]. The preparation of rubbery films may involve the use of a cross-linking agent [8]. This is done to assure dimensional stability of the rubbery material that otherwise possesses too low viscosity for practical use.

1.3.3. Random and block copolymers

An important practically utilized class of polymers is copolymers. In this case, the question of glassy or rubbery nature of the systems is quite complex and often multiple T_g values are found, especially in the case of block copolymers. However, when plasticized with penetrants the copolymers often reside above the highest T_g of the constituents and can be considered rubbers. The systems which involved copolymers, and have been investigated with *in-situ* ellipsometry, are much differentiated reflecting a multitude of potential applications.

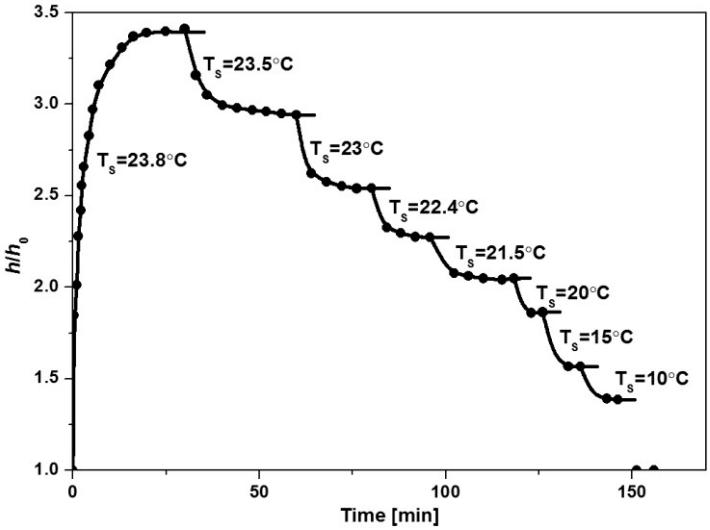

Figure 1.19 Swelling behavior of a PtBMA film in decreasing activity of chloroform vapor (T_P=24 °C, h_0=150 nm). Activity of vapors is tuned by the saturation temperature. Adapted with permission [80]. Copyright 2004 Elsevier

Chen et al. [39], have investigated swelling of various hydrophilic copolymers in humid environments. The polymers used are based on polyacrylates with low M_w poly(ethylene glycol) PEG side chains, and could be potentially used as coatings with tunable wettability and adhesive properties. The researchers have reported on the existence of humidity induced phase transition within the materials as confirmed with QCM complemented with *in-situ* ellipsometry. In their fundamental study Elbs et al. [80], have investigated the organic solvent (vapor) swelling of various homo- and related copolymers, Figure 1.19, and have extracted the Flory-Huggins interaction parameters. Based on that data the researchers have been able to quantify compatibility of the polymers synthesized from different co-monomers in various solvents.

Spin-coated thermosensitive coatings of cross-linked microgels of poly(*N*-isopropyl acrylamide-*co*-acrylic acid) (p(NIPAM-*co*-AA)) have been investigated by Schmidt et al. [93]. The coatings have been prepared to enable tunable surface reflection properties depending on temperature. The fundamentals of scaling behavior of the order – disorder transition in PS-*block*-polyisoprene copolymers in compressed CO_2 has been investigated by Chandler et al. [76]. An interesting confinement effect in PS-*block*-PVP has been shown to control swelling, considered as a macroscopic response, with a maximum effect for films with dry thickness on the order of one-two lamella dimensions [94]. The confinement effects, manifested as a 10% increase of solvent uptake with decreasing film thickness, have also been investigated in cylinder-forming PS-*block*-polybutadiene copolymers [95]. In spectroelectrochemical sensor applications the partially

sulfonated polystyrene-block-poly(ethylene-ran-butylene)-block-polystyrene (SSEBS) thin films have been evaluated towards sensing of $Ru(bpy)_3^{2+}$, phenosafranine and rhodamine analytes in aqueous conditions [96]. Yagüe et al. [97], have shown the possibilities to control the mesh size in poly[(2-hydroxylethyl methacrylate)-*co*-(ethylene glycol diacrylate)] (p(HEMA-*co*-EGDA)) synthesized by initiated chemical vapor deposition (iCVD) during water swelling of the layers. iCVD prepared pH-responsive copolymers have also been investigated with respect to their drug release capabilities [98].

1.3.4. Multilayer films

A significant portion of *in-situ* ellipsometry studies has been dedicated to swelling of multilayer films. These types of materials, in particular polyelectrolyte multilayers prepared by layer-by-layer deposition [99], are known for their stimuli responsive characteristics. They can be used in sensor, electronic, separation, cell adhesion and many other applications. In this section the multilayer systems investigated are outlined. More focus on the particular processes studied is given later in paragraph 1.4.

Kleinfeld et al. [34], have described composite films prepared by alternate adsorption of poly(allylamine hydrochloride) (PAH) and exfoliated sheets of Laponite RD that show dramatic response to ambient humidity. Rapid water penetration depth down to 139 nm has been shown to be accompanied by equally rapid desorption. For the ionic separation applications PAH/poly(styrenesulfonate) (PSS) and PAH/poly(acrylic acid) (PAA) films have been shown to present pH dependent permeability of $Fe(CN)_6^{3-}$ and $Ru(NH_3)_6^{3+}$ [44]. Layer-by-layer self-assembled osmium complex-derivatized PAH and glucose oxidase multilayers, $(PAH\text{-}Os)_n(GO_x)_n$ that change thickness and index in response to electrical potential changes have been investigated by Forzani et al. [45]. History dependent, pH-responsive swelling behavior and molecular conformational memory has been demonstrated in PAH/PSS incorporated into multilayer films [100]. Poly(L-glutamic acid) (PGA) and poly(L-lysine) (PLL) multilayers built on poy(ethylene imine) PEI has been shown to be a stable drying/deweting system, responsive to temperature and pH changes of the surroundings [101]. The dynamic swelling of PAA and PAH under various pH conditions has been studied by Tanchak et al. [102]. Assemblies of PSS and PAH have been characterized with respect to thickness changes in humid environments and the odd-even effect (swelling dependence on the outer layer charge) has been investigated [103]. Swelling of biopolymer multilayers containing hyaluronic acid (HA) and PAH has been reported by Burke et al. [104]. Ph-induced swelling/deswelling transition mechanism in multilayers containing PAH have been investigated by Itano et al. [105]. Permeability/swelling correlations of various polyeletrolyte multilayers have been investigated by Miller et al. [106]. Olugebefola et al. [107], synthesized and characterized a photo-cross-linkable weak polyelectrolyte based on poly(acrylic

acid-*ran*-vinylbenzyl acrylate) (PAArVBA). Electrodes modified by layer-by-layer assembled redox active polyelectrolytes have been investigated by Tagliazucchi et al. [46]. Schmidt et al. [64], investigated electrochemical swelling control capabilities in nanocomposite thin films comprising linear PEI and Prussian Blue nanoparticles, Figure 1.20. As can be seen from the figure, these multilayers showed excellent stability and swelling – deswelling reproducibility. Hysteretic swelling in PAH) and PAA multilayers has been investigated by Secrist et al. [63].

The effects of cross-linking in bioreducible poly(2-dimethylaminoethyl methacrylate) (PDMAEMA) and deoxyribonucleic acid (DNA) have been investigated with respect to their biologically active properties [108]. Electric field controlled orientation of bilayers containing gramicidin and dimyristoylphosphatidylcholine (DMPC) has been described by Fiche et al. [109]. Temperature induced swelling of multilayer triblock copolymers has been investigated by Tan et al. [110]. Diblock copolymer micelles with thermo-sensitive cores have been characterized by Xu et al. [111]. Ionic strength effects on swelling of PSS and poly(diallyldimethylammonium chloride) (PDADMAC) have been investigated in depth by Dodoo et al. [112]. Cell migration through cell-cell interaction on polyelectrolyte multilayers has been characterized by Han et al. [113].

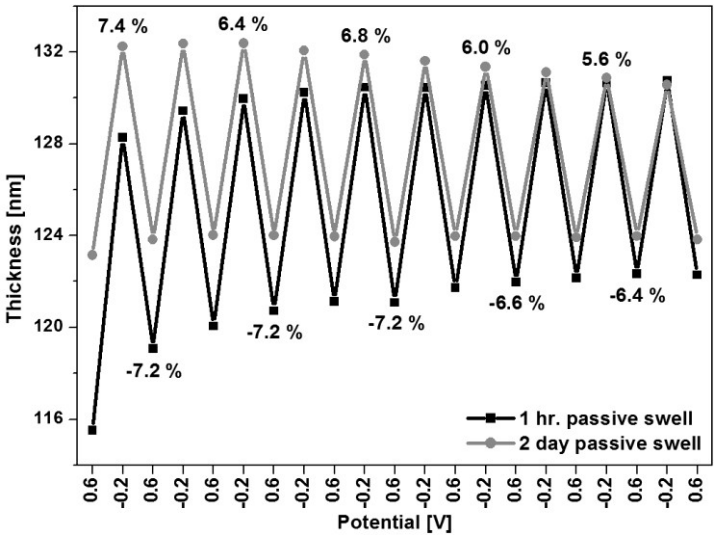

Figure 1.20 Active swelling of two (linear PEI/Prussian Blue)$_{30}$ films subjected to 10 redox cycles after 1 hour and 2 days. Swelling percentage values (calculated relative to thickness in the preceding redox state) are next to the corresponding data points; negative values represent shrinking. Adapted with permission from [64]. Copyright 2009 American Chemical Society

1.3.5. Other systems

Other larger groups of polymeric systems, investigated with *in-situ* ellipsometry, included zwitterionic films based on PC [14, 15, 114, 115], and polysulfobetaine [16]. In contrast to polyelectrolyte multilayers, described in 1.3.4, zwitterionic polymers contain both positively and negatively charged groups within a single monomer unit. This determines their properties, in particular with respect to cell adhesion and biofouling. Cyclic oligomeric molecules of calixarenes have been characterized for sensing of organic vapors by several groups [41, 42, 116]. Hydrogel behavior under aqueous conditions has also been characterized by *in-situ* ellipsometry [50, 117-119]. Swelling of hyperbranched polyesters has been investigated in several cases [25, 37, 120, 121]. Swelling of adsorbed latex particles has been studied by van der Zeeuw et al. [122, 123] by reflectometry. This detailed study has focused on the determination of size changes of the adsorbed particles during swelling.

Other less common polymeric systems include electrochemically grown polyaniline (PANI) [40], 200 nm Pd- fluoropolymer (Pd-CF_x) sputtered films [124], sol-gel processed polyelectrolyte-silica composite films [52], iCVD deposited, cross-linked systems [125], chemical reactions of ferrous ion within thin Nafion films [51], MOFs [126], Nafion nanomembranes [127] and dendritic macromolecule films of oligosaccharide-modified PEI [128].

1.4. Types of polymer-penetrant phenomena studied

In-situ ellipsometry has been applied to study a wide range of polymer-penetrant phenomena. In the most common experiments a dry polymeric thin film sample has been exposed to a penetrant and the change in its properties has been recorded. These types of investigations constitute about 50% of *in-situ* ellipsometry studies on polymer swelling. They are outlined in 1.4.1 where also the distinction is made between the different types of penetrants used in the literature. In the subsequent paragraphs, 1.4.2-1.4.6, the other less commonly found groups of investigations are described.

1.4.1. Penetrant uptake from dry state

In this part the focus is on thin film samples that have been swollen with various penetrants from a dry state. These studies involved samples that have been spin-, dip-coated or prepared *in-situ* and subsequently annealed under inert gas flow or vacuum to remove the solvent and relax post-preparation stresses. Thus the dry sample properties have usually been known. Figure 1.21 shows the change in the Ψ spectrum for a dry and liquid n-hexane swollen ~150 nm PS film [23]. In this case the pronounced change in the amplitude going from a dry to a swollen film has been only weakly related to the change in the film index during swelling of about

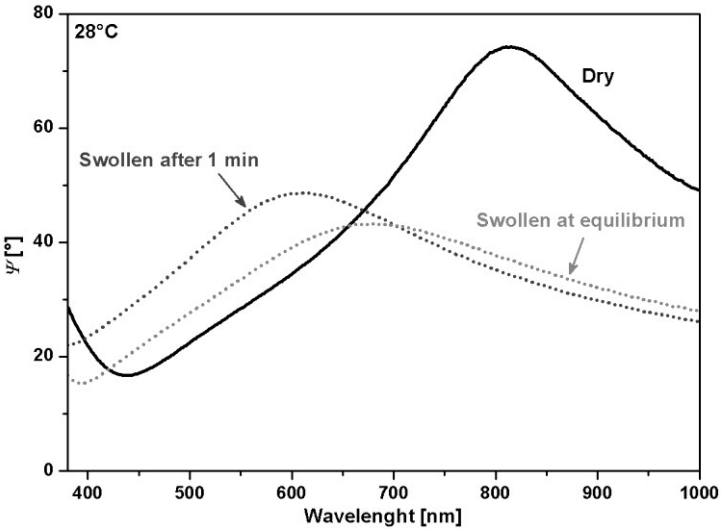

Figure 1.21 Changes in the Ψ spectrum of ~150 nm PS film supported on a silicon wafer upon exposure to liquid n-hexane penetrant at 28 °C, adapted with permission from [23]. Copyright 2013 Elsevier

20% (n_{dry} = 1.585, $n_{swollen}$ = 1.556). Most of the amplitude dampening has originated from the replacement of the experimental ambient (air for the Dry spectrum, n_{air} = 1.000) with liquid n-hexane (for the Swollen spectrum $n_{n\text{-}hex}$ = 1.369). This has caused a very significant reduction in the optical contrast between the layer of interest (PS film) and the ambient. This is a typical issue during *in-situ* ellipsometry swelling experiments.

The loss of contrast contributes to an increase of error in determination of the sample properties because a much smaller change in Ψ has to be detected with the same resolution of the device. If the swollen system possesses refractive index very close to the experimental ambient (which is usually the case for polymers swollen much above 100%), the loss of contrast may even prevent accurate determination of the swollen film refractive index. The solution for the problem could be, in some cases, the assumption that the index of the film doesn't change too much during sorption. This may be especially helpful when only relative swelling or differences between similar samples are investigated.

For the experiments where only penetrant vapors are used, usually the index of the ambient can be assumed not to change significantly from n_{air} = 1.000. The exceptions are high pressure gas experiments where the departure from air index (n_{air} ~1.000) may be significant already for moderate pressures. For example, at 50 bar $n_{CO2,gas}$ = 1.027. Changes in refractive index of the ambient can be expected in particular for highly polarizable molecules, such as VOCs or carbon dioxide. The effects are smaller for He or H_2.

Multilayer and responsive (pH, temperature, ionic strength, etc) samples, highlighted already in paragraph 1.3.4, are often prepared and characterized *in-situ* and dry properties are not known. Therefore, these samples are not discussed here, but in the paragraph 1.4.3. The segregation of studies in the following subparagraphs is done on the basis of the type of penetrant used (aqueous – non-aqueous, liquid – vapor – gaseous), and the examples are selected to give as broad as possible picture of the various types of investigations.

1.4.1.1. Liquid water

Liquid water has a room temperature refractive index of n_{water} = 1.332, which is lower than for most typical polymer systems. The value is also significantly lower than the indices of the most commonly utilized organic solvents ($n_{n\text{-}hexane}$ = 1.386, $n_{toluene}$ = 1.496, $n_{chloroform}$ = 1.446, $n_{ethanol}$ = 1.361). That is why liquid water provides a reasonable optical contrast for not too highly swollen, relatively thick samples and an accurate swollen refractive index determination is possible. Water is also the most widely studied penetrant in the literature, mainly due to the obvious biological and environmental importance.

Swelling studies of a very wide range of polymeric materials in liquid water are available. The following examples represent some of the more interesting measurement approaches found in the literature. One of the first studies, dealing with dynamic *in-situ* spectroscopic ellipsometry determination of swelling, has been conducted on a biocompatible zwitterionic polymer based on PC [14, 15]. The focus has been put on the interplay between the hydrophilic and hydrophobic units of the polymer on the formation of complex morphologies determining the swelling character (like departures from classical Fickian diffusion). The authors have found a two-step swelling where Fickian and relaxational regimes both contributed equally to the total swelling of the material. Water-induced surface swelling of thin polyimide films has been studied in a combined contact angle – ellipsometry measurements reported by Hennig et al. [62]. This class of polymers is widely used in electronic devices where the impact of humidity may cause reliability problems. In this study ellipsometry has been used to correlate the swelling of the layers upon contact with a water droplet to the observed contact angle hysteresis. The impact of layer annealing at high temperature has been reported. Contact angle hysteresis, related to surface reconfiguration of iCVD synthesized hydrogels intended for use in drug release, has been reported by Chan et al. [125]. The authors have used ellipsometry to study the effects of the hydrogel cross-linking on the water uptake and found a significant decrease of water fraction with increasing cross-linking and decreasing incorporation of the hydrophilic monomer. Cross-linking effects on water uptake of electron beam irradiated hydrogels based on PNVP have been reported by Burkert et al. [118].

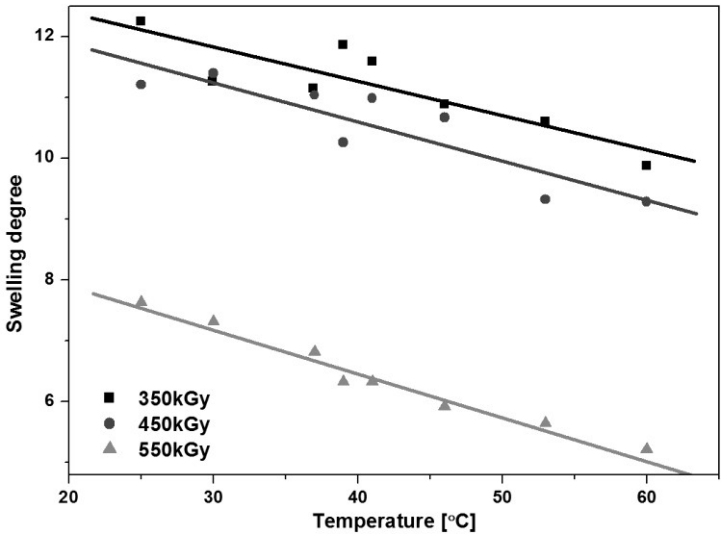

Figure 1.22 Swelling degree of hydrogels as a function of temperature for different irradiation doses. Ellipsometry precision decreases for the highest swelling degrees due to reduction of the optical contrast related to extremely high saturation of the films with experimental ambient. Adapted with permission from [118]. Copyright 2007 Elsevier

The hydrogels have been shown to present very high swelling degrees, defined as $h_{swollen}/h_{dry}$, Figure 1.22, which reduced with increasing temperature of swelling. As can be seen from the figure, due to the low optical contrast as a result of extremely large water fraction the precision of ellipsometry have suffered for the higher swelling degrees. Still, however, the trend with temperature can be identified. The authors have also reported on an irradiation threshold necessary to fix the material to the silicon substrate. Swelling of iCVD synthesized, cylindrical-shape in copolymer hydrogels with controllable mesh sized has been reported by Yagüe et al. [97]. There, the swelling of the network has been used to deduce the degree of cross-linking, which has been in turn correlated with the mesh size.

1.4.1.2. Water vapor

Water vapor *in-situ* ellipsometry measurements have mostly dealt with humid gases close to atmospheric pressures. Swelling and index changes of polymeric samples have been measured as a function of the Relative Humidity (RH). Similarly to the studies described in 1.4.1.1, here also the range of both investigated systems and experimental approaches is very wide.

One of the earliest RH swelling measurements, reported by Kleinfeld et al. [34], have been done on water penetration into composite films of PAH and sheet-silicate mineral, Laponite RD. The control over water vapor saturation has been

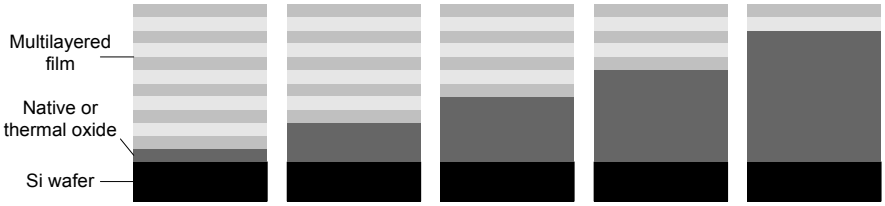

Figure 1.23 Preparation of multilayer composite films on top of variable thermal silicon oxide thickness layers, while keeping the total film thickness constant. Such a sample configuration gives different changes in color upon exposure to the same relative humidity and helps to rule out surface water condensation. Adapted with permission from [34]. Copyright 1995 American Chemical Society

performed by placing the ellipsometer stage in a plastic bag with small holes serving as windows for the polarized laser beam. By a very interesting sample preparation approach, based on the preparation of the composite films on top of variable thickness thermal silicon oxide while keeping the total thickness constant, Figure 1.23, the researchers have been able to rule out surface condensation as a dominant mechanism of the rapid water sorption in the films. Some possibility of fine-tuning the changes in sample color upon exposure to RH has been reported.

A study on water sorption in different biologically relevant polysaccharides, HA and dextran, where significant differences in the swelling behavior at high RH have been found, has been reported by Mathe et al. [38]. The differences have been correlated with internal pressures related to the rearrangement of the sorbed water molecules. The forces operating within the films have been calculated from the disjoining pressure (negative derivative of Gibbs energy with respect to film thickness) being a function of swelling. The hydration forces in ultra-thin (below 20 nm cellulose films) have been investigated by Rehfeldt et al. [36]. The authors have found no dependence of the swelling degree, or the corresponding disjoining pressure, on dry thickness of the films down to several nm. Water vapor swelling of B^+ bombardment modified thin layers of aromatic polyimides has been reported by Eichhorn et al. [86, 87]. The produced partially carbonized material has been shown to be characterized by a very small (2%) and completely reversible water vapor sorption, making it very interesting in sensor applications. An interesting study on the impact of humidity on the changes of refractive index and thickness in thin films of polyimide obtained from 3,3′,4,4′-benzophenone tetracarboxylic dianhydride and diamino-phenylidene (Matrimid) has been presented by Rowe et al. [88]. The researchers considered two limiting cases for the refractive index versus RH dependence: one where the glassy sample volume does not change with sorption (implying sorption into the microporosity, or excess fractional free volume of the polymer), and a second one where volume additivity is obeyed (Henry-type sorption).

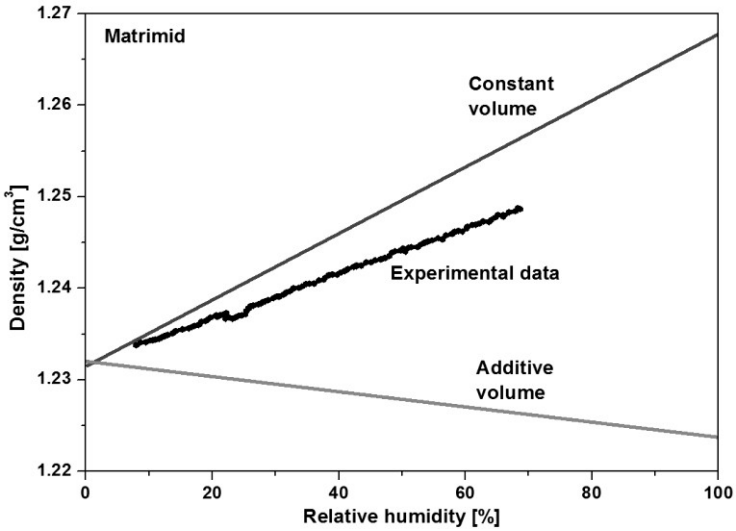

Figure 1.24 Density changes in thin Matrimid films as a function of RH. The limiting cases assume either exclusive sorption into microporosity of the glassy polymer (Constant volume) or perfect additivity of volumes of the polymer and sorbed water (Additive volume). Adapted with permission from [88]. Copyright 2007 American Chemical Society

As can be seen in Figure 1.24, the data falls in-between the limiting cases, but lies closer to the constant volume line which suggests the pronounced hole-filling sorption mechanism in this material. The implications from this study are important for the fundamental understanding of the operation of the glassy membranes. Water vapor sorption in flexible MOFs (MIL-89) has been reported by Horcajada et al. [126]. The researchers have shown the possibility of tunable and remarkably reversible sorption properties with relatively high swelling degrees of these network structures. Abuin et al. [127], have demonstrated substrate effects on the swelling of Nafion nanomembranes with dry thicknesses in a very broad range (17 – 1000 nm). It has been found that the water uptake for the thin films is much smaller than in the case of the bulk, and also that an effect of the supporting substrate is significant.

1.4.1.3. Organic solvents, liquids and vapors

In contrast to water as a penetrant, the studies involving sorption of non-aqueous liquids or vapors into dry polymer films are less common. Here, however, also a variety of topics can be found.

The need for the ability to detect VOCs has stimulated a significant effort in the development of selective sensors. Because these very often involve polymeric thin films able to swell in contact with VOCs, *in-situ* ellipsometry has proved to be a very useful technique in these types of investigations [90, 91, 94, 95, 124].

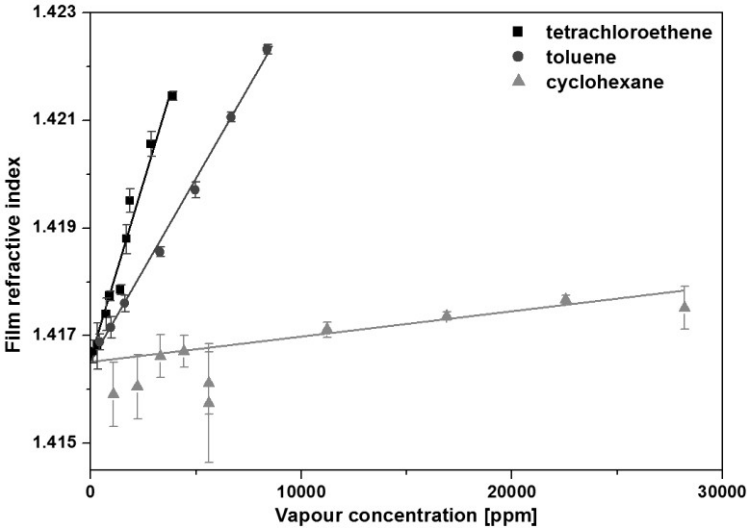

Figure 1.25 Change in PDMS refractive index when exposed to organic vapors; the largest response seen in the case of tetrachloroethane indicating good sensitivity towards this compound. Adapted with permission from [91]. Copyright 1997 Springer

Spaeth et al. [90, 91], have focused on the most widely used VOCs sensing polymer PDMS, as well as its derivatives. The authors have also characterized a polyurethane type material and the choice of organic vapors included toluene, tetrachloroethane and cyclohexane. Due to the measurement of relatively thick films (several hundred nm) the changes in thickness and index could be observed independently. The sensing materials have been shown to swell linearly in response to increasing vapor concentration. The highest sensitivity has been found in the case of the penetrant with the refractive index most different to the index of PDMS (n_{PDMS} = 1.400) – tetrachloroethane (n_{TCE} = 1.505) and has resulted from the largest relative changes in refractive index upon swelling, Figure 1.25. Conversely, a sensor – analyte pair (polyurethane - tetrachloroethane) with almost the same refractive indices has not shown much change of index upon sorption making the polymer a poor sensor for that particular organic compound.

The findings of those studies can be used to choose the sensing material that is very sensitive towards some analytes and not towards others. Linear swelling of nanostructured composites for sensing applications (Pd- and Au-CF_x) towards vapors of acetone, chloroform and 2-propanol has been reported by Cioffi et al. [124]. Swelling of calixarenes, potential candidates for organic vapor sensing with fast and reversible sorption, in several organic vapors has been reported by Nabok et al. [41, 42]. Other studies in the field of sensors include swelling of nano-confined block copolymer films [94, 95].

The theoretical, as well as experimental treatment of organic solvent diffusion into thin polymer films have been presented by Filippov [83] and Filippova [79]. In another fundamental study of Elbs et al. [80], the Flory-Huggins interaction parameters for various glassy polymers in common vapor solvents have been determined. The researchers have used an interesting approach of measuring the sorption in homopolymers, as well as in copolymers. This allowed them to study the compatibility between the different monomers in the presence of different solvents. Buchhold et al. [33], have reported on swelling of various high performance glassy polymers in vapors including water, ethanol, methanol and 2-propanol for the applications in microeletronic devices. In an interesting study of Crossland et al. [47], a systematic control over nucleation density in poly(3-hexylthiophene) thin films has been investigated. It has been achieved by first swelling the films in high activity of good solvent vapors to completely remove crystallites, and subsequently reducing the vapor partial pressure (and swelling) to induce re-crystallization within the films. Depending on the conditions the re-crystallization has yielded different crystalline structures. Fundamentals of temperature-induced n-hexane diffusion mechanism in thin and ultra-thin PS films have been investigated by Ogieglo et al. [23, 24].

In the only to date, high pressure liquid *in-situ* ellipsometry study [8], thin, cross-linked PDMS films supported on porous substrates have been investigated to study their response under non-equilibrium permeation of the liquid n-hexane. The results have been found to be in an excellent agreement with the theoretical description of the transport by solution-diffusion model. This study has demonstrated the applicability of ellipsometry to directly observe the behavior of thin selective layers of membranes during permeation.

1.4.1.4. High pressure gases

There are only a handful of *in-situ* ellipsometry studies involving high pressure gases. All of them focus exclusively on sorption of CO_2, mainly due to its high impact as an environmentally friendly solvent and importance in membrane separations. Sirard et al. [65], have been the first to develop a high pressure ellipsometry cell, described in 1.2.3.3, and show its potential for measuring the swelling of cross-linked PDMS films in CO_2 up to pressures of about 120 bar. The results for these rubbery thin films have been shown to correspond very well with swelling of bulk films done before with a different technique (sorption balance) [89], serving as a validation for the high pressure ellipsometry. A considerable attention has been devoted to the investigations of the unexpected swelling maxima (anomalies) reported first for PMMA [54], in vicinity of the critical point of CO_2, Figure 1.26.

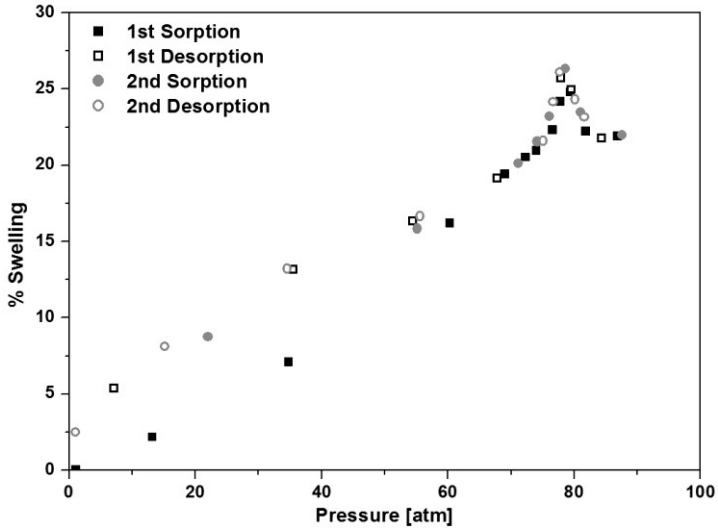

Figure 1.26 Anomalous swelling maxima around 75 bar reported during high pressure CO_2 sorption in thin PMMA films. Onset of sorption – desorption hysteresis visible around 60 bar. Adapted with permission from [54]. Copyright 2002 American Chemical Society

These maxima had never been previously seen in bulk swelling and have been shown to be more pronounced during sorption at 35 °C, as compared with 50 °C, which resembled the compressibility behavior of high pressure CO_2. The maxima have been insensitive towards replacing the silicon wafer substrate with GaAs wafer. The swelling at the maxima has been found to increase proportionally with the dry film thickness in the range from 85 to 325 nm, suggesting that their occurrence could not be solely explained by surface effects and had to be related to the swelling in the whole volume of the films. The anomalies have been further studied by Li et al. [75], for several other polymers including PS, poly(ethylene oxide) (PEO), PDHFOMA and a diblock copolymer PS-*b*-PDHFOMA. All of the polymers have shown the anomalous maxima, and their occurrence has again been found to be related to swelling within the whole volume of the films, rather than to the surface excess CO_2 at interfaces.

Wind et al. [70, 71], have studied the relaxation dynamics in thin and thick polyimide films intended as membrane selective layers. The authors have focused on the effects of annealing on the CO_2 sorption and relaxation in these materials. Interestingly, the thin films have been shown to relax much faster than thick films. The departures of the behavior of thin films from the bulk, and the impact on the gas sorption properties have been further systematically studied with *in-situ* ellipsometry by Horn et al. [74]. The authors have been able to conclusively establish the large deviations in behavior of thin films from bulk behavior with respect to permeability of the thin layer membranes, reported in [129]. The long

term dynamic ellipsometry measurements have revealed refractive index minima in glassy films exposed to penetrant over large timescales (~100 hours) suggesting a competition between plasticization and physical aging. For the longer timescales the aging has been shown to be dominant.

The *in-situ* high pressure ellipsometry has also been used to study the effects of confinement on the glass transition occurring in a polymer – penetrant system. Systems below glass transition temperature are known not to be in their thermodynamic equilibrium, which has consequences for instance in their gas sorption behavior. Common features of such a process include a slightly concave swelling versus pressure isotherm, as well as the existence of sorption – desorption hysteresis. On the other hand due to the interaction with highly plasticizing gases, like CO_2, glass transition temperature in a polymer can be brought down significantly may be transversed during a sorption experiment. Above glass transition the polymer – penetrant the system resides in a rubbery state with a linear (or slightly convex) sorption curvature and no sorption – desorption hysteresis. The first application of *in-situ* high pressure ellipsometry to observation of the penetrant induced glass transition (P_g) has been done by Sirard et al. [54], in their study on anomalous maxima in CO_2 sorption in PMMA. Due to sufficiently high accuracy of ellipsometry, it has been possible to detect a pressure point at which the onset of sorption – desorption hysteresis occurred, Figure 1.26, hence quantifying the P_g. More detailed studies of this phenomenon in highly plasticized PS and PMMA have been done by Pham et al. [69, 81]. In these studies the authors utilized the change of swelling curvature (linear to concave) upon going from rubbery to glassy state. They have been able to determine the dependence of dry film thickness on the P_g even in very thin films, Figure 1.17, by looking at changes of the Ψ parameter at several wavelengths. This approach has been chosen because the change in curvature associated with P_g could be seen in the raw data and the modeling has not been necessary. The thinner films have been shown to be plasticized at significantly lower pressures than the thicker ones. Additionally, the signature of a retrograde vitrification in PS/CO_2 system has been found – a phenomenon not present in the bulk of the polymer [81]. High pressure *in-situ* ellipsometry of highly plasticized glassy polymers has also been used by Carla et al. [73, 130, 131], in their development of a non-equilibrium sorption model. The technique has been used firstly to verify the sorption data (by application of Clausius – Mossotti equation, discussed in more detail in paragraph 1.5.2 of this review) versus the sorption calculated from the developed model, and secondly, to locate the P_g point by the intersection of linear fits from rubbery and glassy regions, in much the same manner as done in the studies of Pham et al.

The other high pressure ellipsometry studies include those of Simons et al. [48], reporting CO_2 swelling and concentration data for several glassy polyetherimides and rubbery PEBAX, and the investigations on order-disorder transition in block copolymers by Chandler et al. [76].

1.4.2. Drying processes

A few studies focused on a much different type of investigations, than the ones described in 1.4.1, namely on the details of solvent removal from the film. In most cases these studies do not require any experimental cell and can be done in a configuration presented in Figure 1.10a. The film properties are observed usually in a dynamic mode as a function of time during the process of drying immediately after film preparation.

The first, both theoretical and experimental, treatment of the drying in thin polymer films has been done by Filippov [83] and Filippova [79]. The authors have derived expressions for the diffusion of the solvent in the films and the apparent activation energy over a wide range of temperatures and solvent concentrations base on the thickness changes during the process. In these cases the diffusion has been observed at relatively high temperatures (55, 75 and 96 °C) and a very clear exponential trend in thickness loss has been found. When, however, the diffusion process occurs at temperatures further below the T_g of the pure polymer the details are more complex and have significant implications for technological applications. In this case the effects related to the transverse of the glass transition during drying significantly influence the kinetics by the appearance of the non-equilibrium glassy

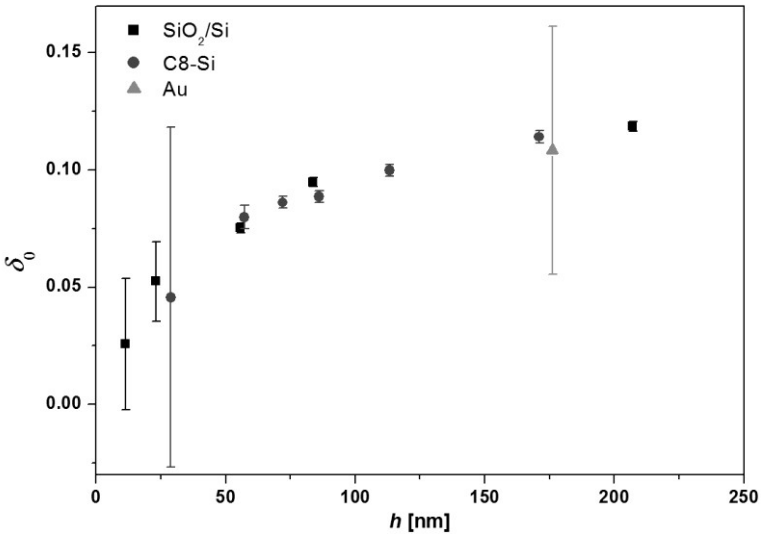

Figure 1.27 Dry thickness dependence, h, of the structural relaxation parameter, δ_0, defined as $(h_t - h_\infty)/h_\infty$, in drying of ultra thin PMMA films. h_t and h_∞ represent film thicknesses at the beginning and end of drying. The data has been measured for several different substrates. The smaller values with decreasing thickness indicate significantly faster drying in the thinner films. Adapted with permission from [53]. Copyright 2004 American Physical Society

structure. In the studies of Richardson et al. [53, 60], for ultra thin films of as spin-cast PMMA the vitrification of the polymer has been associated with the emergence of the glass compression energy barrier that opposed the thickness decrease during the solvent loss. The manifestation of these effects results in a very slow relaxation of ~150 nm films (about 10 hours) during drying, much slower than required if the process is governed solely by the diffusion of the solvent. In

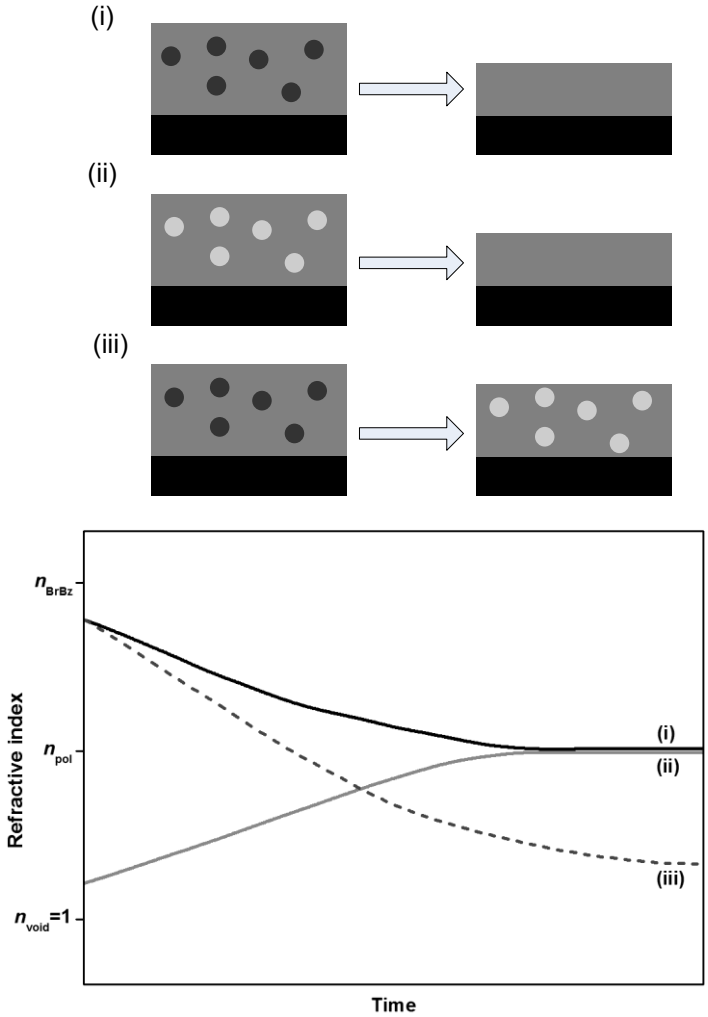

Figure 1.28 a) three different scenarios of structural relaxation and removal of solvent molecules from drying PMMA films, b) the corresponding dynamic refractive index changes. Adapted with permission from [61]. Copyright 2011 Wiley

addition, the authors have investigated the thickness dependence of this structural relaxation, and have found, firstly that the thickness of the films during drying has not returned to its equilibrium thickness (determined when solvent is not present by cooling from the melt) over the whole experiment duration, and secondly, that thinner films relax much faster regardless of the used substrate, Figure 1.27. The results have been discussed in terms of nano-confinement effects in the films manifested as an enhanced mobility within the polymer film closer to its top interface.

Drying of much thicker films of the same polymer, PMMA at ~300 nm, has been investigated by López Garcia et al. [61]. In this case the researchers have chosen a high refractive index solvent, bromobenzene, to maximize the optical contrast between the polymer and the solvent and to slow down its evaporation (due to high boiling point). This has been done to be able to test several scenarios possible to occur during the solvent evaporation, Figure 1.28.

In scenario (i) the structural relaxation occurs together with the removal of solvent, in (ii) the solvent is lost long before the structural relaxation and in (iii) the solvent removal proceeds without any polymer relaxation. The calculated refractive index dynamics are shown in Figure 1.28b. The conclusion has been that some voids are indeed forming during the solvent loss in the thin films. The loss of solvent in PMMA has also been investigated by Atarashi et al. [84], where the surprisingly significant impact of the produced morphology of as cast films on the subsequent water uptake has been shown. The effects have been explained in terms of the formation of unrelaxed pathways for water diffusion within the films. Annealing of the films after preparation would have closed the pathways resulting in the swelling behavior expected solely from thermodynamics of polymer – solvent affinity.

1.4.3. Thermally, pH, and ionic strength induced transitions

In-situ ellipsometry, especially in aqueous solutions, has been widely applied in studies of responsive polymers. Often, the layer preparation (layer by layer or synthesis reaction) is itself carried out *in-situ* and can be followed with ellipsometry (as done, for example in [101]). In this section, the representative examples for temperature, pH and ionic strength responsive polymeric materials investigated with ellipsometry are presented. As discussed before, polymer brushes and other covalently attached to substrate polymers are in general avoided due to their specific physics and properties as well as limitation of scope of this review.

In a study of Harris et al. [44], *in-situ* ellipsometry has been used to explain the changes in permeability of multilayer polyelectrolyte films as a function of pH. The authors have found that at acidic and neutral pH the swelling has been significant (~40%), but stable in time. On the other hand at alkaline pH the films have swelled to a similar magnitude but continued to increase in thickness eventually delaminating. Correspondingly, at the same pH conditions the layers

have shown dramatic increases in permeability indicating a much more solvent saturated structure able to pass molecules faster. A pH responsive derivative of PDMS (Posimca50) has been shown to be well suited for the detection of ammonia in air [92], presenting a good alternative for the conventionally used dye-based ammonia detectors. In this case the changes in the optical thickness ($n \cdot h$) in response to water vapor containing ammonia have been the basis for the sensing mechanism, Figure 1.29. The swelling changes have been primarily due to the interaction of the ammonia with the carboxyl group attached to the polymer matrix.

A general design strategy for the preparation of variable pH-responsiveness polyelectrolyte multilayer films has been presented by Hiller at al. [100]. The material is based on PAH/SPS and has been shown to possess history dependent swelling behavior. At low pH swelling of about 500% has occurred, whereas when the pH has been raised above neutral a very sharp volume transition to a collapsed state (with swelling of 100%) has been reported. Hysteresis between pH increase and decrease run in the response of the film has been observed. A similar hysteresis, explained in terms of the kinetics of changes in the charges density within the films, has been found in polypeptide multilayers built by layer by layer deposition [101]. The films have been shown to be also stable and responsive to changes in temperature (swelling of 8% at 28 °C and 4% at 37 °C) due to conformational rearrangements. Small effects of ionic strength (concentrations of 1-6 mM NaCl) together with pH responsiveness of swelling and swelling kinetics in multilayers of weak polyelectrolytes have been found by Tanchak et al. [102].

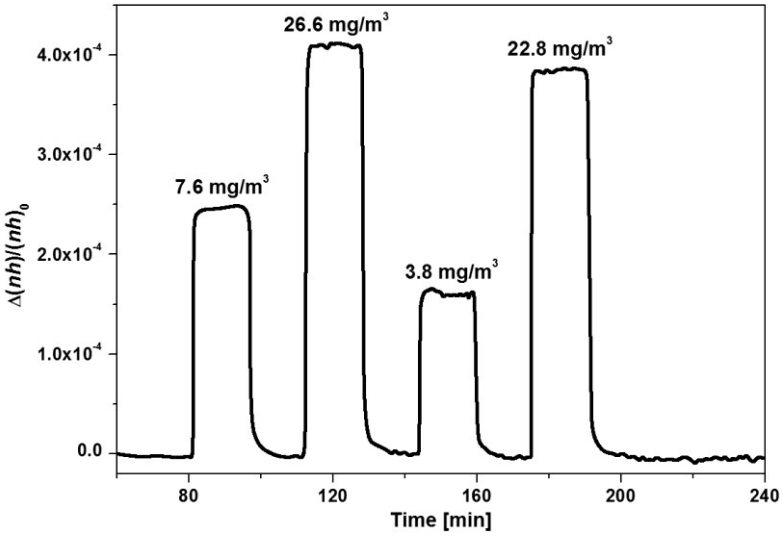

Figure 1.29 Changes in optical thickness of a pH responsive polymer as a result of variable concentration of ammonia in water vapor at RH = 50%. Adapted with permission from [92]. Copyright 2000 Springer

Burke et al. [104], have investigated the effects of assembly pH on the pH and ionic strength responsiveness in multilayers of HA and PAH. The swelling ratio has been found to increase with decreasing assembly pH and the swelling curves have revealed a minimum of swelling at around neutral pH, Figure 1.30. The latter has been explained in terms of the acid – base chemistry of the layers: around neutral pH the majority of the free functional groups within the films are charged. Because of the polyampholytic nature of the films (presence of both acidic and basic groups), this leads to a partial collapse of the structure. On the other hand, for pH significantly different than neutral, chain extension due to like-charges repulsion dominates, causing increase in swelling. The authors have reported also on the swelling changes as a function of NaCl concentration. At higher salt concentrations the swelling has increased, which has been explained by the high salt concentration causing an irreversible weakening of the ionic bonds within the structure. Assembly pH responsiveness of polyelectrolyte multilayers has also been studied by Itano et al. [105] and Nerapusri et al. [117].

Temperature-sensitive hydrogels synthesized by electron beam irradiation of poly(vinyl methyl ether) (PVME) have been described by Hegewald et al. [50] in a combined ellipsometry, surface plasmon resonance (SPR) and optical waveguide spectroscopy study (OWS). Fully reversible swelling – deswelling process has been found with a phase transition temperature around 33 °C. In another study on hydrogels [93], thermo responsive coatings of p(NIPAM-*co*-AA) on silicon wafers have been described. These coatings consisted of, instead a uniform film, a densely

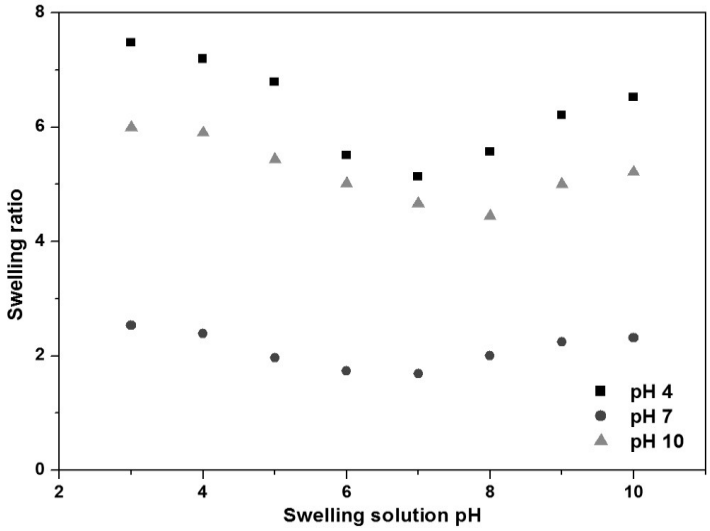

Figure 1.30 Swelling ratio as a function of pH for HA/PAH multilayers assembled at different pH: 4 (■), 7(●), 10 (▲). Adapted with permission from [104]. Copyright 2005 American Chemical Society

packed monolayer of spheres of 600 nm swollen diameter, which constituted a 10 times increase in dimensions from dry state. Despite the confinement effects the layers have been shown to still respond to temperature changes and ellipsometry has been able to resolve these changes due to close packing in the structure, which has allowed assuming a Uniform film model. Close-packed monolayers of hydrogels have also been investigated towards temperature, pH and ionic strength responsiveness by Nerapusri et al. [117].

A slightly different type of a responsive film investigation has been presented by Freudenberg et al. [85]. The authors have investigated the charging and swelling in thin cellulose films in water by combined streaming potential and ellipsometry measurements. It has been found that differences existed in the dissociation behavior of the carboxylic acid groups at the surface of the film and those within the films. The topmost groups have been able to dissociate completely, whereas for the rest only partial dissociation has occurred.

1.4.4. Reactions at interfaces, depositions and formations

In this section some of the examples of *in-situ* ellipsometry studies of reactions at interfaces, depositions and film formations are described. Because such studies are quite common [132-134], especially in biological and protein research, here the focus is only on some examples where significant attention is dedicated to studying the properties of the swollen polymer layers with ellipsometry.

The study of adsorption of lysozyme and bovine serum albumin (BSA) on a surface of highly swollen hydrogel polymer based on PC has been presented by Murphy et al. [115]. This zwitterionic hydrogel, prepared by dip-coating, has been found to significantly reduce adsorption of the proteins, which is important in many medical applications and in surfaces fouling. Combining the neutron reflectivity with ellipsometry the information on the spacial distribution of water within the swollen layers has been obtained. It has been shown that the non-uniformly distributed density (gradient) within the films, with highly diffuse outer interface, is an important factor contributing to the control over protein adsorption. The protein adsorption, in this case on swollen hyperbranched polyesters, has been investigated by Reichelt et al. [25], where the focus has been on the systematic study on the effects of the degree of branching, backbone structure, flexibility and polarity of the materials. Various optical models, taking account for the adsorbed protein layer, the underlayer of the polyesters and ambient solutions have been evaluated. In this case, upon careful evaluation of applicability of the chosen optical models, ellipsometry has been shown to be capable of the simultaneous study of swelling and adsorption. In addition, the IR-ellipsometry has provided chemical evidence for the formation of a thin protein layer on top of the polyester layers. An interesting use of *in-situ* spectroscopic ellipsometry to track a reaction between ferrous ion and 2,2'-bipiridine (bpy) in swollen Nafion films has been made by Pantelić et al. [51]. Here the basis has been the strong changes in optical

absorption spectra upon formation of the complex ion, $Fe(bpy)_3^{2+}$. The optical absorption of the swollen films has been modeled with Urbach and Tauc – Lorentz oscillator functions.

1.4.5. Dissolution or degradation

In fact, studies on polymer dissolution with *in-situ* ellipsometry have been one of the first applications of this technique to investigate highly swollen polymer systems. Already in 1987 Manjkow et al. [17, 18], have investigated kinetics of PMMA dissolution in various organic solvents with a "psi-meter". The authors have investigated the influence of various parameters such as temperature, molecular weight or aging time on the dissolution rate. They have also been able to identify conditions when the process of anomalous Case II diffusion governed the initial stages of dissolution, with the rate of swelling being proportional to time as a result of the progress of a sharp front separating the swollen and the dry layer within the film. Subsequently, the polymer dissolution of the swollen layer occurred, which has been limited kinetically by the presence of the longer polymer chains. It has been shown that both thermodynamics and kinetics of the processes in the system could be mapped out accurately with utilization of the technique. Later, Papanu et. al. [19, 20, 22], have further developed the technique and focused, in particular, on the solvent mixtures, effects of molecular weight and temperature on the dissolution kinetics by Case II penetration. The authors have been able to show that the evidence for Case II description is very clear upon analysis of the Ψ and Δ curves. The spectra have been otherwise impossible to be accurately modeled by a uniform film description (assuming no sharp front within the film).

Dissolution of composite films of PDADMAC and silica particles used in sensor applications has been studied by Zudans et al. [52]. The authors have been able to identify the different stages of the film dissolution. The initial one when the film index approaches that of the surrounding solution while the thickness does not change much, the second one where the disintegration of the matrix occurs together with the large expansion of the polymer network, and the third one where slow dissolution of the swollen film occurs. Interestingly, during the initial exposure to the experimental ambient (0.1 M KNO_3) the thickness decrease has observed, inset in Figure 1.31, after which the network expansion (thickness increase starting after about 36 hours) and subsequent dissolution has occurred.

Although, no certain cause for this initial thickness decrease has been given, it has been speculated that introduction of water into the structure leads to the formation of hydrogen bonding resulting in compaction of the structure. As the driving force for the later dissolution of the films, the very high hydrophilicity of the films has been given.

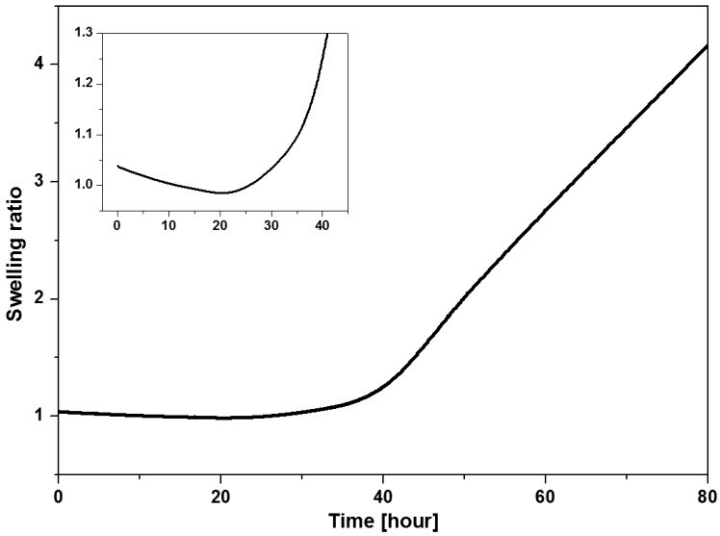

Figure 1.31 Swelling ratio of composite sol-gel films upon immersion in 0.1 M KNO_3. Initial, very slight thickness decrease is observed, after which significant swelling and film dissolution occurs. Adapted with permission from [52]. Copyright 2004 American Chemical Society

In other studies the dissolution of photoresist [135] and plasma-polymerized polyethylene glycol-like films for drug delivery applications [119] has been investigated in a similar manner. Enzymatic degradation of immobilized protein multilayer films has been investigated by Foose et al. [136] also using a dynamic *in-situ* ellipsometry approach.

1.4.6. Electrochemically induced swelling changes

There exist several investigations that focus on the study of electrochemically induced changes in swelling of the polymer and composite layers. In one of them a detailed electrochemical investigation on the PANI anodic pre-peak has been conducted in conjunction with *in-situ* ellipsometry measurements of the film swelling [40]. This anodic pre-peak had been previously found to occur in this important conducting polymer during cyclic voltametry experiments but the reason for its appearance has remained not investigated. The authors have been able to relate the appearance of this pre-peak to the changes in swelling of the polymer during electric potential scans. The either positive or negative shifts in the peak have been related to higher or lower water content within the polymer matrix (swelling differences), which could in turn be tuned by film annealing. Oxidation-reduction has been shown to change the optical properties in self-assembled osmium complex-derivatized poly(allylamine) and glucose multilayers have been investigated by Forzani et al. [45]. The swelling of the films has been shown to be correlated to redox transitions resulting in an exchange of anions and the solvent

with the investigated film. Electrochemical swelling has also been investigated by Schmidt et al. [64], for nanocomposite films containing PEI and Prussian Blue nanoparticles. The incorporation of the particles has allowed electrochemical control over the swelling and mechanical properties of the films. Upon reduction the films have shown reversible swelling decrease and softening. These properties may have useful applications in responsive coatings and nanoscale devices. Oriented bilayer films of gramicidin and DMPC have been shown to respond to electrical potential by the change in water content (swelling) and the resulting changes in circular dichroism of gramicidin molecules within the film [109].

1.5. Types of information extracted with the use of *in-situ* ellipsometry

In about 40% of *in-situ* ellipsometry studies on swollen polymers the technique is mainly used to determine the equilibrium swelling and refractive index of the layers in contact with ambients. Many studies, however, focus in addition on the kinetics of swelling, which may be relatively simple, for instance, sufficiently described by the Fick's law, or more complex. These studies are reviewed in paragraph 1.5.1. Ellipsometry data on swelling and index can also be used to calculate, for example, the penetrant volume fractions, paragraph 1.5.2, which can be subsequently used to determine thermodynamic parameters governing the polymer – penetrant swelling, like the Flory – Huggins interaction parameters, χ, paragraph 1.5.3.

1.5.1. Dynamic studies

In many *in-situ* ellipsometry studies usually no time dependent ellipsometry data is presented. The reasons are mainly the much faster equilibration of the investigated system in relation to data acquisition rate (especially in older studies), or no explicit interest in process kinetics. However, when different techniques are used in parallel (QCM-D, neutron reflectivity etc.) dynamic complementary information obtained with these techniques may be included. The significant progress in instrumentation for dynamic ellipsometry data acquisition in modern devices has allowed high temporal resolutions on the order of several seconds per full spectral scan. This has opened new possibilities to track even relatively fast processes with great accuracy. In this paragraph the focus is on these types of investigations.

1.5.1.1. Simple dynamic phenomena

In a few representative examples, presented in this paragraph, dynamic ellipsometry has been used to study relatively simple diffusion phenomena. The technique has been used to confirm a more or less Fickian type of diffusion with little impact of secondary relaxation phenomena, discussed in more detail in 1.5.1.2. Fickian type of dynamics can be found for glassy samples swollen to a relatively small degree where swelling is fully reversible, or samples swollen sufficiently to become equilibrium rubbers (assuming dissolution doesn't occur).

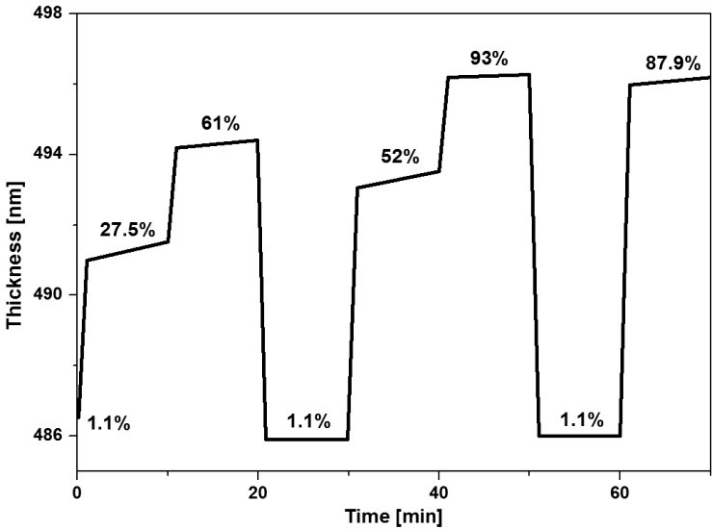

Figure 1.32 Reversible dynamic response to changes in relative humidity in the ambient of ion bombardment modified thin polyimide film. Adapted with permission from [86]. Copyright 2004 Elsevier

An example for the first case is the dynamic spectroscopic ellipsometry study of ion bombardment modified polyimides presented by Eichhorn et al. [86]. In this study the spectra of about 500 nm glassy polyimide films have been recorded in time, while the relative humidity in the ambient air has been varied. The authors have been able to detect the small, fully reversible swelling changes in the material response, Figure 1.32, making it interesting for sensor applications.

The fast swelling of the film in response to immersion in electrolyte solutions has been reported for hyperbranched polyester films by Mikhaylova et al. [37]. In this case the swelling has proceeded very fast towards equilibrium with similar kinetics for all investigated films. The equilibrium swelling degree has been found to be a function of annealing temperature. For longer annealing times, the swelling has decreased which has been explained the formation of a more compact, denser polymer structure due to formation of hydrogen bonding between the –OH groups. Fickian type of diffusion has also been investigated in the investigation of Gensel et al. [94] and Zettl et al. [95], for the swelling of confined block copolymer films.

1.5.1.2. Complex dynamic phenomena

Diffusion phenomena, in particular for glassy matrices but not exclusively, may become much more complex, and the assumption of purely Fickian dynamics does not hold. This is because the diffusion itself may be accompanied by significant sorption induced relaxations leading to reorganizations of the structure of the polymer [137, 138]. Usually, the fast Fickian diffusion occurs first and then the relaxations with much larger characteristic timescales set in. Such processes can be

fitted with semi-empirical relationships established by Berens and Hopfenberg [139], however, the physical meaning of the extracted parameters (like diffusion coefficient and relaxation times) needs to be treated with care. Due to the advantages of *in-situ* spectroscopic ellipsometry, especially related to the possibility of dynamic, independent analysis of many sample properties, such complex phenomena may be studied in great detail. Apart from thickness variation also the dynamic changes in refractive index, refractive index distribution (non-uniformity, anisotropy and gradients), and optical absorption can be analyzed. The dynamic refractive index behavior may often bring even more insights than the thickness variations. In this section some of the more interesting examples are discussed.

One of the first *in-situ* spectroscopic ellipsometry studies where, not only Fickian diffusion but also the relaxation controlled diffusion is identified, has been done by Tang et al. [14, 15]. The researchers have investigated zwitterionic polymer films based on phosphorylcholine (PC), a material important in biomedical applications, Figure 1.33.

Although the temporal resolution of the used device has not been very high (about 40 s per scan), the process of diffusion has been slow enough to be resolvable. The authors have found that the Fickian and relaxational swelling contributed approximately equally to the final equilibrium solvent uptake. Annealing of the films has been found to significantly slow down the relaxational dynamics but has

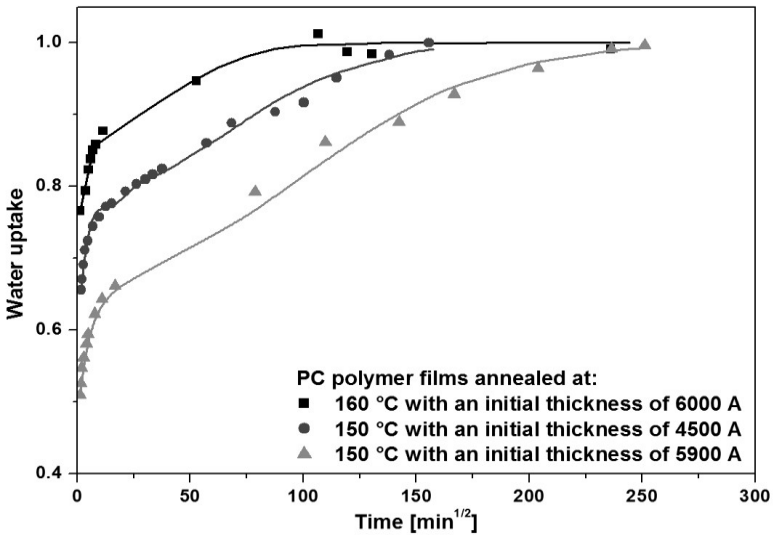

Figure 1.33 Complex swelling of zwitterionic films in aqueous solutions. The initial fast swelling (Fickian) and the subsequent slower relaxation contribute approximately equally to the total swelling of the films. Adapted with permission from [15]. Copyright 2002 American Chemical Society

had little impact on the initial Fickian process. The annealing temperature has been shown to affect the equilibrium penetrant uptake. The authors have used the Berens – Hopfenberg model to characterize the different kinetic parameters governing the diffusion and relaxation, but have indicated the imperfections of the model. For comparative purposes between samples of similar nature the model has, however, been able to yield some interesting relationships, and the extracted diffusion coefficients have been similar to those determined with other methods.

The pronounced relaxational behavior of glassy films exposed to plasticized gaseous penetrants has been investigated by *in-situ* ellipsometry in a few cases [70, 71, 74]. In these cases the extremely high sensitivity of ellipsometry to small changes of both thickness and refractive index in the plasticized films over large timescales has been utilized. In the studies of Wind et al. [70, 71], the dynamics of sorption and diffusion of CO_2 in plasticized polyimide membrane materials have been shown to correlate with permeation measurements, in particular with respect to annealing impact on the properties of the membranes. Importantly, the thin films of the polyimides have been shown to plasticize faster and at lower pressures than bulk films. This has important consequences for membrane technology, where thin selective layers dominate due to larger attainable fluxes of the separated species. Sorptive relaxations and simultaneous physical aging in ultra thin films have been investigated by Horn et al. [74], Figure 1.34. In this study the authors have

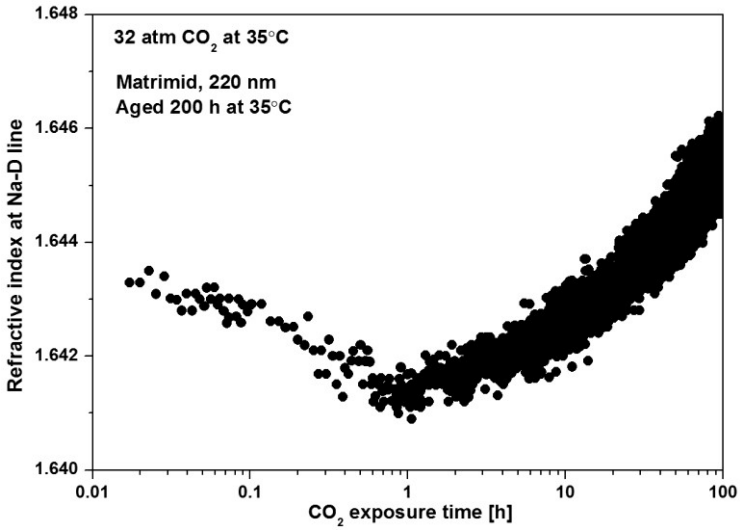

Figure 1.34 Long term changes in the refractive index of Matrimid 220 nm film upon exposure to 32 bar of CO_2. Initially the index drops, being a sign of increasing penetrant uptake. In the later stages the structure densifies signifying an increasing impact of physical aging. Adapted with permission from [74]. Copyright 2012 American Chemical Society

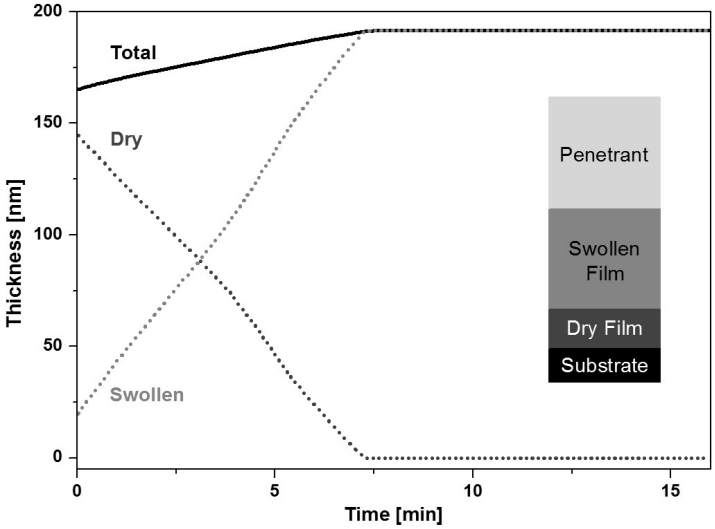

Figure 1.35 Case II diffusion resolved in 150 nm PS film during swelling with liquid n-hexane. A sharp front existing between the swollen and the dry layers of the film allows application of a two-layer model enabling kinetics of the process to be accurately resolved. Adapted with permission from [23]. Copyright 2013 Elsevier

systematically investigated sorptive relaxations in various membrane related polymers, including Matrimid, poly(*p*-phenylene oxide) (PPO), polysulfone (PSF) and PS. The thin film data have been compared with bulk measurements and the significant differences in the behavior of the two groups have been highlighted. Thin films have been shown to sorb significantly less penetrant than the bulk. Interestingly, the thin films have showed greatly accelerated physical aging effects which have dominated the sorption processes at longer timescales.

Sorption induced relaxations can become so important that they may control dynamics of diffusion. If the diffusion process is severely relaxations limited the observation of anomalous diffusion, like Case II type is possible. This has been investigated with *in-situ* ellipsometry in several studies focused on dissolution of PMMA [17-20] and diffusion of n-hexane into PS [23, 24]. The characteristic feature of Case II diffusion is the formation of a sharp front separating the swollen and practically dry regions within the swelling films. Such a phenomenon occurs when the diffusion through the swollen layer is much faster than the relaxations of the polymer chains at the diffusing front. In effect a uniform film is transformed into a two-layer film (swollen and dry regions) with the ratio of thicknesses of these regions changing dynamically as diffusion proceeds, Figure 1.35.

The diffusion proceeds linearly due to constant rate of relaxation at the front that limits the process. Because of the multilayer nature of the diffusion the progress of the penetrant wave can be accurately resolved in time with an appropriate optical

model, Figure 1.8c. The usefulness of such an approach has been demonstrated for the study of surface diffusion in the same system [24]. By the investigation of the speed of the penetrant wave progression into films of variable dry thicknesses the authors have been able to quantify an instantly swollen region existing on the polymer outer surface. This region has been shown to possess a thickness of about 14 nm, which is technologically significant in applications where films with thicknesses below 100 nm are utilized.

Significant deviations from Fickian diffusion have also been found in layer by layer deposited polyelectrolyte films [102]. The authors have shown that the dynamics of water swelling of these films could be tuned by different assembly conditions. The variety of the obtained diffusion mechanisms ranged from Case II (with swelling linearly proportional with time) to Super Case II (with sigmoidal swelling with time).

Upon application of more complex optical models in dynamic studies it is possible to gain insights into the dynamic structural changes occurring in swelling layers. This has been demonstrated in electrolyte solution swelling of zwitterionic films based on sulfobetaine and n-butylacrylate [16]. In this study a strong evidence for the developing optical anisotropy within the swollen films has been found by the detailed investigation of applicability of different optical models in the system. In

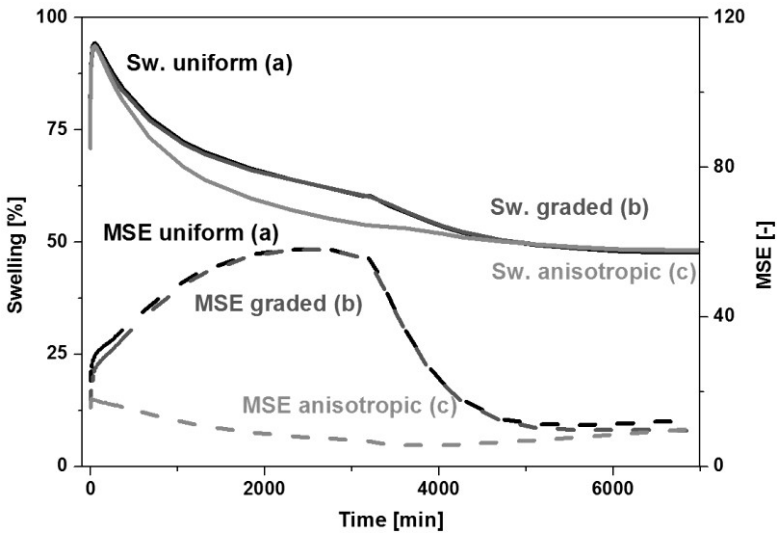

Figure 1.36 Comparison of swelling of zwitterionic films exposed to 1 M NaCl modeled with various optical models. The large reduction of MSE, seen in the case of application of a uniaxial anisotropic model, strongly suggests the existence of anisotropic structure during swelling of the material. Adapted with permission from [16]. Copyright 2013 Elsevier

particular, the very large reductions of MSE going from a uniform and an anisotropic model (from MSE ~ 50 to MSE ~ 8) suggest the applicability of the latter, Figure 1.36.

The optical anisotropy in the structure has been shown to be plausible when the morphology of the polymeric material is considered, in particular the possibility of formation of ionic crosslinks from the highly polarizable zwitterionic groups positioned non-uniformly within the volume of the swollen films. Dynamic data have suggested the overshoot dynamics of the swelling with optical anisotropy emerging and slowly disappearing as the process continued. The authors have also been able to model the structure of the swollen polymer with a model combining a density gradient with anisotropy, and to show that the largest degree of polymer structure deformation occurred close to the substrate where the immobilization of chains has been the strongest. Going towards the outer surface of the film the sample anisotropy has been shown to diminish, eventually producing an almost isotropically swollen outer interface.

1.5.2. Penetrant volume fraction calculations

Very often in *in-situ* ellipsometry investigations, in addition to the determination of swelling (thickness increase) and a change in refractive index upon sorption, the interest is in the determination of the penetrant concentration in the matrix. The simplest approach is based on the assumption of unidirectional swelling of the film (possibility of dilation only in the direction perpendicular to the substrate as a result of film confinement) and polymer – penetrant volume additivity.

As a result, the penetrant volume fraction, $\phi_S^{dil.}$, can be calculated simply from film dilation:

$$\phi_S^{dil.} = \frac{h_{SP} - h_{DP}}{h_{SP}} \qquad (1.3)$$

In this equation h_{SP} and h_{DP} represent the thicknesses of polymer films swollen with penetrant and dry, respectively. Such an approach has been used for the determination of water volume fraction in hydrophilic polyacrylates [39], in zwitterionic polymer films [14, 15], and in polyelectrolyte multilayers [112], as well as organic solvent fractions in block copolymers [95] and poly(3-hexylthiophene) [47].

A more reliable approach, especially if volume additivity may not be easily assumed (i.e. sorption in glassy polymers with non-equilibrium excess fractional free volume [88]), is based on the calculation of penetrant volume fraction from the change of the refractive index of the mixture. For swollen polymer systems two approaches are most frequently utilized: Clausius – Mossotti relationship and Bruggeman Effective Medium Approximation (EMA). The Clausius – Mossotti

takes advantage of the dependence of the refractive index of a pure substance on its mass density [140]:

$$\frac{n^2-1}{n^2+2} = \frac{R}{M_w} \cdot \rho \qquad (1.4)$$

Where R is the molar refractivity and M_w is the molecular weight of the substance. The ratio of R/M_w is often assumed constant and denoted q. In a mixture of a polymer and a solvent the additivity of refractivity contributions can be assumed:

$$\frac{n_{mix}^2-1}{n_{mix}^2+2} = q_{solv.} \cdot C_{solv.} + q_{polym.} \cdot C_{polym.} \qquad (1.5)$$

And the concentration of the polymer can be calculated from the dilation:

$$C_{polym.} = \rho_{polym.} \cdot \frac{h_{DP}}{h_{SP}} \qquad (1.6)$$

When the mixture refractive index, n_{mix}, polymer density, swelling and $q_{solv.}$ for the pure solvent (from eq. 1.6) are known, the mass concentration of the solvent, $C_{solv.}$, can be determined from eq. 1.5.

The Clausius – Mossotti approach has been used for the determination of high pressure gaseous penetrant volume fraction dissolved in glassy and rubbery polymers [48, 65, 70, 71, 73, 74, 88, 141], however, in this case the procedure is somewhat flawed by the need of an assumption about the density of a penetrant dissolved in the polymer. For CO_2 Sirard et al. [65] took the supercritical densities of 0.95 g/cm^3 and corresponding refractive index of 1.22 at room temperature to determine mass concentrations of CO_2 in PDMS. However, whether the state of the dissolved penetrant at relatively low pressures can be assumed identical to that from its critical state is arguable, and the results of such calculations need to be treated as only estimate, as also admitted by the authors.

Bruggeman EMA mixes the optical dispersions of the mixture components (designated as *1* and *2*) in a self-consistent manner, treating the optical dispersion of the mixture as a host material:

$$\phi_1 \cdot \frac{n_1^2-n_{mix}^2}{n_1^2+2n_{mix}^2} + \phi_2 \cdot \frac{n_2^2-n_{mix}^2}{n_2^2+2n_{mix}^2} = 0 \qquad (1.7)$$

This approach is most appropriate when the volume fractions of the components are comparable, which is often the case for significantly swollen polymers. Similarly to the Clausius – Mossotti equations, the penetrant dispersion is assumed to be known and not to change upon sorption in the polymer matrix. The Bruggeman EMA is the most frequently used in literature. The examples include organic solvent fraction determination in PDMS and its derivatives [8, 91], water sorption in polyimides [62], polyacrylates [39], hydrated polysaccharides [38],

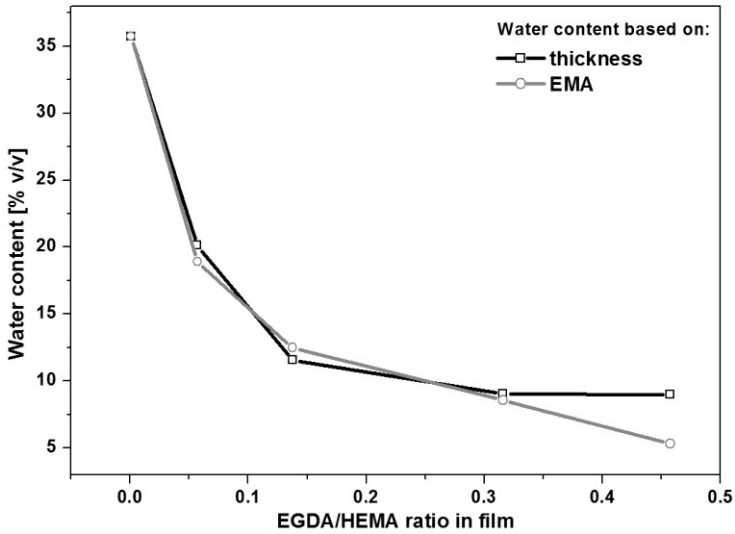

Figure 1.37 EMA and dilation (thickness) approaches for the determination of water fraction in hydrogels shown to agree very well, confirming unidirectionality of swelling. Adapted with permission from [125]. Copyright 2005 American Chemical Society

hydrogels [98, 125], block copolymers [96], and hyperbranched polyesters [25]. In the investigation of Chan et al. [125], the dilation and EMA approaches have been shown to be in a very good agreement which also confirmed the applicability of the unidirectional swelling of the films (only perpendicular to the substrate), Figure 1.37.

In one study of swelling in polyelectrolyte multilayer films by Miller et al. [106], the refractive index of swollen films has been calculated from a linear combination of indices of pure polymer and penetrant according to the relationship using swollen and dry film thicknesses:

$$h_{SP}n_{SP} = (h_{SP} - h_{DP})n_{SP} + h_{DP}n_{DP} \qquad (1.8)$$

Because of the small refractive index differences between the polymer and water this very simple assumption has been shown to be quite accurate. The formula actually corresponds to the use of the lower Wiener bound and its applicability in this study originates from complete transparency of the analyzed films. More information on this topic can be found in optics textbooks, for instance in [140].

1.5.3. Thermodynamic parameters

The volume fractions calculated using one of the approaches, presented in 1.5.2, can be used to quantify the thermodynamic parameters of the polymer – penetrant systems. In investigations of swollen films the most popular approach is via the Flory – Huggins and Flory – Rehner theories [142, 143]. The Flory – Huggins

theory, written in terms of solvent volume fraction and its activity, uses the binary interaction parameter χ:

$$ln(a) = ln(\phi_S) + (1 - \phi_S) + \chi \cdot (1 - \phi_S)^2 \quad (1.9)$$

This parameter describes the interaction energy between the polymer and penetrant and is a useful measure of the strength of this interaction, due to simplicity of equation 1.9. When cross-linked thin film networks are considered the Flory – Huggins expression is modified by the elastic energy, Ω, yielding the Flory – Rehner expression by adding the following term to the right side of equation 1.9:

$$\Omega = \left(1 - \frac{2M_c}{M}\right)\frac{V_S E}{3RT}\left(\alpha - \frac{1}{2\alpha}\right) \quad (1.10)$$

In this expression M_c is the molecular weight between cross-links, M is the molecular weight of the polymer, V_S is the molar volume of the solvent, R is the gas constant, T is the temperature, E is the Young's modulus of the polymer, and α is the swelling factor defined as h_{SP}/h_{DP}. The use of the Flory Rehner expression instead of pure Flory - Huggins is of particular importance for cross-linked strongly swelling supported films. This is because, due to immobilization on the substrate, swelling can only occur in one direction perpendicular to the substrate. It means that the polymer network deformation is much larger than in the case where swelling occurs in all three spacial directions, as in the bulk. In the case of one directional swelling the Ω contribution is usually quite significant and cannot be neglected [8].

There are several *in-situ* ellipsometry investigations where the interaction parameters are calculated. In an interesting study of Elbs et al. [80], the Flory – Huggins interaction parameters have been determined for homo- and copolymers as a function of various organic vapor activities. The polymer films, of about 150 nm dry thickness, have been exposed to vapors at different saturations (p/p_{sat}) until stabilization. The volume fraction of the solvent has been calculated from polymer dilation, as described in 1.5.2, and then equation 1.9 has been used to extract the χ parameters. The authors have discussed the concentration dependence of the interaction parameters (which, according to Flory – Huggins theory should be concentration independent), Figure 1.38. The effect is known to be related to the difference in densities between the polymer and the penetrant and concentration dependence of chain mobility or monomer interactions. Afterwards, the compatibility between different polymer components in block copolymer solutions has been estimated from a Scott – Flory – Huggins mean field approach. Ellipsometry has been shown to be a very consistent and convenient technique which could be easily generalized for similar research problems. The interaction parameters for the non cross-linked polymers have also been investigated in a scaling behavior study for block copolymers by Chandler et al. [76].

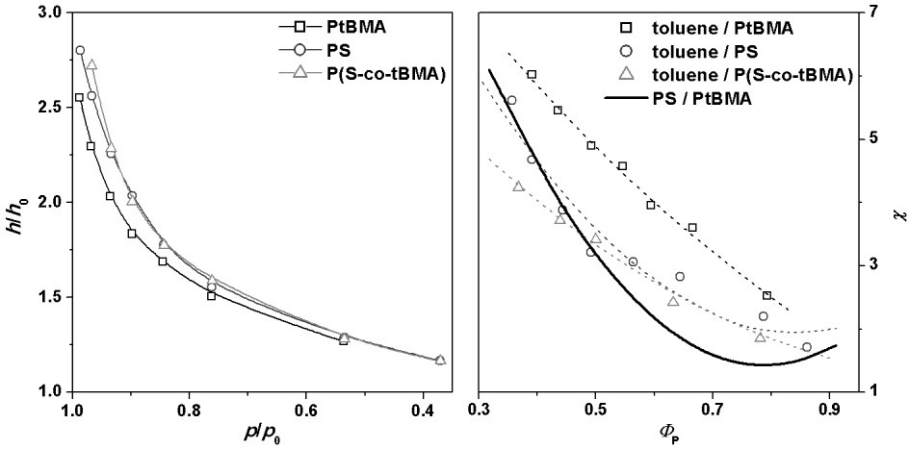

Figure 1.38 Swelling of various polymers and a copolymer in toluene vapors (left), and the extracted Flory – Huggins interaction parameters (right). The concentration dependence of the interaction parameters clearly points to the breakdown of some assumptions in the simplest form of the Flory – Huggins relationship, equation 1.9. Adapted with permission from [80]. Copyright 2004 Elsevier

For the cross-linked materials the Flory – Rehner approach has been utilized in several cases [8, 71, 108]. Wind et al. [71], have used the expression to estimate the effect of cross-linking of thin polyimide and PDMS films on the sorption and relaxation behavior. They have found negligible effects in PDMS, whereas for the glassy polyimides the effect has been very significant. These effects have been related to much more pronounced relaxational behavior of glassy polymers in general as compared to rubbery PDMS. Blacklock et al. [108], have investigated the impact of cross-linking on the behavior of bioreducible polymers. The interaction parameters have been calculated with the Young's modulus determined from rubber elasticity theory ($E = 3\,\nu_E RT$). An increase in the interaction parameter upon cross-linking has been correlated with an increased hydrophobicity of the network and formation of bulk water droplets within the films. The authors have found, in addition, an excellent agreement between results of QCM, AFM and ellipsometry. The impact of cross-linking density on the swelling and interaction parameters in PDMS – n-hexane system has been investigated with high pressure liquid ellipsometry [8]. In this study the parameters calculated from Flory – Huggins, and Flory – Rehner with and without the assumption of perfect network have been compared. It has been concluded that the perfect network assumption does not hold for the lowest degree of cross-linking.

In several investigations also a different type of a thermodynamic parameter, the disjoining pressure, has been investigated [38, 144, 145]. This parameter, also calculable from swelling of the polymer, is a measure for the force per unit area

within the wetting film. This pressure can be created by large macromolecules confined between cells in the extracellular matrix and result in emergence of hydrated pathways for the transport of molecules by separating the cellular barriers.

1.6. Ellipsometry combined with other techniques

More than half of the studies included in this review combine ellipsometry with other *in-situ* techniques, which are able to determine various properties of the swollen layers. There are mainly two reasons for that. One is the inherently indirect nature of ellipsometry. Extraction of useful parameters in almost all ellipsometry investigations on thin films has to be done with the application of the optical model. This is an obvious disadvantage, because the evaluation of the applicability of a given optical model to the morphology of a particular sample may sometimes be problematic, as already discussed in 1.2.2.3. On the other hand, optical models can include many sample features (roughness, gradients, anisotropy etc) that can yield additional information. Therefore, a sensible balance between the sufficiently detailed and overparametrized sample description needs to be found, which can be strengthened by comparison against a more direct method (QCM, AFM etc). The other reason for combining ellipsometry with other techniques is the possibility to gather complementary information on the swollen (or non-swollen, in *ex-situ* mode) polymeric material. The second reason is the most widely represented in the literature.

1.6.1. Ellipsometry concurrently combined with other techniques *in-situ*

Even though ellipsometry has been frequently complemented with other techniques, only very few studies have been done, where ellipsometry measurements have been conducted *in-situ*, concurrently with other methods. Due to the compatible sample configuration utilized in electrochemical, QCM and ellipsometry measurements these 3 techniques have been combined in the study on the PANI anodic pre-peak by Dinh et al. [40]. The authors have constructed a special electrochemical/optical plastic (PMMA) cell with a working electrode consisting of AT-cut quartz crystal with evaporated Ti and Au layers. The counter electrode has been Pt, and the reference electrode has been reversible hydrogen electrode. The measurement cell has given the authors a unique opportunity to observe the swelling responses of the analyzed films to electrochemical stimuli. A similar cell has been used in electrochemical and ellipsometry measurements done by Forzani et al. [45] and Tagliazucchi et al. [46], for the observation of swelling of polyelectrolyte multilayers during redox cycles, Figure 1.39.

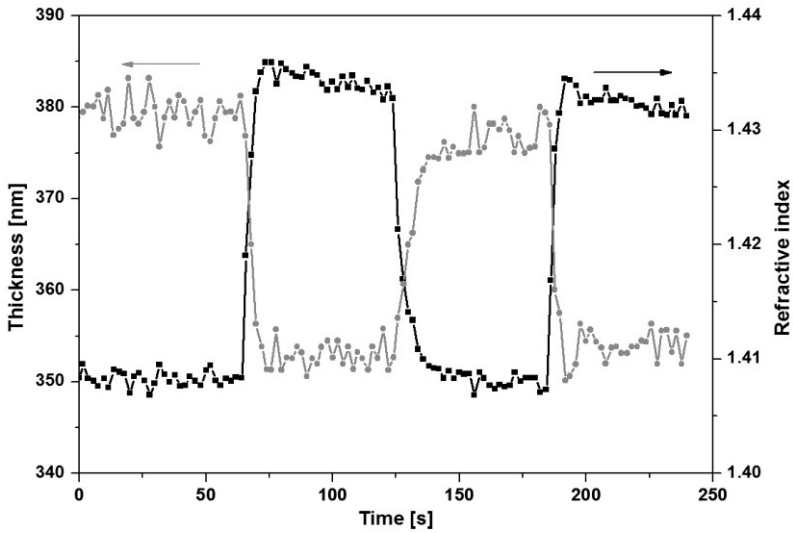

Figure 1.39 Thickness (closed symbols) and refractive index (open symbols) changes induced by alternating electrical potential steps of 0 V and 0.5 V, measured by concurrent ellipsometry and electrochemical measurements. Adapted with permission from [45]. Copyright 2002 American Chemical Society

1.6.2. Ellipsometry complemented with other *in-situ* techniques

A large variety of different *in-situ* techniques have been used in swollen film investigations to complement information gathered with ellipsometry. Among the most common ones are QCM (often with dissipation, QCM-D) for obtaining mass changes and viscoelastic properties of swollen films and AFM, assuring a more direct measurement of the swelling film thickness and its, usually top-view, morphology. Both of these techniques are quite well established in *in-situ* measurements of swollen polymers and some of the most prominent examples, with theoretical and instrumental aspects described, may be found in [146-148] for AFM and in [149, 150] for QCM. In this paragraph the *in-situ* ellipsometry in combination with these and other techniques is described. Principles of each of the techniques are mentioned, however only briefly, and the interested reader should refer to literature for more details.

1.6.2.1. Quartz crystal microbalance (QCM)

In this technique the changes of a resonant frequency of a metal coated (i.e. gold, titanium) quartz crystal are measured with extremely high precision. The analyzed polymer film is either already attached to the electrode or is being formed during the measurement. The changes in mass of the attached film influence the resonant frequency of the crystal and enable accurate measurements of, for instance,

penetrant mass uptake. When also the overtones are analyzed it is possible to determine the changes in viscoelastic properties of the non-rigid samples. Because most swollen polymer systems classify as such, this variation of the technique, denoted QCM-D, is the one most often used. QCM-D is one of the most interesting techniques that can be coupled with ellipsometry, because it is very complementary. Ellipsometry gives access to the volumetric and optical density (refractive index) changes in the films, however, extraction of the changes in mass needs calculations based on the refractive index, 1.5.2. This may become very problematic, or even impossible, if the swelling ambient has a refractive index close, or the same, as that of the analyzed film. This may also become difficult in the limit of very thin films in typical penetrants (below about 25 nm). Because the measurement in QCM-D is based on a completely different principle, this technique can still be sensitive. In addition, it enables the measurement of changes in the viscoelastic properties of the films (energy dissipation) – where ellipsometry has no applicability at all.

QCM and ellipsometry have been used to study water uptake in hydrophilic polyacrylates [39]. Both techniques have been found to agree with each other, also with respect to dynamics of swelling, provided that the water content in the films does not alter the shape of the QCM resonance. The authors have based their conclusions on the discussion of the qualitative features of the resonance peaks upon immersion in water and subsequent sorption in the films. If the resonance peaks maintain the same shape during the whole process of sorption, implying little change in the dissipation properties of the swollen films, then the mass uptake corresponds with ellipsometry swelling very well. If the resonant curves change significantly, that is not the case. Kleinfeld et al. [34], have been able to explain the water uptake in composite multilayer films by independent QCM and ellipsometry measurements, Figure 1.40. The authors have described water uptake process, where the penetrant first fills the void spaces within the films (with little swelling – ellipsometry, but significant mass uptake – QCM) and subsequently swells the structure to a larger extent.

Similar sorption features in Nafion nanomembranes have been investigated with QCM and ellipsometry by Abuin et al. [127]. The complementary nature of ellipsometry (in this case ellipsometry porosimetry) and QCM has been also utilized by Rouessac et al. [151], in their very thorough micro- and mesoporosity studies of supported glassy membrane films. The authors have presented in detail the advantages and disadvantages of all used techniques for this measurement problem. A significant experimental effort in the measurements of the mechanical properties change upon cross-linking in swollen multilayer bioreducible films has been performed with QCM-D, ellipsometry and AFM by Blacklock et al. [108]. Complementarity between QCM and ellipsometry has also been used in organic vapor sorption experiments on calixarene films [41], in the high pressure

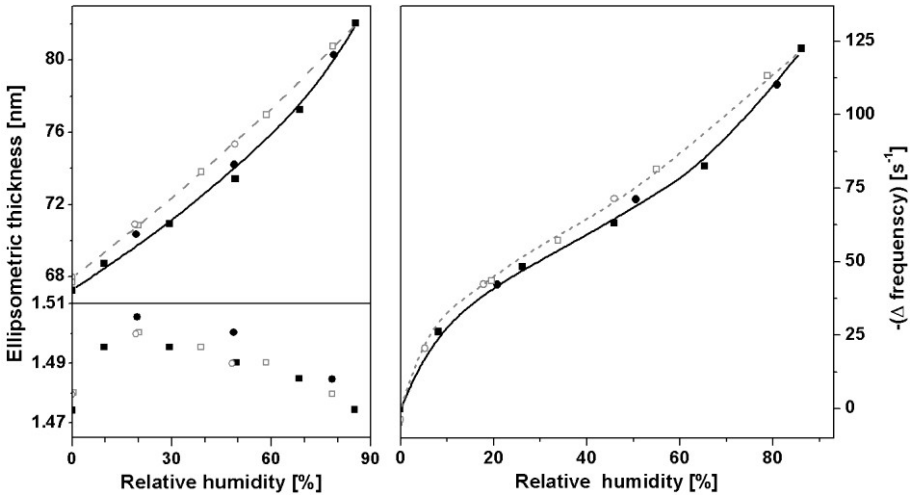

Figure 1.40 Ellipsometry (left) and QCM (right) data on sorption of water vapor in composite multilayer films [34]. At lower humidity the mass uptake dominates without much swelling of the film (little thickness change, but significant index and mass increase). At higher humidity more pronounced swelling as a result of the mass uptake is observed. Adapted with permission from [34]. Copyright 1995 American Chemical Society

ellipsometry study of Carla et al. [73], and in the swelling of nanocomposite layers of Schmidt et al. [64].

1.6.2.2. Atomic force microscopy (AFM)

AFM belongs to the most direct methods to determine film thickness and its top-view morphology. In this type of scanning probe microscopy a few nm area tip of a cantilever scans the surface of the sample, thereby probing the forces between the sample and the tip. The probed forces may include van der Waals forces, capillary forces, electrostatic forces and others. The displacement of the tip is typically measured with a laser reflected of the top of the surface of the cantilever and detected by a photodiode. The measurement of the film thickness can be done by simply making a small scratch on the sample surface with a sharp tool removing the polymeric material locally and exposing the bare substrate. By a linear AFM scan perpendicular to the scratch, it is possible to determine the relative height between the bare substrate and the top surface of the film [100].

The complementarity of the AFM with ellipsometry is best utilized in the surface topology and roughness determination [36, 64, 93, 104, 105, 108, 121, 126]. This is because the probing light spot size in ellipsometry is usually relatively large, ranging from hundreds of microns to several millimeters. Consequently, ellipsometry data represents the average properties of the probed films within this

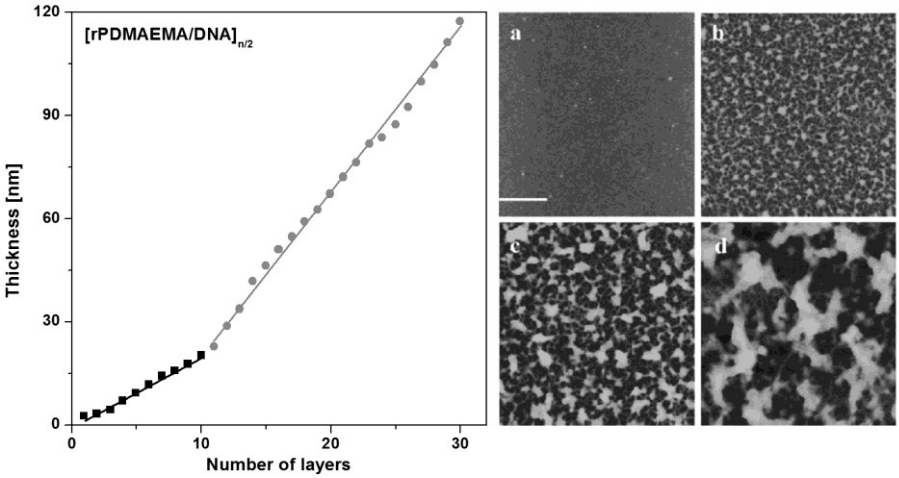

Figure 1.41 Ellipsometry thickness data (left) and the corresponding changes in morphology of the layer by layer films by in-situ AFM (right). Going from a to d (right) the numbers of layers are increasing from 2 (a), 10 (b), 20 (c), 30 (d). The bar in graph a is 1 micron long. In ellipsometry data, two linear regimes of deposition are visible, one from 1 to 10 layers (~2 nm per layer) and the second from 11 to 30 layers (~5 nm per layer). Adapted with permission from [108]. Copyright 2010 American Chemical Society

area. AFM on the other hand, is able to resolve surface features on a length scale of nanometers giving complementary information on the morphology, roughness and homogeneity of the films (defects). In addition, *in-situ* AFM can be used to directly observe both changes in thickness (swelling) of the layers and changes in their morphology when exposed to penetrants [64, 105, 108]. For example, in a study of Blacklock et al. [108], the *in-situ* AFM has been used together with ellipsometry to study the morphology changes in thin bioreducible layer by layer films as a function of number of layers, Figure 1.41, progress of the cross-linking and degradation. *In-situ* AFM has also been used to visualize pore closing as function of time in an interesting study on polyelectrolyte multilayers by Lee et al. [152].

1.6.2.3. Neutron and X-ray reflectivity

Neutron and X-ray reflectivity techniques probe with much smaller wavelengths than visible light, usually on the order of sub-Å to several nm. This allows the techniques to generate complementary data to ellipsometry by accessing much smaller length scales.

In neutron reflectivity measurements, the intensities of the incoming and exiting beams are measured at very low angles (grazing incidence). The reflectivity is usually expressed as a function of the scattering length density which is related to the chemical composition. The scattering length density is a relatively strong function of isotopic composition of the material and allows distinguishing between,

for instance, D_2O and H_2O in, so called, contrast variation measurements. In measurements of swollen polymers, a mixture of 1 mol D_2O and 2 mol of H_2O can be used as the swelling ambient because it has the specular neutron reflectivity very close to the one of the silicon substrate. Thereby, the neutron contrast is caused largely by the polymer layer and can be used to calculate its concentration, also accounting for the spacial distribution (i.e. gradients in density). This can be done for layers of several nm in thickness – as opposed to ellipsometry determination of composition (and gradients), which can usually be done only for at least an order of magnitude thicker films. Such methodology has been used by Murphy et al. [114, 115] and Tang et al. [14], to gain polymer concentration together with its spacial variation for very thin (down to ~5-10 nm) zwitterionic films swollen in water in their protein adsorption studies. Ellipsometry has been shown to be practically insensitive to gradients in such very thin films. Neutron reflectivity has also been used by Atarashi et al. [84], to study the density profiles of as spun PMMA thin layers in their water uptake (measured by ellipsometry) study.

X-ray reflectivity measurements are sensitive to electron density variation in the films. These changes can be correlated with the mass uptake of microporous systems but the technique is also sensitive to the nanopore size distribution. These features make it complementary to ellipsometry. A thorough study comparing results obtained with ellipsometry, QCM and X-ray reflectivity measurements, as well as addressing issues related to the complementarity of the techniques, has been conducted by Rouessac et al. [151].

1.6.2.4. Electrochemical methods

Electrochemical methods require preparation of films on metal substrates serving as electrodes, which include gold, titanium or platinum. Often the sample can be used for the QCM measurements as well [64]. In cyclic voltametry the electric potential applied to the sample is varied at a certain rate (for instance 0.1 V/s [44]). In impedance measurements the response of the sample to sinusoidal voltage of variable frequencies is recorded. In the investigation of Harris et al. [44], changes of swelling obtained with ellipsometry at different pH values have been complemented with electrochemical results to assess the selectivities of layer by layer polyelectrolyte films to different ions. Cyclic voltametry has been used to determine ionic currents in the films and revealed that it increased by almost two orders of magnitude at basic pH, as compared to neutral and acidic pH. These results, together with impedance measurements, have given the authors a possibility to investigate the formation of defects and delaminations, but have also provided data on accessibility of electrodes to the flowing ions and kinetic diffusion parameters. The increase of ionic permeabilities at basic pH has been shown to correlate well with the increase of swelling at the same pH. Ellipsometry has also been complemented by the data on the zeta potential of the polymeric

layers determined by the measurements of the streaming potential in the study of close-packed monolayers of microgel parcitles [117] and swollen cellulose films [49, 85].

1.6.2.5. Gravimetric methods

Apart from the QCM, also other techniques sensitive to mass changes of the analyzed samples have been used to complement ellipsometry. Sorption (micro) balance measurement have the advantage of more direct measurement of the sample mass than QCM, however, they cannot in general be used in the same sample mass range as the QCM (and ellipsometry). This is because of much lower (several orders of magnitude) sensitivity of the balances. However, in studies where the research is aimed at comparison of sorption (or drying) behavior of thin films (by ellipsometry or QCM) and thick films the microbalances have been found useful [60, 88]. In the measurements of Rowe et al. [88], the changes in dilation of a quartz spring with a known spring constant, to which about 30 mg of polymer sample is attached, have been measured. The spring displacement has then been used to calculate mass uptake in several high glass transition polymers. It has been found that the thin films (about 500 nm) behave in agreement with their bulk counterparts with respect to water vapor uptake at low pressures. In the investigation of Richardson et al. [60], the kinetics of drying have been investigated for thin (~150 nm) and bulk (~50 micron) films to study the impact of vitrification of the polymer solution on the residual solvent remaining in the films. In both cases it has been found that the time required for loss of solvent is much larger than that calculated based on the assumption of purely Fickian diffusion, pointing to the importance of the occurrence of glass transition in the course of drying. Horn et al. [74], have compiled the ellipsometry CO_2 sorption data (for thin films) with various balance based data in Matrimid. In their investigation the authors have specifically focused on differences in plasticization and relaxation behavior of thin and thick films, Figure 1.42.

In contrast to the investigation of Rowe et al. [88], the films have been much thinner, on the order of 100 nm, and have been found to behave significantly differently than the bulk. In the studies of Wind et al. [70, 71], also the thick and thin films have been compared with respect to their plasticization, sorption and permeability behavior, however, only permeability (not mass change) behavior of the thick films has been measured.

A relatively simple and direct approach, based on weighing the spin coated samples on 3-inch diameter silicon wafers, has been applied in the investigation of Buchhold et al. [33]. In this case the researchers have reported the precision of weight determination with an analytical mass balance on the order of 15% with an accuracy of 30 μg.

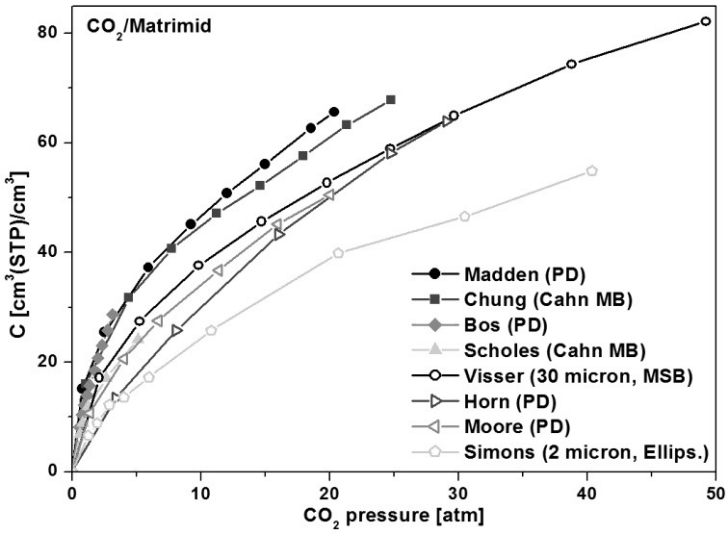

Figure 1.42 CO_2 sorption data in Matrimid from several microbalance (MB), pressure decay (PD), and magnetic suspension balance (MSB) studies of bulk films compared with ellipsometry data for thin films. Adapted with permission from [74]. Copyright 2012 American Chemical Society

1.6.2.6. Contact angle measurements

The phenomena of contact angle hysteresis have been investigated by dynamic contact angle measurements in polyimide [62] and hyperbranched aromatic polyesters [37]. These measurements can give information on the dynamics of changes in hydrophilic – hydrophobic balance during swelling of the investigated polymer layers, which are not accessible by ellipsometry. In these measurements of Hennig et al. [62], the advancing and receding contact angles have been measured in dependence on the contact time with water. The observed hysteresis has been attributed to the small surface swelling of the investigated polymer layers, as determined with ellipsometry. The curing at high temperatures has been found to reduce the water uptake, and accelerated stabilization of the advancing contact angle. Mikhaylova et al. [37], have found no changes in contact angle with thickness of hyperbranched aromatic polyesters, whereas an increase of refractive index with reducing thickness has been found. These results have seemed to confirm the more or less similar hydrophilicity of the surface of the films with increasing overall polymer density for thinner films.

1.6.2.7. UV-VIS spectroscopy

Crossland et al. [47], have used ellipsometry and UV-VIS spectroscopy for the study of crystallization of conjugated polymers displaying π-π interactions. Single

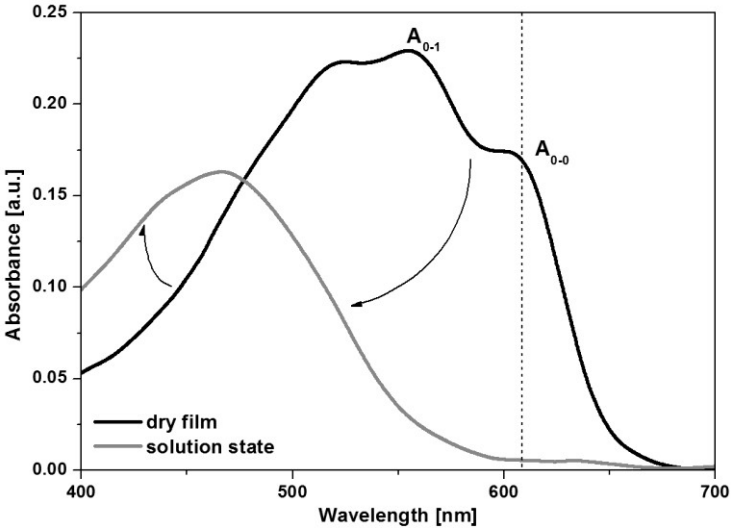

Figure 1.43 UV-VIS spectra of dry and significantly swollen π-π conjugated films. The change in the absorption spectrum is related to dissolution of crystallites going from dry to swollen polymer. At the same time ellipsometry derived film thickness has been observed (not shown). Adapted with permission from [47]. Copyright 2011 Wiley

wavelength *in-situ* ellipsometry has been used to determine swelling changes, whereas UV-VIS spectroscopy allowed tracking the changes in the optical absorption. The optical absorption has been a product of two types of molecular states, Figure 1.43.

The long wavelength absorption has been attributed to chains in a crystalline state (linearized π-stacked chains), the short wavelength absorption has occurred due to interchain states of isolated chains. Thus the changes in the UV-VIS spectrum could be used to quantify and follow crystallinity changes within the swollen films. In principle, similar data could be gathered with spectroscopic ellipsometry *in-situ* provided that the optical absorption of the films is not too strong, or the films are not too thick, and the interference of light can occur at the outer interface of the films. UV-VIS absorption measurements has also been used by Yagüe et al. [97], to track marker (fluorescein) emission signal depending on the mesh size in iCVD deposited hydrogels.

1.6.2.8. IR spectroscopy

IR spectroscopy is able to probe the properties of the swollen films for the much longer wavelengths than typical ellipsometry. This technique is particularly sensitive to chemical changes of the investigated materials, giving rise to its complementary nature with respect to ellipsometry. The utility of combined ellipsometry and IR spectroscopy measurements has been demonstrated in a study

of ammonia sensing in a derivative of PDMS, Posimca50, containing carboxyl acid groups. The changes in IR transmission in a particular region of the spectrum have been interpreted as clear evidence of the acid-base reaction of the analyte (ammonia) with the sensing material. At the same time the changes in swelling of the material upon exposure to ammonia have been detected with ellipsometry. In another study Fourier Transform IR has been employed by Chan et al. [125] to investigate chemical changes related to cross-linking in iCVD deposited films. *In-situ* ATR-IR has been combined with *in-situ* ellipsometry for the study of protein adsorption on oligosaccharide-modified hyperbranched poly(ethylene imine) films [128].

IR ellipsometry, a technique rarely employed *in-situ*, has been used together with VIS ellipsometry to study chemical changes and swelling occurring during the formation of protein adsorption layer on top of hyperbranched polyesters in a study of Reichelt et al. [25]. Recently, *in-situ* IR ellipsometry has been developed for the studies of polymer brushes [153]. Correlation of VIS-ellipsometry with IR-ellipsometry contributed to a significant improvement of water fraction determination in these highly swollen systems.

1.6.2.9. Surface plasmon resonance (SPR)

The excitation of the surface plasmon (collective motion of electrons stimulated by incident light at resonance conditions) can be used as a measure of the response of a polymeric material to adsorbing species. The excitation can be done with a single wavelength *p*-polarized He-Ne laser light [41] and can be performed in *in-situ* arrangement [41, 50, 116]. The relative response in calixarene films studied with SPR by several groups has been shown to be correlated with saturation vapor pressure of the penetrants [41, 116]. SPR measurements have been treated as complimentary to ellipsometry by giving a more direct measure of mass adsorption of the probed vapors, in this sense being quite similar to QCM measurements.

1.6.2.10. Methods to determine mechanical properties

Young's modulus of the thin polymeric films can be extracted by analyzing the laser light diffraction patterns from buckling wavelengths [82]. These simple and elegant measurements have been shown to be applicable *in-situ* (in controlled relative humidity) for PS, PMMA and polyelectrolyte multilayers. The collected data have allowed correlating changes in swelling (ellipsometry) with the changes of the mechanical properties of the investigated materials, Figure 1.44.

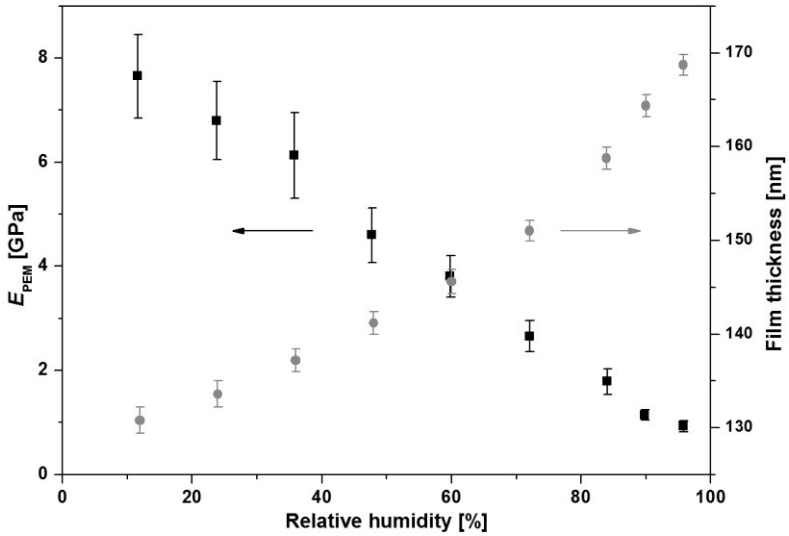

Figure 1.44 Young's modulus (buckling) and film thickness (ellipsometry) obtained for polyelectrolyte multilayer films as a function of relative humidity. Adapted with permission from [82]. Copyright 2008 American Chemical Society

1.7. Concluding remarks and outlook

Based on the analysis of the studies described in this review several conclusions and future projections can be made. Undoubtedly, ellipsometry has established itself as a very useful technique in investigations of thin films interacting with penetrants. It offers a very balanced combination of precision, accuracy, non-intrusive character, and high temporal resolution. It is also relatively inexpensive and well applicable to analysis of films with thicknesses in a practically important range, from nanometers to several microns. High versatility of ellipsometry is signified by a large variety of different processes studied, starting from penetrant uptake from dry state, via drying processes, pH, temperature, ionic strength or electrochemically induced transitions, ending with dissolutions, degradations and complex diffusion phenomena. All of the advantages of the technique have contributed to the situation, where in many studies ellipsometry suffices as the only characterization technique.

A gradual progress in instrumentation has been noticeable in the timeline of the studies, where a shift from single wavelength to spectroscopic ellipsometry going from older to more recent investigations has been well visible. At the same time the type of information extracted with the technique has changed from relatively simple static swelling studies to more complex dynamic ones. However, this trend has certain exceptions, like the early studies of complex dissolution phenomena in PMMA [17-20]. The improvement in the speed of data acquisition and analysis has

made possible investigations of processes occurring on the timescales from seconds to weeks. A significant extension of applicability of ellipsometry has been made by the introduction of high pressure static [65] and permeation cells [8] that opened entirely new possibilities related to fundamental research in, for example, membrane technology. In this area, it is possible to notice that the research attention has been gradually shifting from fundamental studies to investigations on the behavior of practically applied systems.

In-situ ellipsometry has proved to be very successful in fundamental studies on the nature of interactions of glassy and rubbery polymers with liquids and condensable gases. Its potential has also been explored significantly in more complex polymeric materials, like multilayers and composites. It can be expected that also other, emerging classes of macromolecular materials will attract attention in the future. These may include nano- and biocomposites, or hybrid organic – inorganic materials, including metal organic frameworks. The characterization of these more complex systems may benefit especially from combination of ellipsometry with other *in-situ* techniques. In particular, the concurrent ellipsometry - QCM-D studies seem highly complementary, but are not extensively represented in thin polymer film research yet.

1.8. Acknowledgments

The author acknowledges comments and helpful discussions with Michiel Raaijmakers and Emiel Kappert from Inorganic Membranes group and Beata Koziara from Membrane Science and Technology group at the University of Twente.

The author gratefully acknowledges the permissions granted to reproduce the copyright material in this Thesis. The material is used in the Thesis under fair use, non-profit, review conditions.

1.9. Appendix

In this section, the selected mathematical formulae utilized in the conversion of ellipsometric parameters, Ψ and Δ, into sample properties (and vice versa) are briefly presented. The detailed derivation can be found in [5]. Reflectivity ratio for the sample shown in Figure 1.4 can be written, using the well known Fresnel relationships, as:

$$\rho = \frac{r_p}{r_s} = \frac{\frac{N_1 cos\theta_0 - N_0 cos\theta_1}{N_1 cos\theta_0 + N_0 cos\theta_1}}{\frac{N_0 cos\theta_0 - N_1 cos\theta_0}{N_0 cos\theta_0 + N_1 cos\theta_1}} \quad \text{(A1)}$$

The transmission angle can be calculated from the Snell's law using the usually known incidence angle, θ_0:

$$N_0 sin\theta_0 = N_1 sin\theta_1 \quad \text{(A2)}$$

Equation A1 represents a complex number, because $N_0=n_0-ik_0$ and $N_1=n_1-ik_1$.

Ψ and Δ are then directly calculated as:

$$\Psi = tan^{-1}(|\rho|) \quad \text{(A3)}$$

$$\Delta = \begin{cases} tan^{-1}\left[\frac{Im(\rho)}{Re(\rho)}\right] for\ Re(\rho) > 0 \\ tan^{-1}\left[\frac{Im(\rho)}{Re(\rho)}\right] + 180° \ for\ Re(\rho) < 0, Im(\rho) \geq 0 \\ tan^{-1}\left[\frac{Im(\rho)}{Re(\rho)}\right] - 180° \ for\ Re(\rho) < 0, Im(\rho) < 0 \end{cases} \quad \text{(A4)}$$

When light enters a thin film sample it reflects (reflectivity, r) and transmits (transmittance, t) at each of the interfaces. The rays leaving a sample (r_{01} – reflection from topmost interface, t_{10} – transmittance after reflection from second interface, etc.) interfere with each other and produce spectral oscillations in the Ψ and Δ. Figure A1 presents in more detail the light reflection and transmission occurring at the thin film sample.

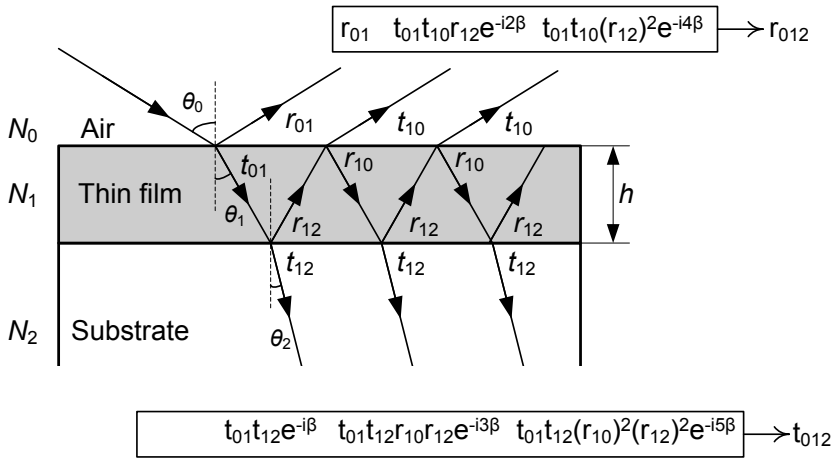

Figure A1 More detailed scheme of light reflection and transmission at the thin film sample, adapted with permission from [5]. Copyright 2007 Maruzen

The reflectivity ratio is expressed as:

$$\rho = \frac{r_p}{r_s} = \frac{\frac{r_{01,p}+r_{12,p}exp\,(-i2\beta)}{1+r_{01,p}r_{12,p}exp\,(-i2\beta)}}{\frac{r_{01,s}+r_{12,s}exp\,(-i2\beta)}{1+r_{01,s}r_{12,s}exp\,(-i2\beta)}} \quad \text{(A5)}$$

With:

$$\beta = 2\pi d N_1 cos\theta_1/\lambda \quad \text{(A6)}$$

Calculation of Ψ and Δ can be performed using again equations A3 and A4. However, for the measured Ψ and Δ values the determination of film thickness and its optical constants is usually done with an optical model, 1.2.2.3, due to mathematical complexity of A5.

1.10. List of abbreviations

Chemical names

BSA	bovine serum albumin
CF_x	fluoropolymer
DMPC	dimyristoylphosphatidylcholine
DNA	deoxyribonucleic acid
HA	hyaluronic acid
Matrimid	polyimide of 3,3′,4,4′-benzophenone tetracarboxylic dianhydride and diamino-phenylidene
p(HEMA-*co*-EGDA)	poly[(2-hydroxylethyl methacrylate)-*co*-(ethylene glycol diacrylate)]
p(NIPAM-*co*-AA)	poly(*N*-isopropyl acrylamide-*co*-acrylic acid)
PAA	poly(acrylic acid)
PAArVBA	poly(acrylic acid-*ran*-vinylbenzyl acrylate)
PAH	poly(allylamine hydrochloride)
PANI	polyaniline
PC	phosphorylcholine
PDADMAC	poly(diallyldimethylammonium chloride)
PDMAEMA	poly(2-dimethylaminoethyl methacrylate)
PDMS	poly(dimethyl siloxane)
PEBAX	poly(amide-6-*b*-ethylene oxide)
PEG	poly(ethylene glycol)
PEI	poly(iminoethylene), poly(ethylene imine)
PEO	poly(ethylene oxide)
PES	poly(ethersulfone)
PFOMA	poly(1,10-dihydroperflurooctyl methacrylate)
PGA	poly(L-glutamic acid)
PHEMA	poly(2-hydroxyethyl methacrylate)
PLL	poly(L-lysine)
PMMA	poly(methyl methacrylate)
PNIPAM	poly(*N*-isopropyl acrylamide)
PNVP	poly(N-vinyl pyrrolidon)
Posimca50	poly(methylcarboxypropyl siloxane)
PPO	poly(*p*-phenylene oxide)
PS	poly(styrene)
PSF	polysulfone
PSS	poly(styrenesulfonate)
PVME	poly(vinyl methyl ether)
PVP	poly(2-vinylpyridine)
PVS	poly(vinyl sulfonate)
SPEEK	sulfonated poly(ether ether ketone)
SSEBS	polystyrene-*block*-poly(ethylene-*ran*-butylene)-*block*-polystyrene

Other abbreviations

AFM	atomic force microscopy
EMA	effective medium approximation
iCVD	initiated chemical vapor deposition
MOFs	metal-organic frameworks
OWS	optical waveguide spectroscopy
P_g	penetrant induced glass transition
QCM	quartz crystal microbalance
RH	relative humidity
RSD	relative standard deviation
sc-CO_2	supercritical carbon dioxide fluid
SPR	surface plasmon resonance
T_g	glass transition temperature
VOCs	volatile organic compounds

1.11. References

[1] Lorentz, H.A., Over de theorie der terugkaatsing en breking van het licht: academisch proefschrift1875: K. van der Zande.

[2] Drude, P., Optische Eigenschaften und Elektronentheorie. Annalen der Physik, 1904. **319**(9): p. 677-725.

[3] Drude, P., Ueber Oberflächenschichten. II. Theil. Annalen der Physik, 1889. **272**(4): p. 865-897.

[4] Drude, P., Ueber Oberflächenschichten. I. Theil. Annalen der Physik, 1889. **272**(2): p. 532-560.

[5] Fujiwara, H. and I. Wiley, Spectroscopic ellipsometry principles and applications, 2007, John Wiley & Sons: Chichester, England; Hoboken, NJ.

[6] Tompkins, H.G. and E.A. Irene, Handbook of ellipsometry, 2005, William Andrew Pub. ; Springer: Norwich, NY; Heidelberg, Germany.

[7] Azzam, R.M.A. and N.M. Bashara, Ellipsometry and polarized light1977, Amsterdam; New York; New York: North-Holland Pub. Co. ; Sole distributors for the U.S.A. and Canada, Elsevier North-Holland.

[8] Ogieglo, W., et al., n-Hexane induced swelling of thin PDMS films under non-equilibrium nanofiltration permeation conditions, resolved by spectroscopic ellipsometry. Journal of Membrane Science, 2013. **437**(0): p. 313-323.

[9] Hale, G.M. and M.R. Querry, Optical Constants of Water in the 200-nm to 200-µm Wavelength Region. Applied Optics, 1973. **12**(3): p. 555-563.

[10] French, R.H., et al. Immersion fluid refractive indices using prism minimum deviation techniques. 2004.

[11] Barbey, R., et al., Polymer Brushes via Surface-Initiated Controlled Radical Polymerization: Synthesis, Characterization, Properties, and Applications. Chemical Reviews, 2009. **109**(11): p. 5437-5527.

[12] Edmondson, S., V.L. Osborne, and W.T.S. Huck, Polymer brushes via surface-initiated polymerizations. Chemical Society Reviews, 2004. **33**(1): p. 14-22.

[13] Hinrichs, K. and K.-J. Eichhorn, Ellipsometry of Functional Organic Surfaces and Films.

[14] Tang, Y., et al., Swelling of Zwitterionic Polymer Films Characterized by Spectroscopic Ellipsometry. Macromolecules, 2001. **34**(25): p. 8768-8776.

[15] Tang, Y., et al., Structural Effects on Swelling of Thin Phosphorylcholine Polymer Films. Macromolecules, 2002. **35**(10): p. 3955-3964.

[16] Ogieglo, W., et al., Relaxation induced optical anisotropy during dynamic overshoot swelling of zwitterionic polymer films. Thin Solid Films, 2013. **545**(0): p. 320-326.

[17] Manjkow, J., et al., INFLUENCE OF PROCESSING AND MOLECULAR PARAMETERS ON THE DISSOLUTION RATE OF POLY-(METHYL METHACRYLATE) THIN FILMS. Journal of the Electrochemical Society, 1987. **134**(8): p. 2003-2007.

[18] Manjkow, J., et al., An in situ study of dissolution and swelling behavior of poly-(methyl methacrylate) thin films in solvent/nonsolvent binary mixtures. Journal of Applied Physics, 1987. **62**(2): p. 682-688.

[19] Papanu, J.S., et al., In situ ellipsometry to monitor swelling and dissolution of thin polymer films. Journal of the Electrochemical Society, 1989. **136**(4): p. 1195-1200.

[20] Papanu, J.S., et al., Dissolution of thin poly(methyl methacrylate) films in ketones, binary ketone/alcohol mixtures, and hydroxy ketones. Journal of the Electrochemical Society, 1989. **136**(10): p. 3077-3083.

[21] Papanu, J.S., et al., Swelling of poly(methyl methacrylate) thin films in low molecular weight alcohols. Journal of Applied Polymer Science, 1990. **39**(4): p. 803-823.

[22] Papanu, J.S., et al., Transport models for swelling and dissolution of thin polymer films. Journal of Applied Polymer Science, 1989. **38**(5): p. 859-885.

[23] Ogieglo, W., et al., Temperature-induced transition of the diffusion mechanism of n-hexane in ultra-thin polystyrene films, resolved by in-situ Spectroscopic Ellipsometry. Polymer, 2013. **54**(1): p. 341-348.

[24] Ogieglo, W., et al., Probing the Surface Swelling in Ultra-Thin Supported Polystyrene Films During Case II Diffusion of n-Hexane. Macromolecular Chemistry and Physics, 2013. **214**(21): p. 2480-2488.

[25] Reichelt, S., et al., Functionalization of solid surfaces with hyperbranched polyesters to control protein adsorption. Colloids and Surfaces B: Biointerfaces, 2009. **69**(2): p. 169-177.

[26] Sturm, J., et al., Optical anisotropy in thin films of a blue electroluminescent conjugated polymer. Thin Solid Films, 1997. **298**(1–2): p. 138-142.

[27] Pettersson, L.A.A., S. Ghosh, and O. Inganäs, Optical anisotropy in thin films of poly(3,4-ethylenedioxythiophene)–poly(4-styrenesulfonate). Organic Electronics, 2002. **3**(3–4): p. 143-148.

[28] Campoy-Quiles, M., et al., On the determination of anisotropy in polymer thin films: A comparative study of optical techniques. physica status solidi (c), 2008. **5**(5): p. 1270-1273.

[29] Campoy-Quiles, M., P.G. Etchegoin, and D.D.C. Bradley, On the optical anisotropy of conjugated polymer thin films. Physical Review B, 2005. **72**(4): p. 045209.

[30] Laskarakis, A. and S. Logothetidis, On the optical anisotropy of poly(ethylene terephthalate) and poly(ethylene naphthalate) polymeric films by spectroscopic ellipsometry from visible-far ultraviolet to infrared spectral regions. Journal of Applied Physics, 2006. **99**(6): p. 066101-3.

[31] Winfield, J.M., C.L. Donley, and J.-S. Kim, Anisotropic optical constants of electroluminescent conjugated polymer thin films determined by variable-angle spectroscopic ellipsometry. Journal of Applied Physics, 2007. **102**(6): p. 063505-063505-7.

[32] Patil, N., et al., Swelling-induced optical anisotropy of thermoresponsive hydrogels based on poly(2-(2-methoxyethoxy)ethyl methacrylate): Deswelling kinetics probed by quantitative mueller matrix polarimetry. Journal of Physical Chemistry B, 2012. **116**(47): p. 13913-13921.

[33] Buchhold, R., et al., Swelling behavior of thin anisotropic polymer layers. Thin Solid Films, 1999. **350**(1–2): p. 178-185.

[34] Kleinfeld, E.R. and G.S. Ferguson, Rapid, reversible sorption of water from the vapor by a multilayered composite film: A nanostructured humidity sensor. Chemistry of Materials, 1995. **7**(12): p. 2327-2331.

[35] Herzinger, C.M., et al., Ellipsometric determination of optical constants for silicon and thermally grown silicon dioxide via a multi-sample, multi-wavelength, multi-angle investigation. Journal of Applied Physics, 1998. **83**(6): p. 3323-3336.

[36] Rehfeldt, F. and M. Tanaka, Hydration forces in ultrathin films of cellulose. Langmuir, 2003. **19**(5): p. 1467-1473.

[37] Mikhaylova, Y., et al., Study of the solid-liquid interface of hydroxyl-terminated hyperbranched aromatic polyesters (HBP-OH) in aqueous media. I. Characterisation of the properties and swelling behaviour of HBP-OH thin films. Colloids and Surfaces A: Physicochemical and Engineering Aspects, 2006. **279**(1-3): p. 20-27.

[38] Mathe, G., et al., Disjoining pressure and swelling dynamics of thin adsorbed polymer films under controlled hydration conditions. Langmuir, 1999. **15**(25): p. 8726-8735.

[39] Chen, W.L., et al., Equilibrium swelling of hydrophilic polyacrylates in humid environments. Macromolecules, 1999. **32**(1): p. 136-144.

[40] Dinh, H.N. and V.I. Birss, Characteristics of the polyaniline anodic pre-peak. Electrochimica Acta, 1999. **44**(26): p. 4763-4771.

[41] Nabok, A.V., A.K. Hassan, and A.K. Ray, Condensation of organic vapours within nanoporous calixarene thin films. Journal of Materials Chemistry, 2000. **10**(1): p. 189-194.

[42] Nabok, A.V., et al., Complexing properties of calix[4]resorcinolarene LB films. Thin Solid Films, 1995. **259**(2): p. 244-247.

[43] Arwin, H., TIRE and SPR-Enhanced SE for Adsorption Processes, in Ellipsometry of Functional Organic Surfaces and Films, K. Hinrichs and K.-J. Eichhorn, Editors. 2014, Springer Berlin Heidelberg. p. 249-264.

[44] Harris, J.J. and M.L. Bruening, Electrochemical and in situ ellipsometric investigation of the permeability and stability of layered polyelectrolyte films. Langmuir, 2000. **16**(4): p. 2006-2013.

[45] Forzani, E.S., et al., Redox driven swelling of layer-by-layer enzyme-polyelectrolyte multilayers. Langmuir, 2002. **18**(25): p. 9867-9873.

[46] Tagliazucchi, M., D. Grumelli, and E.J. Calvo, Nanostructured modified electrodes: Role of ions and solvent flux in redox active polyelectrolyte multilayer films. Physical Chemistry Chemical Physics, 2006. **8**(43): p. 5086-5095.

[47] Crossland, E.J.W., et al., Systematic control of nucleation density in Poly(3-Hexylthiophene) thin films. Advanced Functional Materials, 2011. **21**(3): p. 518-524.

[48] Simons, K., et al., CO2 sorption and transport behavior of ODPA-based polyetherimide polymer films. Polymer, 2010. **51**(17): p. 3907-3917.

[49] Müller, Y., et al., The impact of esterification reactions on physical properties of cellulose thin films. Soft Matter, 2010. **6**(15): p. 3680-3684.

[50] Hegewald, J., et al., Electron beam irradiation of poly(vinyl methyl ether) films. 2. Temperature-dependent swelling behavior. Langmuir, 2006. **22**(11): p. 5152-5159.

[51] Pantelić, N., et al., Dynamic In Situ Spectroscopic Ellipsometry of the Reaction of Aqueous Iron(II) with 2,2‘-Bipyridine in a Thin Nafion Film. The Journal of Physical Chemistry B, 2005. **109**(29): p. 13971-13979.

[52] Zudans, I., W.R. Heineman, and C.J. Seliskar, In Situ Dynamic Measurements of Sol−Gel Processed Thin Chemically Selective PDMDAAC−Silica Films by Spectroscopic Ellipsometry. Chemistry of Materials, 2004. **16**(17): p. 3339-3347.

[53] Richardson, H., et al., Thickness dependence of structural relaxation in spin-cast, glassy polymer thin films. Physical Review E - Statistical, Nonlinear, and Soft Matter Physics, 2004. **70**(5 1): p. 051805-1-051805-8.

[54] Sirard, S.M., et al., Anomalous Properties of Poly(methyl methacrylate) Thin Films in Supercritical Carbon Dioxide. Macromolecules, 2002. **35**(5): p. 1928-1935.

[55] Woollam, J.A., et al. Overview of variable angle spectroscopic ellipsometry (VASE), part I: basic theory and typical applications. 1999.

[56] William, H., Press, et al., Numerical Recipes in C1992: Cambridge University Press.

[57] Jellison Jr, G.E., Data analysis for spectroscopic ellipsometry. Thin Solid Films, 1993. **234**(1–2): p. 416-422.

[58] Johs, B. and J.S. Hale, Dielectric function representation by B-splines. physica status solidi (a), 2008. **205**(4): p. 715-719.

[59] J.A. Woollam Co, I., CompleteEASE™ Data Analysis Manual. 2009.

[60] Richardson, H., M. Sferrazza, and J.L. Keddie, Influence of the glass transition on solvent loss from spin-cast glassy polymer thin films. The European Physical Journal E: Soft Matter and Biological Physics, 2003. **12**(0): p. 87-91.

[61] López García, Í., J.L. Keddie, and M. Sferrazza, Probing the early stages of solvent evaporation and relaxation in solvent-cast polymer thin films by spectroscopic ellipsometry. Surface and Interface Analysis, 2011. **43**(11): p. 1448-1452.

[62] Hennig, A., et al., Contact angle hysteresis: Study by dynamic cycling contact angle measurements and variable angle spectroscopic ellipsometry on polyimide. Langmuir, 2004. **20**(16): p. 6685-6691.

[63] Secrist, K.E. and A.J. Nolte, Humidity swelling/deswelling hysteresis in a polyelectrolyte multilayer film. Macromolecules, 2011. **44**(8): p. 2859-2865.

[64] Schmidt, D.J., et al., Electrochemically controlled swelling and mechanical properties of a polymer nanocomposite. ACS Nano, 2009. **3**(8): p. 2207-2216.

[65] Sirard, S.M., P.F. Green, and K.P. Johnston, Spectroscopic Ellipsometry Investigation of the Swelling of Poly(Dimethylsiloxane) Thin Films with High Pressure Carbon Dioxide. The Journal of Physical Chemistry B, 2001. **105**(4): p. 766-772.

[66] Michels, A. and J. Hamers, The effect of pressure on the refractive index of CO2: The Lorentz-Lorenz formula. Physica, 1937. **4**(10): p. 995-1006.

[67] Xiao, G.Z., et al., Monitoring changes in the refractive index of gases by means of a fiber optic Fabry-Perot interferometer sensor. Sensors and Actuators A: Physical, 2005. **118**(2): p. 177-182.

[68] Besserer, G.J. and D.B. Robinson, Refractive indexes of ethane, carbon dioxide, and isobutane. Journal of Chemical & Engineering Data, 1973. **18**(2): p. 137-140.

[69] Pham, J.Q., et al., Pressure, Temperature, and Thickness Dependence of CO_{2}-Induced Devitrification of Polymer Films. Physical Review Letters, 2003. **91**(17): p. 175503.

[70] Wind, J.D., et al., Relaxation Dynamics of CO2 Diffusion, Sorption, and Polymer Swelling for Plasticized Polyimide Membranes. Macromolecules, 2003. **36**(17): p. 6442-6448.

[71] Wind, J.D., et al., Carbon Dioxide-Induced Plasticization of Polyimide Membranes: Pseudo-Equilibrium Relationships of Diffusion, Sorption, and Swelling. Macromolecules, 2003. **36**(17): p. 6433-6441.

[72] Wind, J.D., et al., Carbon dioxide-induced plasticization of polyimide membranes: Pseudo-equilibrium relationships of diffusion, sorption, and swelling. Macromolecules, 2003. **36**(17): p. 6433-6441.

[73] Carla, V., et al., Nonequilibrium model for sorption and swelling of bulk glassy polymer films with supercritical carbon dioxide. Macromolecules, 2005. **38**(24): p. 10299-10313.

[74] Horn, N.R. and D.R. Paul, Carbon Dioxide Sorption and Plasticization of Thin Glassy Polymer Films Tracked by Optical Methods. Macromolecules, 2012.

[75] Li, Y., et al., Role of interfacial interactions on the anomalous swelling of polymer thin films in supercritical carbon dioxide. Journal of Polymer Science Part B: Polymer Physics, 2007. **45**(11): p. 1313-1324.

[76] Chandler, C.M., et al., Unexpected scaling behavior of the order-disorder transition of nearly symmetric polystyrene-block-polyisoprene diblock copolymers dilated with a nominally neutral solvent at very low dilution. Macromolecules, 2009. **42**(13): p. 4867-4873.

[77] Ogieglo, W., et al., Spectroscopic Ellipsometry Analysis of a Thin Film Composite Membrane Consisting of Polysulfone on a Porous α-Alumina Support. ACS Applied Materials & Interfaces, 2012. **4**(2): p. 935-943.

[78] Struik, L.C.E., PHYSICAL AGING IN AMORPHOUS GLASSY POLYMERS*. Annals of the New York Academy of Sciences, 1976. **279**(1): p. 78-85.

[79] Filippova, N.L., Interdiffusion in Polymer Film by Ellipsometry. Journal of Colloid and Interface Science, 1999. **212**(2): p. 589-592.

[80] Elbs, H. and G. Krausch, Ellipsometric determination of Flory-Huggins interaction parameters in solution. Polymer, 2004. **45**(23): p. 7935-7942.

[81] Pham, J.Q., K.P. Johnston, and P.F. Green, Retrograde Vitrification in CO2/Polystyrene Thin Films. The Journal of Physical Chemistry B, 2004. **108**(11): p. 3457-3461.

[82] Nolte, A.J., et al., Effect of Relative Humidity on the Young's Modulus of Polyelectrolyte Multilayer Films and Related Nonionic Polymers. Macromolecules, 2008. **41**(15): p. 5793-5798.

[83] Filippov, L.K., Study of diffusion in films on planar substrates by ellipsometry. Journal of the Chemical Society, Faraday Transactions, 1993. **89**(22): p. 4053-4057.

[84] Atarashi, H., et al., Uptake of water in as-spun poly (methyl methacrylate) thin films. RSC Adv., 2013. **3**(11): p. 3516-3519.

[85] Freudenberg, U., et al., Charging and swelling of cellulose films. Journal of Colloid and Interface Science, 2007. **309**(2): p. 360-365.

[86] Eichhorn, K.J., et al., Swelling of a thin B+ implanted polyimide layer - A dynamic spectroscopic ellipsometry study. Thin Solid Films, 2004. **455-456**: p. 292-294.

[87] Sahre, K., et al., Water sorption properties of carbonized layers produced by controlled B+ bombardment of thin polyimide and polysulfone films. Analytical and Bioanalytical Chemistry, 2004. **378**(2): p. 396-401.

[88] Rowe, B.W., B.D. Freeman, and D.R. Paul, Effect of sorbed water and temperature on the optical properties and density of thin glassy polymer films on a silicon substrate. Macromolecules, 2007. **40**(8): p. 2806-2813.

[89] Kamiya, Y., et al., Sorption and partial molar volume of gases in poly (dimethyl siloxane). Journal of Polymer Science Part B: Polymer Physics, 1990. **28**(8): p. 1297-1308.

[90] Spaeth, K. and G. Gauglitz, Characterisation of the optical properties of thin polymer films for their application in detection of volatile organic compounds. Materials Science and Engineering C, 1998. **5**(3-4): p. 187-191.

[91] Spaeth, K., G. Kraus, and G. Gauglitz, In-situ characterization of thin polymer films for applications in chemical sensing of volatile organic compounds by spectroscopic ellipsometry. Fresenius' Journal of Analytical Chemistry, 1997. **357**(3): p. 292-296.

[92] Rathgeb, F., et al., Dyeless optical detection of ammonia in the gaseous phase using a pH-responsive polymer - Characterization of the sorption process. Fresenius' Journal of Analytical Chemistry, 2000. **368**(2-3): p. 192-195.

[93] Schmidt, S., et al., Thermoresponsive surfaces by spin-coating of PNIPAM-co-PAA microgels: A combined AFM and ellipsometry study. Polymer, 2008. **49**(3): p. 749-756.

[94] Gensel, J., et al., Micro-structure-macro-response relationship in swollen block copolymer films. Soft Matter, 2009. **5**(13): p. 2534-2537.

[95] Zettl, U., A. Knoll, and L. Tsarkova, Effect of confinement on the mesoscale and macroscopic swelling of thin block copolymer films. Langmuir, 2010. **26**(9): p. 6610-6617.

[96] Pantelić, N., et al., Characterization of partially sulfonated polystyrene-block-poly(ethylene- ran-butylene)-block-polystyrene thin films for spectroelectrochemical sensing. Analytical Chemistry, 2009. **81**(16): p. 6756-6764.

[97] Yagüe, J.L. and K.K. Gleason, Systematic control of mesh size in hydrogels by initiated chemical vapor deposition. Soft Matter, 2012. **8**(10): p. 2890-2894.

[98] Lau, K.K.S. and K.K. Gleason, All-dry synthesis and coating of methacrylic acid copolymers for controlled release. Macromolecular Bioscience, 2007. **7**(4): p. 429-434.

[99] Decher, G., Fuzzy Nanoassemblies: Toward Layered Polymeric Multicomposites. Science, 1997. **277**(5330): p. 1232-1237.

[100] Hiller, J. and M.F. Rubner, Reversible molecular memory and pH-switchable swelling transitions in polyelectrolyte multilayers. Macromolecules, 2003. **36**(11): p. 4078-4083.

[101] Halthur, T.J., P.M. Claesson, and U.M. Elofsson, Stability of polypeptide multilayers as studied by in situ ellipsometry: Effects of drying and post-buildup changes in temperature and pH. Journal of the American Chemical Society, 2004. **126**(51): p. 17009-17015.

[102] Tanchak, O.M. and C.J. Barrett, Swelling Dynamics of Multilayer Films of Weak Polyelectrolytes. Chemistry of Materials, 2004. **16**(14): p. 2734-2739.

[103] Wong, J.E., et al., Swelling behavior of polyelectrolyte multilayers in saturated water vapor. Macromolecules, 2004. **37**(19): p. 7285-7289.

[104] Burke, S.E. and C.J. Barrett, Swelling behavior of hyaluronic acid/polyallylamine hydrochloride multilayer films. Biomacromolecules, 2005. **6**(3): p. 1419-1428.

[105] Itano, K., J. Choi, and M.F. Rubner, Mechanism of the pH-induced discontinuous swelling/deswelling transitions of poly(allylamine hydrochloride)-Containing polyelectrolyte multilayer films. Macromolecules, 2005. **38**(8): p. 3450-3460.

[106] Miller, M.D. and M.L. Bruening, Correlation of the swelling and permeability of polyelectrolyte multilayer films. Chemistry of Materials, 2005. **17**(21): p. 5375-5381.

[107] Olugebefola, S.C., et al., Photo-cross-linkable polyelectrolyte multilayers for 2-D and 3-D patterning. Langmuir, 2006. **22**(13): p. 5958-5962.

[108] Blacklock, J., et al., Cross-linked bioreducible layer-by-layer films for increased cell adhesion and transgene expression. Journal of Physical Chemistry B, 2010. **114**(16): p. 5283-5291.

[109] Fiche, J.B., et al., Influence of an electric field on oriented films of DMPC/gramicidin bilayers: A circular dichroism study. Langmuir, 2010. **26**(2): p. 1057-1066.

[110] Tan, W.S., et al., Temperature-Induced, Reversible swelling transitions in multilayers of a cationic triblock copolymer and a polyacid. Macromolecules, 2010. **43**(4): p. 1950-1957.

[111] Xu, L., Z. Zhu, and S.A. Sukhishvili, Polyelectrolyte multilayers of diblock copolymer micelles with temperature-responsive cores. Langmuir, 2011. **27**(1): p. 409-415.

[112] Dodoo, S., et al., Effect of ionic strength and layer number on swelling of polyelectrolyte multilayers in water vapour. Soft Materials, 2013. **11**(2): p. 157-164.

[113] Han, L., et al., Directional cell migration through cell-cell interaction on polyelectrolyte multilayers with swelling gradients. Biomaterials, 2013. **34**(4): p. 975-984.

[114] Murphy, E.F., et al., Characterization of protein adsorption at the phosphorylcholine incorporated polymer-water interface. Macromolecules, 2000. **33**(12): p. 4545-4554.

[115] Murphy, E.F., et al., The Reduced Adsorption of Proteins at the Phosphoryl Choline Incorporated Polymer - Water Interface. Langmuir, 1999. **15**(4): p. 1313-1322.

[116] Shirshov, Y.M., et al., Optical parameters of thin calixarene films and their response to benzene, toluene and chloroform adsorption. Supramolecular Science, 1997. **4**(3-4): p. 491-494.

[117] Nerapusri, V., et al., Swelling and deswelling of adsorbed microgel monolayers triggered by changes in temperature, pH, and electrolyte concentration. Langmuir, 2006. **22**(11): p. 5036-5041.

[118] Burkert, S., et al., Cross-linking of poly(N-vinyl pyrrolidone) films by electron beam irradiation. Radiation Physics and Chemistry, 2007. **76**(8-9): p. 1324-1328.

[119] Pathak, S.C. and D.W. Hess. Dissolution and swelling behaviour of plasma-polymerized polyethylene glycol-like hydrogel films for use as drug delivery reservoirs. 2008.

[120] Richter, A., et al., PH-stable hyperbranched poly(ethyleneimine)-maltose films for the interaction with phosphate containing drugs. New Journal of Chemistry, 2010. **34**(10): p. 2105-2108.

[121] Beyerlein, D., et al., Preparation and properties of thin films of hyperbranched polyesters with different end groups. Macromolecular Symposia, 2001. **164**(1): p. 117-132.

[122] Van Der Zeeuw, E.A., et al., The suitability of scanning angle reflectometry for colloidal particle sizing. Journal of Chemical Physics, 1996. **105**(4): p. 1646-1653.

[123] Emmerzael, R., E. van der Zeeuw, and G. Koper, The use of reflectometry for the study of swelling of latex particles at a silica surface, in Optical Methods and Physics of Colloidal Dispersions1997, Springer. p. 107-109.

[124] Cioffi, N., et al., Deposition and analytical characterization of fluoropolymer thin films modified by palladium nanoparticles. Thin Solid Films, 2004. **449**(1-2): p. 25-33.

[125] Chan, K. and K.K. Gleason, Initiated chemical vapor deposition of linear and cross-linked poly(2-hydroxyethyl methacrylate) for use as thin-film hydrogels. Langmuir, 2005. **21**(19): p. 8930-8939.

[126] Horcajada, P., et al., Colloidal route for preparing optical thin films of nanoporous metal-organic frameworks. Advanced Materials, 2009. **21**(19): p. 1931-1935.

[127] Abuin, G.C., M. Cecilia Fuertes, and H.R. Corti, Substrate effect on the swelling and water sorption of Nafion nanomembranes. Journal of Membrane Science, 2013. **428**: p. 507-515.

[128] Warenda, M., et al., Fabricating pH-Stable and Swellable Very Thin Hyperbranched Poly(ethylene imine)–Oligosaccharide Films Fabricated Without Precoating: First View on Protein Adsorption. Macromolecular Rapid Communications, 2012. **33**(17): p. 1466-1473.

[129] Horn, N.R. and D.R. Paul, Carbon dioxide plasticization and conditioning effects in thick vs. thin glassy polymer films. Polymer, 2011. **52**(7): p. 1619-1627.

[130] Carlà, V., et al. Modeling solubility isotherms and sorption kinetics of supercritical carbon dioxide in initially glassy polymers using non-equilibrium thermodynamics. 2006.

[131] Carlà, V., et al., Modeling Sorption Kinetics of Carbon Dioxide in Glassy Polymeric Films Using the Nonequilibrium Thermodynamics Approach. Industrial & Engineering Chemistry Research, 2009. **48**(8): p. 3844-3854.

[132] Collins, R.W. and B.Y. Yang, In situ ellipsometry of thin film deposition: Implications for amorphous and microcrystalline Si growth. Journal of Vacuum Science & Technology B: Microelectronics and Nanometer Structures, 1989. **7**(5): p. 1155-1164.

[133] Jellison, G.E., Jr., M.F. Chisholm, and S.M. Gorbatkin, Optical functions of chemical vapor deposited thin film silicon determined by spectroscopic ellipsometry. Applied Physics Letters, 1993. **62**(25): p. 3348-3350.

[134] Elwing, H., Protein absorption and ellipsometry in biomaterial research. Biomaterials, 1998. **19**(4–5): p. 397-406.

[135] Spuller, M.T., R.S. Perchuk, and D.W. Hess, Evaluating photoresist dissolution, swelling, and removal with an in Situ film refractive index and thickness monitor. Journal of the Electrochemical Society, 2005. **152**(1): p. G40-G44.

[136] Foose, L.L., H.W. Blanch, and C.J. Radke, Effect of sodium dodecylbenzene sulfonate on subtilisin carlsberg proteolysis of an immobilized ovalbumin film. Biotechnology and Bioengineering, 2009. **102**(4): p. 1273-1277.

[137] Wessling, M., et al., Plasticization of gas separation membranes. Gas Separation & Purification, 1991. **5**(4): p. 222-228.

[138] Wessling, M., et al., Dilation kinetics of glassy, aromatic polyimides induced by carbon dioxide sorption. Journal of Polymer Science Part B: Polymer Physics, 1995. **33**(9): p. 1371-1384.

[139] Berens, A.R. and H.B. Hopfenberg, Diffusion and relaxation in glassy polymer powders: 2. Separation of diffusion and relaxation parameters. Polymer, 1978. **19**(5): p. 489-496.

[140] Born, M., E. Wolf, and A.B. Bhatia, Principles of Optics: Electromagnetic Theory of Propagation, Interference and Diffraction of Light2000: Cambridge University Press.

[141] Sirard, S.M., et al., Spectroscopic ellipsometry of grafted poly(dimethylsiloxane) brushes in carbon dioxide. The Journal of Supercritical Fluids, 2004. **32**(1–3): p. 265-273.

[142] Flory, P.J., Principles of Polymer Chemistry1953: Cornell University Press, Ithaca, New York.

[143] Flory, P.J. and J.J. Rehner, Statistical Mechanics of Cross-Linked Polymer Networks II. Swelling. The Journal of Chemical Physics, 1943. **11**(11): p. 521-526.

[144] Schneider, M.F., et al., Thermodynamic properties and swelling behavior of glycolipid monolayers at interfaces. Journal of Physical Chemistry B, 2001. **105**(22): p. 5178-5185.

[145] Rehfeldt, F., et al., Static and dynamic swelling of grafted poly(2-alkyl-2-oxazoline)s. Langmuir, 2002. **18**(12): p. 4908-4914.

[146] Lavalle, P., et al., Comparison of the Structure of Polyelectrolyte Multilayer Films Exhibiting a Linear and an Exponential Growth Regime: An in Situ Atomic Force Microscopy Study. Macromolecules, 2002. **35**(11): p. 4458-4465.

[147] Dubas, S.T. and J.B. Schlenoff, Swelling and Smoothing of Polyelectrolyte Multilayers by Salt. Langmuir, 2001. **17**(25): p. 7725-7727.

[148] Suárez, M.F. and R.G. Compton, In situ atomic force microscopy study of polypyrrole synthesis and the volume changes induced by oxidation and reduction of the polymer. Journal of Electroanalytical Chemistry, 1999. **462**(2): p. 211-221.

[149] Takada, K., et al., Redox-Active Ferrocenyl Dendrimers: Thermodynamics and Kinetics of Adsorption, In-Situ Electrochemical Quartz Crystal Microbalance Study of the Redox Process and Tapping Mode AFM Imaging. Journal of the American Chemical Society, 1997. **119**(44): p. 10763-10773.

[150] Liu, G. and G. Zhang, Collapse and Swelling of Thermally Sensitive Poly(N-isopropylacrylamide) Brushes Monitored with a Quartz Crystal Microbalance. The Journal of Physical Chemistry B, 2004. **109**(2): p. 743-747.

[151] Rouessac, V., et al., Three characterization techniques coupled with adsorption for studying the nanoporosity of supported films and membranes. Microporous and Mesoporous Materials, 2008. **111**(1–3): p. 417-428.

[152] Lee, D., et al., pH-Induced Hysteretic Gating of Track-Etched Polycarbonate Membranes: Swelling/Deswelling Behavior of Polyelectrolyte Multilayers in Confined Geometry. Journal of the American Chemical Society, 2006. **128**(26): p. 8521-8529.

[153] Furchner, A., et al., In-situ characterization of the temperature-sensitive swelling behavior of poly(N-isopropylacrylamide) brushes by infrared and visible ellipsometry. Thin Solid Films, 2013. **541**: p. 41-45.

1.12. Summary of the *in-situ* ellipsometry studies included in the review

Number	Polymeric material studied	Penetrant	*In-situ* configuration	Type of ellipsometer used (device/manuf.)	Modeling
1	PMMA	Methyl isobutyl ketone, 2-propanol, methanol	Near atmospheric *in-situ* cell	Single-element rotating-polarizer (AME-500) and home built ellipsometer	Two-layer, moving front model
2	PMMA, PS	Chloroform, toluene	Near atmospheric *in-situ* cell	Not specified	Direct calculation from Fresnel relations
3	Polyimides, polyimide resin, PES	Vapors: water, methanol, ethanol, 2-propanol	Near atmospheric *in-situ* cell	Not specified	Anisotropic model for dry films
4	PMMA	Sc-CO_2	High pressure *in-situ* cell	Spectroscopic (M-44, J.A. Woollam Co. Inc.)	Uniform model
5	PMMA, PS	CO_2 up to 60 bar	High pressure *in-situ* cell	Spectroscopic (J.A. Woollam Co. Inc.)	Uniform model
6	Cellulose	Water vapor	No cell, point humidity delivery	632.8 nm He-Ne laser (Plasmos GmbH Prozesstechnik)	Direct calculation from Fresnel relations
7	PMMA	Toluene	No cell	Spectroscopic (VASE, J.A. Woollam Co. Inc.)	Uniform model
8	Polyimide 6FDA-DAM:DABA 2:1	CO_2 up to 100 bar	High pressure *in-situ* cell	Spectroscopic (M-44, J.A. Woollam Co. Inc.)	Uniform model
9	Polyimide, PES	Water vapor	Near atmospheric *in-situ* cell	Spectroscopic (M-44, J.A. Woollam Co. Inc.)	Anisotropic model
10	PS, poly(2-vinyl pyridine), poly(tert-butyl methacrylate) and their copolymers	Vapors of toluene, chloroform, tetrahydrofurane	Near atmospheric *in-situ* cell	Spectroscopic (SENTECH SE 850)	Uniform model

Substrate	Phenomena studied	Information extracted with ellipsometry	Other *in-situ* techniques used	Remarks	Reference
Si wafer	Case II diffusion and dissolution	Swollen film thickness changes	-	-	[17-20]
Si wafer	Penetrant diffusion	Penetrant concentrations by Lorentz-Lorenz formula	-	-	[79, 83]
Si wafer	Vapor sorption	Swollen film thickness changes	-	Optical anisotropy of dry layers determined	[33]
Si wafer and GaAs wafer	Penetrant sorption and penetrant induced glass transition	Layer swelling and refractive index changes	-	-	[54]
Si wafer	P_g as function of film thickness	Ψ and Δ curvature changes at P_g	-	Attempts at modeling adsorbed CO_2 as extra layer	[69, 81]
Si wafer	Hydration forces, disjoining pressure	Swollen film thickness changes	-	-	[36]
Si wafer	Drying	Film thickness changes	-	-	[53, 60]
Si wafer	Penetrant sorption and relaxation	Penetrant volume fraction from Clausius - Mossotti	-	-	[70, 71]
Si wafer	Swelling dynamics	Swollen film thickness	-	-	[86, 87]
Si wafer	Swelling and penetrant uptake	Penetrant volume fractions from swelling and interaction parameters	-	-	[80]

Number	Polymeric material studied	Penetrant	*In-situ* configuration	Type of ellipsometer used (device/manuf.)	Modeling
11	Polyimide	Liquid water	No cell	Spectroscopic (VASE, J.A. Woollam Co. Inc.)	Uniform model
12	PMMA	CO_2 up to 100 bar	High pressure *in-situ* cell	Spectroscopic (J.A. Woollam Co. Inc.)	Uniform model
13	Cellulose	Liquid water, variable pH	Near atmospheric *in-situ* cell	Spectroscopic (M-2000, J.A. Woollam Co. Inc.)	Uniform model
14	Hyperbranched polyesters	Water vapor	Near atmospheric *in-situ* cell	Spectroscopic (M-44, J.A. Woollam Co. Inc.)	Uniform model
15	PEI – oligosaccharide	Liquid water, variable pH	Near atmospheric *in-situ* cell	Spectroscopic (alpha-SE, J.A. Woollam Co. Inc.)	Uniform model
16	PAH and PAA multilayers	Water vapor	Humidity controlled glove box	Reflectometer (Filmetrics, F20)	Direct calculation from Fresnel relations
17	Polyelectrolyte multilayer, PS and PMMA	Water vapor	-	-	Uniform model
18	Polyelectrolyte multilayer	Liquid water, variable pH	Near atmospheric *in-situ* cell	Spectroscopic (M-2000D, J.A. Woollam Co. Inc.)	Uniform model
19	PFOMA, PS, PEO, and diblock copolymer of PS-*b*-PFOMA	Sc-CO_2	High pressure *in-situ* cell	Spectroscopic (M-44, J.A. Woollam Co. Inc.)	Uniform model
20	Polyetherimides, PEBAX, SPEEK, Matrimid	CO_2 up to 50 bar	High pressure *in-situ* cell	Spectroscopic (alpha-SE, J.A. Woollam Co. Inc.)	Uniform model

Substrate	Phenomena studied	Information extracted with ellipsometry	Other *in-situ* techniques used	Remarks	Reference
Si wafer	Swelling and penetrant uptake	Penetrant volume fraction with EMA	Contact angle	3 angles used 65, 70 and 75°	[62]
Si wafer	Penetrant sorption and penetrant induced glass transition	Penetrant concentration from Clausius - Mossotti	QCM to compare thin film with bulk sorption	-	[73]
Glass slides	Charging and swelling	Swollen film thickness	Electrochemical methods	-	[85]
Si wafer	Swelling and simple swelling dynamics	Swollen film thickness	Zeta potential, contact angle	-	[121]
Si wafer and Thermal oxide	Swelling and stability in different pH	Swollen film thickness	ATR-IR, zeta potential	-	[128]
Si wafer	Swelling – deswelling hysteresis	Relative swelling	-	-	[63]
Si wafer	Swelling and mechanical properties	Swollen film thickness	Buckling	-	[82]
Si wafer	Swelling and reversible gating of pores in thin membranes	Swollen film thickness	AFM	-	[152]
Si wafer	Anomalous swelling maxima near critical CO_2	Swollen film thickness	-	-	[75]
Glass slides	Swelling – deswelling hysteresis	Swelling degree, penetrant concentration with Clausius- Mossotti	-	-	[48]

Number	Polymeric material studied	Penetrant	*In-situ* configuration	Type of ellipsometer used (device/manuf.)	Modeling
21	Poly(3-hexylthiophene)	CS_2 vapors	Near atmospheric *in-situ* cell	Single wavelength, imaging ellipsometer (Accurion)	Uniform model
22	PMMA	Bromobenzene	No cell	Spectroscopic (WVASE, J.A. Woollam Co. Inc.)	Uniform model
23	PPO, Matrimid, PSF, PS	CO_2 up to 45 bar	High pressure *in-situ* cell	Spectroscopic (M-2000D, J.A. Woollam Co. Inc.)	Uniform model
24	PMMA	Liquid water	No cell	M-150 (JASCO Co., Ltd.)	Uniform model
25	PS	Liquid n-hexane	Near atmospheric *in-situ* cell	Spectroscopic (M-2000X, J.A. Woollam Co. Inc.)	Uniform and Two-layer model
26	PS	Liquid n-hexane	Near atmospheric *in-situ* cell	Spectroscopic (M-2000X, J.A. Woollam Co. Inc.)	Uniform and Two-layer model
27	PSF, Matrimid	Water vapor	Near atmospheric *in-situ* cell	Spectroscopic (WVASE, J.A. Woollam Co. Inc.)	Uniform model
28	PDMS and its derivatives, polyurethane	Vapors of cyclohexane, toluene and tetrachloroethane	Near atmospheric *in-situ* cell	Spectroscopic (ES4G, SOPRA)	Uniform model
29	Posimca50	Ammonia in water vapor	Near atmospheric *in-situ* cell	Spectroscopic (ES4G, SOPRA)	Uniform model
30	PDMS, non-crosslinked	Sc-CO_2	High pressure *in-situ* cell	Spectroscopic (M-44, J.A. Woollam Co. Inc.)	Uniform model

Substrate	Phenomena studied	Information extracted with ellipsometry	Other *in-situ* techniques used	Remarks	Reference
Glass slides	Crystallization as function of solvent vapor activity	Polymer fraction from dilation	UV-VIS	Fitting of single wavelength data over multiple angles (for dry films)	[47]
Si wafer	Drying	Thickness, EMA calculations of penetrant, polymer and microporosity (free volume) fractions	-	Bromobenzene (high index solvent) used to enhance contrast	[61]
Si wafer	Sorption, relaxation and aging of films	Penetrant concentration with Clausius - Mossotti	-	-	[74]
Si wafer	Sorption of water in as spun and annealed PMMA films	Thickness and index of film during drying after formation	Neutron reflectivity	-	[84]
Si wafer	Sorption and relaxation kinetics	Swelling dynamics	-	-	[23]
Si wafer	Sorption kinetics	Swelling dynamics	-	-	[24]
Si wafer	Water sorption in microporosity of glassy polymers	Penetrant volume fraction	Gravimetric sorption	-	[88]
Si wafer with 250 nm thermal oxide	Penetrant sorption	Swelling	-	-	[89, 90]
Si wafer	Penetrant sorption and pH responsiveness	Swelling	IR spectroscopy	-	[91]
Si wafer	Penetrant sorption	Swelling, and penetrant mass concentration from Clausius - Mossotti	-	First high pressure study	[65]

Number	Polymeric material studied	Penetrant	*In-situ* configuration	Type of ellipsometer used (device/manuf.)	Modeling
31	PDMS	Liquid n-hexane up to 100 bar	High pressure *in-situ* cell	Spectroscopic (M-2000X, J.A. Woollam Co. Inc.)	Uniform model
32	PEG-PMMA block copolymer	Water vapor and liquid	Near atmospheric *in-situ* cell	Spectroscopic (J.A. Woollam Co. Inc.)	Uniform model
33	PS-*b*-PVP	Vapors of toluene	Near atmospheric *in-situ* cell	Spectroscopic (SE 850, SENTECH)	Uniform model
34	PS-*b*-polyisoprene	Sc-CO_2	High pressure *in-situ* cell	Spectroscopic (GES-5, SOPRA)	Uniform model
35	SSEBS	Liquid water	Near atmospheric *in-situ* cell	Spectroscopic (WVASE, J.A. Woollam Co. Inc.)	Uniform model
36	PS-*b*-polybutadiene	Vapors of chloroform	Near atmospheric *in-situ* cell	Spectroscopic (SE 850, SENTECH)	Uniform model
37	PNIPAM-co-PAA microgels	Liquid water	Near atmospheric *in-situ* cell	632.8 nm He-Ne laser (Optrel Multiskop)	Direct calculation
38	p(HEMA-co-EGDA)	Liquid water	Near atmospheric *in-situ* cell	Spectroscopic (M-2000, J.A. Woollam Co. Inc.)	Uniform model
39	Zwitterionic polymer	Liquid water and NaCl solutions	Near atmospheric *in-situ* cell	Spectroscopic (M-2000X, J.A. Woollam Co. Inc.)	Uniform, Graded and Anisotropic models
40	Composite of polyDADMAC and Laponite RD	Water vapor	Near atmospheric *in-situ* cell	632.8 nm He-Ne laser (Auto-EL III, Rudolph)	Direct calculation from Fresnel relations

Substrate	Phenomena studied	Information extracted with ellipsometry	Other *in-situ* techniques used	Remarks	Reference
Si wafer, glass slide, porous AKP	Swelling changes under non-equilibrium conditions	Swelling, penetrant volume fraction with EMA	-	Cell with permeation possibility	[8]
Au coated QCM crystal	Swelling induced transitions in mechanical properties	Swelling dynamics, penetrant volume fraction from dilation and EMA	QCM	-	[39]
Si wafer	Swelling in confinement	Swelling dynamics	-	-	[94]
Si wafer	Scaling behavior in block copolymers	Swelling, penetrant volume fraction and interaction parameters	-	-	[76]
Glass substrate	Penetrant sorption	Swelling, penetrant volume fraction by EMA	Electrochemical methods	-	[96]
Si wafer	Order-disorder transitions in block copolymers	Swelling dynamics, polymer volume fraction from dilation	-	-	[95]
Si wafer	Thermally induced swelling transitions	Thickness and refractive index	-	Cell with variable angles of incidence	[93]
Si wafer	Mesh size determination in cylinder forming block-copolymers	Swelling, interaction parameters	UV-VIS	-	[97]
Si wafer	Dynamic swelling and relaxation	Dynamic swelling, density gradients and optical anisotropy	-	-	[16]
Si wafer with various oxide thicknesses	Sorption and swelling, hole filling and Henry sorption	Thickness and refractive index	QCM	Plastic bag with holes cut for windows	[34]

Number	Polymeric material studied	Penetrant	*In-situ* configuration	Type of ellipsometer used (device/manuf.)	Modeling
41	PANI	Liquid water	Near atmospheric *in-situ* cell	632.8 nm He-Ne laser (L116C, Gaertner)	Direct calculation from Fresnel relations
42	Hydrogel based on methacrylate and PC	Liquid water, variable pH	Near atmospheric *in-situ* cell	Spectroscopic (WVASE, J.A. Woollam Co. Inc.)	Uniform model
43	PAH/PSS and PAH/PAA multilayers	Liquid water, variable pH	Near atmospheric *in-situ* cell	Spectroscopic (M-44, J.A. Woollam Co. Inc.)	Uniform model
44	calixarenes	Vapors of toluene, p-xylene, aniline, n-hexane, chloroform	Near atmospheric *in-situ* cell	632.8 nm He-Ne laser (3M, LEF)	Direct calculation from Fresnel relations
45	Zwitterionic polymers based on PC	Liquid water	Near atmospheric *in-situ* cell	Spectroscopic (WVASE, J.A. Woollam Co. Inc.)	Uniform and graded models
46	PAH modified by $Os(bpy_2(ClPhCOH]^+$ and glucose oxidase	Liquid water	Near atmospheric *in-situ* cell	3 different wavelengths (2000FT, Rudolf Research)	Uniform model
47	Palladium – fluoropolymer composites	Vapors of acetone, 2-propanol, tetrachloromethane	Near atmospheric *in-situ* cell	632.8 nm He-Ne laser (Jobin Yvon-Sofie)	Direct calculation from Fresnel relations
48	PLL/PGA multilayers	Liquid water, variable pH and temperature	Near atmospheric *in-situ* cell	401.5 nm (436, Rudolf Research)	Direct calculation from Fresnel relations
49	PEG lipid monolayers, polysaccharides	Water vapor	Near atmospheric *in-situ* cell	632.8 nm He-Ne laser (Plasmos GmbH)	Direct calculation from Fresnel relations
50	PAA/PAH multilayers	Liquid water, variable pH	Near atmospheric *in-situ* cell	632.8 nm He-Ne laser (Multiskop, Optrel)	Direct calculation from Fresnel relations

Substrate	Phenomena studied	Information extracted with ellipsometry	Other *in-situ* techniques used	Remarks	Reference
Au coated QCM crystal	Swelling in response to redox cycles	Thickness and refractive index, changes in light absorption	QCM and electrochemical methods all concurrently	-	[40]
Si wafer	Protein adsorption on swollen hydrogels	Swelling and adsorption	Neutron reflection	In some cases index fixed due to low film thickness (>5 nm)	[114, 115]
Au and Ti coated Si wafers	Swelling and ion permeability changes, long term stability	Swelling	Electrochemical methods	-	[44]
Au coated glass slide	Swelling and kinetics of response to penetrants	Swelling dynamics	QCM and surface plasmon resonance	-	[41, 42]
Si wafer	Complex diffusion and relaxation, effect of annealing	Swelling dynamics, water fraction from dilation	Neutron reflection, gravimetric method	-	[14, 15]
Au coated QCM crystal	Redox transitions in multilayer polyelectrolytes	Thickness and refractive index	Concurrently with QCM and electrochemical methods	-	[45, 154]
Si wafer	Response of the layers to organic vapors	Swelling	QCM	Low vacuum experimental cell	[124]
Si wafer with Ti or thermal oxide layer	Stability, temperature and pH induced changes	Swelling	-	-	[101]
Si wafer with thermal oxide	Sorption and sorption kinetics	Swelling, water fraction with EMA and disjoining pressure	AFM	Also point humidity delivery cell	[38, 155]
Si wafer	Complex swelling behavior	Swelling dynamics	-	Observation of Super Case II diffusion	[102]

Number	Polymeric material studied	Penetrant	*In-situ* configuration	Type of ellipsometer used (device/manuf.)	Modeling
51	PDMDAAS-SiO_2 composites	Liquid water	Near atmospheric *in-situ* cell	Spectroscopic (VASE, J.A. Woollam Co. Inc.)	Uniform model
52	HA/PAH multilayers	Liquid water, variable pH and ionic strength	Near atmospheric *in-situ* cell	632.8 nm He-Ne laser (Gaertner)	Direct calculation from Fresnel relations
53	PHEMA via iCVD	Liquid water	Near atmospheric *in-situ* cell	Spectroscopic (VASE, J.A. Woollam Co. Inc.)	Uniform model
54	PAH containing multilayers	Liquid water, variable pH	Near atmospheric *in-situ* cell	632.8 nm He-Ne laser (Gaertner)	Direct calculation from Fresnel relations
55	HA/chitosan, PSS/PDADMAC, and PSS/PAH multilayers	Liquid water	Near atmospheric *in-situ* cell	Spectroscopic (M-44, J.A. Woollam Co. Inc.)	Uniform model
56	Ferrous ion and 2,2'-bipyridine in thin Nafion films	Liquid water, NaCl solution	Near atmospheric *in-situ* cell	Spectroscopic (VASE, J.A. Woollam Co. Inc.)	Uniform model with absorption (oscillators)
57	JSR photoresist	Liquid water, ethanol and water vapors	Near atmospheric *in-situ* cell	Spectroscopic (VASE, J.A. Woollam Co. Inc.)	Uniform model
58	Hydroxyl-terminated hyperbranched aromatic polyesters	Liquid water, buffer solution	Near atmospheric *in-situ* cell	Spectroscopic (M-44, J.A. Woollam Co. Inc.)	Uniform model
59	PNIPAM microgel particles	Liquid water, variable temperature, pH and NaCl concentration	Near atmospheric *in-situ* cell	Spectroscopic (VASE, J.A. Woollam Co. Inc.)	Uniform model
60	PAArVBA multilayers	Liquid water	Near atmospheric *in-situ* cell	632.8 nm He-Ne laser (126B, Gaertner)	Direct calculation from Fresnel relations

Substr.	Phenomena studied	Information extracted with ellipsometry	Other *in-situ* techniques used	Remarks	Reference
Glass slides and ITO glass	Swelling and complex dissolution	Thickness and refractive index	Concurrently with electrochemical methods	Backside configuration	[52]
Si wafer	Swelling as function of prep. conditions, pH, ionic strength and cross-linking	Swelling	Microelectrophoresis (to track layers buildup)	-	[104]
Si wafer	Swelling as function of chemical structure, cross-linking	Swelling, water fraction with EMA	Contact angle	-	[125]
Si wafer	Swelling and stability in water as function of pH	Thickness and refractive index, swelling dynamics	AFM	-	[105]
Si wafer	Swelling correlations with permeability	Thickness and refractive index, penetrant fraction with linear EMA	Permeation experiments	-	[106]
Glass slides	Chemical reaction by changes in light absorption of the swollen layers	Complex swelling dynamics, diffusion coefficients, changes in optical absorption	-	Backside configuration	[51]
Si wafer	Dissolution, degradation and swelling	Swelling dynamics	Reflectometry	-	[135]
Si wafer with thermal oxide	Swelling behavior and surface adsorption	Swelling dynamics	Contact angle	Two-term simplified Cauchy model	[37]
Si wafer	Swelling as function of temperature, pH and ionic strength	Swelling	Streaming potential	-	[117]
Si wafer	Swelling properties as function of preparation and cross-linking	Swelling	-	-	[107]

Number	Polymeric material studied	Penetrant	*In-situ* configuration	Type of ellipsometer used (device/manuf.)	Modeling
61	Osminum bipyridine-pyridine derivatized PAH and PVS	Liquid water, various electrolytes	Near atmospheric *in-situ* cell	632.8 nm He-Ne laser (FT, Sentech)	Direct calculation from Fresnel relations
62	PVP cross-linked by electron beam irradiation	Liquid water	Near atmospheric *in-situ* cell	Spectroscopic (VASE, J.A. Woollam Co. Inc.)	Uniform model
63	iCVD methacrylic acid copolymers	Liquid water, variable pH	Near atmospheric *in-situ* cell	Spectroscopic (M-2000S, J.A. Woollam Co. Inc.)	Uniform model
64	Plasma polymerized PEG	Water vapor	Near atmospheric *in-situ* cell	Spectroscopic (M-2000V, J.A. Woollam Co. Inc.)	Uniform model
65	Ovalbumin multilayer films	Liquid water with enzymes	Near atmospheric *in-situ* cell	632.8 nm He-Ne laser (Sentech)	Direct calculation from Fresnel relations
66	MOFs	Water vapor	Near atmospheric *in-situ* cell	Spectroscopic (VASE, J.A. Woollam Co. Inc.)	Uniform model
67	Hyperbranched polyesters	Liquid water, buffer solutions	Near atmospheric *in-situ* cell	Spectroscopic (M-44 and M-2000 VI, J.A. Woollam Co. Inc.)	Uniform model, multilayer modeling
68	Linear PEI	Liquid water	Near atmospheric *in-situ* cell	Spectroscopic (M-2000, J.A. Woollam Co. Inc.)	Uniform model
69	PDMAEMA and DNA multilayers	Liquid water	Near atmospheric *in-situ* cell	Single wavelength (Beaglehole Instruments)	Uniform model
70	Gramicidin and DMPC multilayers	Liquid water	Near atmospheric *in-situ* cell	632.8 nm He-Ne laser (-)	Direct calculation from Fresnel relations

Substrate	Phenomena studied	Information extracted with ellipsometry	Other *in-situ* techniques used	Remarks	Reference
Si coated with Ti, Pd and Au	Redox driven swelling	Swelling	Concurrently with QCM and electrochemical methods	-	[46]
Si wafer	Penetrant sorption	Swelling	-	-	[118]
Si wafer	Swelling behavior as function of pH	Swelling, water volume fraction with EMA	-	-	[98]
Si wafer	Dissolution and swelling behavior	Thickness and refractive index	-	3 angles of incidence	[119]
Si wafer	Degradation and swelling	Swelling	-	-	[136]
Si wafer	Penetrant uptake, simple swelling	Thickness and refractive index	-	-	[126]
Si wafer, glass slides	Swelling behavior for protein adsorption potential	Swelling, EMA for protein adsorption layer	IR ellipsometry	With IR ellipsometry in backside reflection	[25]
Au coated Si wafer	Electrochemically controlled swelling and mechanical properties	Thickness	AFM, QCM and electrochemical methods	-	[64]
Si wafer	Rigidity, biodegradability, call adhesion studies	Swelling, interaction parameters	AFM, QCM and electrochemical methods	-	[108]
Au coated glass	Swelling behavior as function of static electric field	Swelling	Electrochemical methods and circular dichroism	-	[109]

Number	Polymeric material studied	Penetrant	*In-situ* configuration	Type of ellipsometer used (device/manuf.)	Modeling
71	Cellulose	Liquid water, variable pH	Near atmospheric *in-situ* cell	Spectroscopic (M-44, J.A. Woollam Co. Inc.)	Uniform model
72	Hyperbranched PEI-maltose films	Liquid water	Near atmospheric *in-situ* cell	Spectroscopic (Alpha-SE, J.A. Woollam Co. Inc.)	Uniform model
73	Various triblock copolymers, multilayers	Liquid water, variable pH and temperature	Near atmospheric *in-situ* cell	Spectroscopic (VASE, J.A. Woollam Co. Inc.)	Uniform model
74	PDMS-*b*-PNIPAM multilayers, PSS	Liquid water, variable pH and temperature	Near atmospheric *in-situ* cell	632.8 nm He-Ne laser (-)	Direct calculation from Fresnel relations
75	Nafion nanomembranes	Liquid water	Near atmospheric *in-situ* cell	Spectroscopic (GES5A, SOPRA)	Uniform model
76	PSS/PDADMAC multilayers	Liquid and vapors of water	Near atmospheric *in-situ* cell	632.8 nm He-Ne laser (Optrel Multiskop)	Direct calculation from Fresnel relations
77	PSS/PDADMAC multilayers	Liquid water	Near atmospheric *in-situ* cell	Spectroscopic (M-2000D, J.A. Woollam Co. Inc.)	Uniform model
78	PAH/SPS multilayers	Liquid water, variable pH	Near atmospheric *in-situ* cell	632.8 nm He-Ne laser (Gaertner)	Direct calculation from Fresnel relations
79	PSS/PAH multilayers	Water vapor	Near atmospheric *in-situ* cell	632.8 nm He-Ne laser (Plasmos GmbH)	Direct calculation from Fresnel relations
80	PVME hydrogel	Liquid water, variable temperature	Near atmospheric *in-situ* cell	Spectroscopic (M-44, J.A. Woollam Co. Inc.)	Uniform model

Substrate	Phenomena studied	Information extracted with ellipsometry	Other *in-situ* techniques used	Remarks	Reference
Glass substrate	Swelling as function of preparation and chemical structure	Swelling	Electrochemical methods	-	[49]
Si wafer	Swelling response to nucleic acids and drugs	Swelling	-	-	[120]
Si wafer	Temperature and pH response of the triblock copolymers	Swelling	-	-	[110]
Si wafer	Temperature and pH responsive swelling	Swelling	Fluorescence and AFM	-	[111]
Au coated QCM crystal, Si wafer	Sorption as function of thickn., substrate and aging	Thickness and refractive index	QCM	Ellipsometric porosimetry used	[127]
Si wafer	Swelling as function of layer thickness and formation conditions	Swelling	AFM	-	[112]
Quartz, glass and Si wafer	Swelling behavior of laterally graded (thickness) layers	Thickness and refractive index	-	-	[113]
Si wafer	Reversibility of swelling	Swelling	-	-	[100]
Si wafer	Swelling behavior as function of number of layers deposited	Swelling	Contact angle	-	[103]
Si wafer, Au and glass	Temperature dependent swelling behavior	Swelling, water volume fraction from dilation	Surface plasmon resonance and optical waveguide spectroscopy	-	[50]

1.13. Scope of the Thesis

The Thesis combines studies which explore *in-situ* spectroscopic ellipsometry applicability for various processes that occur in polymer films interacting with liquid and gaseous penetrants. The investigated macromolecular systems include model glassy and rubbery structures, PS and PDMS respectively, as well as zwitterionic thin films and complex composite membranes. Penetrants range from water, aqueous salt solutions and liquid organic solvents, to high pressure fluids. Significant attention is dedicated to the superposition of nano-confinement and penetrant effects on the equilibrium and dynamic properties of the investigated systems. These combined impacts are of particular importance in membrane separations.

Chapter 2 describes a study on a transition in the diffusion mechanism of liquid n-hexane in thin PS films. It is shown that in a very narrow temperature range around room temperature, from 16 - 28 °C, the process changes characteristics from simultaneously occurring Fickian diffusion and polymer relaxation to purely relaxation limited Case II diffusion.

In **Chapter 3** the detailed optical modeling approach of the Case II diffusion, developed in **Chapter 2**, is applied to probe superimposed effects of nano-confinement and penetrant in ultra thin PS films. It is shown that a region of about 14±3 nm exists in the outer surface of these glassy films that is swollen almost instantaneously upon contact with the penetrant. These findings may have significant implications for the areas where small molecule penetrants diffuse through ultra thin glassy polymer layers, i.e. membrane separations.

The very high precision of *in-situ* spectroscopic ellipsometry is utilized in **Chapter 4** to develop a procedure to accurately determine penetrant volume fraction in thin swollen glassy polymer films. The method is based on a Bruggeman effective medium approximation and takes account for the relaxation of non-equilibrium excess fractional free volume (EFFV) of a glassy polymer upon sorption above glass transition temperature of the polymer – penetrant mixture. The newly developed method is compared to those not taking account for the EFFV relaxation, but frequently applied in literature.

Chapter 5 focuses on the sorption and relaxation processes that occur in the vicinity of the penetrant induced glass transition, P_g. It is shown for the first time, that although P_g is phenomenologically similar to thermally induced glass transition, T_g, significant differences in the dynamic behaviors exist. These differences are related to the much more pronounced polymer matrix deformation by the sorbing penetrant around P_g that seems to activate complex long term chain relaxation processes.

Chapters 6 and **7** describe dynamic *in-situ* spectroscopic ellipsometry studies on thin films of zwitterionic polymers based on sulfobetaine methacrylate and n-butylacrylate. This material represents an interesting class of polymers with a large potential in reduction of biofouling in ultrafiltration membranes. **Chapter 6** focuses on the characterization of the overshoot dynamic swelling response in the material upon exposure to 1 M NaCl solution. **Chapter 7** explores the effects of different salts and their concentration on the swelling the same polymer.

Often in membrane technology composite membranes consisting of a porous substrate and a thin separating film are employed. Application of ellipsometry to such systems has been severely limited by the size of the substrate roughness and porosity. These features resulted in unwanted probing light scattering effects. In **chapter 8** appropriate optical models that allow *in-situ* ellipsometry analysis of composite membranes are developed. The models consider the surface roughness of the support as a distinct, graded density layer and are shown to be applicable to composite membranes.

The optical models developed in **chapter 8** are utilized for the non-equilibrium, high pressure permeation investigation of thin PDMS films and membranes in **chapter 9**. The newly developed high pressure *in-situ* ellipsometry chamber is shown to be capable of investigating the membrane behavior in conditions by far exceeding the ones found in nanofiltration.

Chapter 10 extends the application of variable temperature and pressure ellipsometry to supported glassy films. In this chapter the effects of time, temperature, and pressure in the vicinity of the solvent induced glass transition are studied.

Chapter 11 provides an outlook of the remaining and interesting research questions that could be pursued. The examples are divided into several categories, highlighting the entirely new directions, follow-up studies and studies using coupling of *in-situ* ellipsometry with other techniques. Most of the content of this chapter is supported by a significant amount of preliminary results and observations.

Chapter 2

Temperature-induced transition of the diffusion mechanism of n-hexane in ultra-thin polystyrene films, resolved by *in-situ* spectroscopic ellipsometry

This chapter has been adapted from:

Ogieglo W., Wormeester H., Wessling M., Benes N.E., Polymer 2013;54(1):341-348. Copyright 2013 Elsevier

Abstract

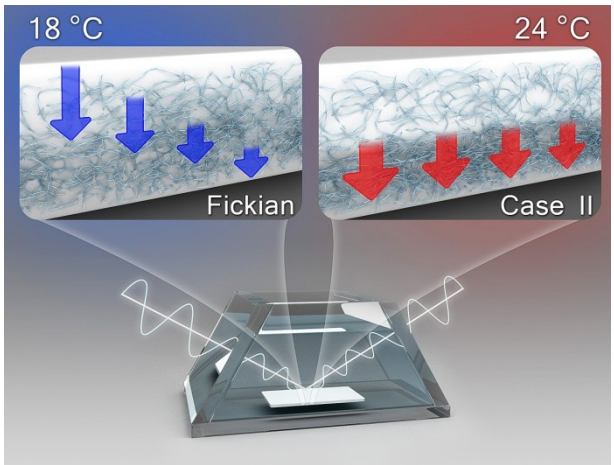

In-situ spectroscopic ellipsometry is used to study diffusion of liquid n-hexane in silicon wafer supported 150 nm thick polystyrene films, in the temperature range 16 – 28 °C. In the higher part of this temperature range Case II diffusion is shown to be dominant. For this diffusion mechanism the temporal evolution of the ellipsometric spectra is adequately described by an optical model that divides the polystyrene into a swollen layer and a non-swollen layer, separated by a sharp diffusion front, i.e. mimicking the essential characteristics of the Case II diffusion process. This description is found to be applicable for tracking of the penetrant wave progressing through films with a thickness between 100 nm – 1000 nm, covering much of the technologically important thin polymer film range. For temperatures below 20 °C the transport is shown to occur by a combination of Fickian diffusion and polymer relaxation (Fickian Relaxation). The temperature induced transition from Case II to Fickian Relaxation finds validation in the spectroscopic ellipsometry modeling and is related to the occurrence of penetrant induced glass transition in the system at around 20 °C. For the kinetics of swelling below the glass transition of the polymer - penetrant mixture Berens – Hopfenberg formalism is applied to extract the penetrant diffusion coefficient and characteristic chain relaxation time.

2.1. Introduction

Case II, non-Fickian diffusion mechanism has been widely studied for many polymer – penetrant systems, including polystyrene, poly(vinyl chloride), and poly(methyl methacrylate) as polymer matrices, and C_5 – C_8 hydrocarbons, vinyl chloride, acetone and methanol as penetrants [1-4]. Sample geometries utilized involved predominantly microspheres or powders [2], sheets [3, 4] and films with a thickness well above 1 μm [5-8]. Very little data are available on the behavior of thin films with a thickness below 1 μm. Thin films in this range are used increasingly in such areas as membranes [9, 10], coatings [11] or micro devices [12]. Particularly in membrane technology films of thickness in the order of 100 nm (referred to as ultra-thin films) have been used as selective layers, due to their low resistance for mass transport combined with high selectivity [13, 14]. There is growing evidence that ultra-thin films may show significant deviations from bulk materials with respect to such properties as glass transition and structural relaxations [15, 16], physical aging [17, 18] or plasticization resistance [9, 19]. The distinct properties of ultra-thin films are commonly assigned to an increased contribution of the interfaces (both free ambient interface, as well as substrate interface) to the overall behavior of the films. Hori et al. have recently shown that there exist interfacial regions where penetrant diffusion coefficients may deviate from the bulk values [20]. However, similar studies are still very rare mainly due to difficulties in experimental procedures applicable to *in-situ* analysis of ultra-thin films.

One suitable technique that has been employed in studies related to properties of thin and ultra-thin films is spectroscopic ellipsometry. This technique is characterized by a high accuracy, high precision and a non-destructive character. The abovementioned features, together with a possibility of very fast data acquisition of modern equipment, make spectroscopic ellipsometry particularly suitable for *in-situ* sorption studies in thin film – fluids systems [21-24]. The technique is, however, indirect and requires appropriate data analysis with utilization of an optical model in order to extract relevant sample properties, such as its thickness or refractive index. Accurate determination of these two properties is particularly important when the sample is exposed to a diffusing penetrant that causes the material to increase its volume and simultaneously reduce its density (swelling).

In this work we attempt to show the significance of appropriate data analysis and modeling in the system involving n-hexane diffusion into polystyrene films with thickness much below 1 μm. Attention is particularly put on the development of an appropriate optical model able to accurately describe the Case II kinetics of the process. Additionally, the transition from Case II diffusion to a combination of Fickian diffusion with polymer relaxation (Fickian Relaxation) in the temperature range 16 - 28 °C for ~ 150 nm polystyrene films is investigated. The temperature-

induced transition in transport mechanism is shown to be related to the occurrence of the glass transition in the investigated system in the probed temperature range.

2.2. Theory

2.2.1. Diffusion descriptions in polymer-liquid penetrant systems

Penetrant sorption in polymeric materials is commonly described by the Berens – Hopfenberg model [1], which attempts to separate the Fickian from the non-Fickian, or relaxational, contributions. The model adapted for unidirectional sample dilation (thin, confined films), according to ref. [25], allows extracting the diffusion coefficients of the penetrant, as well as the characteristic polymer relaxation time, by fitting the experimental dilation curves to the following equation:

$$S_T = S_{F,\infty} \cdot \left[1 - \frac{8}{\pi^2}\sum_{m=0}^{\infty}\frac{1}{(2m+1)^2} \cdot exp\left\{-\frac{D(2m+1)^2\pi^2 t}{h^2}\right\}\right] + \\ +S_R\left[1 - exp\left\{-\frac{t}{\tau_R}\right\}\right] \quad (2.1)$$

In eq. 2.1 S_T, $S_{F,\infty}$ and S_R represent the total, Fickian and relaxational contributions to the overall swelling of the sample. h is the sample thickness, t is the time, and τ_R the polymer characteristic relaxation time. In $S_{F,\infty}$ the ∞ sign indicates equilibrium Fickian swelling in unrelaxed polymer. The swelling percentage is defined in eq. 2.2 as:

$$S = \frac{h_S - h_D}{h_D} \cdot 100\% \quad (2.2)$$

where h_S and h_D are the swollen and dry polymer film thicknesses, respectively. The model, however, is not applicable to the anomalous Case II diffusion, in which the mass uptake is linearly proportional to time. The occurrence of Case II diffusion is associated with a sharp penetrant wave traveling through the swelling film at a constant velocity. This is often expressed by a value of exponent $w = 1$ in the general swelling vs. time relationship:

$$S(t) = const \cdot t^w \quad (2.3)$$

The observed average front velocity, v, can then be expressed as:

$$v = \frac{h_D}{t_{eq}} \quad (2.4)$$

where t_{eq} stands for the time until equilibrium swelling is reached, that is when no further thickness increase is observed. Constant velocity of the front indicates that the diffusion process is purely limited by the polymer relaxation at the front and that the diffusion resistance for the penetrant in the swollen region of the film is negligibly small. The fast diffusion of the penetrant through the swollen region is a

result of glassy to rubbery transition induced in the material at the front. In the swollen rubbery region penetrant diffusion is orders of magnitude faster than in the glassy, non-swollen core. For bulk samples the linearity of swelling versus time may eventually be lost due to relatively large dimensions of the samples [4], however, in ultra-thin films penetrant diffusion in the swollen region above penetrant induced glass transition might be considered infinitely fast.

2.2.2. Spectroscopic ellipsometry

Spectroscopic ellipsometry uses the change of polarization state of light upon reflection from, usually, multi-layer samples to obtain such sample properties as layer thickness and its refractive index. Commonly, *p*- and *s*-polarized components are distinguished, and the ratio of *p*- and *s*-reflectivities, r_p and r_s, is converted into ellipsometric parameters Ψ and Δ:

$$\rho = \frac{r_p}{r_s} = \tan(\Psi) \cdot e^{i\Delta} \quad (2.5)$$

The virtue of spectroscopic ellipsometry, compared to a reflectivity measurement, is that the measured quantities do not depend on the intensity of light reflected from the sample. This feature makes the technique suitable in various *in-situ* studies, where low light intensity might be a consequence of significant extinction of an experimental ambient.

Multiple Ψ and Δ pairs are acquired as a function of wavelength to produce an ellipsometric spectrum, which allows simultaneous determination of various sample properties. In particular, thickness and refractive index of a sample can be reliably determined from a single scan, if an appropriate optical model is used. Currently, the advances in instrumentation have allowed for dynamic studies of various systems due to relatively high time resolution (<1 s per full spectral scan). This presents particular benefits in ultra-thin film *in situ* analyses where, due to very small sample dimensions, for instance, diffusion processes are relatively fast.

One drawback of spectroscopic ellipsometry is its indirect character. To obtain useful information about the sample an optical model needs to be developed that corresponds to sample morphology as closely as possible. The data generated for a constructed optical model is fitted to experimental data. The fit quality is evaluated on the basis of a fitting error, which gives indication about confidence in sample properties determination. The error is often expressed by the Mean Square Error (MSE), which is the square root of the sum of errors between the measured and model-generated Ψ and Δ values. Generally, for simple thin film samples the MSE values of 1-2 present a good fit in the range of thicknesses around 100 nm. For thicker films, but also in *in-situ* experiments, MSE values as high as 10-20 are acceptable. Commonly, an improvement of an optical model, for example by implementation of additional parameters, is considered viable, if the resulting MSE value for the improved model is lowered by about 20-25% compared to original

model. If the improvement is less pronounced, the additional parameters are considered excessive and are omitted to avoid overparametrization [26].

2.3. Experimental part

2.3.1. Sample preparation and post-treatment

Polystyrene (Sigma Aldrich) with a molecular weight of 280 kg/mol, as determined with GPC, and glass transition temperature of 100.0 °C (DSC, onset) was used to prepare thin films. The films were spin coated from polymer solutions in toluene (Merck) onto clean silicon wafers. The resulting film thicknesses were adjusted by changing the concentration of the solution between 2.5 and 10% (w/w). The silicon wafers (111) possessed ~1.5 nm native SiO_2 layer, as determined with spectroscopic ellipsometry, which was left in place. The wafers were carefully immersed in a 3:1 volume part mixture of 98% sulfuric acid and 30% hydrogen peroxide solution to remove organic impurities. Afterwards, they were cleaned with demineralized water and flushed with dry nitrogen. Before spin coating the polystyrene solution was filtered through 0.2 µm syringe filter to ensure removal of any solid impurities.

Spin coated thin films were left to dry in air for 15 minutes and then transported to nitrogen flushed oven set at temperature of 130 °C, which was above the glass transition of the material. After at least 24 hours of annealing the samples were first quenched to room temperature and then immediately placed in another nitrogen flushed oven to physically age at 35 °C. Each of the samples of approximately 150 nm thickness, to be used for n-hexane swelling in the temperature range 16-28 °C, were aged for exactly 60 minutes before the *in-situ* spectroscopic ellipsometry measurement was started. The assurance of exactly the same thermal history of the samples was necessary since the process of diffusion in glassy polymers is non-equilibrium state dependent. In particular, the influence of the physical aging is known [27].

2.3.2. *In-situ* spectroscopic ellipsometry setup

For all measurements a spectroscopic ellipsometer M-2000X (J.A. Woollam Co., Inc.) was used with light reflected at 70° angle of incidence and a spot size of 2 mm in diameter. Ψ and Δ pairs over a wavelength range of 340 – 1000 nm, with spectral resolution of about 2 nm were recorded. The intensity and amount of depolarization of the reflected light were determined as well. The latter is important for the verification of the presence of sample imperfections, for example layer thickness variations within the measured spot. Such effects, if not taken into account properly, lead to inaccurate model values of the ellipsometric parameters. The Complete EASE v.4.64 software package (J.A. Woollam Co., Inc.) was used both to control the instrument, as well as for the data analysis and modeling. For

the *in-situ* measurements the data recording was performed continuously approximately every 2 seconds allowing for a very high time resolution.

For swelling experiments an *in-situ* homemade glass cell with an inner volume of about 70 ml was used. The 5 mm thick glass windows were positioned perpendicular to the light beam and were transparent in the employed wavelength range. The cell was equipped with a temperature control system ensuring the stability of the desired temperature of both the thin film sample and the penetrant. For all measurements the data were corrected for the residual polarization by the windows. This window correction was obtained from a sample with a 25 nm thick SiO_2 layer on a Si wafer. It was found that for 150 nm polystyrene films the window corrections did not influence the modeling results significantly.

2.3.3. Experimental procedure

Both n-hexane and polystyrene could be considered transparent in the used wavelength range [28] (extinction coefficient, k = 0), and thus their optical dispersion was described with a Cauchy formula:

$$n(\lambda) = A + \frac{B}{\lambda^2} + \frac{C}{\lambda^4} \qquad (2.6)$$

In the Cauchy formula A, B and C are adjustable fitting parameters describing the refractive index, n, dependence on light wavelength, λ. The optical dispersion of n-hexane was determined by first performing a full spectral scan of a pure silicon wafer (with native oxide) inside the cell and hence obtaining its optical characteristics. Subsequently, the cell was filled with liquid n-hexane and equilibrated at the desired temperature. After equilibration the spectrum was measured again and the refractive index dispersion of the solvent was fitted as an ambient against the known dispersion of the pure silicon wafer. This procedure was found to result in n-hexane refractive index in agreement within ±0.001 of the literature values [28].

Swelling experiments were performed according to the following protocol. Every time a fresh polymer sample with exactly the same thermal history (24 hours annealing at 130 °C followed by 60 minutes aging at 35 °C for 150 nm films) was used. The aged sample was taken out of the oven and placed inside the *in-situ* cell. Its thickness and optical index dispersion, fitted to eq. 2.6, were determined, and immediately afterwards the cell was filled with n-hexane pre-equilibrated at the desired temperature. The recording of Ψ and Δ parameters was started ~40 seconds after addition of the n-hexane. The time was required to correct for a slight misalignment of the system caused by the presence of the liquid and to ensure settling of its level. The acquisition was continued until the swelling of the polymer reached equilibrium.

2.4. Results and discussion

2.4.1. Spectroscopic ellipsometry optical model for Case II diffusion

Typical Ψ spectra recorded during n-hexane swelling experiments are shown in Figure 2.1. The spectrum for a dry sample, obtained directly before the swelling experiment, is also presented. Compared to the dry sample (n_{DS} = 1.585), Ψ oscillation amplitudes for the swollen films are significantly dampened after addition of n-hexane to the measurement cell. This is because the refractive index of n-hexane (n_{H} = 1.370 at 26 °C) is closer to the refractive index of polystyrene, than the refractive index of air (n_{AIR} = 1.000) is. This decrease in optical contrast, and thus sensitivity of spectroscopic ellipsometry, is often observed during *in-situ* experiments. Here, the remaining optical contrast is sufficiently large to allow high accuracy and precision of the data analysis. With time progression from 1 minute to equilibrium the spectra of the swollen film show a shift towards longer wavelengths accompanied with a further reduction of the amplitude. The shift is related to an increase of thickness as a result of swelling. The reduction in the amplitude is a consequence of a further decrease in the refractive index of the film, and thus the decrease in density, upon penetrant sorption. These changes in spectra can be quantified in terms of changes in film thickness and refractive index, provided that a valid optical model is available.

The analysis of the process of n-hexane diffusion into the films is carried out using optical models schematically presented in Figure 2.2. All of the models consist of

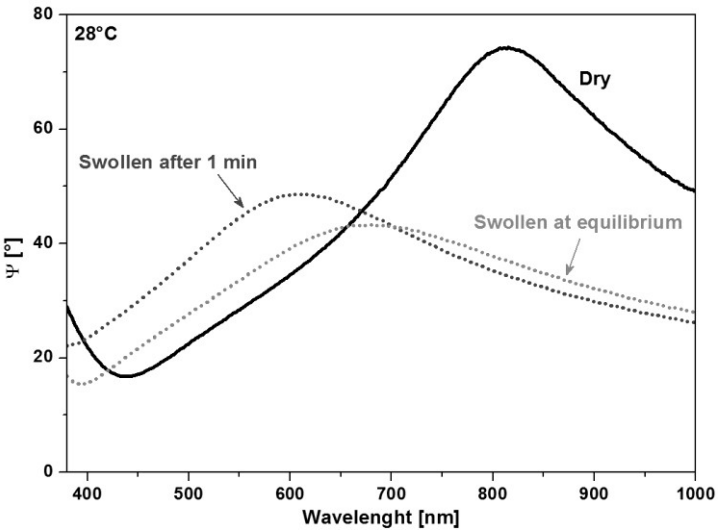

Figure 2.1 Ψ spectrum of a swollen sample compared with the Ψ spectrum for a dry sample

several optically different layers representing the polymer film, as well as the silicon substrate and the ambient medium in contact with the film. In Figure 2.2 the thin native silicon oxide layer is not included for clarity, but its influence is taken into account in the modeling. Data analysis results based on the most simple Single Layer model (Figure 2.2a) are plotted in Figure 2.3, which shows the thickness of

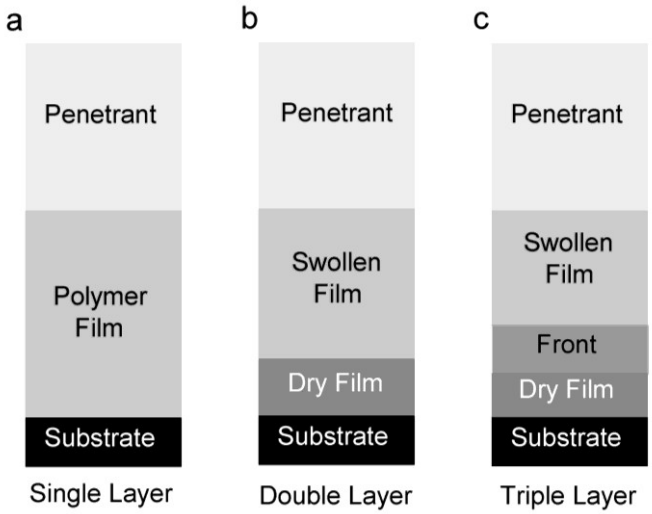

Figure 2.2 Schematics of the optical models utilized in this work

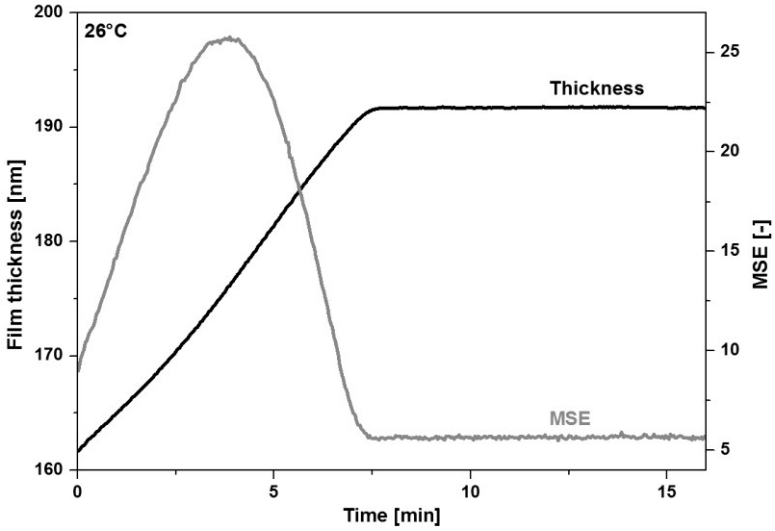

Figure 2.3 Thickness and MSE variations during the n-hexane swelling of a 158 nm polystyrene film at 26 °C; data obtained with a Single Layer model (Figure 2.2a)

the film and the MSE as a function of time for a 158 nm thin film. The swelling was recorded at 26 °C. The Single Layer model assumes uniform properties of the polymer film over the whole period of the experiment, and numerically fits the film thickness and the three Cauchy coefficients.

It has been found, that for ~150 nm films the Single Layer model captures the essential characteristics of the Case II diffusion process, which dominates at that temperature. In the first 8 minutes, the thickness of the film changes linearly with time, which agrees with the steady movement of a diffusion front from the liquid-film interface towards the silicon substrate. After ~8 minutes the film thickness reaches a constant value, indicating that the front has reached the silicon substrate and the film is uniformly swollen. The low MSE in this stage indicates that the optical properties of the film have become fairly homogeneous. The pronounced maximum value in the MSE at ~4 minutes indicates that the Single Layer model is not appropriate in this stage of the n-hexane diffusion. The maximum value of the MSE, i.e., the least accurate fit obtained with the Single Layer model, occurs at the instance when the front has reached the middle of the film. At that moment the film is effectively separated into two layers of equal thickness that are optically different. One of these layers contains a high concentration of n-hexane, the other layer is essentially non-swollen. Further advancement of the front is accompanied by a reduction in the MSE with time. After the front has reached the substrate the MSE attains a constant, relatively low value. This indicates that the refractive index is constant throughout the entire film, which can be adequately described by the Single Layer model.

The model in Figure 2.2b comprises the essential elements of Case II diffusion, i.e. the evolution of a bi-layered film with a swollen and a dry layer. This provides a model with two optically different layers whose thicknesses change with time. The sharp change in optical properties at the interface between dry and swollen state is directly related to the very sharp diffusion front for this type of mass transport. A similar bi-layer modeling approach has been used by others in investigations of relatively thick films (1 – 9 μm) of poly(methyl methacrylate) by means of laser interferometry [7, 8], and thicker films of the same material (50 – 100 μm) by optical microscopy [29]. The description of the evolution of swelling by this model requires only two fitting parameters: the thicknesses of the two distinct layers. The optical properties of the non-swollen film are assumed identical to that of the dry film. The optical properties of the swollen part are assumed identical to those of equilibrated swollen film, at the end of the measurement.

Figure 2.4 shows the variation of the swollen, dry and total thicknesses of a 158 nm polystyrene film, obtained with the Double Layer model. Both the swollen and dry parts of the film change linearly with time, and as a result produce a linear variation of the total film thickness with time. The MSE of this model has greatly

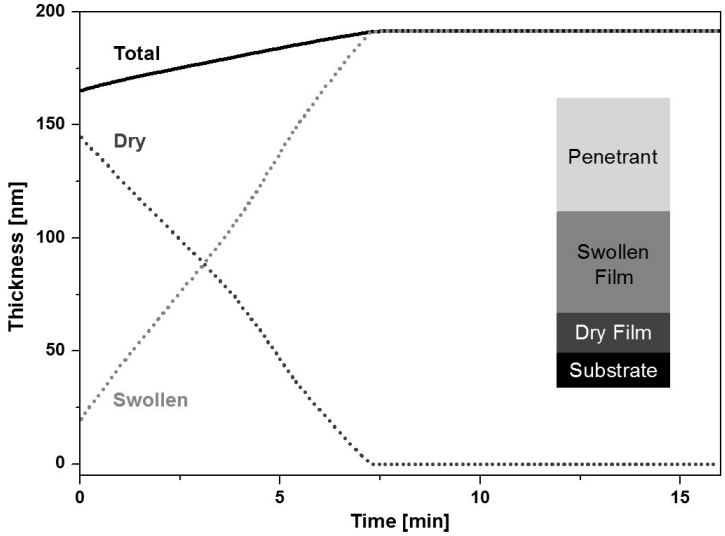

Figure 2.4 Thicknesses of the swollen and dry parts of a 158 nm polystyrene film during n-hexane sorption at 26 °C; data obtained with a Double Layer model (Figure 2.2b). Total thickness is a sum of the swollen and dry parts.

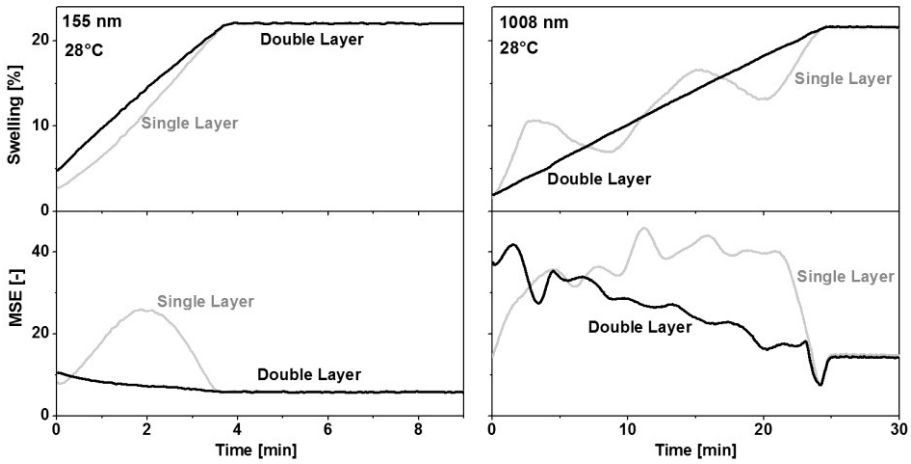

Figure 2.5 Swelling and MSE variation with time obtained with Single and Double Layer models for polystyrene films of different thicknesses

reduced (as discussed later, see Figure 2.5 bottom left), indicating that it is much more appropriate. These results show that ellipsometry is very capable of quantitatively monitoring the propagation of a penetrant induced glass transition front, traveling through a thin film.

In Figure 2.5 the results for the Single and Double Layer models are compared for a 155 nm and a 1008 nm films. At the temperature of the experiment, 28 °C, the Case II diffusion can be assumed. It is evident that the Double Layer model displays superior fit quality for both films, as indicated by the lower values of the MSE. The difference in fit quality of the two models is especially large in the case of the thinner film (155 nm) where the Double Layer yields an almost constant low value for the MSE. For the thicker film (1008 nm), the distinct differences in swelling behavior are obtained with Single Layer and Double Layer models. For the thicker film the Single Layer model is unable to adequately capture the characteristic linearity of swelling. Generally, it has been found that the thicker the sample is, the more pronounced deviation from linearity of swelling is obtained with the Single Layer model. The Double Layer model does yield a linear swelling with time, even though the MSE remains relatively large. The Double Layer modeling is found more appropriate for a film thickness in the range between 120 nm and 1008 nm at conditions where Case II transport dominates.

In the Case II transport, it is assumed that the diffusion front is very sharp. The validity of this assumption can be tested by adding an additional layer as depicted in Figure 2.2c, producing the Three Layer model. This model extends the Double Layer model by implementation of an intermediate layer between the swollen and dry parts of the polymer film. For simplification, its optical constants are considered uniform over its thickness, and equal to the arithmetic average of the

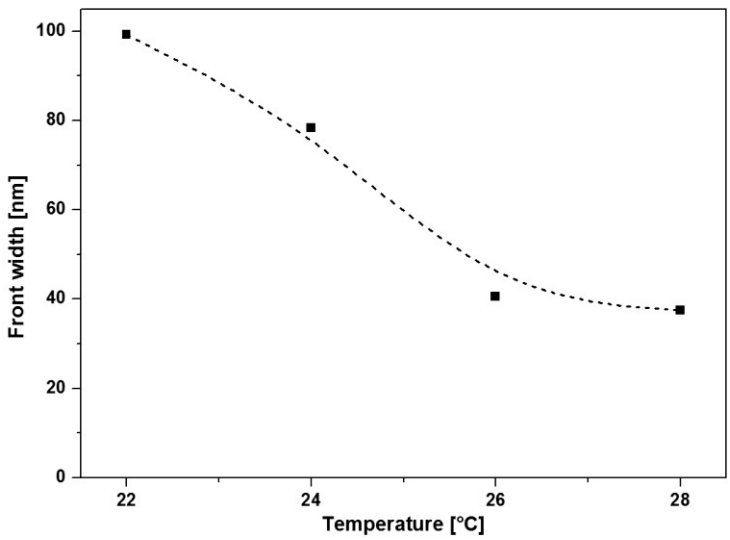

Figure 2.6 Front width values obtained with the Triple Layer model plotted against the temperature of the experiment in the range, where the Case II transport dominates

indices of the two neighboring layers. It has to be noted, that in reality, the diffusion front will possess a non-linear concentration profile. However, the introduction of additional parameters describing a non-linear front profile was found to complicate, rather than improve, the quality of the analysis. This is due to the inability of ellipsometry to decouple thickness and refractive index of the layers below about 25-30 nm, which is the anticipated order of the front width.

The front widths obtained for the experiments conducted in the temperature range 22 - 28 °C are shown in Figure 2.6. The results indicate that the front width increases with decreasing temperature, which is in agreement with experimental findings [8] and the prediction made by theoretical models of Case II diffusion [3]. In their optical reflectivity study Hassan et al have found that the sharpness of the optical signal, coming from the front itself, is reduced with decreasing temperature [8]. The finding was interpreted as a relatively steep decrease of front sharpness with temperature for all analyzed samples of polystyrene with molecular weights larger than ~14 kg/mol. Our findings are also in agreement with the model of Thomas and Windle, which predicts that predominantly the Fickian front precursor width increases with decreasing temperature [3]. The front precursor width would correspond to the front layer thickness indicated in the Triple Layer model, Figure 2.2c.

Table 2.1 shows the fit qualities, expressed as the MSE values, obtained in the middle of the linear swelling period, for all three optical models. For the higher temperatures, at 26 °C and 28 °C, particularly large reductions of the MSE are observed between the Single and Double Layer modeling. Introduction of the third layer, Triple Layer, at those temperatures reduces the MSE further only slightly. This indicates that the front width seems indeed small as compared to the total film thickness, and thus the process is captured by the Double Layer model already sufficiently well. The situation is different for the lower temperatures of sorption. At 24 °C the Double Layer model is still beneficial compared to Single Layer model, however the largest MSE reduction is observed in the case of the Triple Layer model. The particular benefit of the introduction of the third layer at this

Table 2.1 MSE of all optical models obtained in the middle of the swelling period

Temperature [°C]	MSE Single Layer	MSE Double Layer	MSE Triple Layer
28	16.3	6.3	5.9
26	16.1	4.7	4.1
24	12.1	8.9	3.9
22	7.6	14.8	2.9

temperature (24 °C) is related to the fact, that the width of the diffusion front is already significant. The front occupies a major part of the swollen film, about 80 nm according to Figure 2.6. At an even lower temperature of 22 °C the introduction of Double Layer model results in an increase in MSE. The introduction of the second layer appears not to be beneficial. The Triple Layer modeling results in a very large magnitude of the front width and a concurrent large MSE reduction. This suggests that at 22 °C the swelling process starts to lose its Case II characteristics and a large gradient in penetrant concentration, involving much of the film volume, develops.

Although the assumptions of the Triple Layer model are relatively crude, the predicted narrow front widths at higher temperatures (much less than 100 nm at 28 °C and 26 °C) are in agreement with literature predictions and experimental observations [3, 7, 30].

2.4.2. Temperature-induced transition in the range 16 °C - 28 °C

Swelling experiments of ~150 nm polystyrene films have been performed in the temperature range 16 °C - 28 °C, which covers the anticipated penetrant induced glass transition around 20 °C [4]. The particular film thickness was chosen because of the relatively simple MSE behavior for the Single Layer model, and the large fit improvements obtained, when using the Double Layer model, Figure 2.5. Direct experimental observations of Case II diffusion for this thickness range have been rarely described before [20]. The range is, however, of interest for some relevant application areas in membranes or coatings.

In Figure 2.7 the swelling of ~150 nm polystyrene films induced by liquid n-hexane in the temperature range 16 - 28 °C is presented. The thickness has been obtained using the Single Layer model. The thickness variation with time reveals a pronounced dependence of the swelling with temperature. At the higher temperatures, from 28 °C down to 22 °C, the process shows typical Case II diffusion characteristics: a linear increase of the swelling with time. In this temperature range the progress of the advancing front is controlled purely by polymer chains relaxation at the front, to allow accommodation of the penetrant. No significant diffusion resistance exists in the swollen region of the film. The average front velocity, v, is found to obey Arrhenius type temperature dependence:

$$v = K \cdot exp\left(\frac{-E_a}{R \cdot T}\right) \quad (2.7)$$

where K is a fitting constant and R is the gas constant. The activation energy E_a for the velocity of the front is calculated to be 241 kJ/mol and is in a good agreement with the literature value for the bulk, 2 mm, polymer sheets [4].

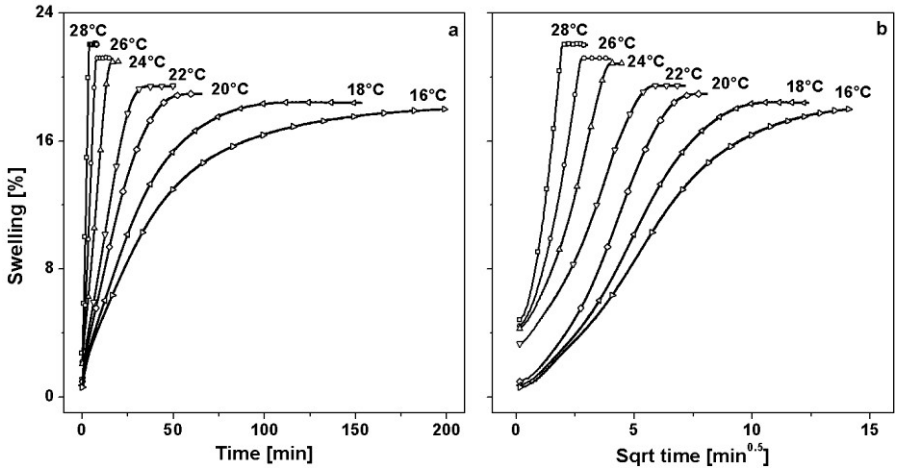

Figure 2.7 Swelling of ~150 nm polystyrene films as a function time (a) and square root of time (b) for different temperatures of liquid n-hexane sorption

As the temperature is decreased below 22 °C the curves of swelling versus time curves are no longer linear, and instead become concave with respect to the time axis. At lower temperatures the equilibrium swelling is observed after longer sorption times, and the corresponding swelling degree is lower. The emergence of this non-linear relation between swelling and time going down with the temperature is a result of a temperature-induced transition in the sorption mechanism, from Case II diffusion at higher temperature to Fickian Relaxation at lower temperatures. At higher temperatures the part of the polymer swollen by n-hexane is above glass transition, in a rubbery state. In the rubbery state the mass transport resistance is much lower as compared to the glassy state. The diffusion process is, therefore, limited by chain relaxation at the front (Case II). At lower temperatures n-hexane is unable to induce the glass transition in the swollen part and as a consequence the penetrant diffuses through a glassy polymer with much higher resistance to transport. As a result a smooth concentration profile develops and relaxation of the polymer chains accompanies the diffusion of the penetrant throughout the thickness of the film (Fickian Relaxation). In Figure 2.7b theswelling degree is depicted as a function of the square root of time. For the lower temperatures the data display the characteristic sigmoidal shape typical for Fickian Relaxation [1].

The temperature-induced transition in diffusion mechanism is also captured in the behavior of MSE of the Single and Double Layer models, presented in Figure 2.8. At 28 °C the Double Layer model yields a much lower fit error as compared to the Single Layer model. This indicates that the assumption of an infinitely thin front is applicable at this temperature. On the other hand at 16 °C the Single Layer model seems more appropriate, indicating that the assumption of two distinct layers with a

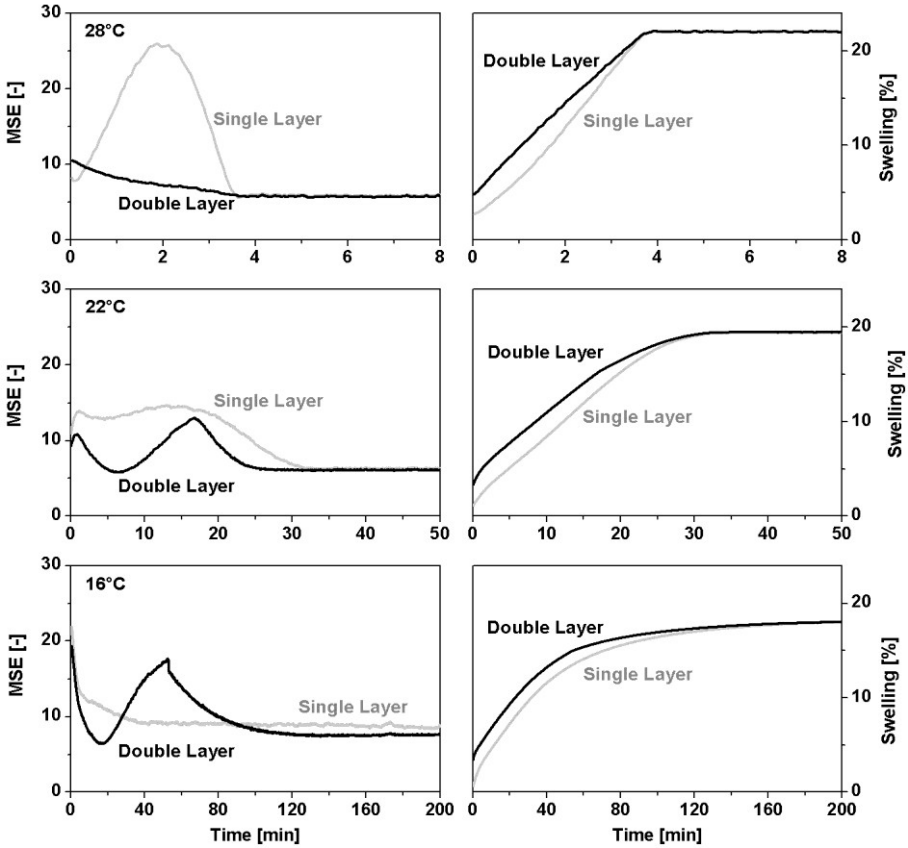

Figure 2.8 Comparison of the fitting results obtained with Single and Double Layer models around the temperature-induced transition from Case II diffusion to Fickian relaxation

sharp optical contrast no longer holds. Instead, the predominant Fickian Relaxation produces a smooth gradient of n-hexane in the film, which is better captured by the Single Layer model despite the assumption of spatially uniform optical properties of the film at any given moment in time. Below the glass transition temperature, at 16 °C, the transport resistance in the swollen layer becomes significant and prevents the persistence of a sharp front. In this case the Double Layer model becomes less adequate. Based on the MSE behavior the glass transition point is estimated between 20-22 °C, which is where, going down on a temperature scale, the MSE of Double Layer begins to be on average larger than the MSE for the Single Layer model. This approach for approximation of the glass transition temperature for penetrant swollen samples by spectroscopic ellipsometry may be applicable for other systems as well.

The curvature of the kinetic swelling in the range 16 - 20 °C, Figure 2.7, can be identified as strongly relaxation controlled diffusion with a very low liquid n-hexane diffusion coefficient in the swollen polymer [1]. This is because the polymer remains in an extensively plasticized, but glassy state. For the lowest temperature of the experiment, 16 °C, it is possible to obtain a good fit of the Berens - Hopfenberg model, given by eq. 2.1. The penetrant diffusion coefficient, Fickian and relaxational contributions to the overall swelling, as well as the characteristic polymer relaxation time can be estimated. The results of the calculations are presented in Table 2.2. The attempts to apply the Berens – Hopfenberg model to 18 °C and 20 °C result in worse fit qualities and some degree of correlation between fitting parameters. Therefore, the model is considered inapplicable to these cases.

The results show that the relaxational contribution to the overall swelling is much larger than the Fickian contribution, which indeed suggests a strongly relaxation controlled regime. The polymer relaxation time is found to be much larger than the value of τ_R = 100 s, usually set by a convention to be characteristic at the glass transition point. This confirms the glassy nature of the system at 16 °C. The obtained diffusion coefficient of n-hexane in the plasticized glassy polystyrene is, as expected, very low. The value is on the same order of magnitude as the value obtained for ultra-small spheres (534 nm) of polystyrene swollen with n-hexane, at experimental conditions interpreted by the author as relaxation controlled diffusion [31]. The n-hexane diffusion coefficient reported for the same system above the glass transition point is on the order of 10^{-10} - 10^{-11} cm^2/s in the range between 30 °C and 50 °C [5]. This means that the diffusion of the penetrant slows down 3 to 4 orders of magnitude upon crossing the glass transition point. Comparable observations were also found in other glassy polymer – penetrant systems, such as ethyl cellulose - dichloroethane [32]. Because of this large change in *D*, going from the higher to lower temperatures the chain relaxation and diffusion timescales start to coincide and the former process does not control the diffusion anymore. As a result the Case II mechanism does not dominate the swelling kinetics in the glassy state, below 20 °C.

Table 2.2 Temperature dependence of the liquid n-hexane diffusion coefficient, *D*, polymer relaxation time, τ_R, and Fickian and Relaxational contributions to the swelling, $S_{\infty,F}$ and S_R. S_{eq} stands for the total swelling at equilibrium.

Temperature [°C]	D [cm^2/s]	τ_R [s]	$S_{\infty,F}$ [%]	S_R [%]	S_{eq} [%]
16	$1.13\pm0.27\cdot10^{-14}$	2753±17	5.68±0.10	12.42±0.11	18.08

2.5. Conclusions

In-situ spectroscopic ellipsometry has been used to study the kinetic and equilibrium properties of liquid n-hexane swelling of 150 nm silicon wafer supported polystyrene films. Suitable optical models have been developed and applied to investigate the temperature dependent kinetics of the process in the vicinity of penetrant induced glass transition. In the temperature range where Case II diffusion is predominant, the system is best modeled by the Two Layer model. This model assumes a sharp boundary between a uniformly swollen region and an essentially non-swollen region. This description is shown to be less valid as temperature of swelling is decreased towards glass transition temperature of the system, where the Case II diffusion characteristics disappear. In the temperature region where Case II diffusion characteristics are apparent it is possible to estimate the front thickness by extending the Double Layer model to a Three Layer model. The resulting thickness of the boundary agrees with literature predictions and indicates that the progressing font of the penetrant is much thinner than 100 nm. Below the glass transition temperature the penetrant diffusion mechanism changes from Case II to Fickian Relaxation. Here the evolution of swelling with time is best modeled with the Single Layer model that assumes spatially uniform optical properties for the swollen film. Berens – Hopfenberg model fitting for the lowest temperature analyzed (16 °C) allows extraction of the diffusion coefficient of the penetrant and the characteristic polymer chains relaxation time. The obtained values indicate that the swollen film is an extensively plasticized glassy polymer.

2.6. Acknowledgements

MW acknowledges support through the Alexander von Humboldt Foundation

2.7. References

[1] Berens, A.R. and H.B. Hopfenberg, Diffusion and relaxation in glassy polymer powders: 2. Separation of diffusion and relaxation parameters. Polymer, 1978. **19**(5): p. 489-496.

[2] Berens, A.R., Diffusion and relaxation in glassy polymer powders: 1. Fickian diffusion of vinyl chloride in poly(vinyl choride). Polymer, 1977. **18**(7): p. 697-704.

[3] Thomas, N. and A.H. Windle, Transport of methanol in poly(methyl methacrylate). Polymer, 1978. **19**(3): p. 255-265.

[4] Nicolais, L., et al., Characterization and effects of n-alkane swelling of polystyrene sheets. Polymer, 1977. **18**(11): p. 1137-1142.

[5] Hopfenberg, H.B., The effect of film thickness and sample history on the parameters describing transport in glassy polymers. Journal of Membrane Science, 1978. **3**(2): p. 215-230.

[6] Buckley, D.A. and F.G. Belli, Study of the effect of film thickness on the sorption/desorption properties of ultra thin polymeric films. Materials Chemistry, 1980. **5**(6): p. 353-360.

[7] Durning, C.J., et al., A Study of Case II Transport by Laser Interferometry. Macromolecules, 1995. **28**(12): p. 4234-4248.

[8] Hassan, M.M. and C.J. Durning, Effects of polymer molecular weight and temperature on case II transport. Journal of Polymer Science Part B: Polymer Physics, 1999. **37**(22): p. 3159-3171.

[9] Scholes, C.A., et al., Plasticization of ultra-thin polysulfone membranes by carbon dioxide. Journal of Membrane Science, 2010. **346**(1): p. 208-214.

[10] Wessling, M., M. Lidon Lopez, and H. Strathmann, Accelerated plasticization of thin-film composite membranes used in gas separation. Separation and Purification Technology, 2001. **24**(1-2): p. 223-233.

[11] Bertrand, P., et al., Ultrathin polymer coatings by complexation of polyelectrolytes at interfaces: suitable materials, structure and properties. Macromolecular Rapid Communications, 2000. **21**(7): p. 319-348.

[12] Ram, M.K., et al., CO gas sensing from ultrathin nano-composite conducting polymer film. Sensors and Actuators B: Chemical, 2005. **106**(2): p. 750-757.

[13] Wind, J.D., et al., Relaxation Dynamics of CO2 Diffusion, Sorption, and Polymer Swelling for Plasticized Polyimide Membranes. Macromolecules, 2003. **36**(17): p. 6442-6448.

[14] Kapantaidakis, G.C., et al., CO2 Plasticization of polyethersulfone/polyimide gas-separation membranes. Aiche Journal, 2003. **49**(7): p. 1702-1711.

[15] Richardson, H., et al., Thickness dependence of structural relaxation in spin-cast, glassy polymer thin films. Physical Review E - Statistical, Nonlinear, and Soft Matter Physics, 2004. **70**(5 1): p. 051805-1-051805-8.

[16] Keddie, J.L., R.A.L. Jones, and R.A. Cory, Interface and surface effects on the glass-transition temperature in thin polymer films. Faraday Discussions, 1994. **98**: p. 219-230.

[17] Priestley, R.D., Physical aging of confined glasses. Soft Matter, 2009. **5**(5): p. 919-926.

[18] Rowe, B.W., B.D. Freeman, and D.R. Paul, Physical aging of ultrathin glassy polymer films tracked by gas permeability. Polymer, 2009. **50**(23): p. 5565-5575.

[19] Zhou, C., et al., The accelerated CO2 plasticization of ultra-thin polyimide films and the effect of surface chemical cross-linking on plasticization and physical aging. Journal of Membrane Science, 2003. **225**(1-2): p. 125-134.

[20] Hori, K., H. Matsuno, and K. Tanaka, Sorption kinetics of methanol in thin poly(methyl methacrylate) films studied by optical reflectivity. Soft Matter, 2011. **7**(21): p. 10319-10326.

[21] Pham, J.Q., et al., Pressure, Temperature, and Thickness Dependence of CO_{2}-Induced Devitrification of Polymer Films. Physical Review Letters, 2003. **91**(17): p. 175503.

[22] Sirard, S.M., et al., Anomalous Properties of Poly(methyl methacrylate) Thin Films in Supercritical Carbon Dioxide. Macromolecules, 2002. **35**(5): p. 1928-1935.

[23] Sirard, S.M., P.F. Green, and K.P. Johnston, Spectroscopic Ellipsometry Investigation of the Swelling of Poly(Dimethylsiloxane) Thin Films with High Pressure Carbon Dioxide. The Journal of Physical Chemistry B, 2001. **105**(4): p. 766-772.

[24] Tang, Y., et al., Swelling of Zwitterionic Polymer Films Characterized by Spectroscopic Ellipsometry. Macromolecules, 2001. **34**(25): p. 8768-8776.

[25] Visser, T. and M. Wessling, When Do Sorption-Induced Relaxations in Glassy Polymers Set In? Macromolecules, 2007. **40**(14): p. 4992-5000.

[26] Woollam, J.A., et al. Overview of variable angle spectroscopic ellipsometry (VASE), part I: basic theory and typical applications. 1999.

[27] Sarti, G.C., A. Apicella, and C. De Notaristefani, Effect of the thermal histories on case II sorption kinetics: Test of a kinetic theory for swelling. Journal of Applied Polymer Science, 1984. **29**(12): p. 4145-4159.

[28] Stokes, R.H., Dielectric constants and molar polarizations of cycloalkanes, benzene, n-hexane, and carbon tetrachloride in the range 278 to 343 K. The Journal of Chemical Thermodynamics, 1973. **5**(3): p. 379-385.

[29] Stamatialis, D.F., M. Sanopoulou, and I. Raptis, Swelling and dissolution behavior of poly(methyl methacrylate) films in methyl ethyl ketone/methyl alcohol mixtures studied by optical techniques. Journal of Applied Polymer Science, 2002. **83**(13): p. 2823-2834.

[30] Thomas, N.L. and A.H. Windle, A theory of case II diffusion. Polymer, 1982. **23**(4): p. 529-542.

[31] Potreck, J., et al., Sorption induced relaxations during water diffusion in S-PEEK. Physical Chemistry Chemical Physics, 2009. **11**(2): p. 298-308.

[32] Artsis, M., et al., Diffusion of organic diluents into ethyl cellulose. European Polymer Journal, 1972. **8**(4): p. 613-626.

Chapter 3

Probing the surface swelling in ultra-thin supported polystyrene films during Case II diffusion of n-hexane

This chapter has been adapted from:

Ogieglo W., Wormeester H., Wessling M., Benes N.E., Macromolecular Chemistry and Physics 2013;214(21):2480-2488. Copyright 2013 Wiley

Abstract

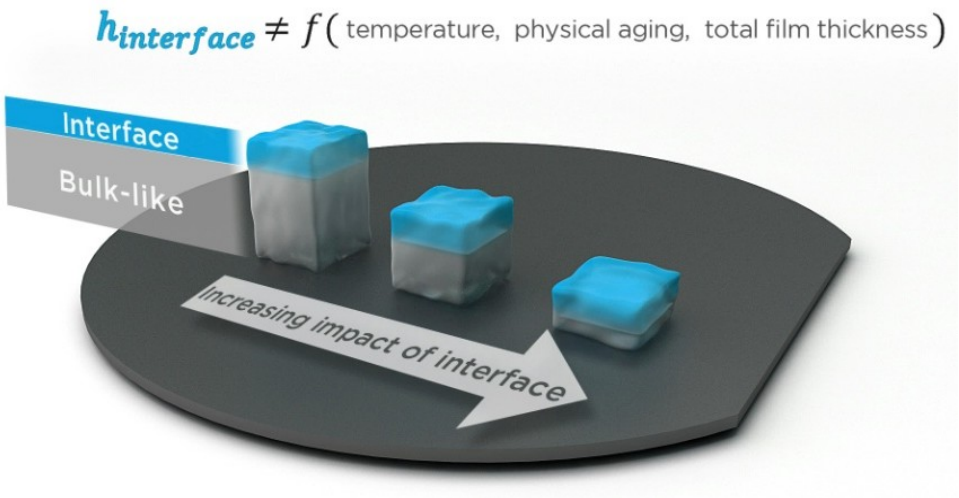

In-situ time resolved spectroscopic ellipsometry has been used to study the dynamics of n-hexane diffusion into, and the corresponding induced swelling of, ultra-thin polystyrene films. The experimental conditions have been carefully selected to facilitate the observation of anomalous Case II diffusion in the system, thereby allowing probing chain relaxation dynamics of a sharp moving penetrant front within the films. The obtained data have been analyzed via two distinct methods. The first method is based on numerical fitting of a multi-layer optical model to the ellipsometry data and yields the time evolution of the thicknesses of a swollen layer and a non-swollen layer. The second method is based on kinetics of the diffusing front, derived from changes in the raw Ψ and Δ data. It has been found that both approaches are in a quantitative agreement and suggest the existence of a finite thickness region of 14±3 nm in the outer film interface that is instantly swollen after contact with the penetrant. The thickness of this fast swelling layer is found to be independent of swelling temperature and physical aging time. After the interface is swollen, the diffusion front velocity shows no significant spatial variations in the direction perpendicular to the substrate, but is strongly dependent on temperature and sample aging history. These findings support the experimental and theoretical body of evidence indicating significantly different than bulk behavior of the surface of ultra-thin polymeric films.

3.1. Introduction

Decreasing the thickness of polymer films below about 100 nm has been claimed to result in deviations of materials properties as compared to those of the bulk polymer. Such phenomena are commonly referred to as nano-confinement effects and are generally explained in terms of an increased contribution of interfaces to the behavior of ultra-thin films [1-15]. A typical result is a deviation of the glass transition temperature (T_g) of a thin film from the characteristic value of the bulk polymer. Although still a subject of an intense debate, the most common explanations for nano-confinement effects are different molecular mobility at the film interfaces, or a gradient of dynamics within the thin film. For polystyrene thin films a reduction of T_g with decreasing thickness is generally reported. This is explained by the increasing contribution of the free film interface that possesses a higher segmental mobility than the bulk [14, 15]. In the case of poly(methyl methacrylate) (PMMA), and other polymers with hydroxyl groups [6, 7, 16, 17], an increase in T_g with decreasing thickness of the film has been reported. The increase in T_g is explained in terms of the dominant contribution of an immobilized (or adsorbed) layer of polymer directly at the interface with the substrate. For PMMA, the evidence of an increased mobility at the outer (free) interface has also been reported [18].

There have been a few investigations dedicated to the direct study of polymer surface dynamics. Most notably, Fakhraai and Forrest [9] have demonstrated, using a nanoparticle embedding technique, that the glassy polymer surface has an orders of magnitude higher mobility as compared to the bulk. In their experiments they followed relaxation of nano-scale indentations (craters) left after removal of gold nanoparticles from the polymer surface. These relaxations occur relatively fast, even at temperatures as low as 100 K below the T_g, suggesting the existence of a liquid-like layer at the surface. Very convincing evidence of increased surface mobility is also provided by the observations of dynamic rigid percolating solid fractal structures near T_g [19, 20]. These time-resolved studies suggest that even well below T_g the surface is characterized by a significant mobility that can be well described by the twinkling fractal theory. The thickness of the layer with increased mobility is estimated to be 0.1 – 10 nm [21, 22]. This thickness is often larger than the length of the cooperatively rearranging region (CRR) at glass transition (1-3 nm) [23], and does not seem to significantly depend on the total film thickness [24]. The surface mobility layer is shown to be characterized by dynamics much faster than for the bulk polymer, with estimates reaching a factor of 10^9 [25]. The increased surface dynamics have also been shown in other glassy systems, including small molecule glass formers [26].

Apart from increased surface chain mobility, other explanations of nano-confinement effects have also been proposed. One of them is the reduced local entanglement density at the polymer interface, which has been suggested based on

experiments involving thinning of suspended polymer fibers [27]. As suggested in that study, a threshold of film thickness exists at $h/R_{ee} < 2$ below which the entanglement density significantly decreases and self-entanglements become more significant. Related to that the viscosity of the polymer network at the interface was found to be orders of magnitude lower, leading to much higher deformability [15, 28-30].

Studies involving *in-situ* experiments of swelling of thin and ultra thin films in liquid penetrants are very rare, mainly due to the associated experimental difficulties [18, 31]. In one investigation Hori et al. analyzed Case II diffusion of methanol in PMMA ultra-thin films, by an optical reflectivity method [18]. They found an increase in diffusion coefficient of methanol at the free surface of the film substantiating the existence of a surface region with increased mobility. Below a certain threshold value of the total film thickness, also the influence of the immobilized substrate layer is noticeable. These mutual effects are shown to occur in surprisingly large thickness range (below about 70 – 90 nm). In the study of Hori et al. the dynamics of Case II diffusion were shown to be a good measure of the polymer chain dynamics, allowing resolving possible spatial deviations in dynamics in the direction perpendicular to the substrate.

In the present study *in-situ* time-resolved spectroscopic ellipsometry has been applied to investigate surface properties of ultra-thin supported polystyrene films, during swelling with n-hexane. The conditions of the experiments have been carefully selected to force transport of n-hexane into the film to occur by Case II anomalous diffusion. This enables to probe spatial variations in the chain dynamics in the direction perpendicular to the substrate, as a function of sample history (aging) and temperature. The obtained data have been analyzed via two distinct methods. The first method is based on numerical fitting of a multi-layer optical model to the ellipsometry data and yields the time evolution of the thicknesses of a swollen part of the film and a non-swollen part. The second method is based on deriving kinetics of the diffusing front from changes in the raw Ψ and Δ data. Both approaches are shown to confirm the existence of an almost instantly swollen layer at the top interface and allow quantifying its thickness. The study presents evidence supporting a different behavior of the surface of a thin film than for bulk material and its consequences for the diffusion of small molecule penetrants. Such processes are relevant in many thin film application areas, e.g., membranes, barriers, and coatings.

3.2. Theory

3.2.1. Anomalous Case II diffusion

Case II diffusion occurs as a result of a difference between the diffusion timescales of a small molecule penetrant in the rubbery and glassy state of the polymer [32, 33]. The diffusion coefficient in a rubbery state is 3-4 orders of magnitude larger

than in the glassy state [34]. The consequence is that an anomalous, non-Fickian, mechanism of diffusion occurs in which the limiting process is polymer chain relaxation, not the Fickian diffusion of the penetrant. Case II diffusion is characterized by a migration of a sharp front that divides the film into a completely swollen region and an essentially dry region [35, 36]. In the swollen region, the penetrant plasticizes the polymer severely and the system becomes a rubber; the dry part of the film still remains far below its T_g. Because of the large difference in penetrant mobility in the two regions the process of diffusion is only limited by the chain relaxations at the glass transition front. This enables to separate polymer chain relaxations, of interest in the studies presented here, from the diffusion process. The approach is valid for polystyrene films thinner than about 1-2 microns, where diffusion through the swollen layer can be considered infinitely fast and the process is manifested by a linear increase of film dilation (or weight) in time. Such behavior is found to occur at temperatures slightly above the penetrant induced T_g, which is about 20-22 °C for a polystyrene – n-hexane system [37, 38]. Below that temperature the swollen region of the film remains glassy and a sharp diffusion front does not develop. That process can be described by the Berens – Hopfenberg model [39], because diffusion and relaxation occur on similar timescales. The linear dependence of swelling on time no longer holds and curves are obtained that are more characteristic for Fickian diffusion.

3.2.2. Spectroscopic ellipsometry principles and data analysis

Spectroscopic ellipsometry is based on the measurement of the change of polarization state of light reflected from a flat sample. Polarization states that are in-plane or out-of-plane of incidence, *p*- and *s*- respectively, are distinguished. The ratio of the reflectivity for these two polarizations is used, characterized by the ellipsometric parameters Ψ and Δ:

$$\rho = \frac{r_p}{r_s} = tan(\psi)\, e^{i\Delta} \qquad (3.1)$$

The Ψ and Δ parameters measured across a broad spectral range from the ellipsometric spectra. They can be converted into useful sample properties, such as film thickness and refractive index, by numerical fitting of an appropriate optical model to the ellipsometric spectra. For swelling of polymer samples, changes in both of these properties are associated with the penetrant uptake. However, since the thickness and the refractive index are determined independently of each other (at least down to a thickness of about 25 nm), the volume dilation data (thickness change) can be, in principle, confronted with sample density changes (refractive index change).

The extraction of sample properties is done based on a numerical fitting of the model generated data to the experimentally obtained Ψ and Δ. As a goodness of fit an *MSE*, (Root) Mean Square Error, parameter is used. This parameter is a measure

of an error between the modeled and experimental spectrum. For samples thinner than about 100 nm a good fit is considered to have an *MSE* of 1-2. For thicker films larger *MSE* values are acceptable. For more details on the technique and optical modeling, the interested reader is referred to a spectroscopic ellipsometry handbook [40, 41]. The advantage of this technique for *in-situ* optical characterization, is that the values of the measured parameters do not depend on the absolute light intensity, only on the polarization state. This implies that the technique is not very sensitive to, for instance, light attenuation by a fluid ambient.

Spectroscopic ellipsometry allows determining, independently, film thickness and refractive index down to a film thickness of about 25 nm. For thinner films the thickness and refractive index become highly correlated to each other. Despite the unfeasibility to separate thickness and refractive index, for very thin films changes in Ψ and Δ spectra can still be determined very accurately, allowing to study for instance the kinetics of transient processes and glass transitions [42, 43].

3.3. Experimental

3.3.1. Film preparation and sample treatment

Thin films of polystyrene (Sigma Aldrich, T_g = 100.0 °C by DSC onset, M_w = 280 kg/mol) were spin coated on silicon wafers from a toluene solvent (Merck). The thicknesses were adjusted by varying the solution concentration in the range of 0.8% to 3%. The rotational speed of the spin coater platform was 2000 rpm and the coating was done on already rotating samples using about 0.5 ml of the polymer solution. The substrates were thoroughly cleaned with 3:1 (vol.) mixture of 98% sulfuric acid (Sigma Aldrich) and 30% hydrogen peroxide (Sigma Aldrich) to remove any organic impurities. Just before spin coating they were flushed with dry nitrogen to remove any dust or particles, which would cause film defects. After spin coating the samples were dried in air and transported to a nitrogen flushed oven set at 130 °C for annealing. After at least 3 hours of annealing the supported thin films were quenched to room temperature and left to physically age for 1 hour or 2 weeks. The aging was done at room temperature (21 °C ± 1 °C).

3.3.2. Measurement procedure

A spectroscopic Ellipsometer (M-2000X, J.A. Woollam Co., Inc.) was used to track the swelling of ultra thin polystyrene films. The data acquisition rate was about 2 s per full spectral scan and the spot size was about 2 mm. The *in-situ* cell used was made of glass with windows positioned perpendicular to the probing light beam. The angle of incidence was fixed at 70° and the wavelength range used for fitting was from 340 nm to 1000 nm. Further details of the experimental setup can be found in ref. [38].

The aged samples (either for 1 hour or for 2 weeks) were swollen with liquid n-hexane at two temperatures: 23 °C and 26 °C. For each experiment a fresh sample was used. The measurement was always done according to the following experimental procedure. The aged sample was transported to the glass *in-situ* cell after exactly 1 hour or 2 weeks of aging time. First, the dry sample parameters (thickness, optical dispersion) were determined. Afterwards, thermally equilibrated liquid n-hexane was introduced to the cell and the measurement was started within a maximum of 45 seconds from that moment. This time was required to correct for minor sample misalignments, mechanical equilibration of the system and setting up the time resolved data acquisition. The amount of time used was slightly different for each sample; therefore, it was carefully recorded and included in the kinetic data. The measurement was continued until no significant change in the raw data occurred (usually within 1.5 hours from the start of the measurement).

Correction for the Δ offset in-plane of incidence was done using an appropriate fitting parameter based on the data for dry films. The parameter was then used as a non-fitting parameter in the n-hexane swelling experiments. The correction for the out-of-plane offset was automatically performed by the software of the ellipsometer utilizing the appropriate design of the instrument.

3.3.3. Data analysis and modeling

To extract properties of dry films and of equilibrium-swollen films (obtained at the end of kinetic experiments) an optical model of stacked layers was used. This model involved a silicon wafer support (with a thin native oxide layer taken into account), onto which a layer representing the polymer film was placed. The polymer layer was considered uniform and homogenous and its optical dispersion of the polymer layer was modeled with a two-term Cauchy relation:

$$n(\lambda) = A + \frac{B}{\lambda^2} \qquad (3.2)$$

The film thickness and parameters A and B were fitted to the Ψ and Δ spectrum. Often a third parameter, C, is used to model the optical dispersion of polymeric films (contributing a term C/λ^4 to the dispersion). However, since already fitting of A and B resulted in sufficiently low *MSE* for all of the analyzed samples, and the decrease of the *MSE* by including C was limited, it was omitted in the optical dispersion to avoid overparametrization. The dispersion of n-hexane with an ellipsometric measurement on a well-characterized substrate (25 nm of thermal SiO_2 on Si) submerged in the fluid after equilibration at the desired temperature. This provides optical dispersion parameters of n-hexane we used $A_{H,23°C} = 1.375$, $B = 0.0008195$ µm^2 and $C = 0.00044098$ µm^4 and $A_{H,26°C} = 1.373$, $B = 0.00073606$ µm^2 and $C = 0.00044781$ µm^4. These data are in a very good agreement with literature [44].

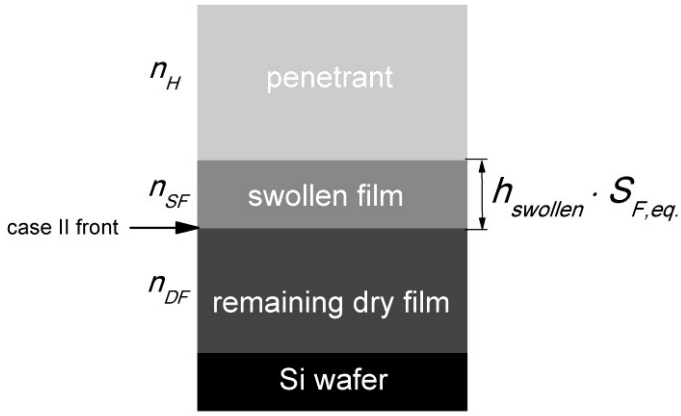

Figure 3.1 Two-layer optical model used to track the Case II mechanism of n-hexane swelling in ultra-thin, silicon wafer supported polystyrene films; n_H, n_{SF} and n_{DF} stand for refractive indices (at 632.8 nm) of n-hexane, swollen and dry parts of the film respectively; $h_{swollen}$ represents thickness of the region of the film that has been swollen to a thickness $h_{swollen}$ $S_{F,eq}$

For the tracking of the Case II wave progression, the layer representing the polymer film was separated in two parts as shown in Figure 3.1. As we showed previously [38], the Case II process can be represented by two distinct layers, separated by a sharp interface (front). The properties of the layer that is in contact with the penetrant (swollen film) were assumed identical to those of the fully swollen films. The other layer, in contact with the support (remaining dry film), was considered non-swollen and to have properties identical to that of the dry film. With this approach, the fitting parameters for this model are limited to the thickness of the swollen layer and the thickness of the dry layer. In such a way the progression of the Case II front could be tracked in time with a relatively high spatial resolution in the direction perpendicular to the substrate [38].

3.4. Results and discussion

In polystyrene swollen by n-hexane the Case II diffusion occurs above the penetrant induced glass transition (20-22 °C) [38]. In the present study, experiments have been conducted at 23 °C and 26 °C. At 23 °C the swollen film is only slightly above the glass transition, allowing the swelling to be tracked in a conveniently long experimental timescale. For instance, equilibrium is obtained after about 50 minutes for ~100 nm samples. Close to the glass transition, the diffusion front is not very sharp but has a small, yet significant, finite thickness. As a consequence, the two-layer model, Figure 3.1, may be inaccurate. However, as will be seen later in Figure 3.2a, the obtained kinetic swelling results do show the expected linearity of swelling versus time, at least in the later part of the kinetics,

before a constant swelling at equilibrium is obtained. This suggests that Case II dominates the process of diffusion at 23 °C and the two-layer model is justified. For the higher temperature, 26 °C, the Case II front can be considered infinitely sharp, and the two-layer optical model holds very accurately. The higher temperature, however, causes relaxations to become much faster, and the diffusion process is completed within just a few minutes (about 9 minutes for ~ 120 nm films). This makes accurate measurements more challenging, especially for thinner films, because the time spent for setting up of the experiment (<45 seconds) becomes more significant. The large effect of temperature is a result of a high activation energy of the chain relaxation process at the front, E_a = 241 kJ/mol [38]. Temperatures outside of the range 23-26 °C were considered not suitable for our measurements. Below 23 °C the timescales of diffusion and chain relaxation start to overlap and the Case II character is lost, above 26 °C the progression of the diffusion front is too fast to accurately resolve Case II kinetics for thinner films (<50 nm).

3.4.1. Ellipsometric modeling of dynamic swelling

Swelling kinetics at 23 °C and 26 °C, for samples aged for 2 weeks, are presented in Figure 3.2. The swelling factor has been obtained using the two-layer optical model, and can be expressed by:

$$S_{F(t)} = \frac{h_{swollen}(t)\cdot S_{F,eq.} + (h_{dry} - h_{swollen}(t))}{h_{dry}} = \frac{h_{swollen}(t)\cdot(S_{F,eq.} - 1)}{h_{dry}} + 1 \quad (3.3)$$

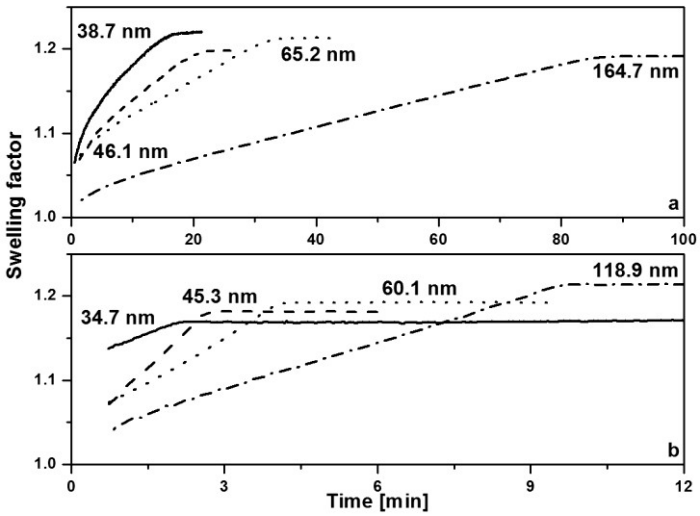

Figure 3.2 Kinetics of swelling obtained with the two-layer optical model, for 23 °C (a) and 26 °C (b) for samples aged for 2 weeks, only 4 data series, out of 9 (a) or 10 (b) measured, are shown on each graph

In this equation h_{swollen} is the thickness of the part of the dry film that is replaced by a penetrant swollen layer of thickness $h_{\text{swollen}} \cdot S_{F,\text{eq}}$ (assuming relative dilation equal to that at equilibrium swelling of the entire film: $S_{F,\text{eq}}$). The thickness of the layer that is not yet swollen is $h_{\text{dry}} - h_{\text{swollen}}$, with h_{dry} the initial thickness of the completely dry film.

All films presented in Figure 3.2 exhibit similar qualitative behavior; faster swelling at the beginning of the curve with a slight exponential character, followed by a linear increase in thickness. Similar observations have been made by Hori et al. [18] for methanol diffusion in PMMA. These authors have interpreted the faster initial swelling as faster diffusion through the outer interface of the thin film, suggesting that this outer interface has a region with different than bulk dynamics. Our results support a similar proposition for the n-hexane – polystyrene system. At the beginning, when the penetrant enters a thin film, its diffusion speed is higher than in a later stage in a bulk-like region. The initial fast swelling is observed consistently for all analyzed samples, at both swelling temperatures (23 °C and 26 °C), and at both aging histories (1 hour and 2 weeks).

In particular, the results for the thinnest films (38.7 nm in Figure 3.2a and 34.7 nm in Figure 3.2b) suggest the presence of an interfacial layer that is swollen almost instantly at the beginning of the experiments. For these thinnest films, the swelling curves show a discontinuity in the initial stage.

To quantify the thickness of the instantly swollen interfacial layer Figures 3.3 and 3.4 are presented. Figure 3.3 shows the swelling factor, $S_{F(t)}$, versus dry film thickness for two time slices, 1 min and 5 min, for 9 thin film samples swollen at 23 °C aged for 2 weeks. For thinner films the swelling factor is larger, due to the relatively larger contribution of the swollen film to the overall film thickness at the same time slice. The lines in Figure 3.3 correspond to a numerical fit of equation 3.3 to the swelling of all nine samples simultaneously, using only h_{swollen} as fitting parameter, therefore extracting the swollen layer thickness at a given time slice. As value for $S_{F,\text{eq}}$, the average swelling at equilibrium of all 9 samples is taken. The value of $S_{F,\text{eq.}}$ is found to be within ±0.015 from the equilibrium swelling of thicker samples (>80 nm) where a more accurate determination of thickness and refractive index by ellipsometry is possible. This additional finding suggests no significant deviations of $S_{F,\text{eq.}}$ for the ultra-thin films. The simultaneous fit for all samples allows moderating the scatter in h_{swollen} obtained for thinner films.

Fit values for $h_{\text{swollen}}(t)$ (23 °C, 9 samples aged for 2 weeks, $S_{F,\text{eq.}}$=1.21) are shown in Figure 3.4 as a function of the time of exposure to n-hexane. The solid line represents a linear fit through the data points. The slope of this line corresponds to the velocity of the front, moving in the direction perpendicular to the substrate interface. The linear behavior indicates that, during the time intervals in between 1 and 5 minutes (well after the penetration of the interface), the velocity of the front

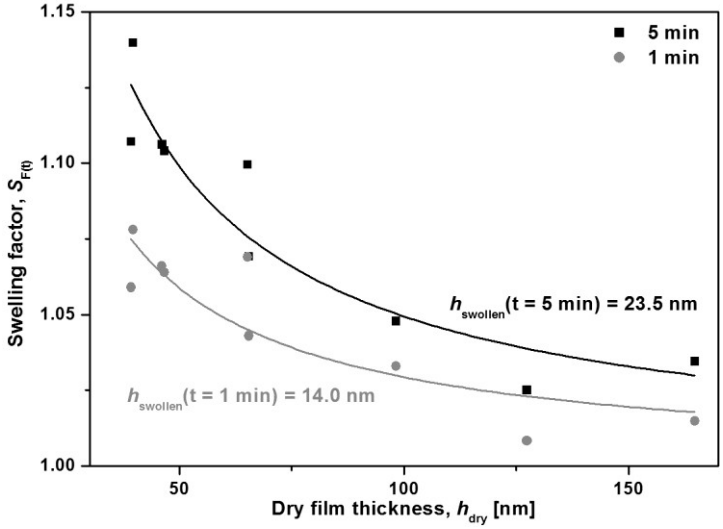

Figure 3.3 Swelling factor after 1 min and after 5 min as a function of a dry film thickness for 9 samples swollen at 23 °C aged for 2 weeks; solid line represents numerical fits of the equation 3 assuming a two-layer mobility profile with $h_{swollen}$ as a single fit parameter

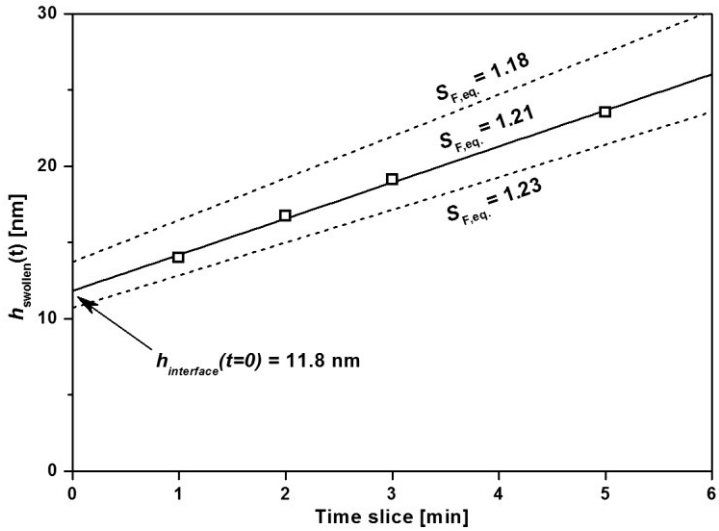

Figure 3.4 Interfacial swollen layer thickness, $h_{swollen}$, at several time slices for thin films swollen at 23 °C aged for 2 weeks; intercept at t = 0 represents a region of the film swollen instantly

is independent of the position in the film. The numerical value of the front velocity is calculated to be ~ 2.4 nm/min. The intercept corresponds to the thickness of an

interfacial layer that is *swollen instantly* when the film comes in contact with n-hexane. The value of the thickness of this fast swelling layer is $h_{\text{interface}}(t=0)$ = 11.8±0.3 nm. The extrapolation of the linear trend to t=0 implies that swelling of the thin interface layer is assumed infinitely fast. The persistence of the linear trend (R^2 = 0.9975) to short experimental times (1 minute) suggests that indeed a very significant difference in dynamic behavior between the outer polymer interface and the rest of the film exists. This is also in agreement with swelling curves shown in Figure 3.2. A similar description of ultra-thin polystyrene films supported on silicon substrates was found to be valid for polymer viscosity profiles, where evidence of very fast mobility layer at the outer film interface has been found [22].

The dashed lines in Figure 3.4 demonstrate the sensitivity of the value of $h_{\text{swollen}}(t)$ and $h_{\text{interface}}(t=0)$ for an experimental error in $S_{F,\text{eq}}$. Results for the two most extreme values for $S_{F,eq}$, obtained for the 9 samples, are plotted. Similar results were obtained for the 3 remaining sets of samples and the resulting $h_{\text{interface}}(\text{t=0})$ values are presented in a comparative Figure 3.6 as open symbols. The error bars represent the limits as demonstrated with dashed lines in Figure 3.4.

The quantification of the interfacial layer thickness, based on our modeling data, involves some assumptions. One assumption is that the effects of interactions between PS layer and the substrate are regarded negligible due to unfavorable interaction of the polymer and SiO_x surface of the wafer [24]. In contrast to PMMA supported on silicon wafers, for the PS significant immobilization of the polymer chains does not seem to occur [22, 24]. Another assumption is that the interfacial layer is assumed to be swollen instantly upon contact with n-hexane, and that the swelling degree of the interfacial layers is identical to that of the bulk. This last assumption is based on the nonexistence of statistically significant deviations in equilibrium bulk swelling with decreasing film thickness. The equilibrium swelling of all analyzed films (7-10 films for each set) is within a range $S_{F,\text{eq.}}$ = 1.18 – 1.23 with no apparent trends with thickness. This rather broad obtained range of $S_{F,\text{eq.}}$ is also related to the inaccuracies inherent to the modeling of the ellipsometric data for very thin films (decoupling of thickness and refractive index) [40]. Because of that, unfortunately, increased or decreased overall swelling of the thinner films could not be conclusively determined.

3.4.2. Kinetic analysis of raw Ψ and Δ spectra

As an alternative to the model-dependent approach of the previous paragraph, it is possible to analyze dynamic evolution of raw Ψ and Δ parameters. This analysis is simplified by the fact that for pure Case II diffusion the front velocity is constant, which is manifested by a linear proportionality between the swelling and the time of exposure to the solvent. The duration for equilibration of the system (the time

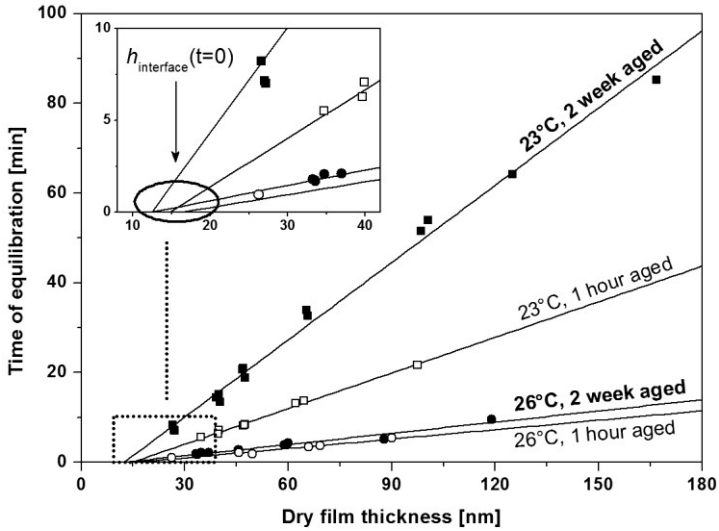

Figure 3.5 Time of equilibration as a function of dry polystyrene thin film thickness for all analyzed samples; inset shows a finite apparent film thickness at the time of equilibration = 0

required for the front to travel through the entire film) is readily available from the raw spectra, from the instance after which no significant changes in the Ψ and Δ are observed. This instance can be extracted by finding the intersection of linear fits of either the Ψ or Δ time evolution; one fit from the constant speed of swelling (bulk-like dynamics) and one fit from the equilibrated system. The results of this approach for all analyzed sample sets are presented in Figure 3.5.

From Figure 3.5 it is apparent that the swelling kinetics are strongly affected by the sample thermal history, in particular for the temperature close to the T_g. This is rationalized by the fact that the kinetics of Case II diffusion are dictated by chain relaxations. For aged samples, that are closer to their equilibrium state, n-hexane induced chain relaxations are known to be slower [37, 38, 45]. For the experiments at 23 °C, close to the T_g, the chain dynamics are very slow and the effects of aging are amplified; the samples aged for 2 weeks require more than twice the time to equilibrate as compared to the samples aged for one hour. For the 26 °C, further away from the T_g, the chain dynamics are much faster. The required equilibrium times at this temperature are much shorter as compared to the experiments at 23 °C, and the effects of aging are less pronounced. For all datasets, the data points can be fitted reasonably well using a simple linear fit (R^2 from 0.9628 to 0.9936). This is in agreement with the findings from section 4.1., and implies that, after the interface is swollen, the front velocity shows no significant spatial variations in the direction perpendicular to the substrate. The constant front velocity allows accurate extrapolation of the time of equilibration for thinner films, from characterization of thicker films, at least in the range studied (up to about 165 nm), and possibly much

further. This may have some practical utility, for instance, when knowledge of differences in diffusion timescales for different thicknesses of thin selective membranes is required.

All four linear fits *do not* go through the origin of the graph, but cross the *x*-axis at around 12-17 nm. The intersection point with the *x*-axis is shown more clearly in the inset of Figure 3.5. The *x*-intercept can be interpreted as the thickness of an interfacial region of the film that became swollen instantaneously within the time resolution of this experiment. Values for the thickness of such a layer, derived from solely the process kinetics, are in a reasonable agreement with the values obtained from the results of ellipsometric modeling presented in section 4.1. The extracted *x*-axis intersection values for all datasets are collected in Figure 3.6 as closed symbols. The error bars are calculated from the combination of a standard error in the determination of the slope and offset of the linear fits.

3.4.3. Comparison of the modeled and kinetic results

Figure 3.6 combines the values of $h_{\text{interface}}(t=0)$ obtained from the modeling (section 3.4.1.) and the kinetic analysis (section 3.4.2.). The results obtained from the two distinct methods are in a reasonable agreement and seem to provide a strong evidence for different than bulk swelling behavior of the thin polystyrene film interface. The $h_{\text{interface}}(t=0)$ is found to be, more or less, insensitive to the swelling temperature and the aging time. Higher error bars for the kinetic data for 26 °C are a result of larger error in determination of time of equilibration, due to much faster swelling of the samples swollen at this temperature. The obtained value of 27.4 nm for the modeling results (open triangle) is also larger than the smallest film thickness analyzed (26.8 nm), and therefore, has to be considered erroneous. This is probably an effect of the large impact of even small experimental errors on the results obtained with ellipsometry modeling for ultra-thin films. In contrast, analysis of kinetic raw data, which avoids modeling issues, for that set of samples (closed triangle) yields a value for the interfacial film thickness that is in agreement with the results for the rest of the sample sets. The average $h_{\text{interface}}(t=0)$ for all of the samples (excluding the modeling result for the 26 °C 1 hour aged sample), can be estimated at 14±3 nm. This value is in a relatively good agreement with the reported range of increased polymer mobility for dry polymer systems (up to 10 nm).

The very fast swelling of the polymer interface can be arguably a manifestation of a few properties reported by other researchers. It can be assigned to much faster than bulk chain mobility of the polymer interface. In this case the argument is that, since in Case II mechanism the front progression is related to local chain mobility, the interface mobility is much higher than in the rest of the film. On the other hand, the much faster swelling of the interface can be related to reduced viscosity (increased deformability and thus easier swelling) of the network at the interface

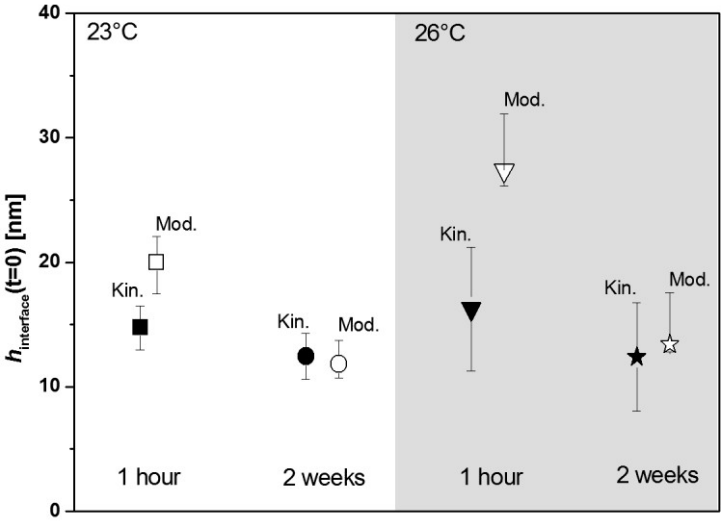

Figure 3.6 Thickness of the increased mobility layer obtained from modeling (section 3.4.1) and kinetic analysis (section 3.4.2) as a function of swelling temperature and aging time; for the kinetic data the error bars are calculated from combination of standard errors in slope and offset determination, for the modeling data the error bars represent limits when extreme values of $S_{F,eq.}$ are taken (see section 3.4.1.)

[30]. Consistent with that interpretation we find that the aging has no significant impact on the quantified thickness of the fast swollen layer, Figure 3.6.

3.5. Conclusions

We have investigated the interfacial and bulk swelling kinetics of ultra-thin, silicon wafer supported, polystyrene films in liquid n-hexane in the temperature range where anomalous Case II diffusion is dominant. In this diffusion mechanism a sharp front between the swollen and the non-swollen regions of a film develops and the progression velocity of this front depends on local polymer chain mobility. By means of time-resolved spectroscopic ellipsometry, spatial variations in the progression velocity can be determined *in-situ*. Two distinct methods have been used for data interpretation. One method involves numerical fitting of a two-layer optical model to the ellipsometry spectra. The other method is based monitoring the time evolution of the raw ellipsometry data. For both methods it is found that the diffusion of the liquid penetrant in the free surface of the film is much faster than the diffusion in the bulk, confirming the existence of a layer with significantly different than bulk properties at the ambient/film interface. The thickness of the fast interfacial region can be estimated to be 14±3 nm, and does not depend on swelling temperature or physical aging time of the entire film. After the interface is swollen, the diffusion front velocity shows no significant spatial variations in the

direction perpendicular to the substrate, but is strongly dependent on temperature and sample aging history. The obtained results are interpreted in terms of the increased polymer chain mobility or decreased viscosity at the surface of the polymer films. The experimental study presented here further strengthens the body of evidence indicating significantly different than bulk dynamics of the surfaces of glassy polymers and may be helpful in rationalizing outcomes of other studies found in literature.

3.6. Acknowledgements

MW acknowledges support through the Alexander von Humboldt Foundation.

3.7. References

[1] Frank, B., et al., *Polymer Mobility in Thin Films.* Macromolecules, 1996. **29**(20): p. 6531-6534.

[2] DeMaggio, G.B., et al., *Interface and Surface Effects on the Glass Transition in Thin Polystyrene Films.* Physical Review Letters, 1997. **78**(8): p. 1524.

[3] Keddie, J.L., R.A.L. Jones, and R.A. Cory, *Interface and surface effects on the glass-transition temperature in thin polymer films.* Faraday Discussions, 1994. **98**: p. 219-230.

[4] Jones, R.A.L., *The dynamics of thin polymer films.* Current Opinion in Colloid & Interface Science, 1999. **4**(2): p. 153-158.

[5] de Gennes, P.G., *Glass transitions in thin polymer films.* The European Physical Journal E: Soft Matter and Biological Physics, 2000. **2**(3): p. 201-205.

[6] Tate, R.S., et al., *Extraordinary elevation of the glass transition temperature of thin polymer films grafted to silicon oxide substrates.* Journal of Chemical Physics, 2001. **115**(21): p. 9982-9990.

[7] Fryer, D.S., P.F. Nealey, and J.J. de Pablo, *Thermal Probe Measurements of the Glass Transition Temperature for Ultrathin Polymer Films as a Function of Thickness.* Macromolecules, 2000. **33**(17): p. 6439-6447.

[8] Forrest, J.A. and K. Dalnoki-Veress, *The glass transition in thin polymer films.* Advances in Colloid and Interface Science, 2001. **94**(1-3): p. 167-195.

[9] Fakhraai, Z. and J.A. Forrest, *Measuring the Surface Dynamics of Glassy Polymers.* Science, 2008. **319**(5863): p. 600-604.

[10] Fakhraai, Z. and J.A. Forrest, *Probing Slow Dynamics in Supported Thin Polymer Films.* Physical Review Letters, 2005. **95**(2): p. 025701.

[11] Peter, S., H. Meyer, and J. Baschnagel, *Thickness-dependent reduction of the glass-transition temperature in thin polymer films with a free surface.* Journal of Polymer Science Part B: Polymer Physics, 2006. **44**(20): p. 2951-2967.

[12] Pye, J.E. and C.B. Roth, *Two Simultaneous Mechanisms Causing Glass Transition Temperature Reductions in High Molecular Weight Freestanding Polymer Films as Measured by Transmission Ellipsometry.* Physical Review Letters, 2011. **107**(23): p. 235701.

[13] Pye, J.E., et al., *Physical Aging in Ultrathin Polystyrene Films: Evidence of a Gradient in Dynamics at the Free Surface and Its Connection to the Glass Transition Temperature Reductions.* Macromolecules, 2010. **43**(19): p. 8296-8303.

[14] Rotella, C., S. Napolitano, and M. Wübbenhorst, *Segmental Mobility and Glass Transition Temperature of Freely Suspended Ultrathin Polymer Membranes.* Macromolecules, 2009. **42**(5): p. 1415-1417.

[15] Yang, Z., et al., *Glass Transition Dynamics and Surface Layer Mobility in Unentangled Polystyrene Films.* Science, 2010. **328**(5986): p. 1676-1679.

[16] Kim, J.H., J. Jang, and W.-C. Zin, *Thickness Dependence of the Glass Transition Temperature in Thin Polymer Films.* Langmuir, 2001. **17**(9): p. 2703-2710.

[17] Pham, J.Q., et al., *Pressure, Temperature, and Thickness Dependence of CO_{2}-Induced Devitrification of Polymer Films.* Physical Review Letters, 2003. **91**(17): p. 175503.

[18] Hori, K., H. Matsuno, and K. Tanaka, *Sorption kinetics of methanol in thin poly(methyl methacrylate) films studied by optical reflectivity.* Soft Matter, 2011. **7**(21): p. 10319-10326.

[19] Stanzione Iii, J.F., K.E. Strawhecker, and R.P. Wool, *Observing the twinkling fractal nature of the glass transition.* Journal of Non-Crystalline Solids, 2011. **357**(2): p. 311-319.

[20] Wool, R.P. and A. Campanella, *Twinkling fractal theory of the glass transition: Rate dependence and time–temperature superposition.* Journal of Polymer Science Part B: Polymer Physics, 2009. **47**(24): p. 2578-2590.

[21] Wong, D., et al., *Surface Dynamics of Polymer Glasses: Sub-Tg Surface Reorganization in End-Functional Polymers.* Macromolecules, 2012.

[22] Peng, D.-d., et al., *Two-layer model description of polymer thin film dynamics.* Chinese Journal of Polymer Science, 2012: p. 1-9.

[23] Cangialosi, D., A. Alegria, and J. Colmenero, *Route to calculate the length scale for the glass transition in polymers.* Physical Review E, 2007. **76**(1): p. 011514.

[24] Paeng, K., R. Richert, and M.D. Ediger, *Molecular mobility in supported thin films of polystyrene, poly(methyl methacrylate), and poly(2-vinyl pyridine) probed by dye reorientation.* Soft Matter, 2012.

[25] Dutcher, J. and M. Ediger, *Glass surfaces not so glassy.* Science, 2008. **319**(5863): p. 577-578.

[26] Sepúlveda, A., et al., *Accelerated Aging in Ultrathin Films of a Molecular Glass Former.* Physical Review Letters, 2011. **107**(2): p. 025901.

[27] Rathfon, J.M., et al., *Confinement Effects on Chain Entanglement in Free-Standing Polystyrene Ultrathin Films.* Macromolecules, 2011: p. null-null.

[28] Brochard Wyart, F. and P.G. de Gennes, *Viscosity at small scales in polymer melts.* The European Physical Journal E, 2000. **1**(1): p. 93-97.

[29] Dubourg, F., et al., *Probing the relationship between the scales of space and time in an entangled polymer network with an oscillating nanotip.* Journal of Physics: Condensed Matter, 2003. **15**(36): p. 6167.

[30] Napolitano, S., C. Rotella, and M. Wübbenhorst, *Can Thickness and Interfacial Interactions Univocally Determine the Behavior of Polymers Confined at the Nanoscale?* ACS Macro Letters, 2012: p. 1189-1193.

[31] Singh, A. and M. Mukherjee, *Swelling Dynamics of Ultrathin Polymer Films.* Macromolecules, 2003. **36**(23): p. 8728-8731.

[32] Thomas, N.L. and A.H. Windle, *A theory of case II diffusion.* Polymer, 1982. **23**(4): p. 529-542.

[33] Thomas, N.L. and A.H. Windle, *Diffusion mechanics of the system PMMA-methanol.* Polymer, 1981. **22**(5): p. 627-639.

[34] Artsis, M., et al., *Diffusion of organic diluents into ethyl cellulose.* European Polymer Journal, 1972. **8**(4): p. 613-626.

[35] Durning, C.J., et al., *A Study of Case II Transport by Laser Interferometry.* Macromolecules, 1995. **28**(12): p. 4234-4248.

[36] Sanopoulou, M. and D.F. Stamatialis, *Study of the transition from Fickian to Case II sorption kinetics in the system poly(ethyl methacrylate)–liquid methyl alcohol.* Polymer, 2001. **42**(4): p. 1429-1439.

[37] Nicolais, L., et al., *Characterization and effects of n-alkane swelling of polystyrene sheets.* Polymer, 1977. **18**(11): p. 1137-1142.

[38] Ogieglo, W., et al., *Temperature-induced transition of the diffusion mechanism of n-hexane in ultra-thin polystyrene films, resolved by in-situ Spectroscopic Ellipsometry.* Polymer, 2012.

[39] Berens, A.R. and H.B. Hopfenberg, *Diffusion and relaxation in glassy polymer powders: 2. Separation of diffusion and relaxation parameters.* Polymer, 1978. **19**(5): p. 489-496.

[40] Fujiwara, H. and I. Wiley, *Spectroscopic ellipsometry principles and applications*, 2007, John Wiley & Sons: Chichester, England; Hoboken, NJ.

[41] Tompkins, H.G. and E.A. Irene, *Handbook of ellipsometry*, 2005, William Andrew Pub. ; Springer: Norwich, NY; Heidelberg, Germany.

[42] Meli, L., et al., *Polystyrene thin films in CO_{2}.* Physical Review E, 2004. **69**(5): p. 051601.

[43] Pham, J.Q., K.P. Johnston, and P.F. Green, *Retrograde Vitrification in CO2/Polystyrene Thin Films.* The Journal of Physical Chemistry B, 2004. **108**(11): p. 3457-3461.

[44] Stokes, R., *Dielectric constants and molar polarizations of cycloalkanes, benzene, n-hexane, and carbon tetrachloride in the range 278 to 343 K.* The Journal of Chemical Thermodynamics, 1973. **5**(3): p. 379-385.

[45] Sarti, G.C., A. Apicella, and C. De Notaristefani, *Effect of the thermal histories on case II sorption kinetics: Test of a kinetic theory for swelling.* Journal of Applied Polymer Science, 1984. **29**(12): p. 4145-4159.

Chapter 4

Effective medium approximations for penetrant sorption in glassy polymers accounting for excess free volume

This chapter has been accepted for publication in Polymer, authored by:

Ogieglo W., Wormeester H., Wessling M., Benes N.E.

Abstract

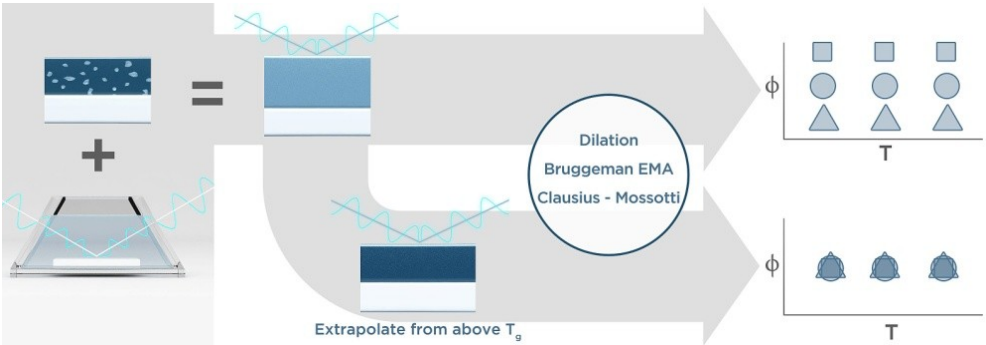

An accurate determination of a penetrant volume fraction in a swollen polymer (partial molar volume) is of crucial importance in a range of different technologies. Using optical methods, such as *in-situ* spectroscopic ellipsometry, it is possible to extract the thickness and refractive index of dry and swollen polymer films. The volume fraction of the penetrant can then be calculated using from the change in thickness, or from the refractive index using effective medium approximations. For thermodynamically equilibrated and ideal swollen rubbery polymers, these calculations yield accurate results. However, for glassy polymers the influence of the excess free volume trapped within the polymer network during vitrification is rarely taken into account. In this work we investigate the effect of excess free volume in the calculations of penetrant volume fraction in a model glassy polymer - penetrant system. The influence of the excess free volume is included by extrapolating the properties of an equilibrium polymer matrix from above its glass transition temperature. The error between the approaches that do and do not take account for the non-equilibrium of the glassy polymer is quantified and the implications for other systems are discussed. The errors are shown to be very significant; especially when the dry polymer has a large excess free volume. Such materials are particularly relevant in membrane applications.

4.1. Introduction

Penetrant-swollen thin films are encountered in a range of technologies, including drying processes, coatings, and membrane applications [1-3]. The properties of such thin films are strongly affected by the presence of the penetrant. This calls for methods that allow accurate study of the extent of penetrant uptake in the thin film.

Properties of thin swollen films have been studied with different optical methods, such as *in-situ* spectroscopic ellipsometry [4-26], white light or laser interferometry [27-31] and optical reflectivity [32]. These optical methods usually provide the extent of thickness dilation, as well the change in the refractive index of the films upon penetrant (de)sorption. It is possible to estimate the solvent volume fraction from this information. The changes in dilation can be directly related to changes in volume, and hence in a volume fraction. From the refractive index of the swollen films, a volume fraction of solvent can be estimated using effective medium approximation (EMA) methods [33]. An EMA method describes the macroscopic properties of a mixture by averaging the properties of the components it consists of on a molecular level. EMA's have been successfully used for accurate quantification of sorption of, chemically similar, penetrants in rubbers [4, 14-16, 19, 23, 34, 35]. For these binary systems, it is reasonable to assume that the individual properties of the penetrant and polymer matrix remain unchanged upon mixing. In contrast to rubbers, dry glassy polymers are inherently non-equilibrium systems. In glassy polymers excess free volume exists. This excess free volume is trapped kinetically within the polymer matrix due to a dramatic increase of polymer chain relaxation times upon vitrification. In effect, the excess free volume renders the dry polymer to be a two-component mixture; an equilibrium polymer matrix containing an additional void fraction. In EMA calculations on polymer swollen from an initial non-equilibrium state, the excess free volume is often not accounted for [6, 10, 11, 15, 18, 20, 21, 24, 36-42]. This may lead to inaccurate, usually underestimated, results. Optical investigations of sorption in glassy polymers that do consider the influence of the unrelaxed excess free volume are very rare [26, 31].

In this work, the effect of excess free volume on the quantitative determination of solvent uptake by an initially glassy polymer film is investigated. Two well-known EMA methods are compared and confronted with a simple volume balance based on dilation. An approach is proposed to appropriately take the excess free volume fraction into account by considering the extrapolated properties of a hypothetical equilibrium liquid polymer, below the glass transition. Sorption of n-octane by polystyrene (PS) is used here as an illustrative model glassy polymer – liquid penetrant system. The method can be readily extended to other systems, and estimates are given for the error introduced in typical polymer – penetrant systems.

4.2. Theory

4.2.1. Contributions to volume in glassy polymers

According to the Free Volume Theory of glass transition [43], glassy polymers contain a certain excess free volume fraction that is trapped within the material structure below the glass transition temperature. In Figure 4.1 the specific volume of a glassy polymer in the temperature range covering the glass transition is schematically presented.

The molar volume of a polymer is often divided into several components. The occupied volume is the hard sphere volume of atoms and molecules building the polymer chains. It is sometimes referred to as van der Waals volume and can be approximated by the group contribution methods [45]. It is usually hard to access it experimentally. The interstitial volume represents the effective volume of a polymer chain. It is considered non-permeable neither for macromolecular segments or diffusing small molecules. The difference between the interstitial free volume and the macroscopic volume of a polymer specimen, represented by the topmost line in Figure 4.1, is referred to as fractional or hole free volume. The macroscopic volume of a dry liquid polymer, v_{DL}, can be considered a sum of the interstitial and hole free volumes.

For ideal systems above their glass transition temperature, rubbers or liquids, it is expected that macroscopic partial liquid volumes of the polymer and a liquid penetrant mix additively. The partial molar volumes of the components in the mixture do not differ from their pure partial molar volumes. In a dry glassy

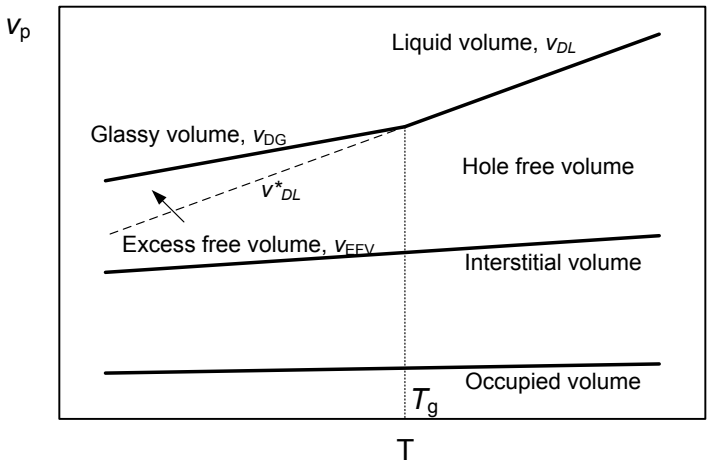

Figure 4.1 Schematic representation of contributions to the molar volume in a glassy polymer in the glass transition temperature range. Adapted with permission from [44]. Copyright 1996 Marcel Dekker

polymer, however, a certain excess free volume exists, v_{EFV}, which is a result of inability of the material volume to relax to its equilibrium liquid volume upon vitrification. This excess free volume contributes to the macroscopic volume of a dry glassy system, v_{DG}. When a penetrant mixes with a glassy polymer and the sorption induces glass transition in the mixture, the excess free volume is fully relaxed, and its fraction becomes zero. The mixture can then be again considered an ideal equilibrium mixture of a penetrant and a liquid polymer. This time, however, the molar volume of the liquid polymer is different to its macroscopic (glassy) molar volume. It can be obtained by extrapolation of the equilibrium liquid volume down to the temperature where the sorption occurs, v^*_{DL}.

In optical reflection methods, instead of volumes the refractive indices of thin film samples are often measured. Independently, also thicknesses of thin film samples are determined. This gives the possibility to measure changes both in the (optical) density and volume of the polymer films upon sorption of various penetrants.

4.2.2. Methods to determine volume fractions of components in polymer – penetrant mixtures

4.2.2.1 Polymer film dilation

The simplest approach uses the change in the dimensions of the sample upon sorption of the penetrant. This approach inherently implies volume additivity of the components. For thin films the samples are assumed to swell only in the direction perpendicular to the substrate, thus the volume dilation is equal to thickness dilation (swelling). The solvent volume fraction from dilation, $\phi_S^{dil.}$, can be calculated as:

$$\phi_S^{dil.} = \frac{v_{SP} - v_{DP}}{v_{SP}} = \frac{h_{SP} - h_{DP}}{h_{SP}} \quad (4.1)$$

In eq. 4.1 v_{SP}, h_{SP} stand for the volume and thickness of the swollen polymer, v_{DP}, h_{DP} stand for the volume and thickness of the dry polymer. Eq. 4.1 does not distinguish whether the dry polymer is a liquid or a glass.

4.2.2.2. Bruggeman effective medium approximation (BEMA)

The optical properties of a mixture of two or more materials can be calculated using an EMA. Such an EMA theory provides a mix of the optical dispersions of the components, using their dielectric constants, ε, or refractive indices, n. For transparent materials $\varepsilon = n^2$ holds. The most commonly used EMA formulation by Bruggeman (BEMA) [33], is expressed for two materials as:

$$\phi_1 \cdot \frac{n_1^2 - n_{mix}^2}{n_1^2 + 2n_{mix}^2} + \phi_2 \cdot \frac{n_2^2 - n_{mix}^2}{n_2^2 + 2n_{mix}^2} = 0 \quad (4.2)$$

where ϕ_1 and ϕ_2 are the volume fractions of material 1 and 2; n_1, n_2, n_{mix} are refractive indices of material 1, 2, and their mixture, respectively. The volume fraction of material 2 can be also expressed as (1-ϕ_1). For porous materials, for instance, material 2 is void (n_2 = 1) and eq. 4.2 can be used to determine the porosity. Eq. 4.2 uses the n_{mix} as a reference, which makes it self-consistent. The BEMA assumes that the mixing of both materials occurs on a length-scale that is much smaller than the wavelength of the probing light. This usually is valid for the sorption of small molecules in polymers when light around visible region is used. The mixture is assumed isotropic.

4.2.2.3. Clausius – Mossotti relationship

For the estimation of mass concentrations in binary mixtures (for example polymer – penetrant) the effective medium approximation approach based on Clausius – Mossotti relationship is frequently used. It takes advantage of the dependence of the refractive index of a pure substance on its mass density, ρ:

$$\frac{n^2-1}{n^2+2} = \frac{R}{M_w} \cdot \rho \qquad (4.3)$$

Here R represents the molar refractivity and M_w the molecular weight of the substance. The ratio of R/M_w, often denoted q, shows only very weak temperature dependence. For most practical applications q can be treated as a material constant. This implies that from the optical properties of a mixture and those of the constituting solvent and polymer, the mass concentration of the penetrant, $C_{solv.}$, can be calculated from:

$$\frac{n_{mix}^2-1}{n_{mix}^2+2} = q_S \cdot C_S + q_{polym.} \cdot C_{polym.} \qquad (4.4)$$

For thin films that are only able to swell in the direction perpendicular to the substrate, the polymer concentration, $C_{polym.}$, is directly related to the initial and swollen film thicknesses, h_{DP} and h_{SP}:

$$C_{polym.} = \rho_{polym.} \cdot \frac{h_{DP}}{h_{SP}} \qquad (4.5)$$

For samples able to swell in three dimensions, the thicknesses should be replaced with the corresponding volumes. The solvent volume fraction, ϕ_S^{C-M}, can then be obtained by dividing the solvent concentration by its pure density:

$$\phi_S^{C-M} = \frac{C_S}{\rho_S} \qquad (4.6)$$

In analogy, the polymer volume fraction follows from: $\phi_P^{C-M} = \frac{C_{polym.}}{\rho_{polym.}}$.

4.2.3 Spectroscopic ellipsometry

The thickness and the refractive index of a thin supported film can be simultaneously measured by spectroscopic ellipsometry. In this technique linearly polarized light is reflected of a multi-layer sample system and the change in the polarization state upon reflection is measured. The change in the polarization state is often expressed in terms of psi (Ψ) and delta (Δ) parameters:

$$\tan(\Psi)\, e^{i\Delta} = \frac{r_p}{r_s} \qquad (4.7)$$

where r_p and r_s refer to reflectivities of p and s polarized light, respectively. To extract useful sample properties, an optical model representing the sample is used. The model-generated data for a particular set of sample properties (for instance: film thickness and refractive index) is then fitted numerically to the measured spectrum and the fit quality is quantified by the root mean square error between the measured and model generated spectra. In spectroscopic ellipsometry the fitting is often done across an entire light spectrum divided into many (200 – 400) discreet wavelengths. This improves both accuracy and precision of the technique. The accuracy depends on the validity of assumptions made about the multi-layer sample system (such as uniformity of density distribution, roughness etc.). The precision of the technique for relatively simple samples, such as well-relaxed, uniform and isotropic polystyrene films on silicon wafer, is usually on the order of < 0.1 nm. This allows resolving very small changes and makes the technique very powerful in ultra thin film studies.

A Cauchy relationship is often used to model the optical dispersion of transparent dielectric samples:

$$n(\lambda) = A + \frac{B}{\lambda^2} + \frac{C}{\lambda^4} \qquad (4.8)$$

Here, A, B and C are constants. Often the last term can be omitted to reduce the amount of fitted parameters, if including this term does not provide a significant improvement in fit quality.

4.3. Experimental

4.3.1. Sample preparation

Polystyrene (Sigma Aldrich, M_w = 280 kg/mol, T_g = 100.0 °C by DSC, onset) thin films were spin coated from toluene (Merck) solutions onto clean silicon wafer substrates. The substrates were thoroughly cleaned by immersion in 3:1 (volume) mixture of 98% sulfuric acid and 30% hydrogen peroxide and subsequently washed with ultra pure water. Spin coating was done at 2000 rpm and afterwards the films were annealed at 120 °C under nitrogen flow for at least 16 hours to remove the

remaining solvent and relax the structure. Swelling of the dry PS films was done in n-octane (Merck).

4.3.2. Ellipsometric measurements

An M-2000X (J.A. Woollam Co.) spectroscopic ellipsometer was used for the temperature scans of dry and swollen polystyrene films. In the employed wavelength range (370 – 1000 nm) polystyrene and n-octane were considered optically transparent. A light beam with an incident diameter of 2 mm was used at an angle of 70°. The thermal evolution of the properties of the dry films was measured with an INSTEC high temperature cell; films were first heated 120 °C and subsequently cooled at a rate of 10 °C/min. A spectrum was recorded every ~2 s. The temperature dependence of swollen films was determined in a custom built solvent cell. The films in this cell were first exposed to a thermally equilibrated n-octane solvent at 42 °C. After stabilization, the temperature was reduced stepwise down to 10 °C. Each step of 2 °C was done within 15 minutes, followed by 85 minutes for equilibration. Full spectra were recorded every 30 s.

In both *in-situ* ellipsometry cells the optical dispersion influence of the windows was taken into account with a calibrated delta offset parameter. The optical dispersion of n-octane, n_S, was measured by fitting its optical properties against the known properties of a 25 nm SiO_2/Si calibration wafer at every temperature used. The data was in a very good agreement with the literature [46].

All of the samples were modeled by a multilayer optical model, involving a crystalline silicon substrate with a ~ 2 nm thick native oxide, and a Cauchy layer representing the polystyrene film. The optical dispersions of crystalline silicon and the native oxide were taken from literature [47]. The temperature dependence of these optical dispersions was taken into account, to improve the accuracy in determination of the properties of the polystyrene films (in particular its refractive index). The polymer films were considered perfectly isotropic with no density gradients and negligible roughness.

4.4. Results and discussion

4.4.1. Calculation of the excess fractional free volume in a dry thin polymer film

Figure 4.2 shows the thickness and refractive index of a dry 179 nm PS film in a region covering the glass transition temperature. The transition temperature, $T_{g,dry}$, is determined from the intersection of linear fits through liquid and glassy regions, as is commonly done.

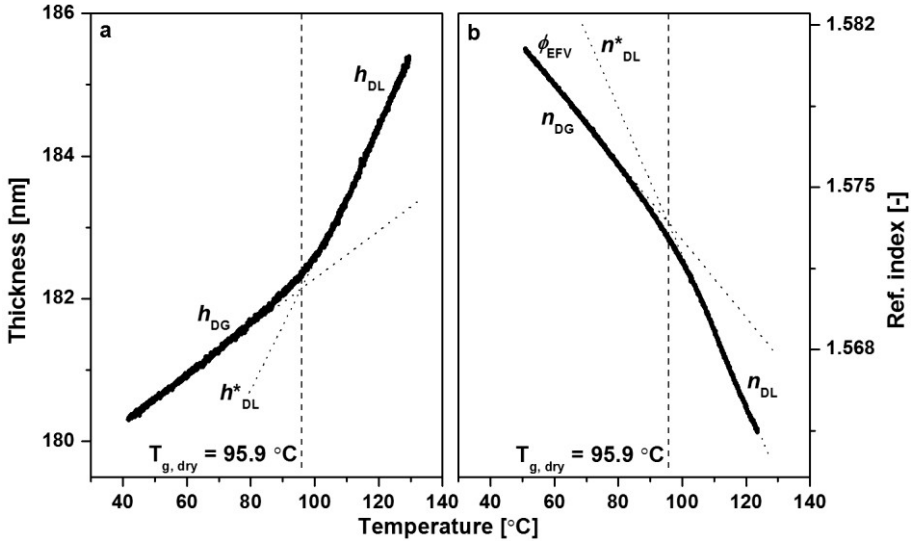

Figure 4.2 a) Thickness and b) refractive index of a 179 nm PS film determined via spectroscopic ellipsometry in a region covering glass transition

The thickness and refractive index show a consistent behavior. Above the glass transition they follow a linear trend that corresponds to the behavior of a dry liquid polymer: h_{DL} and n_{DL}. Below the glass transition both values start to deviate from their equilibrium liquid lines, extrapolated from above the glass transition. A glassy state is obtained, and the corresponding variables are denoted h_{DG} and n_{DG}. From the difference between the glassy thickness, h_{DG}, and the extrapolated liquid thickness, h^*_{DL}, the excess fractional free volume, $\phi_{EFV}^{dil.}$, can be calculated using a relationship similar to the dilation approach:

$$\phi_{EFV}^{dil.} = \frac{h_{DG} - h_{DL}^*}{h_{DG}} \quad (4.9)$$

The excess fractional free volume can also be calculated using the BEMA that considers the glassy polymer (for which n_{DG} is measured directly) to be a mixture of liquid polymer matrix extrapolated down to the glassy region, n^*_{DL}, and void (n_{EFV} = 1.000):

$$\phi_{EFV}^{BEMA} \cdot \frac{n_{EFV}^2 - n_{DG}^2}{n_{EFV}^2 + 2n_{DG}^2} + (1 - \phi_{EFV}^{BEMA}) \cdot \frac{(n_{DL}^*)^2 - n_{DG}^2}{(n_{DL}^*)^2 + 2n_{DG}^2} = 0 \quad (4.10)$$

In a sense, this approach treats the glassy polymer as a porous structure where the porosity corresponds to ϕ_{EFV}^{BEMA}, and the matrix has the properties of hypothetical equilibrium liquid polymer. $\phi_{EFV}^{dil.}$ and ϕ_{EFV}^{BEMA} are plotted together in Figure 4.3.

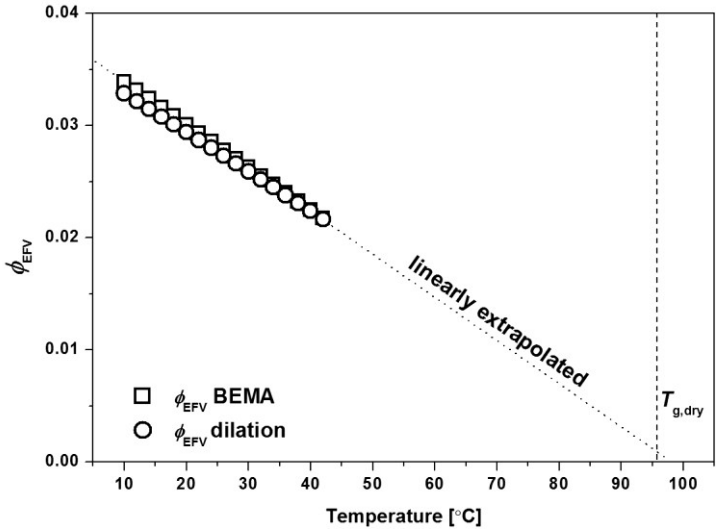

Figure 4.3 Excess fractional free volumes calculated for a dry glassy polymer from the Bruggeman effective medium approximation and from the thickness change around the glass transition temperature.

In the figure the values are calculated in a temperature range 10 – 42 °C, where the solvent swelling experiments, discussed later, are conducted. The values indicate that in the dry glassy PS film about 2% (at 42 °C) to about 3.3% (at 10 °C) of void is kinetically trapped. When the polymer is swollen with a penetrant to form an equilibrium mixture, the influence of this trapped free volume is often neglected. An excellent agreement between $\phi_{EFV}^{dil.}$ and ϕ_{EFV}^{BEMA} strongly suggests the equivalency of both approaches. Additionally, a linear extrapolation towards higher temperatures intersects the ϕ_{EFV} = 0 very close to $T_{g,dry}$. This is expected, because at $T_{g,dry}$ the excess fractional free volume vanishes and the polymer is at equilibrium.

4.4.2. Polystyrene film swollen with n-octane

When a polymer film comes in contact with a liquid penetrant, it often swells and dilates. In the case of sufficiently favorable interactions between the polymer and the penetrant, a plasticization effect can be observed. This is manifested by a reduction in the glass transition temperature of the film, due to the enhancement of polymer chain mobility by a lubricating effect of the penetrant. This is illustrated by swelling PS with n-octane. This hydrocarbon swells PS considerably (to about 12% around room temperature), but it does not dissolve it. The combination of PS and n-octane pair allows convenient observation of the glass transition of the swollen film, close to room temperature, as shown in Figure 4.4.

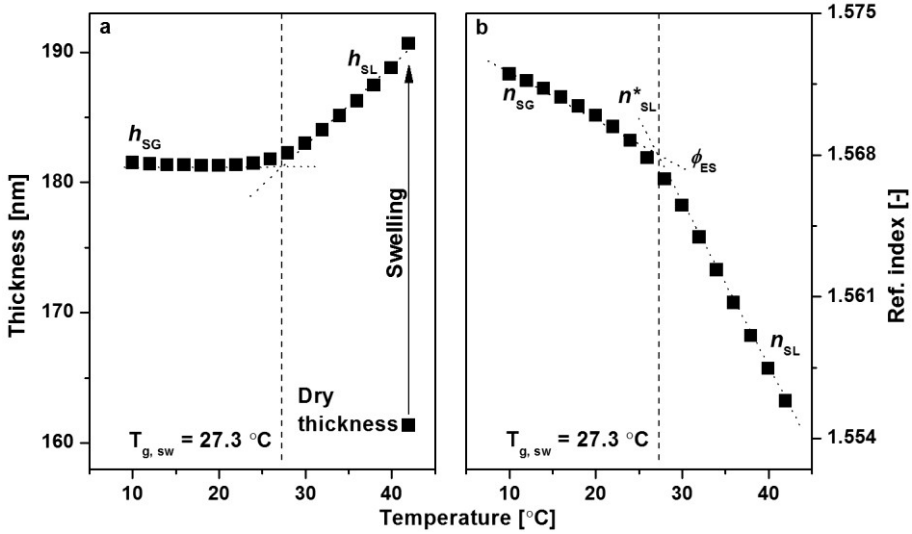

Figure 4.4 a) Thickness and b) refractive index of PS film swollen with liquid n-octane; the system shows glass transition temperature, $T_{g,sw}$, at 27.3 °C. This corresponds to significant plasticization (reduction of T_g by 68.6 °C from 95.9 °C for a dry polymer).

In the swollen system both the dilation and refractive index show an analogous behavior as compared to the dry film. The glass transition of the swollen film can also be determined from the intersection of the extrapolated linear regions above and below the transition. The value of $T_{g,sw}$, = 27.3 °C indicates a significant plasticization, manifested by a reduction in $T_{g,dry}$ from 95.9 °C by 68.6 °C. The physical interpretation of the transition in a swollen system changes as compared to the interpretation the dry glass transition. In the dry glass transition, Figure 4.2, the mobility of the polymer matrix is influenced by solely by the thermal energy. In the case of the swollen system both temperature and penetrant volume fraction (associated with swelling) change. Above the $T_{g,sw}$ an equilibrium amount of n-octane is dissolved in the PS film. When the temperature is reduced the equilibrium concentration of n-octane reduces. At $T_{g,sw}$ the penetrant concentration and thermal energy no longer allow a sufficient polymer chain mobility to follow a perturbation of the system. Upon further decrease in temperature the polymer structure becomes kinetically arrested, with significant excess amount of penetrant in it. This phenomenon, as well as its dynamic characteristics, is investigated in more detail in chapter 10 of this Thesis. In this chapter, the focus is on the calculations of the penetrant volume fraction in the swollen system.

In the literature, the optical measurements of swelling polymers have been used to calculate the penetrant volume fractions using the dilation or EMA approaches. For already rubbery dry polymers, and their mixtures which could be considered ideal, such calculations have yielded accurate results [4, 14-16, 19, 23, 34, 35]. In those

cases the straightforward volume additivity in the dilation approach, eq. 4.1, holds, because the thickness of the dry film corresponds always to equilibrium, liquid state, h_{DL}. For the EMA approaches, Bruggeman and Clausius – Mosotti, the refractive index of the matrix in a swollen state can be considered identical to that from the dry state, n_{DL}. For glassy polymers, on the other hand, the h_{DG} and n_{DG} , that are readily available from the optical measurements of dry glassy films, correspond to non-equilibrium values and carry the contributions of the excess fractional free volume. If these non-equilibrium properties are used either in the dilation or EMA approaches, as is often done [6, 10, 11, 15, 18, 20, 21, 24, 36-42], the obtained penetrant volume or mass fractions can be underestimated.

This is demonstrated in Figure 4.5, where the dilation, BEMA, and C-M approaches are used, without (closed symbols) and with (open symbols) accounting for the excess free volume that was initially present in the dry glassy polymer. In the temperature range of the swelling experiments, 10 – 42 °C, the dry polymer is glassy. For the experiments above $T_{g,sw}$ = 27.3 °C the swollen system is an equilibrium liquid, below $T_{g,sw}$, the swollen system is glassy.

The calculations not taking account for the relaxation of excess fractional free volume can be formulated as:

In the dilation approach, eq. 4.1:

$$\phi_S^{dil.} = f(h_{SP}, h_{DG}) \quad (4.11)$$

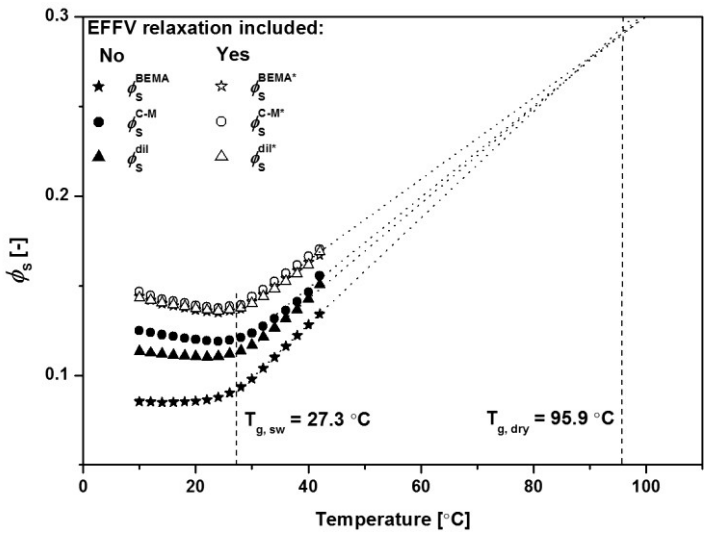

Figure 4.5 Comparison of solvent volume fractions calculated for the PS swollen with n-octane using approaches that do not (closed symbols) or do (open symbols) take into account the relaxation of excess fractional free volume in the polymer upon penetrant sorption

In the Bruggeman EMA, eq. 4.2:

$$\phi_S^{BEMA} = f(n_S, n_{SP}, n_{DG}) \quad (4.12)$$

Where the refractive index of swollen polymer, n_{SP}, is either n_{SL}, for the swollen system above $T_{g,sw}$, or n_{SG} for the swollen system below $T_{g,sw}$.

In the Clausius – Mossotti, eqs. 4.3-4.6:

$$\phi_S^{C-M} = f(n_S, n_{SP}, n_{DG}, h_{DG}, h_{SP}, \rho_S) \quad (4.13)$$

For the calculations, which do take into account the relaxation of the excess fractional free volume upon sorption, h_{DG} is replaced by h^*_{DL}, and n_{DG} is replaced by n^*_{DL}:

$$\phi_S^{dil.,*} = f(h_{SP}, h_{DL}^*) \quad (4.14)$$

$$\phi_S^{BEMA,*} = f(n_S, n_{SP}, n_{DL}^*) \quad (4.15)$$

$$\phi_S^{C-M,*} = f(n_S, n_{SP}, n_{DL}^*, h_{DL}^*, h_{SP}, \rho_S) \quad (4.16)$$

Therefore, by using either the hypothetical equilibrium film thickness and/or its refractive index extrapolated from liquid state of the dry polymer, equations 4.14 – 4.16, the influence of the non-equilibrium state of a dry sample before it comes in contact with the solvent is included.

It is clear from Figure 4.5, that when the relaxation of ϕ_{EFV} is taken into account all of the 3 approaches agree with each other, in contrast to the approaches that use the dry glassy sample properties in a straightforward way. Moreover, the obtained solvent volume fractions are significantly lower (underestimated), when the relaxation of ϕ_{EFV} is not taken into account. In addition, a striking indication of the inapplicability of the Clausius – Mossotti approach using the dry glassy polymer properties, eq. 4.16, is that the sum of ϕ_S^{C-M} and ϕ_P^{C-M} is significantly larger than 1 (data not shown).

The underestimated ϕ_S values for approaches not correcting for the relaxation of ϕ_{EFV} result in overestimated Flory-Huggins interaction parameters, χ, calculated from the well-known Flory-Huggins expression [48], connecting the solvent activity with the volume fraction of the solvent. In its simplest form, for non-crosslinked systems, the expression is written as:

$$ln(a) = ln(\phi_S) + (1 - \phi_S) + \chi \cdot (1 - \phi_S)^2 \quad (4.17)$$

For a liquid solvent, $a = 1$. Figure 4.6 shows the χ values calculated based on the six approaches to calculation of ϕ_S as a function of the inverse temperature, as is commonly presented. For simplification only one χ^* is showed, representing the $\chi^{BEMA,*}$, $\chi^{dil.,*}$, and $\chi^{C-M,*}$which all lie very close to each other (as seen before for solvent volume fractions in Figure 4.5).

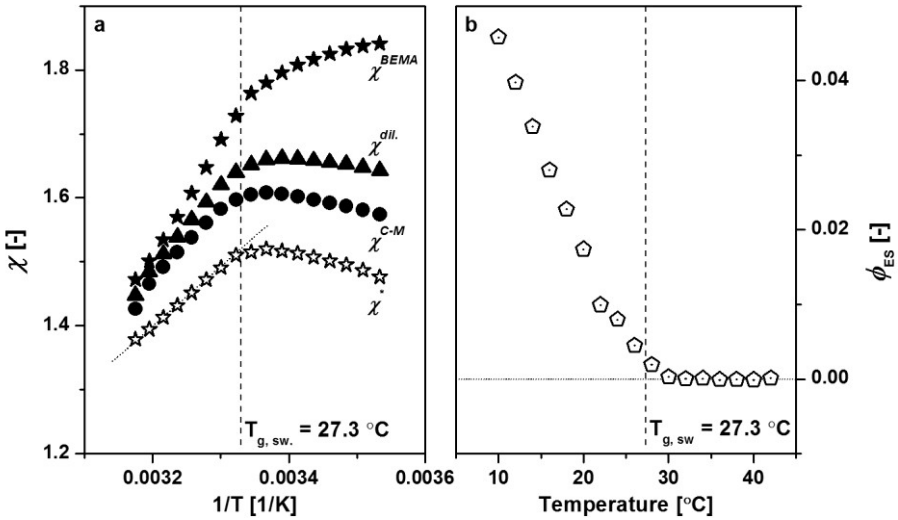

Figure 4.6 a) Flory – Huggins interaction parameters calculated from eq. 4.17 b) Excess solvent fraction trapped below $T_{g,sw}$

As can be seen from the figure, the values of χ^{BEMA}, $\chi^{dil.}$ and χ^{C-M} are all much larger than that of χ^{*}. Thus, the interaction strength between PS and n-octane is underestimated for the three approaches that do not include the relaxation of excess free volume. For the liquid region, above $T_{g,sw.}$, $\chi^{BEMA,*}$ shows the usually obtained linear dependence on the inverse temperature. From the slope of this relationship the difference in the solubility parameters of the polymer and penetrant can be accurately calculated [49].

The curvature change of the swollen polymer refractive index below the glass transition temperature of the swollen polymer, Figure 4.4b, indicates that in the glassy swollen system a certain excess volume of solvent, ϕ_{ES} is kinetically trapped. Such a configuration is analogous to the trapped ϕ_{EFV} in the dry system. This means that a swollen system, cooled down from its liquid state to below the glass transition, will possess an excess amount of solvent as compared to its equilibrium state. The influence of ϕ_{ES} is visible both in Figure 4.5 and Figure 4.6a where the curves change their slope around glass transition point. By quantifying the difference between the $\phi_S^{BEMA,**}$(representing here the values of $\phi_S^{BEMA,*}$ extrapolated from above $T_{g,sw}$) and $\phi_S^{BEMA,*}$ calculated below $T_{g,sw}$, it is possible to *estimate* ϕ_{ES}, Figure 4.6b. The figure shows, as expected, a sharp increase with decreasing temperature below the glass transition in the swollen film. Noticeably, at relatively small degrees of undercooling already significant ϕ_{ES} seems to exist in the swollen polymer.

In Figure 4.5 below the $T_{g,sw}$ the calculated volume fractions represented by the open symbols, seem to slightly increase. This, rather unexpected and probably

unphysical behavior, may be a result of the breakdown of the assumptions behind the dilation and EMA approaches below the glass transition of the swollen system. In particular, it seems questionable whether in this highly swollen, non-equilibrium system the refractive index of the polymer matrix can still be assumed the same as the one extrapolated from the dry liquid state, n^*_{DL}. A more detailed discussion is considered outside of the scope of this study, because the focus here is put on the situation where the solvent induces glass transition, and the swollen system is in an equilibrium rubbery state (between $T_{g,sw}$ = 27.3 °C and 42°C).

4.4.3. General implications for solvent – glassy polymer systems

The approach presented here, for calculation of the n-octane fraction in PS, includes relaxation of ϕ_{EFV} by extrapolation of the polymer properties from the liquid region, that is, from above to below the glass transition. This approach can be generalized to other glassy polymer – liquid penetrant systems. For the most accurate results the swelling should induce a glass transition. In addition, the swollen film should behave as an ideal liquid mixture, i.e., the assumption of constant partial molar properties upon mixing must be valid. Being above $T_{g,sw}$ can be confirmed by measuring relaxation times of the plasticized polymer by, for instance, dielectric relaxation spectroscopy, by measuring the influence of a change in temperature on swelling (instant response in a liquid region), or, in some cases, by the lack of significant changes in swelling in time (indication of equilibrium). In addition the n_{DL} should be measurable, which implies that the polymer is stable above its $T_{g,dry}$. This may become problematic for some high $T_{g,dry}$ polymers due to their thermal decomposition. In those cases n_{DL} could be estimated otherwise, for instance by positron annihilation studies of the free volume distribution, or approximately calculated from group contribution theories [45]. Complications may also arise if a polymer matrix under consideration is characterized by a substantial degree of crystallinity. In such a case n_{PM} might be difficult to accurately define.

Based on the presented approach it is possible to derive an expression for the error that is made in the determination of the solvent volume fraction in a swollen glassy polymer, when the relaxation of excess free volume is neglected. The calculation assumes that the experiments are performed above $T_{g,sw}$. The error quantifies the difference between the penetrant volume fraction obtained from dilation that uses the extrapolated liquid index of the dry polymer, as in eq. 4.14, and the one obtained from straightforward dilation without accounting for EFV, eq. 4.11:

$$Error = \left(\frac{\phi_S^{dil.,*}}{\phi_S^{dil,}} - 1\right) \cdot 100\% \qquad (4.18)$$

Combining eq. 4.9 and swelling factor of a polymer, defined as $S_F = h_{SP}/h_{DP}$, eq. 4.18 can be rewritten:

$$Error = \left(\frac{S_F - \frac{1}{1+\phi_{EFV}}}{S_F - 1} - 1 \right) \cdot 100\% \qquad (4.19)$$

In this form the equation can be conveniently used for a polymer swollen above its glass transition, with a known swelling factor S_F, and a particular non-equilibrium ϕ_{EFV} before the swelling experiment. In fact, membrane films for water and organic solvent separations are usually swollen above glass transition of the mixture to assure high enough values of the solvent diffusion coefficient. The *Error* parameter, eq. 4.19, is plotted in Figure 4.7 as a function of S_F for several ϕ_{EFV}. The filled dot indicates polystyrene swollen with n-octane at 30 °C.

For example in the case of a polymer with ϕ_{EFV} = 0.08 swollen to a factor of 1.2 the error is already 40%. In the case of polystyrene and n-octane the error is moderate due to its low ϕ_{EFV}. Several other interesting conclusions can be drawn from the figure. As anticipated, for lower swelling factors, polymers with extremely large ϕ_{EFV} (for instance, in polymers with intrinsic microporosity (PIMs), like poly(1-trimethylsilyl-1-propyne) (PTMSP), [50-52]) will introduce very high errors. The error will diminish for higher swelling factors – in this case the higher swelling (larger film dimension change) will overshadow the effect of not accounting for the relaxation of ϕ_{EFV}. Moreover, the error that is introduced when the excess free volume is not taken into account depends on the sample history because it uses the non-equilibrium glassy properties that change over time.

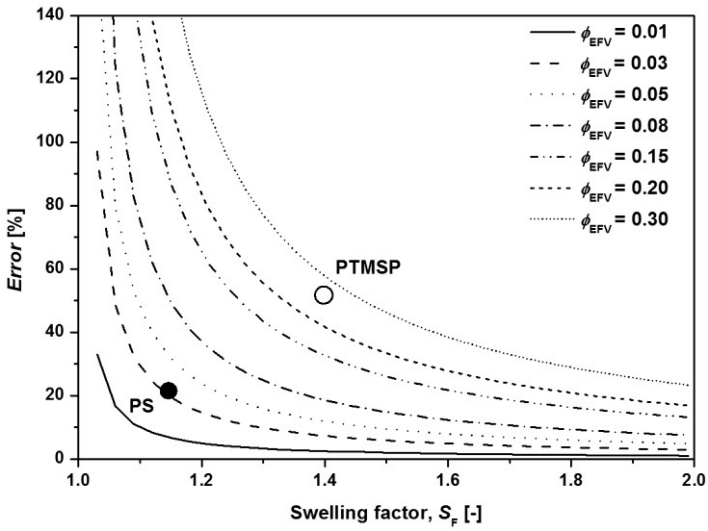

Figure 4.7 Error in the determination of solvent volume fraction of a swollen glassy polymer when relaxation of excess fractional free volume upon sorption is neglected; the filled dot represents PS swollen with n-octane at 30 °C, the open dot is illustrative for PTMSP swollen to a factor of 1.4

This is not the case for the approach that does consider the relaxation of the excess free volume.

4.4.4. Remarks on Clausius – Mossotti approach in high pressure gas sorption measurements

Due to its relative simplicity the Clausius – Mossotti approach has been frequently applied in high pressure ellipsometry studies of gas sorption in ultra thin rubbery and glassy films [6, 10, 11, 14-16, 22, 26]. However, these results need to be considered as *only* an estimate, even in rubbery materials as highlighted by Sirard et al [14]. The main reason is that the use of eqs. 4.3-4.6 requires knowledge of the dissolved penetrant partial molar volume (or density). This is extremely difficult for gas sorption experiments and frequently the properties of the penetrant in its critical state are used. These, however, show a very strong dependence on the conditions (p, T) and are valid for pressures and temperatures usually much higher than typical experimental conditions. For glassy polymers additional complications arise. The density of a plasticized polymer matrix is pressure and concentration dependent which causes the n_{DG} to change in the course of an experiment gradually approaching the n^*_{DL}. Therefore, the (at least partial) relaxation of ϕ_{EFV} in highly plasticized polymer matrices is rarely accounted for. All of the above reasons contribute to significant inaccuracies in the determination of the gaseous penetrant concentration in swollen thin and ultra-thin films.

4.4.5. Summary of the method to determine solvent volume fraction in a swollen polymer in contact with a liquid solvent (a = 1) taking account for excess free volume relaxation

In this part a short summary is presented for a procedure to determine ϕ_S^* based on ellipsometry measurements of swollen and dry polymer films with the relaxation of ϕ_{EFV} taken into account.

a. Determine h_{DL}, n_{DL}, and h_{DG}, n_{DG}, of a dry polymer at the temperature of swelling, from temperature dependent scan covering $T_{\mathrm{g,dry}}$.
b. Extrapolate the h_{DL}, n_{DL} from above $T_{\mathrm{g,dry}}$ to obtain h^*_{DL}, n^*_{DL}.
c. From eq. 4.9 and eq. 4.10 calculate $\phi_{EFV}^{dil.}$ and ϕ_{EFV}^{BEMA}. Confirm that $\phi_{EFV}^{dil.} = \phi_{EFV}^{BEMA}$.
d. Determine the refractive index of the liquid solvent, n_S, at the temperature of swelling, for instance by fitting its dispersion against a calibration silicon wafer.

e. Determine the refractive index of the swollen film, n_{SP}, at the temperature of swelling.

f. From eq. 4.14-4.16 calculate the respective ϕ_S^*.

4.5. Conclusions

We have investigated the effect of the excess free volume fraction on calculations of the penetrant volume fraction in glassy polymers, using a as an example a polystyrene – n-octane model system. Two well-known effective medium approximation (EMA) approaches, the Bruggeman EMA and Clausius – Mossotti, and a simple dilation approach have been used for the calculations. For the determination of the excess free volume fraction in a thin film of a dry glassy polymer, the Bruggeman EMA and dilation are shown to be equivalent. For the calculations of the penetrant volume fraction it is shown that the three different approaches do not agree with each other and yield sample history dependent results. This is a result of neglecting the influence of the excess free volume fraction that is trapped in a glassy polymer upon vitrification, by using the properties of a non-equilibrium glassy system. If the influence of the excess free volume is accounted for, by extrapolating the properties of a hypothetical liquid polymer down to the temperatures where glassy state is obtained, all three approaches yield the same values. In this case, the obtained penetrant volume fractions are significantly larger than those obtained without including the excess free volume fraction. In addition, they are not dependent on the sample history. The error between the two approaches is calculated and shown to be particularly large for polymers that possess high excess free volume fractions. Such systems are of great importance, for instance in membrane separations.

4.6. References

[1] Hölck, O., et al., *Gas sorption isotherms in swelling glassy polymers—Detailed atomistic simulations.* Journal of Membrane Science, 2013. **428**(0): p. 523-532.

[2] Wijmans, J.G. and R.W. Baker, *The solution-diffusion model: a review.* Journal of Membrane Science, 1995. **107**(1-2): p. 1-21.

[3] Wessling, M., et al., *Plasticization of gas separation membranes.* Gas Separation & Purification, 1991. **5**(4): p. 222-228.

[4] Ogieglo, W., et al., *n-Hexane induced swelling of thin PDMS films under non-equilibrium nanofiltration permeation conditions, resolved by spectroscopic ellipsometry.* Journal of Membrane Science, 2013. **437**(0): p. 313-323.

[5] Ogieglo, W., et al., *Temperature-induced transition of the diffusion mechanism of n-hexane in ultra-thin polystyrene films, resolved by in-situ Spectroscopic Ellipsometry.* Polymer, 2013. **54**(1): p. 341-348.

[6] Horn, N.R. and D.R. Paul, *Carbon Dioxide Sorption and Plasticization of Thin Glassy Polymer Films Tracked by Optical Methods.* Macromolecules, 2012.

[7] El Ouakili, A., et al., *Glass transition temperatures of isotactic poly(methymethacrylate) thin films and individual chains probed by multi wavelength ellipsometry.* EPJ Applied Physics, 2011. **56**(1).

[8] Elbs, H. and G. Krausch, *Ellipsometric determination of Flory-Huggins interaction parameters in solution.* Polymer, 2004. **45**(23): p. 7935-7942.

[9] Pham, J.Q., et al., *Pressure, Temperature, and Thickness Dependence of CO_{2}-Induced Devitrification of Polymer Films.* Physical Review Letters, 2003. **91**(17): p. 175503.

[10] Wind, J.D., et al., *Relaxation Dynamics of CO2 Diffusion, Sorption, and Polymer Swelling for Plasticized Polyimide Membranes.* Macromolecules, 2003. **36**(17): p. 6442-6448.

[11] Wind, J.D., et al., *Carbon Dioxide-Induced Plasticization of Polyimide Membranes: Pseudo-Equilibrium Relationships of Diffusion, Sorption, and Swelling.* Macromolecules, 2003. **36**(17): p. 6433-6441.

[12] Richardson, H., M. Sferrazza, and J.L. Keddie, *Influence of the glass transition on solvent loss from spin-cast glassy polymer thin films.* The European Physical Journal E: Soft Matter and Biological Physics, 2003. **12**(0): p. 87-91.

[13] Sirard, S.M., et al., *Anomalous Properties of Poly(methyl methacrylate) Thin Films in Supercritical Carbon Dioxide.* Macromolecules, 2002. **35**(5): p. 1928-1935.

[14] Sirard, S.M., P.F. Green, and K.P. Johnston, *Spectroscopic Ellipsometry Investigation of the Swelling of Poly(Dimethylsiloxane) Thin Films with High Pressure Carbon Dioxide.* The Journal of Physical Chemistry B, 2001. **105**(4): p. 766-772.

[15] Simons, K., et al., *CO2 sorption and transport behavior of ODPA-based polyetherimide polymer films.* Polymer, 2010. **51**(17): p. 3907-3917.

[16] Sirard, S.M., et al., *Spectroscopic ellipsometry of grafted poly(dimethylsiloxane) brushes in carbon dioxide.* The Journal of Supercritical Fluids, 2004. **32**(1–3): p. 265-273.

[17] Mendoza-Galván, A., et al., *Effect of a temperature gradient on ellipsometry measurements in supercritical CO2.* The Journal of Supercritical Fluids, 2012. **64**(0): p. 25-31.

[18] Tang, Y., et al., *Swelling of Zwitterionic Polymer Films Characterized by Spectroscopic Ellipsometry.* Macromolecules, 2001. **34**(25): p. 8768-8776.

[19] Spaeth, K., G. Kraus, and G. Gauglitz, *In-situ characterization of thin polymer films for applications in chemical sensing of volatile organic compounds by spectroscopic ellipsometry.* Fresenius' Journal of Analytical Chemistry, 1997. **357**(3): p. 292-296.

[20] Chen, W.L., et al., *Equilibrium swelling of hydrophilic polyacrylates in humid environments.* Macromolecules, 1999. **32**(1): p. 136-144.

[21] Filippov, L.K., *Study of diffusion in films on planar substrates by ellipsometry.* Journal of the Chemical Society, Faraday Transactions, 1993. **89**(22): p. 4053-4057.

[22] Carla, V., et al., *Nonequilibrium model for sorption and swelling of bulk glassy polymer films with supercritical carbon dioxide.* Macromolecules, 2005. **38**(24): p. 10299-10313.

[23] Chan, K. and K.K. Gleason, *Initiated chemical vapor deposition of linear and cross-linked poly(2-hydroxyethyl methacrylate) for use as thin-film hydrogels.* Langmuir, 2005. **21**(19): p. 8930-8939.

[24] Crossland, E.J.W., et al., *Systematic control of nucleation density in Poly(3-Hexylthiophene) thin films.* Advanced Functional Materials, 2011. **21**(3): p. 518-524.

[25] Dodoo, S., et al., *Effect of ionic strength and layer number on swelling of polyelectrolyte multilayers in water vapour.* Soft Materials, 2013. **11**(2): p. 157-164.

[26] Rowe, B.W., B.D. Freeman, and D.R. Paul, *Effect of sorbed water and temperature on the optical properties and density of thin glassy polymer films on a silicon substrate.* Macromolecules, 2007. **40**(8): p. 2806-2813.

[27] Stamatialis, D.F., M. Sanopoulou, and I. Raptis, *Swelling and dissolution behavior of poly(methyl methacrylate) films in methyl ethyl ketone/methyl alcohol mixtures studied by optical techniques.* Journal of Applied Polymer Science, 2002. **83**(13): p. 2823-2834.

[28] Stamatialis, D.F., et al., *Optical vs. direct sorption and swelling measurements for the study of stiff-chain polymer-penetrant interactions.* Journal of Membrane Science, 1997. **130**(1-2): p. 75-83.

[29] Durning, C.J., et al., *A Study of Case II Transport by Laser Interferometry.* Macromolecules, 1995. **28**(12): p. 4234-4248.

[30] Tong, H.M., K.L. Saenger, and C.J. Durning, *A study of solvent diffusion in thin polyimide films using laser interferometry.* Journal of Polymer Science Part B: Polymer Physics, 1989. **27**(3): p. 689-708.

[31] Bolton, B.A., et al., *Ethanol sorption and partial molar volume in cellulose acetate films.* The Journal of Physical Chemistry, 1986. **90**(6): p. 1207-1211.

[32] Hori, K., H. Matsuno, and K. Tanaka, *Sorption kinetics of methanol in thin poly(methyl methacrylate) films studied by optical reflectivity.* Soft Matter, 2011. **7**(21): p. 10319-10326.

[33] Bruggeman, D., *The calculation of various physical constants of heterogeneous substances. I. The dielectric constants and conductivities of mixtures composed of isotropic substances.* Annalen der Physik, 1935. **24**(7).

[34] Miller, M.D. and M.L. Bruening, *Correlation of the swelling and permeability of polyelectrolyte multilayer films.* Chemistry of Materials, 2005. **17**(21): p. 5375-5381.

[35] Lau, K.K.S. and K.K. Gleason, *All-dry synthesis and coating of methacrylic acid copolymers for controlled release.* Macromolecular Bioscience, 2007. **7**(4): p. 429-434.

[36] Filippova, N.L., *Interdiffusion in Polymer Film by Ellipsometry.* Journal of Colloid and Interface Science, 1999. **212**(2): p. 589-592.

[37] Tang, Y., et al., *Structural Effects on Swelling of Thin Phosphorylcholine Polymer Films.* Macromolecules, 2002. **35**(10): p. 3955-3964.

[38] Hennig, A., et al., *Contact angle hysteresis: Study by dynamic cycling contact angle measurements and variable angle spectroscopic ellipsometry on polyimide.* Langmuir, 2004. **20**(16): p. 6685-6691.

[39] Pantelić, N., et al., *Characterization of partially sulfonated polystyrene-block-poly(ethylene- ran-butylene)-block-polystyrene thin films for spectroelectrochemical sensing.* Analytical Chemistry, 2009. **81**(16): p. 6756-6764.

[40] Zettl, U., A. Knoll, and L. Tsarkova, *Effect of confinement on the mesoscale and macroscopic swelling of thin block copolymer films.* Langmuir, 2010. **26**(9): p. 6610-6617.

[41] López García, Í., J.L. Keddie, and M. Sferrazza, *Probing the early stages of solvent evaporation and relaxation in solvent-cast polymer thin films by spectroscopic ellipsometry.* Surface and Interface Analysis, 2011. **43**(11): p. 1448-1452.

[42] Hegewald, J., et al., *Electron beam irradiation of poly(vinyl methyl ether) films. 2. Temperature-dependent swelling behavior.* Langmuir, 2006. **22**(11): p. 5152-5159.

[43] Gibbs, J.H. and E.A. DiMarzio, *Nature of the Glass Transition and the Glassy State.* The Journal of Chemical Physics, 1958. **28**(3): p. 373-383.

[44] Neogi, P., *Diffusion in polymers*. Vol. 32. 1996: CRC.

[45] Krevelen, W.v., *Properties of Polymers.* Elsevier, 1990. Amsterdam.

[46] Orge, B., et al., *Mixing properties of (methanol, ethanol, or 1-propanol) with (n-pentane, n-hexane, n-heptane and n-octane) at 298.15 K.* Fluid Phase Equilibria, 1997. **133**(1–2): p. 213-227.

[47] Herzinger, C.M., et al., *Ellipsometric determination of optical constants for silicon and thermally grown silicon dioxide via a multi-sample, multi-wavelength, multi-angle investigation.* Journal of Applied Physics, 1998. **83**(6): p. 3323-3336.

[48] Flory, P.J., *Principles of Polymer Chemistry*1953: Cornell University Press, Ithaca, New York.

[49] Sanopoulou, M. and D.F. Stamatialis, *Study of the transition from Fickian to Case II sorption kinetics in the system poly(ethyl methacrylate)–liquid methyl alcohol.* Polymer, 2001. **42**(4): p. 1429-1439.

[50] Budd, P.M., et al., *Polymers of intrinsic microporosity (PIMs): robust, solution-processable, organic nanoporous materials.* Chemical Communications, 2004(2): p. 230-231.

[51] McKeown, N.B. and P.M. Budd, *Polymers of intrinsic microporosity (PIMs): organic materials for membrane separations, heterogeneous catalysis and hydrogen storage.* Chemical Society Reviews, 2006. **35**(8): p. 675-683.

[52] McKeown, N.B., et al., *Towards Polymer-Based Hydrogen Storage Materials: Engineering Ultramicroporous Cavities within Polymers of Intrinsic Microporosity.* Angewandte Chemie International Edition, 2006. **45**(11): p. 1804-1807.

Chapter 5

Polymer relaxations in thin films in the vicinity of penetrant or temperature induced glass transition

This chapter is in preparation for publication, authored by:

Ogieglo W., Wessling M., Benes N.E.

Abstract

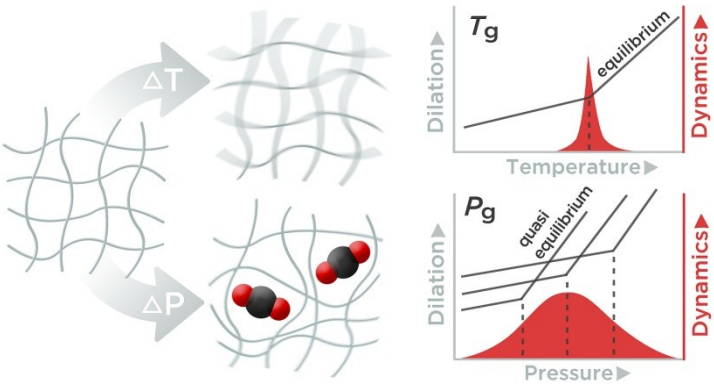

In this chapter the transient properties of thin glassy polymer films in the vicinity of the glass transition are investigated. We compare the differences and similarities between a sorption and temperature induced glass transitions, referred to as P_g and T_g, respectively. The experimental technique used is *in-situ* spectroscopic ellipsometry, which allows for a very precise dynamic measurement of the changes in the thickness and the refractive index of the thin films. It is shown that significant differences exist between the penetrant and the temperature induced transitions. The T_g is relatively well-defined with a sharp change in polymer dynamics, causing a well-known curvature change, a kink, in the dilation curve. In contrast, the relaxations in the vicinity of P_g do not show a sharp change. In particular, the large degree of matrix deformation associated with the P_g may actuate additional relaxation processes that are not probed during transversing the glass transition via temperature scans. The interplay between various polymer relaxation modes can even lead to a kink in the dilation curve that cannot be interpreted as true glass transition. In fact, significant polymer relaxations are manifested upon slight desorption of penetrants from an excessively swollen system, which can be considered a quasi-equilibrium liquid. The important practical implications of the findings are discussed.

5.1. Introduction

Polymers exhibit a distinct transition of various properties (volume, heat capacity) from a glassy state to a liquid state. In the liquid state the (cooperative) movements of polymer elements are fast, and the timescale of polymer relaxation is very small as compared to the time-scale of a typical macroscopic experiment. In the glassy state the timescale of relaxation is very large, resulting in a material with a non-equilibrium state that depends on its prior history. This non-equilibrium status of a material has important implications for its application. Often it is manifested by unwanted time dependent changes of the material properties. Examples include polymer plasticization [1-3] and aging effects [4, 5] that deteriorate the performance of barrier materials and membranes for molecular separation.

The glass transition is a dynamic phenomenon that can be induced by varying the free energy of the system. When the free energy is increased by raising the temperature, the mobility of polymer segments becomes larger. Generally, the glass transition is studied by varying the temperature over time, providing a so-called temperature induced glass transition (T_g). This approach benefits from the fact that, with respect to the T_g, time and temperature are to some extent interchangeable quantities. It is well-recognized as well, that the T_g can be influenced by the presence of small penetrant molecules. The presence of such penetrants dilates the material, thereby allowing increased macromolecular mobility. This is referred to as plasticization and is manifested by a reduction in the T_g. Varying the concentration of a penetrant, at isothermal conditions, can result in the so-called concentration induced glass transition, C_g. This transition is due to an enhanced "lubricating" effect at higher penetrant concentrations. Thermodynamics of glassy polymers swollen by a penetrant have been extensively studied by many researchers, including Sanchez and Lacombe [6], Doghieri and Sarti [7], Vrentas and Vrentas [8-10], and others [11]. Many of these studies take into account the excess energy associated with the non-equilibrium status of the polymers and enable the prediction of penetrant sorption in the glassy polymer. The shape of the corresponding isotherms has been used to derive the C_g. This transition is postulated to correspond to the point where the isotherm shows a kink [12-15], similar to the approach for determining the T_g from the kink in the dilation versus temperature curve. In the case of gaseous penetrants the C_g is often expressed in terms of the pressure at which the kink is observed, rather than by the corresponding concentration of penetrant in the polymer. This pressure-induced glass transition is denoted as P_g.

Although similarities between the temperature and penetrant induced glass transitions exist, the following needs to be considered. For not too large samples thermal conduction is fast as compared to the heating or cooling rates, and the system can be considered quasi-isothermal at any time during the experiment. In contrast, the transport of a penetrant into a polymer material is relatively slow and

concentration-dependent [16-18]. As a consequence the timescale of penetrant diffusion may be comparable to that of the experiment. In addition, the degree of polymer matrix deformation arising from the uptake of a penetrant can be significantly larger than a temperature induced dilation. This extensive polymer matrix dilation may actuate more and other relaxation processes, resulting in a distinct change in macromolecular dynamics.

In this work the relaxational phenomena of thin glassy films in the vicinity of the T_g and the P_g are investigated and compared. The experimental technique used for this purpose is high-pressure *in-situ* spectroscopic ellipsometry. This technique allows the very precise measurement of dynamic changes in thickness and refractive index of penetrant-exposed or temperature perturbed films. The study reveals that the characteristics of the penetrant and the temperature glass transitions are very distinct. As compared to the T_g, the P_g involves very extensive matrix dilation. In addition, sorption-induced matrix relaxations persist over a broad concentration range, below, as well as above the P_g. The consequence of this is that surprisingly long pre-treatment times are required to fully equilibrate a penetrant swollen polymer, even well above the P_g. In addition, the interplay of various penetrant induced relaxations can be manifested by an apparent kink in the isotherm that does not correspond to a glass transition.

5.2. Experimental part

The thin film samples were prepared by a spin coating technique on cleaned silicon wafers at about 2000 rpm (30 seconds) from 5% toluene (Merck, analytical grade) solution of polystyrene (PS) (Sigma Aldrich, M_w = 280 000 g/mol, T_g by DSC, onset = 100.0 °C). After preparation the thin films were annealed at 125 °C for at least 3 hours under vacuum to remove residual solvent and relax post-preparation stresses. For the isobaric measurements an M-2000X spectroscopic ellipsometer (J.A. Woollam Co. Inc.) was used together with a computer controlled high temperature cell (INSTEC). The films were exposed to increasing temperature in a stepwise manner with an increment of 5 °C (within 1 minute) and then 59 minutes of constant temperature. Afterwards, the temperature was reduced in analogous stepwise manner. The full ellipsometric spectra between 210 and 1000 nm (~490 wavelengths) were recorded every 2 seconds. For the high pressure measurements an Alpha SE ellipsometer (J.A. Woollam Co. Inc.) was utilized in combination with a custom build high-pressure stainless steel cell. Polarized light was allowed to enter and leave the cell through 1 cm thick windows, at an angle of incidence of 70°. A detailed description of the experimental setup can be found elsewhere [19]. The device recorded full Ψ and Δ spectra between 390 and 900 nm (~180 wavelengths) continuously every 8 seconds. Pressurized CO_2 gas (purity grade 4.5, Praxair) was introduced via a high pressure syringe pump (Teledyne ISCO, 500D). The pump assured very stable and accurate (to within 0.1 bar) control of the

pressure. Before each high-pressure measurement the films were exposed to vacuum at 125 °C for 3 hours, inside the measurement cell.

Two high-pressure measurement protocols were used. In the first protocol the sample was exposed from vacuum to 60 bar of CO_2 in a single step, and conditioned for a predefined period of time (from 0.5 to 22 hours). Subsequently, the pressure was reduced in a stepwise manner, with steps of 3 bar, with 5 minutes for the pressure change, followed by 10 minutes of system equilibration. The relatively long time required for the pressure changes was to assure that the Joule-Thompson effects were negligible. The relatively quick desorption, ~15 minutes per step, corresponds to a similar protocol as used in other high-pressure ellipsometry studies [14, 15, 20]. In the second protocol the pressure was increased in a stepwise manner, with pressure increments of 3 bar. Time for the pressure increments was 5 minutes, followed by 55 minutes for sample equilibration; an analogues stepwise depressurization was followed.

The properties of the thin films were extracted using a layered Cauchy-type optical model taking account for the presence of the high pressure ambient. For the details of ellipsometry instrumentation and modeling the interested reader is directed to one of the references [19, 21] and handbooks [22-24].

5.3. Results and discussion

We begin by discussing the phenomenon of an isobaric temperature induced glass transition, T_g. In Figure 5.1a the evolution of film thickness with temperature is presented for a ~360 nm thick PS film. The diminutive changes in the thickness highlight the very high sensitivity of spectroscopic ellipsometry. The experimental temperature range covers the anticipated glass transition temperature of PS. The glass transition temperature can be determined from the change in the slope of the curve observed upon cooling. The value obtained from this kink (T_g = 96.9 °C) is lower than that obtained by DSC (T_g = 100.0 °C) for the same material. The difference is due to the well known cooling rate dependency of the glass transition. The slight mismatch between cooling and heating curves is a result of evaporation of the last traces of the solvent or slight thermal decomposition of PS as a consequence of long annealing above T_g. The rubbery state above glass transition is confirmed by the concurrence of the heating and cooling curves.

In Figure 5.1b three desorption isotherms for ~350 nm thick PS films are presented. These isotherms are obtained from stepwise depressurization at 50 °C and 70 °C, after conditioning for a selected time period at 60 bar CO_2 at the respective temperature. For the temperatures studied, this conditioning pressure has been reported to be sufficient to obtain the fully liquid state of CO_2 swollen thin PS films [14, 15] and PS bulk [25] within 10-20 minutes. All three curves show two linear dilation regimes. At higher pressures the slope of the dilation curve is larger

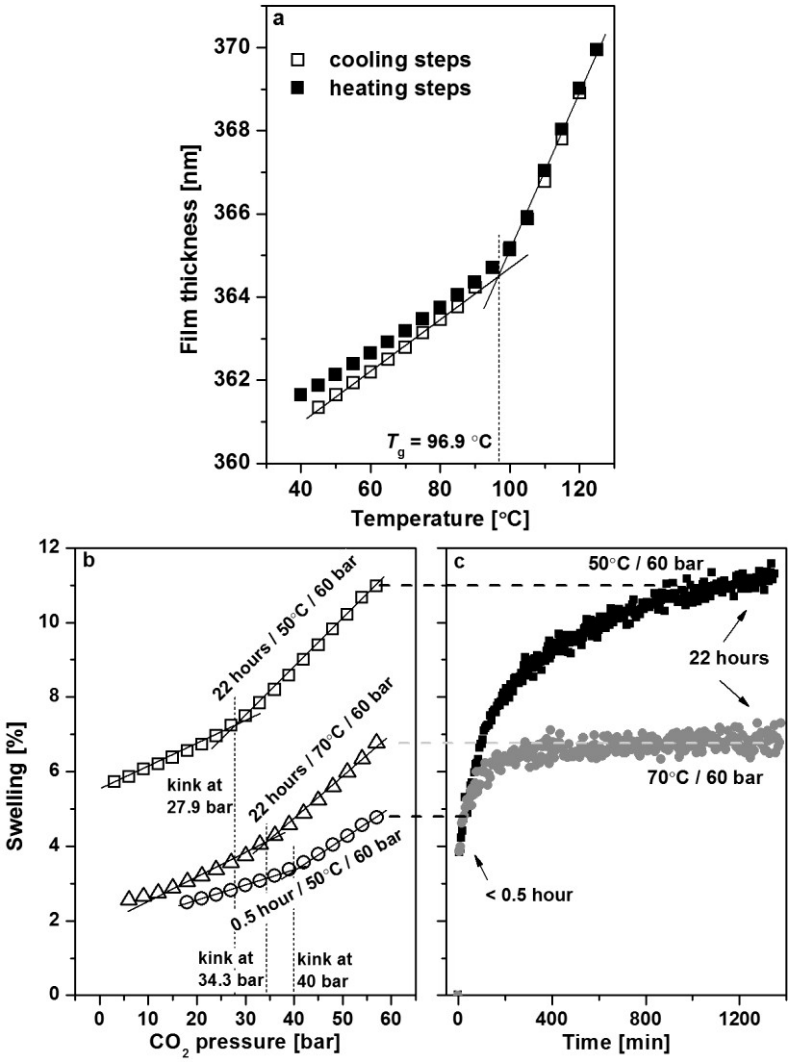

Figure 5.1 a) Thermally induced glass transition determined from the kink in the thermal evolution of thickness of a ~360 nm PS film supported by a silicon wafer b) CO_2 induced swelling of ~350 nm PS films during desorption at 70 °C and 50 °C, and different conditioning times at 60 bar c) long term swelling kinetics of PS films instantly exposed to 60 bar CO_2, at 70 °C and 50 °C; the magnitudes of swelling where a desorption cycle was started are indicated by the vertical dashed lines.

as compared to that at lower pressures. The more pronounced changes at higher pressures are consistent with more dynamic characteristics of the film at these pressures, as compared to lower pressures. The reduced response of the film to pressure changes in the lower pressure range is consistent with a manifestation of

limited polymer dynamics. The kinks in the curves would indicate the onset of these limitations, corresponding to a P_g. However unexpectedly, the location of the kink is strongly correlated with the duration of the conditioning of the films. At 50 °C, conditioning at 60 bar for 0.5 hour or 22 hours results in a kink at 40 or 27.9 bar, respectively. The strong correlation indicates that the equilibrated liquid state is not necessarily obtained during the 60 bar CO_2 exposure. This implies that during conditioning, the timescale of polymer relaxations is too long to consider the material a liquid, and hence the kink cannot correspond to a glass transition. In fact, the origin of the kink is related to correlation between so-called primary and secondary relaxations, as will be discussed in detail later.

The considerable non-equilibrium characteristics of the polymer, during conditioning, are also apparent from Figure 5.1c. In this figure the dynamics of swelling are presented upon immediate exposure to 60 bar CO_2. At 50 °C the swelling is a monotonic function of time. Initially, the slope of the curve is highest, but even after 22 hour the swelling of the film still increases. The difference in swelling after 0.5 hour and 22 hour is almost a factor 3. Such pronounced swelling of thin PS films has not been reported previously, because most studies have focused on short equilibration times [14, 15, 20]. Evidently, at 50 °C even conditioning for 22 hours is insufficient to equilibrate the material. At 70 °C the polymer seems to reach a final constant swelling degree of about 7%, but only after several hours.

Further evidence of the pronounced non-equilibrium characteristics of the films exposed to 60 bar CO_2 is presented in Figure 5.2. In this figure the kinetics of stepwise desorption are presented for samples that have been immediately exposed to 60 bar CO_2. As compared to Figure 5.1b the duration of the depressurization steps has been chosen differently: 5 minutes for the pressure change followed by 55 minutes at constant pressure. The longer time of desorption allows better observation of polymer relaxations. In the inset of Figure 5.2a the response of the polymer to a pressure step is divided into two parts. The first part is denoted primary relaxation, and directly follows the pressure change in the system. The second part is denoted secondary relaxation, and occurs while the pressure is kept constant. Similar to Figure 5.1b, overall the curves show a curvature change, or kink. In contrast, the secondary relaxations undoubtedly prove that the polymer film is in a highly non-equilibrium state throughout the entire depressurization experiment. The curvature change, or kink, can therefore not be classified as glass transition.

The persistence of polymer relaxation during exposure to the high-pressure CO_2 is related to the extensive dilation of the polymer matrix, allowing for relaxations that are not accessible in a less dilated polymer material. This is why at the lower of the two temperatures studied, with the higher dilation, polymer relaxations are

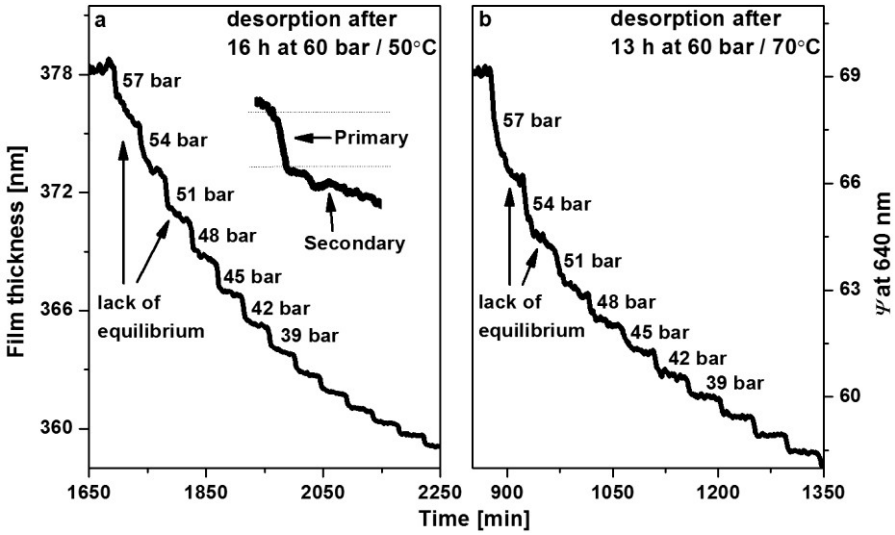

Figure 5.2 Stepwise desorption (5 min pressure step + 55 min constant pressure) after conditioning at 60 bar CO_2 for a) 16 hours at 50 °C b) 13 hours at 70 °C. The inset in a) shows our definition of primary and secondary relaxations. In b) Ψ, at the most sensitive wavelength (640 nm), is plotted instead of the film thickness. The trend of Ψ provides the same information with respect to relaxation as the trend of the thickness, but allows avoiding noise observed in the modeling of the spectroscopic data at 70 °C.

observed over a longer time period. The significant polymer relaxations during conditioning imply that the swelling follows a non-equilibrium path, the end of which is not pre-determined, as it would be for an equilibrium material. In other words, when the pressure evolution during conditioning is chosen differently, the final degree of swelling will be different as well. This can be seen in Figure 5.3, where the second protocol for pressurization/depressurization has been used. Here, instead of immediate pressurization to 60 bar the pressure is increased in a stepwise manner. For comparison the dilation as a function of a stepwise increased temperature is shown (Figure 5.3a). This figure shows that initially the glassy polymer responds quickly to a stepwise increase in temperature. The dilation is however limited, because of the high rigidity of the frozen-in glassy matrix. The relaxation time (τ_p) of the larger polymer segments, associated with glassy to liquid transition, is still much longer than the experimental dwell time (59 minutes) and as a result after the temperature step a constant dilation in time is observed (no sec relax). Only very close to the transition, ~100 °C, secondary relaxations are observed. At 105 °C the timescale of polymer relaxation is similar to the experimental timescale (τ_{exp}), allowing the polymer matrix to equilibrate within the 59 minutes dwell time. Above the glass transition the liquid state is obtained. This state is characterized by a larger thermal expansion coefficient as a result of the

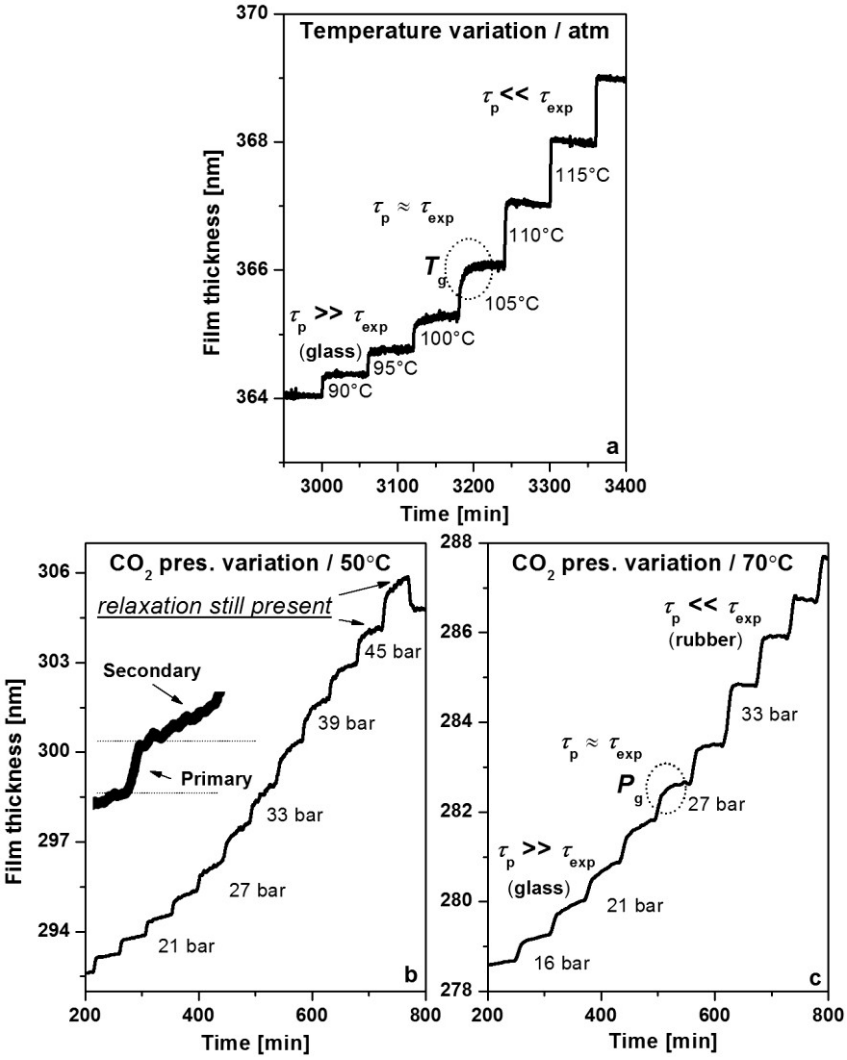

Figure 5.3 a) Film thickness as a function of stepwise increase in temperature in air at 1 atm; around 105 °C polymer relaxation occurs on experimental timescale b) Film thickness as a function of stepwise increase in CO_2 pressure at 50 °C and c) at 70 °C. The data shown for isothermal experiments have been smoothed using adjacent averaging over 10 data points, in order to allow a more clear observation of the polymer film response.

ability of the polymer matrix to fully equilibrate at each temperature. These fast dynamics are confirmed by the absence of secondary relaxations. The temperature induced glass transition occurs in a small range of matrix dilation, about 1% (~5 nm).

In the case of isothermal experiments, Figure 5.3b and c, the relaxational behavior of the polymer is much more pronounced and occurs over a large pressure range. For both of the experiments at 50 °C and 70 °C, secondary relaxations are already observed at pressures well below the kink. The prompt observation of secondary relation is due to the distinct nature of polymer dilation, as compared to the isobaric experiment. In the isobaric experiment the change in the free energy of the polymer is done in a homogeneous manner, with respect to location within the polymer. In the isothermal experiments the dilation is induced predominantly at locations where the penetrant molecules reside. This leads to less homogeneous polymer dilation, at least on a molecular scale. At 50°C the secondary relaxations persist up to the highest applied pressure, 48 bar. This pressure exceeds the pressures at which the kinks occur in Figure 5.1b. In addition, the overall shape of the curve in Figure 5.3b also suggests a kink around 27 bar, which is more apparent later in Figure 5.4. The significant secondary relaxations above this kink again demonstrate that, in contrast to isobaric experiment in Figure 5.3a, it may be inappropriate to attribute the presence of a kink to a penetrant induced glass transition. In the experiment at 70 °C, the secondary relaxations are no longer apparent above ~ 27 bar. This indicates that above this pressure the characteristic polymer relaxation time is similar to the timescale of the experiments, and the polymer does behave like a liquid.

In Figure 5.4 the sorption isotherms derived from the data in Figure 5.3b and c are shown, together with the isotherms obtained during subsequent desorption. The data points represent the degree of swelling obtained immediately after a step in the

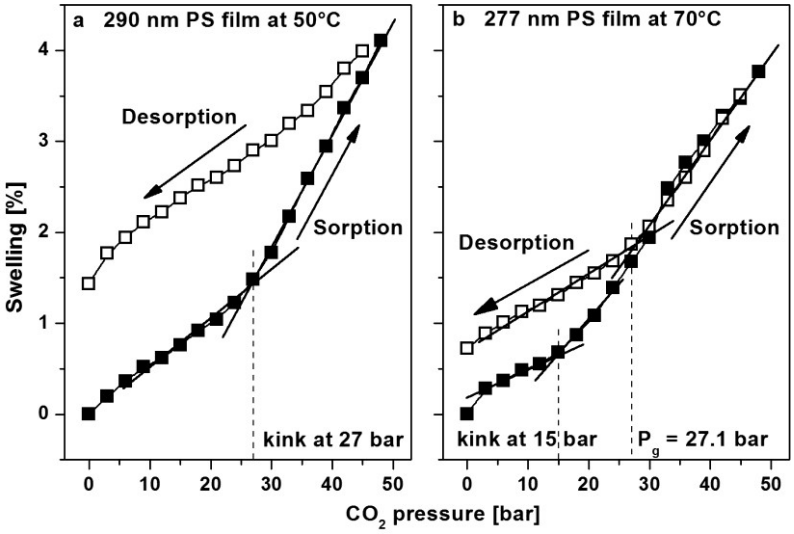

Figure 5.4 Polymer swelling as a function of stepwise increase and decrease of CO_2 pressure up to 48 bar at a) 50°C and b) at 70°C

pressure. At 50°C the sorption curve shows a kink around 27 bar. At this pressure the polymer is still far from equilibrium, as is apparent from the hysteresis in dilation observed upon desorption from 48 bar. This sorption-desorption hysteresis is a well-known feature of the glassy state. The isotherm obtained at 70 °C does not exhibit such a hysteresis above 27 bar. Below 27 bar the sorption and desorption curves do separate, suggesting a glass transition at this pressure. The sorption isotherm at 70 °C shows a kink at ~15 bar. Similar to what has been discussed for the data at 50 °C, this kink should not be associated with a P_g.

The equilibrium swelling characteristics above 27 bar, of the polymer exposed at 70 °C to a stepwise pressure increase to 48 bar (Figure 5.3c), can be confronted with the dynamic behavior observed in the same pressure range when the polymer was immediately exposed to 60 bar (Figure 5.1c). The immediate exposure to 60 bar results in far more pronounced polymer dilation as compared to the stepwise exposure, 4% and 2%, respectively. The extensive dilation upon immediate pressurization allows for additional relaxation processes in the polymer that are not activated in the stepwise experiment. This is revealed by the secondary relaxations observed above the kink, in the 60 bar experiment, and the absence of secondary relaxation in the stepwise experiment for higher pressures. This further signifies that the temperature and penetrant induced glass transitions are disparate. Above the temperature induced glass transition a polymer can be considered to behave as a liquid that is truly in equilibrium, and that does not show any history effects. Above the penetrant induced transitions, an extensive further dilation of the polymer can result in secondary relaxations and conceivable sample history effects.

The kinks in Figure 5.4a and b do not correspond to a glass transition, but do correspond to a sudden amplification of polymer relaxation. This can be understood from a more detailed study of the pressure evolution of the primary and secondary polymer relaxations, as depicted in Figure 5.5. In the case of the temperature induced glass transition (Figure 5.5a) secondary relaxations are only evident very close to the glass transition, where the primary relaxations show a sudden increase that is sustained at higher temperatures. In the case of penetrant induced dilation (Figure 5.5b and c) a more complicated behavior is observed. At 50 °C, up to about 21 bar, the magnitude of the primary relaxations reduces. In other words, in this pressure range each successive pressure step is accompanied by a smaller additional dilation. This can be attributed to more pronounced exclusion effects in sorption, at increasing pressure. This is a well-known feature of sorption in glassy matrices, and is for instance referred to as hole-filling mechanism in dual sorption model. Concurrent with the decrease in primary relaxations, the secondary relaxations increase. This is a result of the more and more pronounced dilation of the polymer. The two effects combined result in an approximately constant total relaxation, producing the constant slope of the sorption curve below 27 bar in Figure 5.4a. Remarkably, in Figure 5.5b at about 21 bar both primary and

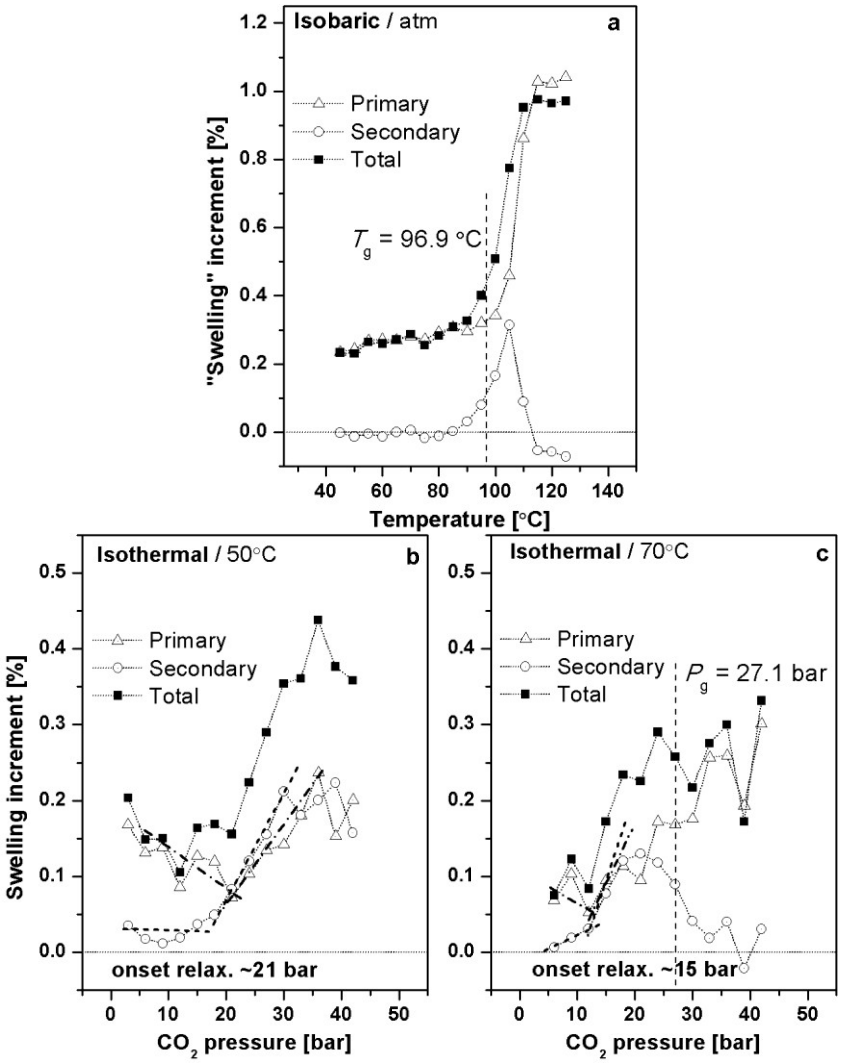

Figure 5.5 Magnitudes of primary, secondary and total relaxation contributions to swelling during a) isobaric, thermal glass transition and during isothermal experiments at b) 50 °C and c) 70 °C.

secondary contributions start to increase. The enhanced dilation of the polymer allows for a larger uptake of penetrant molecules (primary relaxation) whereas it simultaneously allows for more enhanced macromolecular dynamics (secondary relaxation). The combined mutual amplification effect produces the change of the slope, kink, of the sorption isotherm at 27 bar in Figure 5.4a. The pressure of 21 bar marks the onset of the pronounced matrix plasticization. It should be noted that the secondary relaxations do not disappear up to the maximum probed pressure of

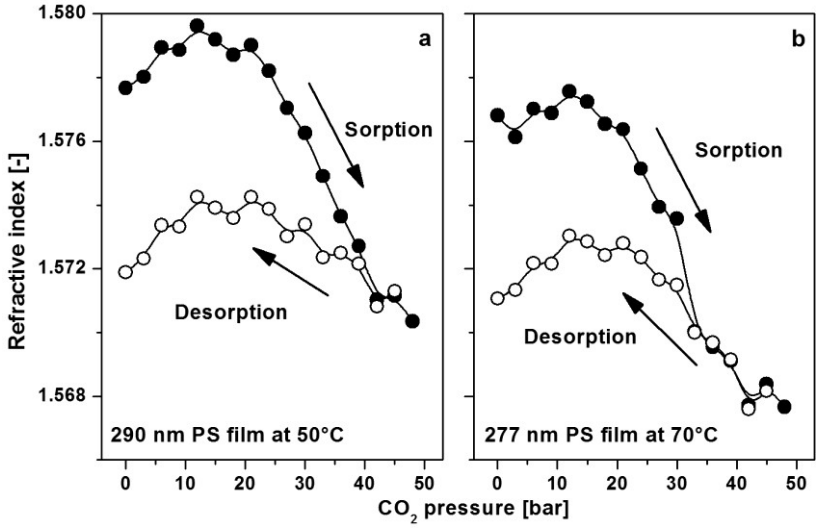

Figure 5.6 Refractive indices of corresponding to the dilation data from Figure 5.4 for CO_2 sorption experiments at a) 50 °C and b) 70 °C

48 bar, thus the slope change may not be assigned as P_g. At 70 °C the onset of plasticization occurs at about 15 bar and the true P_g can be assigned at almost twice higher pressure, where the secondary relaxations are no longer significant and the rubbery state is obtained.

At the pressures corresponding to the onset of relaxations the refractive indices of the swollen polymer films go through maxima, Figure 5.6. This confirms that below these pressures excess free volume in the glassy polymer becomes filled with the sorbing penetrant. This behavior has been previously reported a few times, for instance by Horn et al [26]. A further increase in pressure results in a decline of the refractive index of swollen polymer. This is due to the increasing amount of the penetrant with a lower refractive index, predominantly dissolved in the polymer matrix, with a higher index. This leads to an overall decrease of the refractive index of the film. At 50 °C, Figure 5.6a, over the whole pressure range a sorption-desorption hysteresis is visible, signifying the non-equilibrium, glassy state of the polymer consistent with dilation behavior in Figure 5.4a. At 70 °C, Figure 5.6b, the hysteresis is observed only below about 30 bar. Above that pressure the polymer seems to be in an equilibrium state, which is consistent with the data from Figure 5.4b.

5.4. Implications of the findings

The dynamics of penetrant induced relaxation, as presented in this study, have several important implications. The most obvious one is that values reported for the P_g, derived from dilation studies, should be treated with caution. This is for two reasons. The first reason is that the duration of the conditioning of the polymer

film, prior to a desorption experiment, may have been insufficient to reach an equilibrium liquid polymer. In that case the desorption occurs from a non-equilibrium polymer, implying that a kink in the dilation curve cannot correspond to an actual P_g. Also the location of an observed kink will be undetermined; a too short conditioning time will result in a kink shifted to a higher pressure. This can even lead to a situation where the kink observed at a lower temperature occurs at lower pressure than the kink observed at a higher temperature. An example can be seen in Figure 5.1b, when comparing the experiment at 70 °C and 50 °C (22 hours conditioning). Such a situation might be misinterpreted as retrograde vitrification, while in fact it evidently is not. The second reason for caution is that, even when the polymer is conditioned such that it is in equilibrium at the start of the experiment, irreversible relaxations can be observed above the P_g. This occurs in particular for extensively swollen polymers, in which relaxation processes are activated that are not significant at lower dilation. An example is the desorption at 70 °C depicted in Figure 5.2b, where during desorption above the P_g secondary relaxations are apparent. The irreversible relaxations imply that the sample retains history effects.

The penetrant induced dynamics may also be reflected in thickness dependent polymer properties. It is relatively well established that dynamics in confined PS films can be significantly different than those in the bulk. Various explanations have been proposed for such thickness effects, for instance a larger contribution of a relatively mobile outer surface of the film [27]. Recently, it has been shown that the onset of mechanical plasticization of ultra-thin PS films occurs at much lower strains (on the order of 10^{-3} [28]), than in bulk films. Strains imposed by a condensable penetrant, as is probed during experiments in our study, are of a comparable order. Other researchers have also suggested the existence of very slow relaxation processes in confined polymer films that occur even above T_g of the bulk [29]. These effects were attributed directly to the change of polymer properties (strain hardening) due to confinement on the substrate.

Compelling data exists supporting thickness-dependent physical aging of ultra-thin swollen films. Thinner films are known to age faster than the thicker ones [26, 30-32]. With respect to polymer densification by physical aging, dilation by a penetrant sorption, as done in this study, can be considered a reversing process, and as such it is reasonable to assume, that its dynamics are affected by the film thickness. Pham et al. [14], have reported that the P_g of thin PS films decreases for thinner films. The extent of this decrease is reported to depend on the temperature. It should be noted that the experiments of Pham et al. have been conducted only after short (10-20 min) equilibration of the system. Based on our results it is, therefore, plausible to at least partly explain the thickness dependence of the observed P_g kinks by the different non-equilibrium states of films of different thicknesses conditioned at the same pressures and for the same amount of time.

The practical consequences of thickness and time dependent penetrant imposed film properties are omnipresent. Examples include changes in performance of thin polymer films used as membrane for molecular separation, when exposed to a high pressure or strongly sorbing solvent. Extensive swelling of these films typically results in an increased permeance, at the cost of a loss in selectivity. Implications can also be important for materials synthesis. For example, the plasticizing effect of carbon dioxide can be used to prepare nano-foams from glassy polymers. In this respect, Krause et al. have reported a foaming diagram that specifies a temperature-(CO_2) concentration window in which foaming occurs [33]. An upper border of this window quantifies a transition from porous to a dense polymer indicating that the CO_2 nucleation process and bubble growth process cannot be completely frozen-in in the rubber state of the polymer. Hence the polymer remains non-porous. However, this transition has been reported to occur well above the glass transition of the polymer. The persistence of penetrant induced relaxations well above the dynamic kink in the dilation isotherm, reported in our work, may explain these findings.

5.5. Conclusions

The relaxational phenomena of thin glassy films in the vicinity of the thermally and penetrant induced glass transitions, T_g and P_g respectively, are investigated and compared. It is found that significant differences in the polymer matrix relaxational behavior associated with T_g and P_g exist. Exposure of the glassy polymer films to pressures, usually reported to be sufficient to induce full matrix plasticization, hence an equilibrium liquid state, are shown to give history dependent results. This is observed even well above the kink in the sorption isotherm, broadly associated with the P_g, where the swollen polymer can be considered a quasi-equilibrium system. These results are explained by considering significant differences related to the dynamic dilation behavior in the vicinity of T_g and P_g. The larger deformation of the polymer matrix by a sorbed penetrant results in the actuation of the pronounced polymer relaxations that persist over very long timescales. These relaxations are a result of mutually influencing timescales of penetrant diffusion and the corresponding inhomogeneous matrix dilation on a molecular scale. Such long term relaxations are absent in the vicinity of the thermally induced glass transition, mainly due to immediacy and more homogenous character of the temperature transport in the material. The kinks in the sorptive dilation isotherms are shown to be related to points where the sudden amplification of the primary and secondary relaxation processes occurs in a glassy state. Therefore, the kinks should not be associated with penetrant induced glass transition.

The findings have important implications for the fundamental understanding of the penetrant induced glass transition, time dependent plasticization in membrane technology, and foaming processes in plasticized glassy polymers. The results, combined with other literature studies, may also help to better understand the

dependence of some penetrant induced plasticization phenomena on film thickness in the ultra thin range (< 100 nm).

5.6. References

[1] Ismail, A.F. and W. Lorna, *Penetrant-induced plasticization phenomenon in glassy polymers for gas separation membrane.* Separation and Purification Technology, 2002. **27**(3): p. 173-194.

[2] Wessling, M., M. Lidon Lopez, and H. Strathmann, *Accelerated plasticization of thin-film composite membranes used in gas separation.* Separation and Purification Technology, 2001. **24**(1-2): p. 223-233.

[3] Wessling, M., et al., *Plasticization of gas separation membranes.* Gas Separation & Purification, 1991. **5**(4): p. 222-228.

[4] Rowe, B.W., B.D. Freeman, and D.R. Paul, *Influence of previous history on physical aging in thin glassy polymer films as gas separation membranes.* Polymer, 2010. **51**(16): p. 3784-3792.

[5] Rowe, B.W., B.D. Freeman, and D.R. Paul, *Physical aging of ultrathin glassy polymer films tracked by gas permeability.* Polymer, 2009. **50**(23): p. 5565-5575.

[6] Sanchez, I.C. and R.H. Lacombe, *Statistical Thermodynamics of Polymer Solutions.* Macromolecules, 1978. **11**(6): p. 1145-1156.

[7] Doghieri, F. and G.C. Sarti, *Nonequilibrium Lattice Fluids: A Predictive Model for the Solubility in Glassy Polymers.* Macromolecules, 1996. **29**(24): p. 7885-7896.

[8] Vrentas, J.S. and C.M. Vrentas, *Sorption in glassy polymers.* Macromolecules, 1991. **24**(9): p. 2404-2412.

[9] Vrentas, J.S. and C.M. Vrentas, *Hysteresis Effects for Sorption in Glassy Polymers.* Macromolecules, 1996. **29**(12): p. 4391-4396.

[10] Vrentas, J.S. and C.M. Vrentas, *Integral sorption in glassy polymers.* Chemical Engineering Science, 1998. **53**(4): p. 629-638.

[11] Leibler, L. and K. Sekimoto, *On the sorption of gases and liquids in glassy polymers.* Macromolecules, 1993. **26**(25): p. 6937-6939.

[12] Chiou, J.S., Y. Maeda, and D.R. Paul, *Gas and vapor sorption in polymers just below Tg.* Journal of Applied Polymer Science, 1985. **30**(10): p. 4019-4029.

[13] Sefcik, M.D., *Dilation and plasticization of polystyrene by carbon dioxide.* Journal of Polymer Science Part B: Polymer Physics, 1986. **24**(5): p. 957-971.

[14] Pham, J.Q., K.P. Johnston, and P.F. Green, *Retrograde Vitrification in CO2/Polystyrene Thin Films.* The Journal of Physical Chemistry B, 2004. **108**(11): p. 3457-3461.

[15] Pham, J.Q., et al., *Pressure, Temperature, and Thickness Dependence of CO_{2}-Induced Devitrification of Polymer Films.* Physical Review Letters, 2003. **91**(17): p. 175503.

[16] Böhning, M. and J. Springer, *Sorptive dilation and relaxational processes in glassy polymer/gas systems--I. Poly(sulfone) and poly(ether sulfone).* Polymer, 1998. **39**(21): p. 5183-5195.

[17] Visser, T. and M. Wessling, *When Do Sorption-Induced Relaxations in Glassy Polymers Set In?* Macromolecules, 2007. **40**(14): p. 4992-5000.

[18] Wessling, M., et al., *Dilation kinetics of glassy, aromatic polyimides induced by carbon dioxide sorption.* Journal of Polymer Science Part B: Polymer Physics, 1995. **33**(9): p. 1371-1384.

[19] Ogieglo, W., et al., *n-Hexane induced swelling of thin PDMS films under non-equilibrium nanofiltration permeation conditions, resolved by spectroscopic ellipsometry.* Journal of Membrane Science, 2013. **437**(0): p. 313-323.

[20] Li, Y., et al., *Role of interfacial interactions on the anomalous swelling of polymer thin films in supercritical carbon dioxide.* Journal of Polymer Science Part B: Polymer Physics, 2007. **45**(11): p. 1313-1324.

[21] Sirard, S.M., P.F. Green, and K.P. Johnston, *Spectroscopic Ellipsometry Investigation of the Swelling of Poly(Dimethylsiloxane) Thin Films with High Pressure Carbon Dioxide.* The Journal of Physical Chemistry B, 2001. **105**(4): p. 766-772.

[22] Fujiwara, H. and I. Wiley, *Spectroscopic ellipsometry principles and applications*, 2007, John Wiley & Sons: Chichester, England; Hoboken, NJ.

[23] Azzam, R.M.A. and N.M. Bashara, *Ellipsometry and polarized light*1977, Amsterdam; New York; New York: North-Holland Pub. Co. ; Sole distributors for the U.S.A. and Canada, Elsevier North-Holland.

[24] Tompkins, H.G. and E.A. Irene, *Handbook of ellipsometry*, 2005, William Andrew Pub. ; Springer: Norwich, NY; Heidelberg, Germany.

[25] Condo, P.D., D.R. Paul, and K.P. Johnston, *Glass transitions of polymers with compressed fluid diluents: type II and III behavior.* Macromolecules, 1994. **27**(2): p. 365-371.

[26] Horn, N.R. and D.R. Paul, *Carbon Dioxide Sorption and Plasticization of Thin Glassy Polymer Films Tracked by Optical Methods.* Macromolecules, 2012.

[27] Dutcher, J. and M. Ediger, *Glass surfaces not so glassy.* Science, 2008. **319**(5863): p. 577-578.

[28] Gurmessa, B.J. and A.B. Croll, *Onset of Plasticity in Thin Polystyrene Films.* Physical Review Letters, 2013. **110**(7): p. 074301.

[29] Kanaya, T., et al., *Thermal expansion and contraction of polymer thin films.* physica status solidi (b), 2005. **242**(3): p. 595-606.

[30] Horn, N.R. and D.R. Paul, *Carbon dioxide plasticization and conditioning effects in thick vs. thin glassy polymer films.* Polymer, 2011. **52**(7): p. 1619-1627.

[31] Huang, Y. and D.R. Paul, *Effect of Temperature on Physical Aging of Thin Glassy Polymer Films.* Macromolecules, 2005. **38**(24): p. 10148-10154.

[32] Huang, Y. and D.R. Paul, *Experimental methods for tracking physical aging of thin glassy polymer films by gas permeation.* Journal of Membrane Science, 2004. **244**(1-2): p. 167-178.

[33] Krause, B., et al., *Microcellular Foaming of Amorphous High-Tg Polymers Using Carbon Dioxide.* Macromolecules, 2001. **34**(4): p. 874-884.

Chapter 6

Relaxation-induced optical anisotropy during dynamic overshoot swelling of zwitterionic polymer films

This chapter has been adapted from:

Ogieglo W., de Grooth J., Wormeester H., Wessling M., Nijmeijer K., and Benes N.E., Thin Solid Films 2013;545(0):320-326. Copyright 2013 Elsevier

Abstract

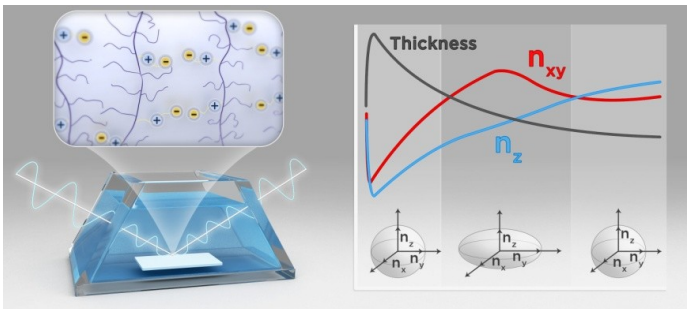

In-situ spectroscopic ellipsometry was used to investigate the swelling behavior of thin supported zwitterionic polymers based on sulfobetaine methacrylate and n-butylacrylate. This material represents an interesting class of zwitterionic polymers, with large potential in reduction of biofouling of ultrafiltration membranes. It was found that the swelling rate and magnitude depend strongly on the content of zwitterionic groups incorporated in the polymer structure. Overshoot anomalous swelling dynamics were observed, explained by an interplay between enthalpic and entropic effects in various stages of the process. To elucidate the changes in the film properties a detailed ellipsometric analysis was conducted during polymer dilation and relaxation. For the polymer with 11.6 mol % zwitterionic groups, the thickness relaxation process after the swelling maximum is shown to be best described by a thin film with a time dependent uniaxial anisotropy. The behavior is rationalized via the orientations of polymer backbone and zwitterionic side chains, as a result of swelling and relaxation in the presence of the screening electrolyte.

6.1. Introduction

Polymers with incorporated zwitterionic moieties have gained a significant research attention due to their interesting potential application in a variety of fields, including oil recovery [1, 2], ion chromatography [3], biocatalysis [4], removal of metal ions from water [5], drug delivery [6] and, recently, in membrane technology. When used for the modification of ultrafiltration membranes, zwitterionic moieties have been shown to greatly improve anti-fouling properties [7-14]. The resistance of membranes functionalized with zwitterionic groups towards biofouling is often explained by severe hindrance of cell adsorption on the modified membrane surface [15]. The same property is reported to be responsible for a very good blood compatibility of zwitterionic polymers, because of limited protein and blood platelets adhesion [16]. The implementation of zwitterionic groups into membrane polymers has been accomplished via routes of random copolymerization [7, 8, 10] or polymer modification [11-14], and already very low molar contents of zwitterionic groups (below 10 mol %) are reported to show a significant impact. In the case of zwitterionic polymers based on sulfobetaine methacrylate (SBMA) the explanations for the observed effects focus on the existence of self-assemblies of the zwitterionic moieties, which influence the character of hydrophobic-hydrophilic interactions within the polymer chains [17, 18]. Such self-assemblies, based on dipole – dipole interactions between the zwitterionic side chains, have also been frequently reported to be formed in other similar polymers both in dry [19-21] and swollen state [22, 23]. When the polymer is swollen in the presence of dissolved small molecule electrolytes these interactions are weakened. This is responsible for the so-called antipolyelectrolyte effect. It is manifested by an increase of chain expansion with increasing salt concentration as a result of screening of the dipole-dipole interactions by the small molecule electrolyte. Though the antipolyelectrolyte effect is relatively well understood on a qualitative level, there still seems to be a lack of understanding of the impact of specific small ions, polymer structure and other factors. In particular, little is known about the dynamics of the swelling behavior of zwitterionic thin polymer films in the presence of small molecule electrolyte.

A thin film geometry is especially beneficial in membrane applications, where the membrane separation performance is dictated by a dense polymeric layer (thickness ~ a few hundred nanometer), in contact with a fluid penetrant. In studies of thin and ultra-thin films, spectroscopic ellipsometry (SE) is a powerful technique. SE is based on the change of the polarization state of a specularly reflected light beam and has a very high sensitivity and accuracy for the determination of thin film properties such as thickness and refractive index. SE relies on changes in polarization state, rather than changes in light intensity. This makes it particularly suitable for measurements performed *in-situ*, where the ambient might cause attenuation of light. There are a few studies in which *in-situ* SE has been applied to study swelling of polymer brushes [24], immobilized thin

films [25] and polyelectrolytes [26] in liquid penetrant environment. The technique has also been used in dynamic water swelling of biocompatible zwitterionic polymers based on phosphorylcholine [27, 28] and polyzwitterionic brushes on gold surfaces [29]. Similar studies are very rare andstudies on dynamic swelling behavior of zwitterionic polymer thin films in the presence of strong small molecule electrolytes are not available.

In this work we use *in-situ* spectroscopic ellipsometry to study the dynamic swelling behavior of a thin film of supported zwitterionic random co-polymer of n-butylacrylate (nBA) and sulfobetaine methacrylate (SBMA) in the presence of an electrolyte (NaCl). The effect of the amount of zwitterionic monomer in the polymer is investigated and particular focus is put on the details of spectroscopic ellipsometry modeling of the swelling process. Various optical models, involving uniform, graded and anisotropic thin film representations are compared.

6.2. Spectroscopic ellipsometry

Spectroscopic ellipsometry measures the change in ellipticity of the reflected light, commonly quantified by the amplitude ratio Ψ and the phase difference Δ, over a wide wavelength range. Deriving film properties from the spectroscopic ellipsometry spectra requires the sample to be represented by an appropriate optical model that can be fitted to the experimental spectra. Generally the optical model involves a stack of multiple layers, each characterized by a thickness, h, and optical dispersion: the wavelength, λ, dependent refractive index, $n(\lambda)$, and extinction coefficient, $k(\lambda)$. For optically transparent dielectrics k=0, and the optical dispersion is often accurately described by the Cauchy relation:

$$n(\lambda) = A + \frac{B}{\lambda^2} + \frac{C}{\lambda^4} \qquad (6.1)$$

where A, B and C are fit parameters.

The fit quality is evaluated based on the value of root Mean Square Error (MSE). For thin (100 – 200 nm) single layer uniform samples (dense SiO_2 on Si wafer) MSE values indicating a good fit are ~ 1–2. For thicker films, characterized by more complex morphologies, much higher MSE values (~10) are considered acceptable. Model modification (addition of fitting parameters, implementation of window corrections etc.) is considered an improvement when the change in MSE is significant.

An appropriate optical model needs to be complex enough to capture the main characteristics of the sample, while overparameterization must be avoided. [30]. The optical models used in this study are depicted in Figure 6.1. The models comprise a crystalline silicon (100) wafer (with thin ~1.5 nm native oxide layer, not shown for clarity), supporting a polymer film that is in contact with an ambient:

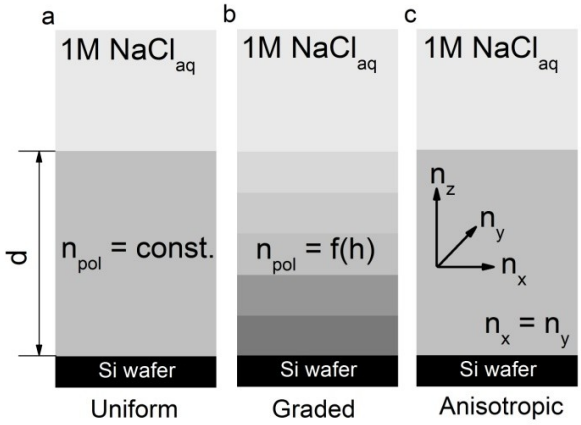

Figure 6.1 Schematic representation of the optical models employed in this study

either a salt solution or air. The models differ in the description of the polymer film. In the uniform model (Figure 6.1a) the film is considered to be isotropic and is characterized by a uniform refractive index, n_{pol} across its thickness. In the graded model (Figure 6.1b), n_{pol} is allowed to be a linear function of the film thickness and the layer is divided into 5 equal thickness sublayers (the obtained value of n_{pol} corresponds to the middle sublayer). The last anisotropic model (Figure 6.1c) considers the polymer film to be uniaxially anisotropic, with distinct n_z (perpendicular to the plane of the substrate) and $n_x = n_y$ (in the plane of the substrate).

In all of the optical models the refractive indices are fitted dynamically for the time resolved experiments. The values of refractive indices given in this work relate to the index at 632.8 nm.

6.3. Experimental details

6.3.1. Polymer synthesis and characterization

The nBA-SBMA random copolymer was prepared via a free-radical polymerization mechanism. A typical reaction involved the dissolution of 17.4 g nBA (135.7 mmol) and 5 gram SBMA (17.9 mmol) in 100 ml of dimethyl sulfoxide in a 250 ml round bottom flask under a nitrogen atmosphere. The solution was heated to 70 °C, and subsequently 0.20 gram $(NH_4)_2S_2O_8$ (0.9 mmol) was added. This mixture was left to react under reflux for at least 12 hours to ensure complete conversion of the monomers. After the reaction, the mixture was poured into demineralized water to form a precipitate. The precipitate was washed three times with 50 ml of water for 30 minutes and dried for 24 hours in a vacuum

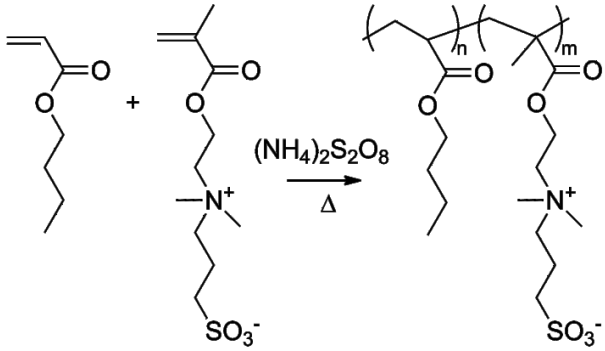

Figure 6.2 Reaction scheme for the free radical polymerization of n-butyl acrylate (nBA) and sulfobetaine methacrylate (SBMA)

oven at 30 °C. The overall procedure gave the p(SBMA-nBA) copolymer, Figure 6.2, with an 88 % yield. The polymer was stored under vacuum and used without any other purification steps. The amount of added SBMA, relative to nBA, was tuned to obtain two polymer batches each with different content of the zwitterionic moieties.

Elemental analysis showed incorporation of 5.0 mol % and 11.6 mol % of the zwitterionic groups in the two polymer batches. Further in the text the two polymers are referred to as P1 and P2 respectively. The molecular weights of the obtained polymers were determined using size exclusion chromatography in tetrahydrofurane with 0.1 M LiCl against a polystyrene standard and resulted in M_w of approximately 55 kg/mol. Thermal stability of the copolymer was determined with thermogravimetric analysis (TGA 4000, Perkin Elmer) and no significant weight loss (< 5 %) was found until 300 °C. Differential scanning calorimetry (DSC 8000, Perkin Elmer) measured at 20 °C per minute showed one glass transition temperature at -37 °C. The results of the thermal characterization are comparable to those found in [31].

6.3.2. Sample preparation and *in-situ* measurement procedure

Silicon wafers used as supports were cleaned by immersion in 98 % H_2SO_4 with 30 % H_2O_2 mixture (3:1 volume ratio) for 24 hours. Afterwards, they were flushed with demineralized water and ultra pure acetone. This procedure resulted in clean wafers with a native oxide layer of approximately 1.5 nm as determined with spectroscopic ellipsometry. Thin films of the polymer were spin coated at 2000 rpm from a solution in 2,2,2-trifluoroethanol (Sigma Aldrich) and the film thickness was tuned by adjusting the solution concentration. Before *in-situ* spectroscopic ellipsometry measurement, the samples were conditioned in a vacuum oven at 30 °C for 16 hours to remove solvent residues.

All ellipsometry measurements were performed with a Rotating Compensator Ellipsometer (M-2000X, J.A. Woollam Co., Inc.). The wavelength range employed for the fitting was limited to 370 – 920 nm (330 equidistant wavelengths per spectrum), to avoid light absorption of the glass cell windows at shorter wavelenght and light absorption of water at longer wavelength. A full spectral scan was performed within approximately 2 s, the light beam diameter was approximately 2 mm.

The *in-situ* spectroscopic ellipsometry measurements were performed in a glass cell with 5 mm thick windows positioned symmetrically at both sides perpendicular to the incident and reflected light beams. The cell was equipped with a dry nitrogen gas flushing and temperature control system. The angle of incidence was fixed at 70 °. In order to improve the measurement accuracy, particularly with respect to refractive index determination of both dry and swollen films, a calibration procedure was run before the measurement of each sample. It involved the determination of in-plane Δ parameter offsets from a measurement on a 25 nm SiO_2 on Si wafer prior to an actual measurement. These parameters were used to correct the *in-situ* measurement of both dry and wet samples. The out-of-plane windows offsets were largely corrected by the design of the instrument and implemented internal calibration procedures.

To avoid the undesired influence of air humidity, all of the dry samples were flushed with dry nitrogen for at least 5 minutes already in the *in-situ* measurement cell after transporting from the vacuum oven. After the measurements showed stable sample optical properties, sodium chloride solution was poured in the cell. The moment that the liquid wetted the sample surface was considered $t = 0$. The dynamic ellipsometric measurement was started after 1 minute, allowing time to fill the cell (usually 1 min), system stabilization and slight correction of sample alignment. All experiments were performed at 21 ± 0.5 °C.

Optical constants of supporting silicon wafer and native oxide were taken from literature [32] and fixed throughout the analysis. Ambient optical dispersion of 1M NaCl was measured *in-situ* against a 25 nm SiO_2/Si calibration wafer (the dispersion of the calibration wafer was fixed), assuming a transparent medium (k = 0). This assumption is valid as already a very small value of k would strongly attenuate the light beam as a result of several cm path length in the used cell. The ambient refractive index obtained by *in-situ* ellipsometry was within ~0.001of the value obtained with a standard laboratory refractometer (Carl Zeiss). The values for Cauchy dispersion were: $A = 1.335$, $B = 0.00262$ µm^{-2} and $C = 9.267 \cdot 10^{-5}$ µm^{-4}.

When in contact with the penetrant the swelling of a polymer film was calculated as:

$$S = \frac{h_s - h_d}{h_d} \qquad (6.2)$$

where h_s and h_d are thicknesses of the polymer film in swollen and dry state.

6.4. Results and discussion

6.4.1. Spectroscopic ellipsometry modeling of swelling

The ellipsometric characterization of the spin coated films revealed only small depolarization of the light beam. This implies that all films have high thickness uniformity. No dewetting during film preparation or during *in-situ* swelling experiments was noticed. In Figure 6.3, Ψ for sample P2 in dry and swollen state is shown. For the dry sample the uniform optical model (Figure 6.1a) yields a film thickness of 414.5 nm and refractive index n_{P2} = 1.488, with MSE = 15.1. For the dry P1 film, the obtained values are 347.4 nm and n_{P1} = 1.481, with MSE = 6.7. The lower index of P1 compared to P2 can be related to its lower content of highly polarizable zwitterionic groups [33]. Sufficiently accurate description of optical dispersions for both polymer films is already obtained when only the A and B parameters of the Cauchy function are used. Influence of fitting parameter C is found to reduce the fitting error only slightly (less than 0.5 % MSE reduction) and its use is omitted.

After the polymer film P2 is immersed in an aqueous 1 M NaCl solution, the oscillations amplitude of the Ψ parameter in Figure 3 shows a significant reduction in comparison to the spectra for the dry sample. This originates from the fact that

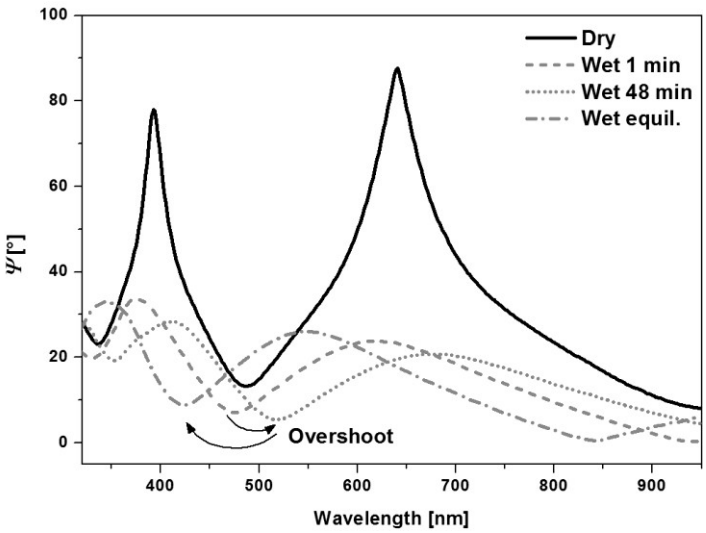

Figure 6.3 Ψ spectra of the dry and swollen ~400 nm films of zwitterionic polymer P2 (with 11.6 mol % of zwitterionic groups). The spectra for the swollen film show a dynamic overshoot: oscillations first move to the right (from 1 min to 48 min) and then to the left (from 48 min till equilibrium)

the experimental ambient refractive index (n_{NaCl} = 1.342) is much closer to the refractive index of the polymer (n_{P1} = 1.488) than the refractive index of air (n_{air} = 1.000). The Ψ spectra for the wet sample show an interesting evolution in time. After 48 minutes the Ψ oscillations have shifted towards longer wavelengths, indicating an increase of polymer film thickness (and/or an increase in its refractive index). At equilibrium, the Ψ oscillatory pattern has reversed towards shorter wavelengths, even beyond the pattern at 1 minute of swelling. This raw data analysis suggests that the film thickness initially increases, reaches a maximum and then decreases. These overshoot dynamics for P2 are clearly visible in Figure 6.4, where the modeling results using the Uniform Film model (Figure 6.1a) are shown.

Figure 6.4 for P2 reveals a maximum swelling ~94-102%, occurring after 48 minutes followed by a period of relaxation during which the thickness reduces. Concurrently, the refractive index initially decreases, shows a minimum, and then slowly increases. The overshoot behavior is very reproducible and relatively independent of dry film thickness in the presented range (240 - 760 nm). A different swelling behavior is observed for polymer P1: the initial thickness increase occurs much slower, and a less distinct maximum (~37 %) in the swelling curve occurs after 2100 minutes. The refractive indices of swollen P1 and P2 films are much smaller than those for the dry samples, due to dilution of the polymer with the salt solution of lower refractive index (n_{NaCl} = 1.342). For the highly swelling P2 the index is much lower than for P1. The evolutions of the refractive indices and swelling of P1 and P2 are consistent: maximum swelling coincides with minimum index (n_{minP1} = 1.440, n_{minP2} = 1.409).

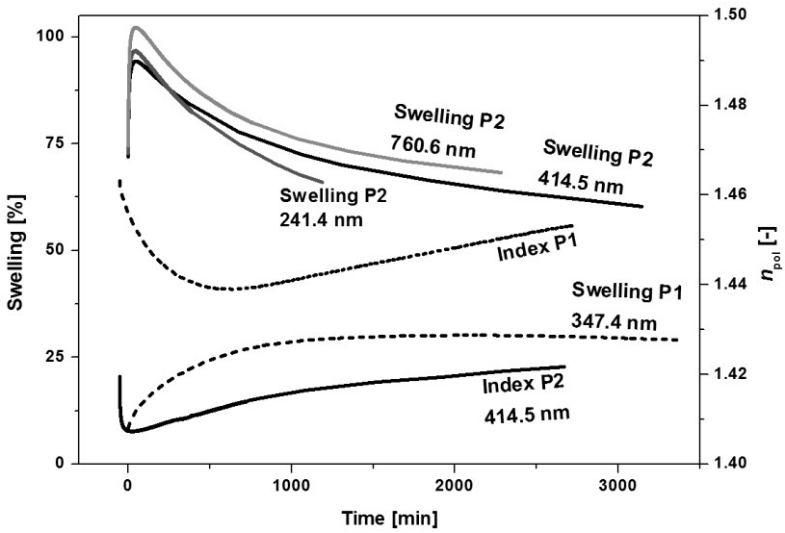

Figure 6.4 Results of uniform model obtained swelling and refractive index for three different film thicknesses of polymer P2 (with 11.6 mol % of zwitterionic groups) and one for polymer P1 (with 5.0 mol % of zwitterionic groups)

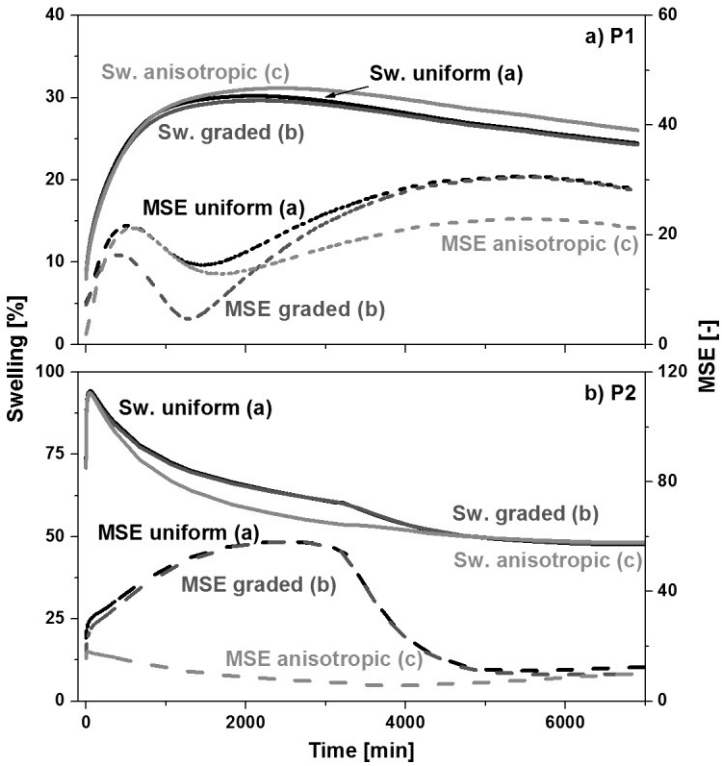

Figure 6.5 Swelling of polymers a) P1 and b) P2 obtained with all of the employed optical models in 1 M NaCl solution. Right Y axes indicate the MSE values of the corresponding models.

Results of fitting, using the three models depicted in Figure 6.1, are presented in Figure 6.5, where swelling and MSE are plotted as a function of time. For polymer P1 the swelling curves for the different models lie close together. Up to ~2000 minutes, the MSE for Uniform and Anisotropic models separate significantly from the MSE for the Graded model. When the swelling maximum is reached, at about 2150 min, the MSE values stay relatively close. The MSE for the graded model shows a clear minimum at about 1300 min with a value of 4.7. This value is much lower than the MSE for both uniform and anisotropic models (14.8, 14.1 respectively).

The optical dispersion of P1 at 1 min and 1300 min, obtained from the Graded model fit, is shown in Figure 6.6a. In this figure a distinction is made between the top (with salt solution) and bottom (with substrate) interfaces of the polymer film. All of the obtained curves are physically viable, with refractive indices increasing towards shorter wavelengths, and characteristic for organic dielectric materials. The results show that at the beginning of swelling (1 min) the polymer refractive

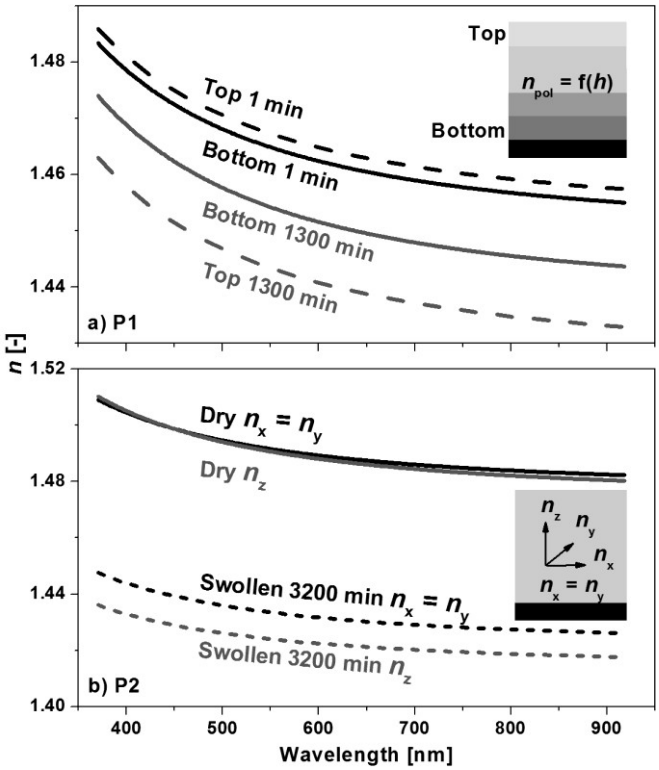

Figure 6.6 Optical dispersions obtained using the graded model for a) P1 and the anisotropic model for b) P2. In a) the graded optical dispersion at the top and bottom of the film is shown at 1 minute (immediately after contact with salt solution), and after 1300 min of swelling. In b) the optical dispersion of a dry film is compared with that for the swollen film at the time slice where the largest anisotropy occurs.

index is relatively uniform and that a gradient in the index between top and bottom parts of the film develops as swelling continues. At both time slices low MSE values for the Graded model are recorded (MSE of 7.2 and 4.7 respectively). The data modeling for polymer P1 suggests a significant gradient in refractive index or density during the diffusion of salt into the polymer film, which is physically realistic and consistent with a development of a penetrant concentration profile across the film. Penetrant diffusion towards the substrate corresponds to a decrease in the density of the film in that direction. This is reflected in the difference in the refractive indices at 1300 minutes at the top (lower index meaning lower density) and the bottom (higher index meaning higher density) of the film.

The results obtained for polymer P2 (Figure 6.5b) indicate that initially a remarkably large difference between fit qualities obtained with Uniform or Graded and Anisotropic models develops. The MSE values of Uniform and Graded models

go through a maximum value of about 58 around 2700 minutes, which is approximately 6 times higher than the MSE value obtained with the Anisotropic model. Significant (~ 8 %) differences are also seen in the swelling curves. After going through the maxiumum, the MSE values of the Uniform and Graded models decrease sharply, within about 1200 minutes, and then remain close to the MSE of anisotropic model. The relatively abrupt change in the MSE of the Uniform and Graded models around 3200 minutes is unlikely to be caused by experimental artifacts because the behavior is found to be reproducible for 2 separate fresh samples of polymer P2. However, since spectroscopic ellipsometry results are often highly model-sensitive the data has to be examined more carefully and the pertinence of using an advanced uniaxially anisotropic model has to be further substantiated.

In Figure 6.6b the results for the Anisotropic model, applied to a dry and swollen P2 sample, are presented as optical dispersion. For the swollen film the time slice is chosen when the difference in MSE values between the Uniform and Anisotropic models is the largest (3200 min). The refractive index of the dry sample shows a physically realistic increase towards shorter wavelengths, and the values of n_{xy} overlap almost completely with n_z. Additionally, no significant reduction of MSE is found between fits with the Uniform and Anisotropic models for the dry sample (*MSE* of 15.12 and 15.03, respectively). The n_{xy} and n_z dispersions for the swollen sample clearly separate. The difference ($\Delta n \sim 0.01$) is approximately constant over the entire wavelength range. Both refractive index components are lower than the refractive indices obtained for the dry sample, and the optical dispersions show physically plausible shapes.

There are several modeling related reasons in favor of the Anisotropic model. The first is the very significant reduction of MSE, as high as 6 fold around ~3000 min, in comparison to Uniform and Graded models (Figure 6.5b). This reduction in MSE is many times larger than a commonly advised 25 % improvement of the fit quality that supports the employment of additional fitting parameters. Another reason is that the Anisotropic model yields a much smoother swelling. The distinct change of slope for swelling obtained with the Uniform and Graded models, ~3300 min, is likely to be a modeling artifact, rather than actual swelling behavior. Furthermore, the obtained n_{xy} and n_z parameters are found to represent unique numerical solutions, which is confirmed by a uniqueness analysis of the anisotropic fit parameters (data not shown). In this analysis, n_{xy} or n_z is varied *ceteris paribus* within certain range and the minimum MSE is recorded. It is found that the data present well-separated parabola-resembling curves, indicating a high degree of uniqueness of (or little correlation between) of the fitted values of n_{xy} and n_z. Finally, the dispersions of n_{xy} and n_z in Figure 6.6b, are physically plausible; the slight increase of refractive index in the ultra-violet range is commonly observed for organic materials. The results for a dry sample seem to suggest a highly isotropic system, even though the Cauchy parameters A and B are not restricted.

When the polymer swells n_{xy} and n_z dispersions suggest slight, but well resolved, anisotropy development in the polymer.

The only parameter that could lower the numerical MSE value of the Uniform model is the Δ offset, related to experimental cell window birefringence. However, physical validity of this is ruled out due to the following reasons. The Δ offsets related to possible window birefringence, determined beforehand against a calibration wafer, are found to be of minor impact on values of sample parameters (refractive index, thickness, shape of dispersion). Furthermore, if Δ offset are included as fit parameters in the time resolved analysis, their values are 1 to 2 orders of magnitude larger than those determined against a calibration wafer. Moreover, the dynamically fitted window effects are found to vary drastically during the measurement, which is highly unlikely. Finally, if window effects are included in the dynamic analysis using the Anisotropic model, the resulting optical dispersion behavior still resembles very closely the one shown in Figure 6.6b, for which window effects are neglected.

There are numerous studies on the determination of uniaxial anisotropy with spectroscopic ellipsometry in thin organic and polymeric films analyzed *ex-situ* [34-42]. In such studies ellipsometry is shown to be capable of the determination of especially uniaxial dispersion of thin polymer films, in the directions parallel and perpendicular to the film plane, on various substrates. Moreover, even measurements performed at a single angle of incidence are reported to accurately characterize anisotropic silicon wafer supported polymer films [41]. Optical anisotropy in polymeric materials has also been studied by other methods [43-47]. Some authors have suggested limitations of spectroscopic ellipsometry with respect to thin polymer film anisotropy determination [48]. These sensitivity issues are only relevant for organic films with thicknesses far below 200 nm, whose spectra do not show interference oscillations. The film thickness range in this work is 450 – 800 nm allows fitting of the Ψ and Δ spectra covering two full interference oscillations (Figure 6.3).

The detailed modeling analysis suggests that implementation of uniaxial anisotropy in the optical model to describe dynamic swelling behavior of thin P2 polymer film seems substantiated.

At longer timescales the MSE curves for polymer P1 modeled with the anisotropic model are about 50 % lower as compared to the MSE curves of the other two models. This indicates that in the case of polymer P1 some degree of anisotropy in the polymer might occur as well. However, the reduction of the MSE values is not as large as in the case of P2 and the preference for the Anisotropic model seems not that clear.

6.4.2. Polymer structure changes during swelling – proposed interpretation

In this section a possible physical interpretation of the modeling results, discussed in paragraph 6.4.1., is given. In the random copolymer of nBA and SBMA 5 mol % (for polymer P1) or 11.6 mol % (for polymer P2) of the side chains of n-butyl acrylate are replaced by the zwitterionic SBMA unit. This facilitates strong specific electrostatic interactions between the zwitterionic units attached to the weakly polar backbone matrix. It is known that when larger fractions of the zwitterionic monomers are used for the polymerization, the resulting copolymers may even show microphase separation due to strong preference of the interaction between the charged units [18, 20, 22, 49, 50]. Zwitterionic moieties can also act as ionic crosslinks, which is manifested in the mechanical properties of the studied polymers [51]. In the case of polymer P2 with 11.6 mol % of SBMA monomer, some degree of association of charged groups may be present in a dry state [52]. In the dry rubbery state, the charged group associations have random orientation, and polymer P2 is isotropic (Figure 6.6b).

Figure 6.7 displays the evolution of the refractive index components n_{xy} and n_z and the swelling of film P2. During the initial fast thickness increase, both refractive index components decrease but remain close to each other. After the maximum swelling, thickness relaxation is observed and n_{xy} and n_z increase. Component n_{xy} increases faster and deviates from n_z until a maximum difference around 3200 min occurs. After that the n_z component continues to increase whereas the n_{xy} reduces and approaches n_z. In the time period from about 5000 min onwards both refractive index components have similar values.

The observed dynamic anisotropic behavior of the optical dispersion can be considered to be related to the macromolecular structure of the zwitterionic polymer. Swelling of the polymer by the aqueous electrolyte solution results in screening of the dipole-dipole interactions within the polymer. The breakdown of the associations between zwitterionic groups, and the loss of the ionically cross linked character of the network, result in increased chain separation. The transport of the electrolyte solution into the polymer is driven predominantly by the tendency to solvate the localized charges of the zwitterionic groups. The contribution of the backbone remains very small because of its weakly polar, hydrophobic character. The large dominance of the enthalpic effects in the initial phase of sorption leads to the very high degree of swelling (Figure 6.5b). Since the polymer remains strongly bound to the surface of the substrate it can only swell in one direction perpendicular to it, as opposed to a three-dimensional swelling of a free standing film. As a result significant degree of chain stretching in the direction perpendicular to the support is induced. The enforced orientation of the chains corresponds to reduced entropy. This is highly unfavorable and leads to the onset of thickness relaxation, during which the entropy is slowly regained. The interplay

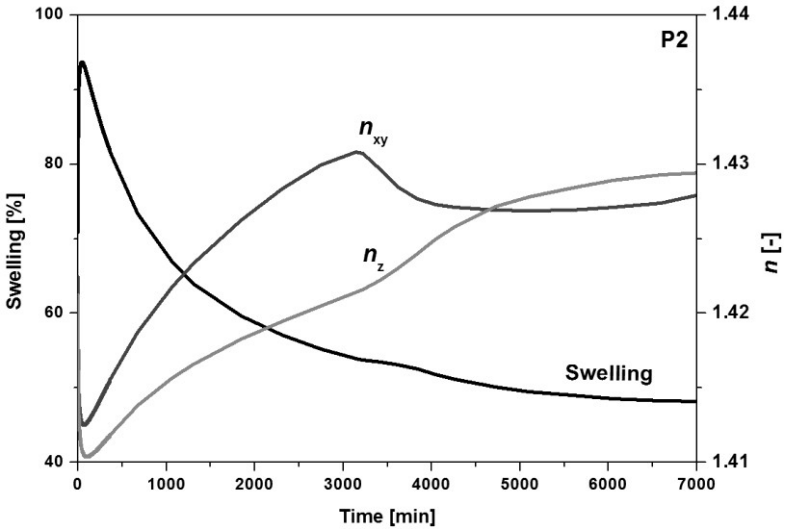

Figure 6.7 Time evolution of optical anisotropy in a swollen ~400 nm film of P2 plotted together with swelling

between enthalpic and entropic effects is responsible for the observed overshoot dynamics.

The dynamic changes in the polymer film thickness are accompanied by changes in the degree of anisotropy of the material. The dynamic anisotropic modeling results (Figure 6.7), suggest that as the swelling reduces from its maximum of 93 %, to about 55 %, the difference between n_{xy}, and n_z increases. This can be interpreted as follows. In the initially highly swollen state, around the maximum swelling, the polymer chains are largely separated. Because of that, there is little interchain interaction between the zwitterionic side chains and these groups remain more or less randomly oriented. During entropically driven polymer relaxation, disclosed by a decrease in thickness, the chains come closer together and the dielectrically screening electrolyte is being expelled from the swollen polymer. This causes an overall increasing trend in refractive index components, n_{xy} and n_z. Such increase of swollen film refractive index during thickness relaxation after overshoot of swelling has been reported previously for anomalous water diffusion dynamics in poly(vinyl alcohol)-poly(acrylic acid) composite films [25], and has also been interpreted as solvent removal from the film during thickness relaxation. Because of the increasing density within the sample, the zwitterionic side chains of neighboring polymer chains start to interact with each other. The developing interaction causes the increasing orientation of the zwitterionic moieties in the plane of the substrate (perpendicular to the orientation of the backbone). Evidence of similar interchain interactions of zwitterionic side chains in highly aligned chains has been previously suggested for zwitterionic brushes of similar chemical

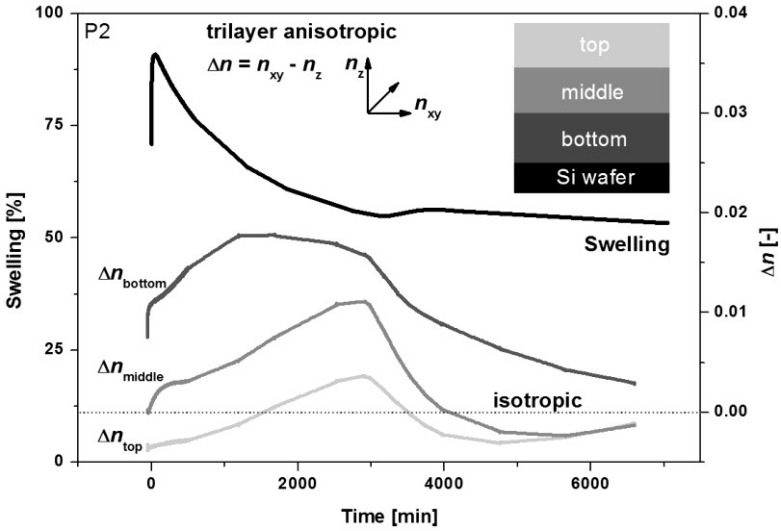

Figure 6.8 Time evolution obtained with the trilayer anisotropic model for the swollen ~400 nm sample of P2. Optical anisotropy (represented as $\Delta n = n_{xy} - n_z$) in three equal thickness regions within the film is shown. Dashed line at $\Delta n = 0$ represents an isotropic film.

composition [29]. The larger, and more electron rich zwitterionic side chains, possess higher polarizability than the backbone of the polymer. The alignment of zwitterionic side chains in the plane of the substrate results in a larger *xy* refractive index component as compared to the *z* component. The progressing orientation of the side chains, therefore, might drive the increase of anisotropy observed in the initial phase of thickness relaxation up to about 3200 minutes.

At about 3200 minutes, when the swelling reduces to about 55 %, n_{xy} and n_z start to converge. This process lasts for about 1200 minutes, during which the swelling reduces further to about 51%. The convergence of the indices is a sign of the loss of preferential directionality within the polymer when a certain swelling threshold is reached. During the later period of thickness relaxation the polymer chains start to regain their random coil configurations and are no longer highly oriented perpendicular to the substrate. As the process continues, the developed interchain and intrachain zwitterionic interactions lose their preferential direction and become more and more randomly oriented. Finally, the sample becomes predominantly isotropic when equilibrium swelling is reached.

To gain further insight into the anisotropy development as function of the position within the swollen film a tri-layer anisotropic model is used (Figure 6.8). The model is based on the Anisotropic model (Figure 6.1c) adapted by dividing the film in three parts that are equal in thickness. The total film thickness is used as fitting parameter and the refractive index components n_{xy} and n_z are fitted separately for each part of the film. For simplification the *B* parameters of the Cauchy relation are

coupled for each of the dispersion curves, and the resulting single value for B is also a fitting parameter. For each of the three parts of the swollen polymer a parameter $\Delta n = n_{xy} - n_z$ is defined to indicate the degree of optical anisotropy within the specific layer. The MSE of the fit is very low over the entire duration of the experiment (MSE < 9). The results indicate that the anisotropy in the swollen film shows a gradual increase from the substrate interface towards the top interface. During the whole experiment $\Delta n_{\text{bottom}} > \Delta n_{\text{middle}} \geq \Delta n_{\text{top}}$ holds. The chain confinement to the substrate results in the highest degree of anisotropy (Δn_{bottom} reaching 0.02), whereas the outer part of the polymer, in direct contact with the penetrant, stays more or less isotropic throughout the whole time of the experiment. It is also possible to notice that during the initial phase of thickness relaxation (between the maximum and about 2000 min) most molecular orientation occurs close to the substrate interface (Δn_{bottom} rises steeply). This can be interpreted as a chain anchoring effect, which leads to the highest degree of orientation closer to the substrate, especially during initial fast and significant swelling. Farther from the substrate, a more random conformation is possible, which results in lower anisotropy. The results after 3200 min show that loss of anisotropy in the later period of the thickness relaxation occurs relatively quickly in the middle and top parts of the film and slower at the bottom. This can be rationalized from immobilization of the polymer close to the substrate. The application of the single layer Anisotropic model, Figure 6.1c, to films in the range of about 240 nm to 760 nm yielded the largest anisotropy in the thinnest swollen films, and progressively lower anisotropy for thicker ones. These findings suggest that confinement to the substrate has a pronounced effect on both the magnitude and dynamics of anisotropy progression.

In the case of polymer P1, characterized by a more than two times lower content of zwitterionic groups, the swelling process is significantly different (Figure 6.5a). In the dry state the interchain associations between the charged groups are unlikely to form due to their low density. This fact, together with the more hydrophobic character of P1 due to overall lower amount of charged groups as compared to P2, reduces the driving force for electrolyte diffusion. As a result the diffusion process is a few orders of magnitude slower and the maximum of swelling is significantly lower. The polymer film P2 still shows, however, the overshoot dynamic behavior, which implies entropically driving relaxation. In contrast to polymer P1, during the thickness relaxation the fit improvement by the introduction of anisotropic model is not as significant as for P2 and the *MSE* of the anisotropic model remains relatively high (about 21-23). This suggests that orientations of the zwitterionic side chains are less pronounced. The lower degree of swelling results in less chain orientation perpendicular to the substrate (much less disturbed random coil configuration) and the overall lower content of zwitterionic side chains in P1 makes the occurrence of interchain interactions less likely.

6.5. Conclusions

Dynamic swelling behavior of thin films of random zwitterionic copolymers of suflobetaine methacrylate (SBMS) and n-butylacrylate (nBA) in 1 M NaCl solution is investigated using *in-situ* spectroscopic ellipsometry. Both the swelling rate and magnitude are shown to depend strongly on the content of zwitterionic groups incorporated in the polymer structure. For the materials investigated, an overshoot anomalous dynamic swelling is observed, indicating interplay between enthalpic and entropic effects in various stages of the process. Detailed ellipsometry data modeling is conducted to gain further insights into the changes in the film properties during polymer dilation and relaxation. For the polymer with 5.0 mol % content of the zwitterionic groups, the evidence of a density gradient in the initial phase of penetrant induced dilation is presented. In the case of the polymer with 11.6 mol % zwitterionic groups, the thickness relaxation process after maximum in swelling is shown to be best described when time dependent uniaxial anisotropy within the thin film is assumed. The behavior is rationalized by accounting for the orientation of polymer backbone and zwitterionic side chains as a result of swelling and relaxation in the presence of the screening electrolyte.

6.6. References

[1] Sabhapondit, A., A. Borthakur, and I. Haque, *Adsorption behavior of poly(N,N-dimethylacrylamide-co-na 2-acrylamido-2-methylpropanesulfonate) on sand surface.* Journal of Applied Polymer Science, 2004. **91**(4): p. 2482-2490.

[2] Didukh, A.G., et al., *Synthesis and characterization of novel hydrophobically modified polybetaines as pour point depressants.* Journal of Applied Polymer Science, 2004. **92**(2): p. 1042-1048.

[3] Arasawa, H., et al., *Grafting of zwitterion-type polymers onto silica gel surface and their properties.* Reactive and Functional Polymers, 2004. **61**(2): p. 153-161.

[4] Miyamoto, D., J. Watanabe, and K. Ishihara, *Molecular design of reactive amphiphilic phospholipid polymer for bioconjugation with an enzyme.* Journal of Applied Polymer Science, 2005. **95**(3): p. 615-622.

[5] Noh, J.-G., et al., *Synthesis, characterization, and stimuli-sensitive properties of novel polycarbobetaines.* Polymer, 2005. **46**(7): p. 2183-2190.

[6] Xu, J.-P., et al., *Novel biomimetic polymersomes as polymer therapeutics for drug delivery.* Journal of Controlled Release, 2005. **107**(3): p. 502-512.

[7] Zhao, J., et al., *Improved biocompatibility and antifouling property of polypropylene non-woven fabric membrane by surface grafting zwitterionic polymer.* Journal of Membrance Science, 2011. **369**(1-2): p. 5-12.

[8] Sun, Q., et al., *Improved antifouling property of zwitterionic ultrafiltration membrane composed of acrylonitrile and sulfobetaine copolymer.* Journal of Membrance Science, 2006. **285**(1-2): p. 299-305.

[9] Liu, J., T. Xu, and Y. Fu, *A novel route for the preparation of hybrid zwitterionic membranes containing both sulfonic and carboxylic acid groups.* Journal of Applied Polymer Science, 2008. **107**(5): p. 3033-3041.

[10] Liu, J., et al., *Preparation and characterizations of novel zwitterionic membranes.* Journal of Membrance Science, 2008. **325**(1): p. 495-502.

[11] Shi, Q., et al., *Zwitterionic polyethersulfone ultrafiltration membrane with superior antifouling property.* Journal of Membrance Science, 2008. **319**(1-2): p. 271-278.

[12] Yang, Y.-F., et al., *Surface hydrophilization of microporous polypropylene membrane by grafting zwitterionic polymer for anti-biofouling.* Journal of Membrance Science, 2010. **362**(1-2): p. 255-264.

[13] Zhang, Q., et al., *Novel zwitterionic poly(arylene ether sulfone)s as antifouling membrane material.* Journal of Membrance Science, 2010. **349**(1-2): p. 217-224.

[14] Chiang, Y.-C., et al., *A facile zwitterionization in the interfacial modification of low bio-fouling nanofiltration membranes.* Journal of Membrance Science, 2012. **389**(0): p. 76-82.

[15] Carr, L., et al., *Engineering the Polymer Backbone To Strengthen Nonfouling Sulfobetaine Hydrogels.* Langmuir, 2010. **26**(18): p. 14793-14798.

[16] Yang, C., et al., *Zwitterionic sulfobetaine-modified non-woven fabric for blood filtration.* Polymer International, 2010. **59**(9): p. 1296-1302.

[17] Wong, D., et al., *Surface Dynamics of Polymer Glasses: Sub-Tg Surface Reorganization in End-Functional Polymers.* Macromolecules, 2012.

[18] Kudaibergenov, S., W. Jaeger, and A. Laschewsky, *Polymeric Betaines: Synthesis, Characterization, and Application*, 2006, Springer Berlin / Heidelberg. p. 157-224.

[19] Galin, M., et al., *Poly(sulphopropylbetaines): 3. Bulk properties.* Polymer, 1987. **28**(11): p. 1937-1944.

[20] Mathis, A., Y.-L. Zheng, and J.-C. Galin, *Sulfonatopropylbetaine random copolymers: Zwitterionic analogues of ionomers.* Die Makromolekulare Chemie, Rapid Communications, 1986. **7**(6): p. 333-337.

[21] Castaño, V.M., et al., *Evidence of ionic aggregates in some ampholytic polymers by transmission electron microscopy.* Journal of Materials Research, 1990. **5**(03): p. 654-657.

[22] Nedelcheva, A.N., et al., *Electrostatic self-assembly of thermally responsive zwitterionic poly(N-isopropylacrylamide) and poly(ethylene oxide) modified with ionic groups.* Polymer, 2005. **46**(7): p. 2059-2067.

[23] Kharlampieva, E., V.A. Izumrudov, and S.A. Sukhishvili, *Electrostatic Layer-by-Layer Self-Assembly of Poly(carboxybetaine)s: Role of Zwitterions in Film Growth.* Macromolecules, 2007. **40**(10): p. 3663-3668.

[24] Habicht, J., et al., *Swelling of Thick Polymer Brushes Investigated with Ellipsometry.* Langmuir, 1999. **15**(7): p. 2460-2465.

[25] Pantelić, N. and C.J. Seliskar, *Anomalous Diffusion in Poly(vinyl alcohol)−Poly(acrylic acid) Thin Films.* Journal of Physical Chemistry C, 2007. **111**(5): p. 2054-2062.

[26] Patra, L., A. Vidyasagar, and R. Toomey, *The effect of the Hofmeister series on the deswelling isotherms of poly(N-isopropylacrylamide) and poly(N,N-diethylacrylamide).* Soft Matter, 2011. **7**(13): p. 6061-6067.

[27] Tang, Y., et al., *Structural Effects on Swelling of Thin Phosphorylcholine Polymer Films.* Macromolecules, 2002. **35**(10): p. 3955-3964.

[28] Tang, Y., et al., *Swelling of Zwitterionic Polymer Films Characterized by Spectroscopic Ellipsometry.* Macromolecules, 2001. **34**(25): p. 8768-8776.

[29] Cheng, N., et al., *Thickness-Dependent Properties of Polyzwitterionic Brushes.* Macromolecules, 2008. **41**(17): p. 6317-6321.

[30] Woollam, J.A., et al. *Overview of variable angle spectroscopic ellipsometry (VASE), part I: basic theory and typical applications*. 1999.

[31] Wu, T., et al., *Influence of Zwitterions on Thermomechanical Properties and Morphology of Acrylic Copolymers: Implications for Electroactive Applications.* Macromolecules, 2011. **44**(20): p. 8056-8063.

[32] Herzinger, C.M., et al., *Ellipsometric determination of optical constants for silicon and thermally grown silicon dioxide via a multi-sample, multi-wavelength, multi-angle investigation.* Journal of Applied Physics, 1998. **83**(6): p. 3323-3336.

[33] Galin, M., A. Chapoton, and J.-C. Galin, *Dielectric increments, intercharge distances and conformation of quaternary ammonioalkylsulfonates and alkoxydicyanoethenolates in aqueous and tirfluoroethanol solutions.* Journal of the Chemical Society, Perkin Transactions 2, 1993(3): p. 545-553.

[34] Samoc, A., et al., *Refractive-index anisotropy and optical dispersion in films of deoxyribonucleic acid.* Journal of Applied Polymer Science, 2007. **105**(1): p. 236-245.

[35] Ramsdale, C.M. and N.C. Greenham, *Ellipsometric Determination of Anisotropic Optical Constants in Electroluminescent Conjugated Polymers.* Advanced Materials, 2002. **14**(3): p. 212-215.

[36] Winfield, J.M., C.L. Donley, and J.-S. Kim, *Anisotropic optical constants of electroluminescent conjugated polymer thin films determined by variable-angle spectroscopic ellipsometry.* Journal of Applied Physics, 2007. **102**(6): p. 063505-063505-7.

[37] Sturm, J., et al., *Optical anisotropy in thin films of a blue electroluminescent conjugated polymer.* Thin Solid Films, 1997. **298**(1–2): p. 138-142.

[38] McBranch, D., et al., *Optical determination of chain orientation in electroluminescent polymer films.* Applied Physics Letters, 1995. **66**(10): p. 1175-1177.

[39] Pettersson, L.A.A., S. Ghosh, and O. Inganäs, *Optical anisotropy in thin films of poly(3,4-ethylenedioxythiophene)–poly(4-styrenesulfonate).* Organic Electronics, 2002. **3**(3–4): p. 143-148.

[40] Dressick, W.J., et al., *Divalent–Anion Salt Effects in Polyelectrolyte Multilayer Depositions.* Langmuir, 2012.

[41] Artsis, M., et al., *Diffusion of organic diluents into ethyl cellulose.* European Polymer Journal, 1972. **8**(4): p. 613-626.

[42] Lodge, T.P. and G.H. Fredrickson, *Optical anisotropy of tethered chains.* Macromolecules, 1992. **25**(21): p. 5643-5650.

[43] Gent, A.N. and T.H. Kuan, *Stress-optical coefficients of swollen polymer networks.* Journal of Polymer Science Part A: Polymer Chemistry, 1971. **9**(5): p. 927-937.

[44] Herminghaus, S., et al., *Large anisotropy in optical properties of thin polyimide films of poly(p‐phenylene biphenyltetracarboximide).* Applied Physics Letters, 1991. **59**(9): p. 1043-1045.

[45] Fischer, T., et al., *Photoinduced optical anisotropy in films of photochromic liquid crystalline polymers.* Journal of Photochemistry and Phobiology A: Chemistry, 1994. **80**(1–3): p. 453-459.

[46] Wang, C.H. and H.W. Guan, *Second harmonic generation and optical anisotropy of a spin-cast polymer film.* Journal of Polymer Science Part B: Polymer Physics, 1993. **31**(13): p. 1983-1988.

[47] Lin, L. and S.A. Bidstrup, *Processing effects on optical anisotropy in spin-coated polyimide films.* Journal of Applied Polymer Science, 1993. **49**(7): p. 1277-1289.

[48] Campoy-Quiles, M., P.G. Etchegoin, and D.D.C. Bradley, *On the optical anisotropy of conjugated polymer thin films.* Physical Review B, 2005. **72**(4): p. 045209.

[49] Galin, M., et al., *Poly(ammonioalkanesulfonate) Blends with Polar Organic Species and Alkali Metal Salts: Structure, Glass Transition and Ionic Conductivity.* Polymers for Advanced Technologies, 1997. **8**(2): p. 75-86.

[50] Bredas, J.L., R.R. Chance, and R. Silbey, *Head-head interactions in zwitterionic associating polymers.* Macromolecules, 1988. **21**(6): p. 1633-1639.

[51] Gauthier, M., T. Carrozzella, and G. Snell, *Sulfobetaine zwitterionomers based on n-butyl acrylate and 2-ethoxyethyl acrylate: Physical properties.* Journal of Polymer Science Part B: Polymer Physics, 2002. **40**(19): p. 2303-2312.

[52] Galin, M. and J.C. Galin, *Water sorption in butyl acrylate zwitterionomers of the ammoniopropanesulfonate and ammonioethoxydicyanoethenolate type.* Macromolecular Chemistry and Physics, 1997. **198**(4): p. 1021-1034.

Chapter 7

Swelling dynamics of zwitterionic copolymers: the effects of concentration and type of anion and cation

This chapter is in preparation for publication, authored by:

de Grooth J., Ogieglo W., de Vos W.M., Gironès M., Nijmeijer K., and Benes N.E..

Abstract

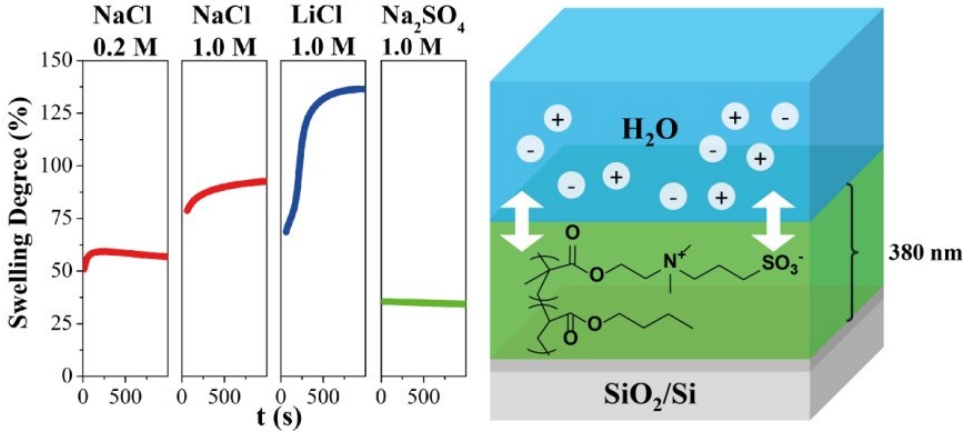

The effect of different salts and their concentration on the swelling of zwitterionic copolymers has been investigated for bulk polymer samples as well as for thin films. Relatively low ratios of the zwitterionic monomer already radically change the swelling properties of the copolymer. Increasing the NaCl concentration results in a significant increase of the swelling, which is indicative of the so-called anti-polyelectrolyte effect. The dynamic swelling experiments on the thin film show that only at high NaCl concentrations, the swelling is limited by solute diffusion. These swelling characteristics are distinctly affected by the type of ions present in the aqueous solution. The changes in maximum swelling degree are most sensitive to the type of anion, where the order of the extent of the effect of the anions follows the Hofmeister lyotropic series. For different cations, smaller changes in maximum swelling degree are found that only partially comply with the Hofmeister series. In most cases similar semi-Fickian swelling behavior is found, except in the case of LiCl concentrations above 0.8 M, where anomalous sigmoidal swelling curves are obtained. This behavior in high LiCl concentrations can be explained by the loss of interchain molecular interactions during swelling. This work provides meaningful insights on the behavior of zwitterionic copolymer films for applications such as membrane filtration, that utilize different ions and ionic strengths.

7.1. Introduction

Zwitterionic polymers are a special class of polymers containing both positive and negative ionic charges. This special characteristic makes this group of polymers an interesting candidate for a variety of applications, ranging from detergents [1], chromatographic processes and biomedical applications [2, 3]. Thin layers and brushes of such polymers have been shown to reduce cell adhesion and protein adsorption, which is relevant for different biomedical coatings. Furthermore, zwitterionic layers proved to be successful as antifouling layers in different industrial applications [4-7]. Especially the latter has resulted in an increased attention for zwitterionic polymers. A particular field where zwitterionic polymers show a large potential is membrane technology, where fouling reduction is critical. In membrane systems, the operating costs and energy consumption are negatively affected by fouling. Membrane fouling results in mandatory downtime of the system and degradation of the membranes due to harsh chemical cleaning steps required. Fouling resistant membranes based on zwitterionic polymers may reduce or even prevent the necessity of cleaning, improving the lifetime and operating costs of membrane processes. Furthermore, in dense polymeric membranes (e.g. desalination membranes) the retention of charged low molecular weight solutes (e.g. salts) is determined by the solution-diffusion model [8, 9]. As a result the retention is amongst others, a function of the polymer charge [10]. The incorporation of both positive and negative charges via polyzwitterions affects the rejection performance of dense membranes.

Another very interesting property, which the polyzwitterions are known to show, is the anti-polyelectrolyte effect: an increase in solubility or swelling of the polymer at increasing salt concentrations [11, 12]. The reason is that the addition of ions leads to a screening of the intra- and interchain interactions of the polyzwitterions, resulting in a solubilizing effect. Similar to solubility of proteins and polyelectrolytes, this effect in zwitterionic polymers is dependent on the nature of the specific ions [11-16]. Already in 1888, Hofmeister arranged ions with respect to their ability to precipitate (salt out) egg white from aqueous solutions [17]. Since then, similar trends have been found in numerous reports, including for zwitterionic polymers. Still the mechanism behind this effect is not very well understood [18]. In the case of zwitterionic polymers, the conformation of the polymer chains was shown to be highly sensitive to the asymmetry of the counterion adsorption [19]. The anti-polyelectrolyte effect has been linked to anti-fouling behavior [20, 21], and can be explained by an unfavorable entropy of conformation during protein adsorption onto swollen polymer networks [21]. Other work has also indicated the importance of electrolyte concentration and the nonspecific adsorption onto zwitterionic films [22, 23].

Recently a detailed ellipsometric study was performed into the swelling of a thin copolymer film of n-butyl acrylate and SBMA [24]. It was shown that the layer

swells significantly in a 1 M NaCl aqueous solution. A key result of this investigation, was that the swelling can cause chain orientation and anisotropy in these thin zwitterionic copolymer films. The focus of that work, however, was the development of a good optical model to study the swelling. In this work we present the dynamic swelling behavior of zwitterionic copolymers in different aqueous electrolyte solutions. As both the separation performance in membranes and the anti-fouling properties of zwitterionic polymers are dependent on both ion type and concentration [10, 25, 26], we examined both the static and dynamic swelling behavior of a zwitterionic copolymer for different electrolytes and concentrations. Since the specific properties of zwitterionic polymers are mainly utilized in thin films or coatings (thickness < 500 nm), we specifically study the effects occurring in thin films using *in-situ* spectroscopic ellipsometry (SE). SE is a precise and non-destructive measurement technique with a high acquisition rate, which allows the study of the behavior of thin films in the nano- to micrometer range [27-29]. With the appropriate experimental setup, *in-situ* swelling experiments can also be performed. The dynamic swelling data are used as input values in the diffusion model developed by Berens and Hopfenberg [30], in order to obtain information on the kinetic sorption behavior of electrolytes in zwitterionic polymer films. The results presented in this study provide a better insight in the dynamic interactions of zwitterionic polymers and different aqueous electrolyte solutions, which can be utilized to improve antifouling properties of coatings or enhance the separation properties of dense membranes.

7.2. Theory - characterization of swelling behavior of thin polymer films

The swelling degree (*SD*) can be calculated as a ratio of the swollen to the dry sample thicknesses as obtained from the *in-situ* SE experiments. *SD* changes over time yield information on the kinetics of the swelling of polyzwitterions in the presence of electrolyte solutions. However, the kinetics of polymer swelling are complex. During swelling not only Fickian diffusion takes place, but due to stretching of the polymer, several polymer chain relaxational phenomena will occur as well. Non-Fickian swelling dynamics can be empirically described by a model devised by Berens and Hopfenberg [30], which distinguishes between the Fickian and relaxational contributions of swelling and sorption in polymers:

$$SD(t)_{total} = SD(t)_{Fick} + SD(t)_R \qquad (7.1)$$

where the ideal Fickian regime is assumed to have a constant diffusion coefficient:

$$SD(t)_{Fick} = SD_{Fick,\infty}\left[1 - \frac{8}{\pi^2}\sum_{n=0}^{\infty}\frac{1}{(2n+1)^2} \times e^{\left\{-\frac{D(2n+1)^2\pi^2 t}{h^2}\right\}}\right] \qquad (7.2)$$

In eq. 7.2 $SD_{\mathrm{Fick},\infty}$ is the total swelling degree due to Fickian diffusion at infinite time, D is the diffusion coefficient (cm^2/s), h is the sample thickness (cm) and t is

the time (s). The relaxational contributions ($SD(t)_R$), and can be quantified according to equation 7.3, with the polymer relaxation time constants k_{Ri} (min^{-1}). Often, it is sufficient to limit the number of relaxational contributions to two.

$$SD(t)_R = \sum_{i=1}^{\infty} SD_{R_i}\left[1 - e^{\{-k_{Ri}t\}}\right] \quad (7.3)$$

The model is only applicable when the diffusion and relaxational contributions occur at different time scales [31, 32]. Since the difference in time scale between Fickian diffusion and polymer relaxations becomes more prominent for thin films, it is assumed that in our case these processes indeed do not overlap. As already pointed out by other researchers [33], the model lacks a physicochemical explanation of the relaxation phenomena. However, it is useful to compare the swelling and sorption behavior resulting from the diffusion of gasses and liquids into polymer films in order to get insight in the Fickian diffusion coefficients upon sorption and the relative contributions of Fickian swelling and relaxational phenomena [34-39].

7.3. Experimental part

7.3.1. Synthesis and characterization of p(SBMA-nBA)

All chemicals were obtained from Sigma Aldrich (The Netherlands) and used without any further purification steps. For a typical synthesis, 17.4 gram n-butyl acrylate (nBA) (135.7 mmol) and 5 gram N-(3-Sulfopropyl)-N-(methacryloxyethyl)-N,N-dimethylammonium betaine (SBMA) (17.9 mmol) were dissolved in 100 ml DMSO in a 250 ml round bottom flask under a nitrogen atmosphere. For other copolymer fractions, the comonomer ratios were changed accordingly whilst keeping the same total moles of monomer. The solution was heated to 70 °C and subsequently 0.20 gram $(NH_4)_2S_2O_8$ (0.9 mmol) was added (Figure 7.1). The mixture was left to react under reflux for at least 12 hours to

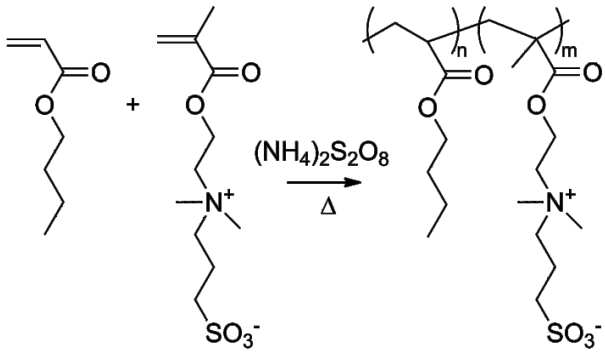

Figure 7.1 p(SBMA-nBA) synthesis via random copolymerisation in DMSO at 70 °C

ensure complete conversion of the monomers. After the reaction, the mixture was poured into demineralized water to form a precipitate. The precipitate was washed three times with 50 ml ultra-pure water for 30 minutes and subsequently dried in a vacuum oven at 30 °C for 24 hours. For further experiments, the polymer was stored under vacuum at 30 °C to prevent water uptake and used without any other purification steps.

Copolymer molecular weights were determined using size exclusion chromatography (SEC) in THF with 0.1 M LiCl against a polystyrene standard. The thermal stability of the copolymer was determined on a PerkinElmer TGA4000 at 20 °C min^{-1}. Differential scanning calorimetry (DSC) was measured on a PerkinElmer DSC8000 at 20 °C min^{-1}. Thin layers were prepared by spin coating the polymer on a piranha (3:1 98% H_2SO_4 : 30% H_2O_2) treated silicon wafer. Spin coating was performed at 2000 rpm for 2 minutes using a solution of 5% of the polymer in 2,2,2-trifluoroethanol (TFE).

The initial swelling experiments of bulk samples were performed by immersing approximately 0.5 grams of dried copolymer in 100 ml of the appropriate solution for at least 24 hours to ensure that the swelling equilibrium has been reached. Before measuring the mass of the swollen polymer, care was taken that any excess solution was removed. The swelling degree for the bulk samples was calculated with the swollen weight of the sample as a percentage of the dry polymer mass.

7.3.2. Spectroscopic ellipsometry

Spectroscopic ellipsometry measurements were performed using a rotating compensator ellipsometer M-2000X (J. A. Woollam Co., Inc.,) operated in a wavelength range from 370 – 920 nm. The wavelength range used was dictated by significant light absorption by the windows of the test cell below 370 nm, and by water absorption above 920 nm. The time resolution was around 2 seconds per full spectral scan, and the light spot size was about 2 mm. The test cell consisted of glass windows, positioned perpendicularly to the incident light, and the measurements were done at a fixed angle of incidence of 70°. The cell was equipped with a temperature control system, and the temperature was set at 21 °C. Before the swelling measurement the film thickness of the dry sample was measured, under nitrogen flow to avoid the influence of moisture. Afterwards the cell was filled with the desired salt solution and the measurement was started within 1 minute after filling the cell. This short period was required for slight corrections of the sample alignment and stabilization of the liquid surface. The ambient refractive index of each salt solution was taken from independent measurements using a standard laboratory refractometer (Carl Zeiss). For a more detailed experimental procedure the reader is referred to our previous work [24]. More information about the experimental technique itself can be found in one of the references [27-29].

The data were fitted dynamically, using an optical model in which uniaxial anisotropy within the thin polymer film was assumed. In the model, a distinction between the in-plane of the sample index (n_{xy}) and the out-of-plane index (n_z) was made and both components were modeled using a simple Cauchy type ($n(\lambda)=A+B/\lambda^2$) optical dispersion, assuming a transparent medium in the range of 370 to 920 nm.

7.4. Results and discussion

7.4.1. Properties of p(SBMA-nBA) and initial swelling experiments

The random copolymerization (Figure 7.1) results in a slightly tacky, ductile polymer. The overall synthetic procedure gives the p(SBMA-nBA) copolymer at a yield of 89%. The product is still soluble in DMSO due to the relatively low zwitterionic content. Elemental analysis was used to determine the SBMA content (based on the C-N ratio) in the polymer chain.SEC results show that the obtained polymer has a molecular weight average (Mw) of 55,000 g/mol. No significant weight loss (< 5%) has been found until 300 °C, while at 450 °C the polymer has completely degraded. DSC measurements indicate the presence of one glass transition temperature (T_g) at -37 °C. The thermal behavior of the copolymer is typical for this kind of polymers [40].

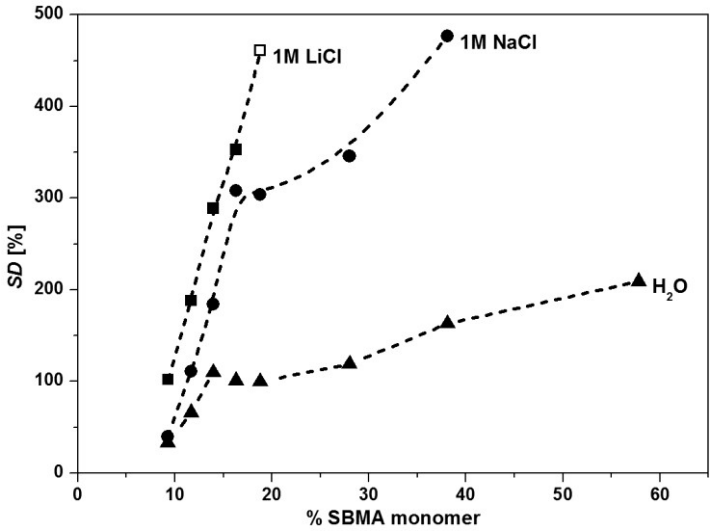

Figure 7.2 Swelling degree, *SD*, of 0.5 gram of p(SBMA-nBA) as a function of SBMA content for aqueous solutions as indicated. At 18% SBMA, partial dissolution is already occurring in 1 M LiCl, hence the open symbol. Lines are intended as a guide for the eye.

Initial swelling experiments of bulk polymers were performed as a function of SBMA content (Figure 7.2) in the copolymer. The results demonstrate that with a higher content of SBMA a higher degree of swelling in pure water is obtained. Moreover, addition of salt leads to a strong increase in the *SD*: a first indication of the anti-polyelectrolyte effect typical for zwitterionic polymers. Finally, the *SD* also depends on the type of anion added. The addition of 1 M LiCl leads to a much higher degree of swelling than the addition of an equal quantity of NaCl. For 1M of LiCl, the measurements were only possible up to about 18% SBMA, as above that value the polymer partially or totally dissolved. For 1M of NaCl, dissolution was observed above 40% of SBMA.

The bulk swelling data in Figure 7.2 clearly demonstrates the rich swelling behavior and interesting interactions with salt of the copolymer under investigation. However, for the application of zwitterions as anti-fouling layers, but also for the possible use of zwitterions in dense membranes, it is of interest to study the copolymer in the confined geometry of a thin film. Furthermore, the kinetics of swelling cannot be measured properly using the weighing technique. For these reasons, the study is continued with spectroscopic ellipsometry. The focus is on a copolymer containing 11.6% of SBMA. For this copolymer, the relative effect of the addition of salt is found to be large, while a relatively low *SD* is best suited to the technique of ellipsometry. In addition, the low SBMA content ensures that no dissolution of the polymer takes place, even at high ionic strengths.

Spin coating of the polymer solution in TFE results in uniform films, with thicknesses ranging from 340 to 390 nm. Due to the low T_g, no stress orientations are found in the dry thin films, as measured by ellipsometry. During all swelling experiments, sample integrity is maintained without any dewetting or dissolution of the polymer layers. Spectroscopic ellipsometry has revealed that for these polymers, during swelling experiments, relaxation of the polymer can be accompanied by the evolution of significant optical anisotropy of the films. A suitable anisotropic optical model is described and justified in [24].

7.4.2. Swelling dynamics in aqueous solutions of NaCl

Figure 7.3 shows the effect of the NaCl concentration on the swelling dynamics of a thin film of the zwitterionic copolymer. A substantially higher swelling degree (*SD*) is found for increasing electrolyte concentrations being a clear indication of the anti-polyelectrolyte effect. The ions diffusing into the polymer film break up the intra-chain and intra-group ionic interactions. The ion dissociation results in a more hydrophilic nature of the polymer and an increase in swelling of the polymer [11]. For our SBMA-nBA copolymer it is especially interesting that, even though the copolymer contains just 11.6% SMBA, we still observe a pronounced and gradual anti-polyelectrolyte effect. The swelling effect is clearly dominated by the SBMA minority, a result of the high degree of hydrophilicity these groups have at sufficient ionic strength [11].

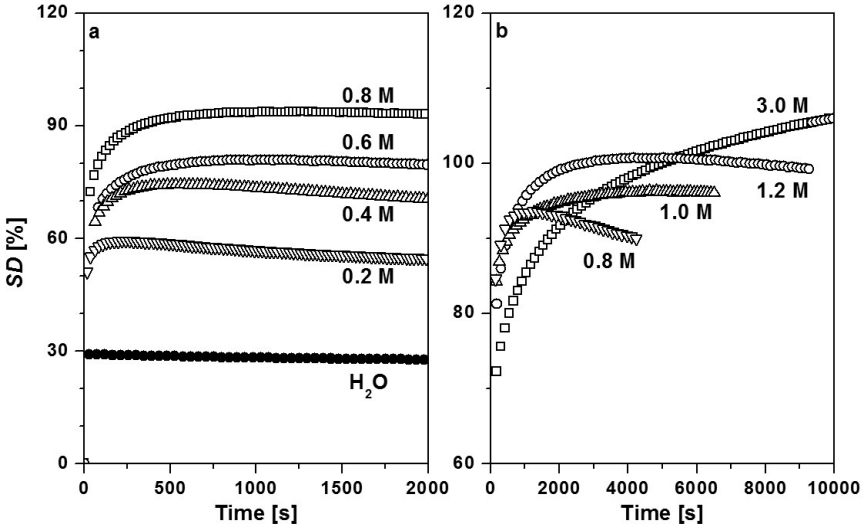

Figure 7.3 Effect of NaCl concentration on the swelling of thin p(SBMA-nBA) films; a) 0-0.8 M; b) 0.8-3.0 M NaCl.

For all concentrations qualitatively similar swelling behavior is observed. In all cases, three distinct contributions can be distinguished: an initial fast Fickian region, a positive relaxational contribution, and a subsequent slight decrease in *SD* due to secondary relaxations and orientation of the polymer chains [24]. The decrease of the *SD* is typically manifested after prolonged swelling, as shown in Figure 7.3b. The magnitude and rate of the different contributions are dependent on the NaCl concentration. Table 7.1 shows the dynamic and relaxational parameters extracted by numerically fitting the kinetic swelling data to the Berens-Hopfenberg relations (eqs. 7.1 - 7.3).

In these measurements, the data acquisition was always started about 60 seconds after exposure to the aqueous solution. This allowed for slight corrections of the sample alignment and stabilization of the liquid surface. Although we realize we exclude the initial measurement data from our analysis, the data still include the most relevant time span: the curvature of the Fickian diffusion component. This is considered sufficient to accurately and reliably calculate the Fickian diffusion in most cases. In the situations where this was not possible, for example for pure water, the reported values provide the minimum value for the Fickian diffusion coefficient. For concentrations up to 1.0 M NaCl, the experimental results can be well described with the empirical Berens – Hopfenberg relationships, indicating that the Fickian contribution and the two relaxational terms (a positive one and a negative one) are sufficient to describe the experimental data. A representative example of a fit is given in Figure 7.4. The results show the apparent differences

Table 7.1: Film thicknesses, Fickian diffusion coefficients and relaxational contributions as obtained from the Berens-Hopfenberg model for different [NaCl].

[NaCl] (M)	h_0 (nm)	D (cm^2/s)	SD_{Fick}	SD_{R1}	SD_{R2}	k_{R1} (min^{-1})	k_{R2} (min^{-1})
0	369	> 1 10^{-8}	-	-	-	-	-
0.2	343	3 10^{-10}	44.7	9.2	-6.4	1.54	6 10^{-2}
0.4	371	6 10^{-12}	62.7	14.7	-17.0	0.32	2 10^{-2}
0.6	382	5 10^{-12}	66.9	16.9	-27.0	0.19	5 10^{-3}
0.8	340	5 10^{-12}	76.2	15.7	-39.2	0.17	2 10^{-3}
1.0	330.	4 10^{-12}	83.5	23.3	-12.8	0.08	8 10^{-2}

h_0 = dry film thickness; D = diffusion coefficient; SD_{Fick} = Fickian swelling contribution; SD_{Ri} = polymer relaxational contribution; k_{Ri} = polymer relaxational time constant

between the time scales of the different processes. The Fickian contribution manifests itself in the first minutes, while both the positive and negative relaxations are significantly slower and become more pronounced at longer time scales.

The analysis of the fitted data from Table 7.1, reveals that the contribution of the Fickian swelling goes up with increasing concentration, due to a more pronounced anti-polyelectrolyte effect. Although the swelling at the start of data acquisition (t = 60 s) increases with increasing NaCl concentration, the diffusion coefficients are relatively stable in this range of concentrations, indicating no concentration dependence of the diffusion coefficient through the polymer films. At concentrations above 1 M NaCl the results suggest a change in the characteristics of the swelling dynamics (Figure 7.3b). First of all, at concentrations above 1M NaCl, the initial swelling rate (after 60 s) is reduced, even though the maximum swelling degree continues to increase up to 3 M. This effect can be attributed to concentration dependence of the diffusion coefficient. It is known that both water and ion diffusivity significantly decrease at higher salt concentrations in water and polymer matrices [41-43]. We therefore suggest that at the higher concentrations, the pronounced diffusion limitations prolong the timescale of initial swelling, causing it to overlap more with the timescale of the positive relaxation. The diffusion limitations are associated with the development of non-linear

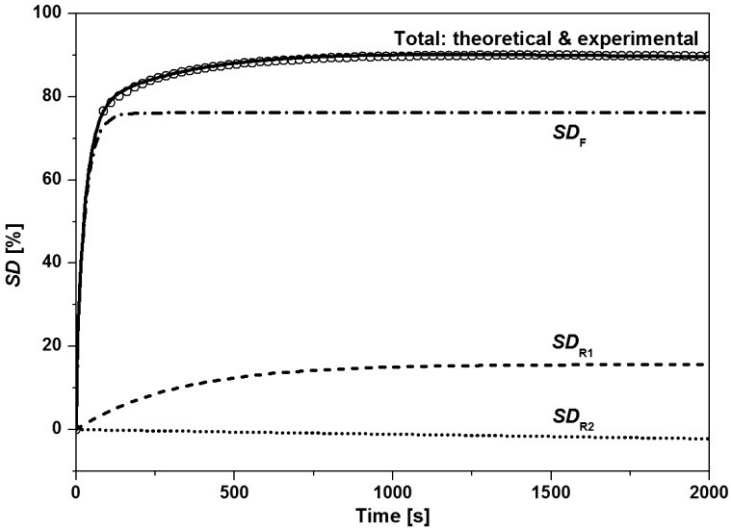

Figure 7.4 Fickian and relaxational contributions to the total swelling of a thin film; The experimental results for 0.6 M NaCl are also shown (○).

concentration profiles inside the film [44]. Modeling results of the raw optical data from spectroscopic ellipsometry indeed suggest the existence of a salinity gradient through the thickness of the film at the initial stages [24]. The existence of a salinity gradient also implies a variation of the diffusion coefficient over the film, and with that the Berens-Hopfenberg diffusion-relaxation model is no longer valid. In agreement with this, at concentrations above 1M, the initial swelling dynamics are not described well by a Fickian diffusion, a single positive relaxation, and a single negative relaxation (fitting results are not shown). These effects are more pronounced at higher NaCl concentrations. A second positive relaxation has to be added to obtain an adequate fit, limiting the physical significance of the fitting parameters.

The observed anti-polyelectrolyte effect, and the related strong dependence of the swelling on the ionic strength, makes this copolymer very interesting for certain dense membrane applications. The hydration of such a dense layer membrane is a key parameter in its retention behavior, with more swollen layers allowing larger molecules to pass through the membrane [45]. With this polymer it thus becomes possible to build a responsive membrane, where the ionic strength can be a control parameter for it swelling and retention behavior. While such responsive membranes exist, they are usually based on polyelectrolyte behavior, with a higher ionic strength leading to a collapse of the layer [46, 47]. Zwitterion-based membranes would have a unique inverse dependence on the ionic strength.

Several researchers have pointed out the importance of ionic strength and the anti-fouling behavior of zwitterionic polymers [21-23]. The observed increase in

swelling with NaCl concentration in our system is in all cases accompanied by polymer chain orientations[24], and this may subsequently result in increased antifouling effects at higher ionic strengths according to the theory of Ruhe and co-workers [21], This is supported by the increased nonspecific adsorption at higher ionic strengths as observed by Zhang et al. [25]. If the interactions between foulants, e.g., proteins, and the zwitterionic polymer are weak, the contribution of enthalpy to the change in free energy upon adsorption is small. Variations in the free energy of the adsorption process are in this case mainly entropy driven. This is also the case for swollen neutral networks or swollen charged networks from strong polyelectrolytes [21]. During adsorption, the entropy of mixing is opposed by loss of conformational entropy of the polymer chains. The loss of conformational entropy is referred to as 'entropic shielding'. With sufficient entropic shielding, adsorption or fouling, becomes unfavorable. Here we show that the relative change in swelling degree is the highest at lower NaCl concentrations, and subsequently the relative change in entropic shielding will thus be larger at the lower NaCl concentrations. This is in accordance with results showing that the largest change in protein adsorption is also found at low ionic strengths [21, 25].

7.4.3. Effect of type of ion on the swelling degree

Zwitterionic polymers are known to behave differently in electrolyte solutions containing different ionic species [11, 13-16]. For the zwitterionic p(SBMA-nBA) thin films, this is apparent from the differences in dynamic swelling in electrolyte solutions with different anions (cation Na^+) and different cations (anion Cl^-).

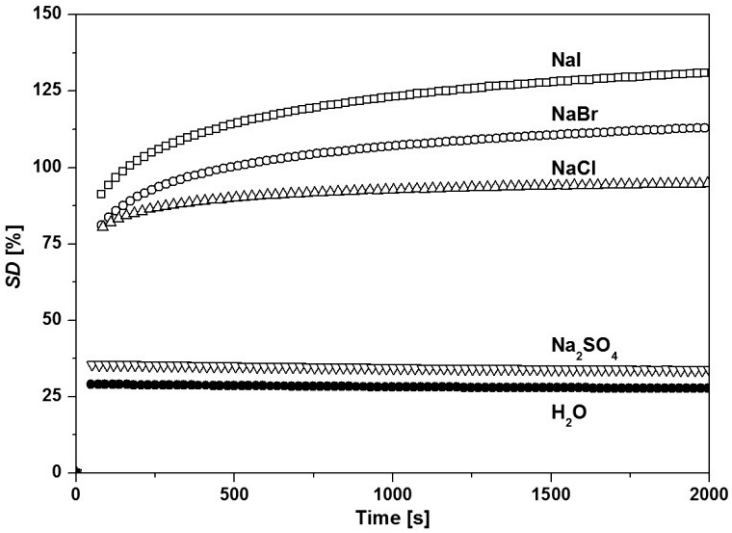

Figure 7.5 Effect of type of anion on the swelling dynamics of thin p(SBMA-nBA) films at 1M Na^+.

Figure 7.5 shows that the response of the zwitterionic polymer is very sensitive to the type of anion for sodium salts at 1 M. At different concentrations, an identical order in the sensitivity was observed.

The observed order of the magnitude of swelling, for the anions, is:

$$SO_4^{2-} < Cl^- < Br^- < I^-$$

This order is similar to trends found by other researchers, although sulfate was not regarded in any of those cases [11, 13-16]. There is no consensus on the rationalization of this order. It seems highly probable that it must be linked to the complex electrostatic interactions of the electrolytes, water and the zwitterionic groups on the polymer chain. It cannot be readily explained based on the size, either by the crystalline radii or the hydrated radii (Table 7.2), of the different ions. A slight correlation can be seen with the Stokes radii, especially for the considerable differences between the halogens and the sulfate ion. However, the differences in Stokes radii for the halogens are relatively small compared to the differences in swelling degree. Lee et al. attributed the solubility power of anions to the ratio of charge to radius [15], and although this theory holds for the monovalent anions, it fails for the divalent sulfate.

The magnitude of swelling does follow the well-known empirical Hofmeister lyotropic series related to the ability of salt to precipitate protein or polyelectrolyte from water [17, 50]. For a certain concentration of anion the lyotropic series (in their ability to salt out a protein) is as follows:

$$CO_3^{2-} > \mathbf{SO_4^{2-}} > S_2O_3^{2-} > H_2PO_4^- > OH^- > F^- > HCO_2^- > CH_3CO_2^- > \mathbf{Cl^-} > \mathbf{Br^-} > NO_3^- > \mathbf{I^-} > ClO_4^- > SCN^-$$

Although a complete understanding of the mechanism behind the effect of different ions from the series is not yet obtained [18], it is thought to be due to changes in the water structure at the interface of the polymer or protein in the presence of different ions, leading to changes in chain conformations and subsequently to precipitation [18, 50]. We assume that similar interfacial mechanisms between water, ions and the zwitterionic polymer are responsible for the changes in *SD* that we observed for different aqueous electrolyte systems.

In addition to the type of anion, also the effects of the type of cation (with a similar anion, Cl^-) on the swelling dynamics have been investigated (Figure 7.6). The swelling dynamics depend on the type of cation, although the observed differences are less pronounced as compared to the anions. Such relatively less pronounced effects induced by cations, as compared to anions, have been observed before for polyelectrolytes [50], and polyzwitterions [13, 16].

Table 7.2: Comparison of the maximum *SD* of thin p(SBMA-nBA) films for different anions and cations and their corresponding radii. [a] *I* = 1.5 M, [b] *I* = 1 M, [c] 0.4 M (*I* = Ionic strength).

	Ion	SD_{max} (%)	Crystal ionic radii (nm) [48]	Stokes radii (nm) [49]	Hydrated Radii (nm) [49]
Anions	SO_4^{2-}	35.5 [a]	0.290	0.230	0.379
	Cl^-	96.2 [b]	0.181	0.121	0.332
	Br^-	118.5 [b]	0.196	0.118	0.330
	I^-	133.2 [b]	0.220	0.119	0.331
Cations	Li^+	64.4 [c]	0.060	0.238	0.382
	Na^+	74.3 [c]	0.095	0.184	0.358
	K^+	77.5 [c]	0.133	0.125	0.331
	Ca^{2+}	80.9 [c]	0.099	0.310	0.329

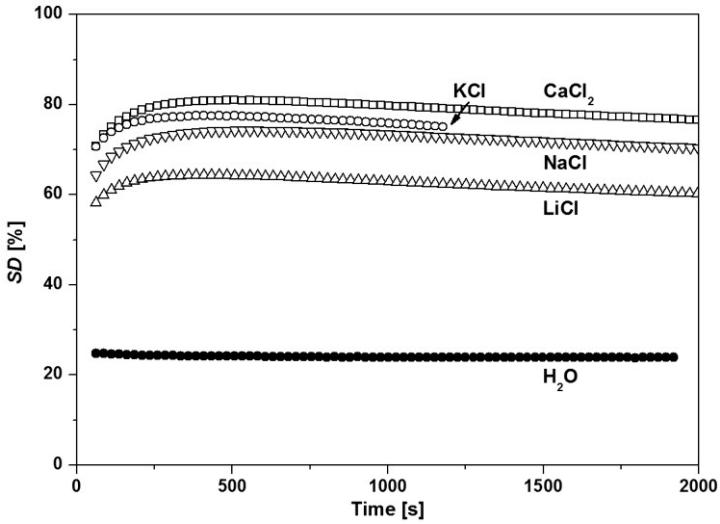

Figure 7.6 Effect of type of cation on the swelling of thin p(SBMA-nBA) films; all concentrations are 0.4 M.

Unlike for the different anions, the order of the swelling per cation depends on the ion concentration. At concentrations below 0.8 M, the order of the swelling per cation is:

$$Li^+ < Na^+ < K^+ < Ca^{2+}$$

The order of the swelling of cations does follow the Hofmeister series for the monovalent ions, but Ca^{2+} is a clear trend-breaker. For cations the, less well defined, Hofmeister series is [50]:

$$(CH_3)_2NH_2^+ > K^+ > Na^+ > Cs^+ > Li^+ > NH_4^+ > Mg^{2+} > Ca^{2+}$$

The results obtained in our dynamic swelling experiments on copolymers, can be compared to the results for the solubility of homopolymers of sulfobetaines in different electrolyte systems. In the case of homopolymers there exists a critical (θ) salt concentration above which the polymers become soluble in water. Comparable trends as presented here were found by Lee et al. for all the cations [15], Salamone et al for the monovalent ions [14], and Wielema et al. for the alkaline metal chlorides [13]. Nevertheless, other orders for the cations have also been found [14], with the order being sensitive to differences in concentrations of both homopolymer and ions [11].

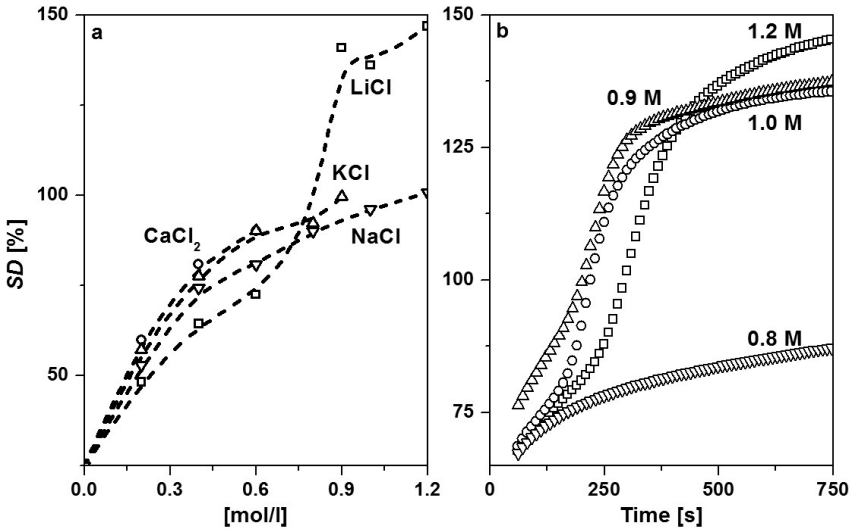

Figure 7.7 The effect of electrolyte concentration on the swelling of thin p(SBMA-nBA) films. a) maximum swelling degree for a range of concentrations for different chloride salts (LiCl ●, NaCl □, KCl ○, $CaCl_2$ ▲); b) change of swelling dynamics in LiCl solutions from 0.8 to 1.2 M.

The reason that Ca^{2+} is found to be a trend-breaker is likely due to its valence. Typically, the same molar concentrations of the salt (and thus cations) have been used in our investigation and in the literature studies. For divalent cations this means that double the amount of the anion Cl^- is present as compared to the amount of the cation. Since the influence of anion is usually more significant as compared to that of cations, this complicates comparison between cations with different valences. The extra Cl^- can easily explain the relatively high level of swelling observed for Ca^{2+}, and thus why Ca^{2+} does not follow the Hofmeister series.

Swelling experiments with different types of cations and different electrolyte concentrations show concentration dependence in the order of the cations (Figure 7.7a). At higher concentrations, the cation order with respect to swelling degree changes. This change is mainly due to a change in the behavior of LiCl and manifests itself at concentrations above 0.8 M LiCl. Such a change is in accordance with the findings of Schultz et al. [11], who concluded that the cation order for solubility is a function of the concentration ratio between the polymer and electrolyte and showed a significant concentration dependence for lithium salts. The change in degree of swelling of LiCl above 0.8 M is accompanied by a striking change in swelling dynamics from a semi-Fickian-like to a sigmoidal swelling behavior (Figure 7.7b). Sigmoidal swelling in polymers is often attributed to the superposition of simultaneous processes [44, 51]. One of these processes may be a loss in strength of the interactions between the polymer chains. The anomalous swelling observed for lithium is not found for the other electrolyte systems. Even at significantly higher concentrations and consequently higher swelling degrees, Fickian-like curves are observed for the other electrolytes (up to 3 M NaCl). This means that the sigmoidal swelling cannot be attributed solely to ductile failure of the material, as has been suggested for other polymer systems [51]. According to Diez-Pena et al., the sigmoidal behavior could be caused by an autocatalytic water up-take mechanism, where the uptake of the first water molecules aids in the uptake of the next ones [52]. A comparable behavior has been found for a copolymer of methacrylic acid with an poly(ethylene glycol) side chain, where an increase in pH and the subsequent ionization of the carboxylic groups leads to the loss of hydrogen bonds between the polymer chains [53]. Similar to this, a high lithium concentration may result in a complete deionization of the SO_3^- group in the polymer chain, significantly reducing the interchain interactions. To confirm this, swelling experiments were also done at different HCl concentrations, both above and below the pKa of the SO_3^- group. However, even at a pH as low as 0.1 no sigmoidal behavior was observed and the swelling dynamics were comparable to all other experiments. Most probably, the solvation shell around the lithium, and consequently the water structure at the surface of the polymer, changes at high lithium concentration. This may result in a complete loss of intermolecular polymer chain interactions, and thus extended swelling degrees. A lot of work has already

been done to comprehend the solvation of lithium in water [42, 54, 55]. Egorov et al. used molecular dynamic simulations to show that lithium fits well in the hydrogen bonded water network [42]. However, at higher concentrations of LiCl, the tetrahedral network can deteriorate [55]. These results indicate that indeed the solvation of lithium may change at higher concentrations. Still, a full explanation of this behavior in the complex matrix of water, zwitterionic polymer and LiCl is lacking. Our results do suggest a change in electrostatic interactions between the polymer chain upon the onset of the sigmoidal swelling, as the anisotropy observed for all experiments[24] is lost during the sigmoidal expansion and a fully isotropic swollen layer is obtained.

The significant differences in swelling of the p(SBMA-nBA) copolymer film indicate a potential use as an ion-selective membrane. Ions that have a high affinity for a membrane might selectively pass through that membrane. For our copolymer layer, there is a very unfavorable component to swelling of the copolymer layer, as increased swelling brings more of the hydrophobic nBA groups in direct contact with water. A higher degree of swelling must thus be compensated by a higher affinity of the ions for the SBMA groups to overcome these unfavorable solvent interactions. Our data thus seems to indicate that the zwitterionic copolymer has a different affinity for several ions, which could be an excellent basis for a membrane separation process.

The significant differences in the effect of the concentration and the type of anion and cation can be used in antifouling studies, as interactions between the electrolytes in solution and zwitterionic polymers determine the antifouling behavior of zwitterionic layers [21-23]. We therefore reason that fouling will be dependent on the type of electrolyte in the environment, similar to the ionic strength being coupled to the anti-polyelectrolyte effect and the anti-fouling behavior. However, to the best of our knowledge no extensive data exist on the fouling rate of zwitterionic films in different electrolyte solutions.

7.5. Conclusions

In this work we have evaluated the kinetic swelling behavior of zwitterionic thin films from p(SBMA-nBA). The diffusion/relaxation model of Berens and Hopfenberg has been used to quantify the semi-Fickian swelling dynamics, distinguishing between solute diffusion and polymer chain relaxations. A significant dependence of the swelling degree and dynamics on the NaCl concentration is found. At higher NaCl concentrations the swelling degree and rate both increase, corresponding to a more pronounced anti-polyelectrolyte effect. The value of the diffusion coefficient, obtained from the Berens-Hopfenberg model remains constant. At NaCl concentrations above 1 M, the diffusion coefficient decreases, causing diffusion and relaxation of the polymer processes to overlap. Furthermore, the results clearly show a dependence on the type of ion on the

swelling dynamics. The effects are most pronounced for anions, and are in accordance with the well-known Hofmeister series. For varying types of cations, less significant effects are found and these do not comply with the Hofmeister series. LiCl shows an anomalous behavior at concentrations above 0.8M. Sigmoidal swelling curves indicate additional loss of intermolecular polymer chain interactions during swelling. This is supported by the distinct evolution of the materials anisotropy at the higher LiCl concentrations, as derived from spectroscopic ellipsometry.

The above results indicate that the p(SMBA-nBA) copolymer under investigation has a real potential as a material for dense membranes. The observed anti-polyelectrolyte effect could be the basis for a responsive membrane, for which hydration and thus the retention behavior are controlled by the ion type and concentration. Furthermore, the significant differences in swelling for different ion-types indicate a potential use of this copolymer as an ion selective membrane. Finally, copolymers containing zwitterionic groups are known to exhibit excellent anti-fouling properties [15, 21, 22], an added benefit to using the copolymer for membrane applications.

7.6. References

[1] Luche, S., V. Santoni, and T. Rabilloud, Evaluation of nonionic and zwitterionic detergents as membrane protein solubilizers in two-dimensional electrophoresis. Proteomics, 2003. **3**(3): p. 249-253.

[2] Umemura, T., et al., Evaluation of sulfobetaine-type zwitterionic stationary phases for ion chromatographic separation using water as a mobile phase. Analytica Chimica Acta, 1997. **349**(1-3): p. 231-238.

[3] Guo, Y. and S. Gaiki, Retention behavior of small polar compounds on polar stationary phases in hydrophilic interaction chromatography. Journal of Chromatography A, 2005. **1074**(1-2): p. 71-80.

[4] Zhang, Z., et al., Superlow fouling sulfobetaine and carboxybetaine polymers on glass slides. Langmuir, 2006. **22**(24): p. 10072-10077.

[5] Li, M.-Z., et al., Grafting zwitterionic brush on the surface of PVDF membrane using physisorbed free radical grafting technique. Journal of Membrance Science, 2012. **405–406**(0): p. 141-148.

[6] Zhao, Y.-H., K.-H. Wee, and R. Bai, Highly hydrophilic and low-protein-fouling polypropylene membrane prepared by surface modification with sulfobetaine-based zwitterionic polymer through a combined surface polymerization method. Journal of Membrance Science, 2010. **362**(1-2): p. 326-333.

[7] Yuan, J., et al., Chemical graft polymerization of sulfobetaine monomer on polyurethane surface for reduction in platelet adhesion. Colloids and Surfaces B, 2004. **39**(1-2): p. 87-94.

[8] Schafer, A.I., A.G. Fane, and T.D. Waite, Nanofiltration - Principles and Applications, ed. A.I. Schafer, A.G. Fane, and T.D. Waite2005, Oxford: Elsevier.

[9] Mulder, M.H.V., Basic principles of membrane technology1996, Dordrecht: KluwerPublishers Group.

[10] Peeters, J.M.M., et al., Retention measurements of nanofiltration membranes with electrolyte solutions. Journal of Membrane Science, 1998. **145**(2): p. 199-209.

[11] Schultz, D.N., et al., Phase behaviour and solution properties of sulphobetaine polymers. Polymer, 1986. **27**(11): p. 1734-1742.

[12] Xue, W., M.B. Huglin, and B. Liao, Observations on the swelling characteristics of the zwitterionic hydrogel of poly(1-3-sulfopropyl)-2-vinyl-pyridinium-betaine hydrogel. European Polymer Journal, 2006. **42**(11): p. 3015-3023.

[13] Wielema, T.A. and J.B.F.N. Engberts, Zwitterionic polymers—III. Salt effects on the solubility of poly(vinyl sulphobetaines) and poly(vinyl betaines) in aqueous solution. European Polymer Journal, 1990. **26**(6): p. 639-642.

[14] Monroy Soto, V.M. and J.C. Galin, Poly(sulphopropylbetaines): 2. Dilute solution properties. Polymer, 1984. **25**(2): p. 254-262.

[15] Lee, W.-F. and C.-C. Tsai, Synthesis and solubility of the poly(sulfobetaine)s and the corresponding cationic polymers: 2. Aqueous solution properties of poly[N,N′-dimethyl-(acrylamido propyl) ammonium propane sulfonate]. Polymer, 1995. **36**(2): p. 357-364.

[16] Salamone, J.C., et al., Aqueous solution properties of a poly(vinyl imidazolium sulphobetaine). Polymer, 1978. **19**(10): p. 1157-1162.

[17] Hofmeister, F., Zur Lehre von der Wirkung der Salze. Naunyn-Schmiedeberg's Archives of Pharmacology, 1888. **24**(4): p. 247-260.

[18] Zhang, Y. and P.S. Cremer, Interactions between macromolecules and ions: the Hofmeister series. Current Opinion in Chemical Biology, 2006. **10**(6): p. 658-663.

[19] Kumar, R. and G.H. Fredrickson, Theory of polyzwitterion conformations. J. Chem. Phys., 2009. **131**(10): p. 104901.

[20] Georgiev, G.S., et al., Self-Assembly, Antipolyelectrolyte Effect, and Nonbiofouling Properties of Polyzwitterions. Biomacromolecules, 2006. **7**(4): p. 1329-1334.

[21] Worz, A., et al., Protein-resistant polymer surfaces. Journal of Materials Chemistry, 2012. **22**(37): p. 19547-19561.

[22] Estephan, Z.G., P.S. Schlenoff, and J.B. Schlenoff, Zwitteration As an Alternative to PEGylation. Langmuir, 2011. **27**(11): p. 6794-6800.

[23] Yang, Q. and M. Ulbricht, Novel Membrane Adsorbers with Grafted Zwitterionic Polymers Synthesized by Surface-Initiated ATRP and Their Salt-Modulated Permeability and Protein Binding Properties. Chemistry of Materials, 2012. **24**(15): p. 2943-2951.

[24] Ogieglo, W., et al., Relaxation induced optical anisotropy during dynamic overshoot swelling of zwitterionic polymer films. Thin Solid Films, 2013(0).

[25] Zhang, Z., et al., Nonfouling Behavior of Polycarboxybetaine-Grafted Surfaces: Structural and Environmental Effects. Biomacromolecules, 2008. **9**(10): p. 2686-2692.

[26] Holmlin, R.E., et al., Zwitterionic SAMs that Resist Nonspecific Adsorption of Protein from Aqueous Buffer. Langmuir, 2001. **17**(9): p. 2841-2850.

[27] Azzam, R.M.A. and N.M. Bashara, Ellipsometry and polarized light1977, Amsterdam; New York; New York: North-Holland Pub. Co. ; Sole distributors for the U.S.A. and Canada, Elsevier North-Holland.

[28] Fujiwara, H. and I. Wiley, Spectroscopic ellipsometry principles and applications, 2007, John Wiley & Sons: Chichester, England; Hoboken, NJ.

[29] Woollam, J.A., et al. Overview of variable angle spectroscopic ellipsometry (VASE), part I: basic theory and typical applications. 1999.

[30] Berens, A.R. and H.B. Hopfenberg, Diffusion and relaxation in glassy polymer powders: 2. Separation of diffusion and relaxation parameters. Polymer, 1978. **19**(5): p. 489-496.

[31] Joshi, S. and G. Astarita, Diffusion-relaxation coupling in polymers which show two-stage sorption phenomena. Polymer, 1979. **20**(4): p. 455-458.

[32] Sun, Y.-M., Sorption/desorption properties of water vapour in poly(2-hydroxyethyl methacrylate): 2. Two-stage sorption models. Polymer, 1996. **37**(17): p. 3921-3928.

[33] Tang, Y., et al., Swelling of Zwitterionic Polymer Films Characterized by Spectroscopic Ellipsometry. Macromolecules, 2001. **34**(25): p. 8768-8776.

[34] Pantelić, N. and C.J. Seliskar, Anomalous Diffusion in Poly(vinyl alcohol)−Poly(acrylic acid) Thin Films. Journal of Physical Chemistry C, 2007. **111**(5): p. 2054-2062.

[35] Kim, B., K. La Flamme, and N.A. Peppas, Dynamic swelling behavior of pH-sensitive anionic hydrogels used for protein delivery. Journal of Applied Polymer Science, 2003. **89**(6): p. 1606-1613.

[36] Hallinan, D.T., et al., Non-Fickian Diffusion of Water in Nafion. Macromolecules, 2010. **43**(10): p. 4667-4678.

[37] van der Wel, G.K. and O.C.G. Adan, Moisture in organic coatings — a review. Progress in Organic Coatings, 1999. **37**(1–2): p. 1-14.

[38] Potreck, J., et al., Sorption induced relaxations during water diffusion in S-PEEK. Physical Chemistry Chemical Physics, 2009. **11**(2): p. 298-308.

[39] Visser, T. and M. Wessling, When Do Sorption-Induced Relaxations in Glassy Polymers Set In? Macromolecules, 2007. **40**(14): p. 4992-5000.

[40] Wu, T., et al., Influence of Zwitterions on Thermomechanical Properties and Morphology of Acrylic Copolymers: Implications for Electroactive Applications. Macromolecules, 2011. **44**(20): p. 8056-8063.

[41] Wang, J.H., Effect of Ions on the Self-diffusion and Structure of Water in Aqueous Electrolytic Solutions. Journal of Physical Chemistry, 1954. **58**(9): p. 686-692.

[42] Egorov, A.V., et al., Temperature and Concentration Effects on Li+-Ion Hydration. A Molecular Dynamics Simulation Study. Journal of Physical Chemistry B, 2003. **107**(14): p. 3234-3242.

[43] Pajonk, A.S., R. Saurel, and J. Andrieu, Experimental study and modeling of effective NaCl diffusion coefficients values during Emmental cheese brining. Journal of Food Engineering, 2003. **60**(3): p. 307-313.

[44] Crank, J., The mathematics of diffusion. Vol. 1. 1979: Clarendon press Oxford.

[45] Bruening, M.L. and M. Adusumilli, Polyelectrolyte Multilayer Films and Membrane Functionalization. Material Matters 2011. **6**(3): p. 76-81.

[46] Huang, R., et al., Environment-responsive hydrogel-based ultrafiltration membranes for protein bioseparation. Journal of Membrane Science, 2009. **336**(1–2): p. 42-49.

[47] Liu, H., M. Zhen, and R. Wu, Ionic-Strength- and pH-Responsive Poly[acrylamide-co-(maleic acid)] Hydrogel Nanofibers. Macromolecular Chemistry and Physics, 2007. **208**(8): p. 874-880.

[48] Marcus, Y., Ion solvation1985: Wiley.

[49] Nightingale, E.R., Phenomenological Theory of Ion Solvation. Effective Radii of Hydrated Ions. Journal of Physical Chemistry, 1959. **63**(9): p. 1381-1387.

[50] Marcus, Y., Effect of Ions on the Structure of Water: Structure Making and Breaking. Chemical Reviews, 2009. **109**(3): p. 1346-1370.

[51] Neogi, P., Diffusion in polymers. Vol. 32. 1996: CRC.

[52] Díez-Peña, E., I. Quijada-Garrido, and J.M. Barrales-Rienda, Hydrogen-Bonding Effects on the Dynamic Swelling of P(N-iPAAm-co-MAA) Copolymers. A Case of Autocatalytic Swelling Kinetics. Macromolecules, 2002. **35**(23): p. 8882-8888.

[53] Prior-Cabanillas, A., et al., Swelling behaviour of hydrogels from methacrylic acid and poly(ethylene glycol) side chains by magnetic resonance imaging. Polymer International, 2007. **56**(4): p. 506-511.

[54] Tielrooij, K.J., et al., Cooperativity in Ion Hydration. Science, 2010. **328**(5981): p. 1006-1009.

[55] Harsanyi, I. and L. Pusztai, On the structure of aqueous LiCl solutions. Journal of Chemical Physics, 2005. **122**(12): p. 124512.

Chapter 8

Spectroscopic ellipsometry analysis of a thin film composite membrane consisting of polysulfone on a porous *α*-alumina support

This chapter has been adapted from:

Ogieglo W., Wormeester H., Wessling M., Benes N.E., ACS Applied Materials & Interfaces 2012;4(2):935-943. Copyright 2012 American Chemical Society

Abstract

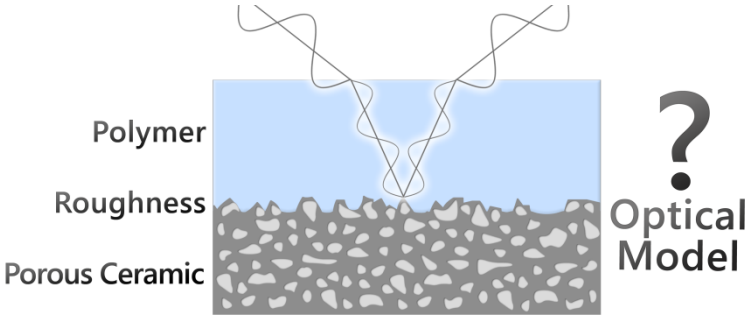

Exposure of a thin polymer film to a fluid can affect such properties of the film as the density and thickness. In particular in membrane technology, these changes can have important implications for membrane performance. Spectroscopic ellipsometry is a convenient technique for *in-situ* studies of thin films, due to its non-invasive character and very high precision. The applicability of spectroscopic ellipsometry is usually limited to samples with well-defined interfacial regions, while in typical composite membranes often substantial and irregular intrusion of the thin film into the pores of a support exists. In this work we provide a detailed characterization of a polished porous alumina membrane support, using variable angle spectroscopic ellipsometry in combination with atomic force microscopy and mercury porosimetry. Two spectroscopic ellipsometry optical models are presented that can adequately describe the surface roughness of the support. These models consider the surface roughness as a distinct layer in which the porosity gradually increases towards the outer ambient interface. The first model considers the porosity profile to be linear; the second model assumes an exponential profile. It is shown that the models can be extended to account for a composite membrane geometry, by deposition of a thin polysulfone film onto the support. The developed method facilitates practicability for *in-situ* spectroscopic ellipsometry studies of non-equilibrium systems, i.e., membranes under actual permeation conditions.

8.1. Introduction

Thin films are widely used in many areas of science and technology, serving as coatings [1] or membranes [2, 3], and for the fabrication of sensors [4] and microelectronic devices [5]. Application areas of thin films often involve their use as an interface between fluid phases with different thermodynamic status. For instance, in membrane technology molecular selectivity is often provided by a thin film serving as semi-permeable barrier. Separation performance of such a thin selective film is strongly dependent on penetrant concentration profiles inside film. These profiles are in turn dictated by the interactions between the thin film and the fluid mixtures it separates. In the case of polymer membranes, penetrant induced sorptive dilation or swelling [6] may significantly change the molecular structure and macromolecular dynamics of the material. For instance, in gas separation large concentrations of highly interacting penetrants can be responsible for undesired plasticization phenomena, thereby limiting the window of membrane operation [3, 7]. Fundamental understanding of such penetrant induced phenomena will aid membrane material choice and optimization of process parameters.

The majority of commercial membranes have an asymmetric composite geometry, comprising a thin selective film deposited on a highly porous support [3]. The support and the film can be organic [8] as well as inorganic [9]. Characterization of supported thin films can be accurately performed with many techniques, including such as Brillouin light scattering [10], particle embedding [11], dielectric relaxation spectroscopy [12, 13], buckling instability [14], positron annihilation spectroscopy [15], X-ray photon correlation spectroscopy[16], and spectroscopic ellipsometry [17, 18]. Few of these techniques have been applied for *in-situ* characterization of thin films exposed to a penetrant [8, 12, 17, 19-21]. For example, for thin films in contact with liquid or gaseous penetrant *in-situ* spectroscopic ellipsometry allows determination of the swelling degree and the estimation of the concentration of the dissolved penetrant [18]. Such *in-situ* spectroscopic ellipsometry analyses are normally limited to equilibrium conditions, when the films are supported on non-porous substrates such as silicon wafers or glass slides. In actual membrane applications the film separates two phases that are not in thermodynamic equilibrium, and mass transport occurs from one side of the film to the other. This requires the layer that supports the thin selective film to be very permeable, i.e., highly porous. Typically, however, porosity introduces roughness in the sample structure which makes the ellipsometry analysis difficult due to diffuse light scattering or depolarization effects. Moreover, if the interface between the dense skin and the porous support of the membrane is not well defined (i.e. pore intrusion) the interpretation of ellipsometry parameters, Ψ and Δ, may be hindered. To characterize thin membrane films in realistic membrane application conditions, the *in-situ* spectroscopic ellipsometry approach will need to be extended to account for porous substrates.

The purpose of this work is to study the applicability of *in-situ* spectroscopic ellipsometry in investigations involving composite flat disk membranes, in which a ceramic porous support is covered with a thin polymer film. The support chosen here is a very well defined, chemically and mechanically stable porous alumina material characterized by uniform roughness. On the alumina support a thin polysulfone film is deposited by a floating technique which minimizes the polymer pore intrusion. For the sample designed in such a way a viable optical model is provided.

8.2. Spectroscopic ellipsometry principles

Spectroscopic Ellipsometry is a non-destructive optical technique that allows very precise *in-situ* analysis of the properties of thin films. Combined with appropriate data analysis and modeling, the technique can yield information on the film thickness and refractive index.

In spectroscopic ellipsometry light of a well-defined polarization state (usually linearly polarized) is reflected of a thin film – substrate system. The reflection results in the change of the polarization state of light, in general into elliptically polarized. The parameters that describe the change of the polarization state upon reflection are Ψ and Δ, which are defined in equation 8.1.

$$\rho = \frac{r_p}{r_s} = \tan(\Psi) \cdot e^{i\Delta} \quad (8.1)$$

The symbols r_p and r_s refer to reflectivity of *p*- and *s*- polarized light, respectively. For further details on the basics of ellipsometry the reader is referred to one of the handbooks[22, 23].

The measured Ψ and Δ are collected over a range of wavelengths of light. Extracting meaningful physical information from this ellipsometric spectrum requires the construction of an optical model of the sample. In general, this optical model takes into account a number of distinct layers with individual optical dispersions. Interfaces between these layers are optical boundaries at which light is refracted and reflected according to the Fresnel relations. The total reflected light is a product of constructive and destructive interferences of light rays reflected from all of the optical interfaces. The Ψ and Δ values generated for a given optical model are numerically matched to the measured Ψ and Δ, by adjusting the values of fitting parameters. Fitting parameters can include the thickness, the real part of the refractive index n (or the optical dispersion) and the imaginary part of the refractive index k (extinction coefficient) of the different layers. In case of weakly or non-absorbing dielectric materials the extinction coefficient is close to zero and the optical dispersion can be successfully fitted to the well-known Cauchy dispersion,(eq. 8.2):

$$n(\lambda) = A + \frac{B}{\lambda^2} + \frac{C}{\lambda^4} \quad (8.2)$$

The difference between the optical response predicted by an optical model and the measured data (the quality of fit) can be expressed by the Mean Square Error (MSE). The MSE is defined as the square root of the sum of errors between the measured and model generated values. The lower the value of the MSE, the closer the data generated from a model are to the measured data. Generally, it is considered that an MSE value between 1 and 2 describes a good fit for single angle of incidence of incoming light and layer thickness in the range 100 - 200 nm. For thicker layers higher values of MSE are considered acceptable. For thicker layers ellipsometry spectra display more oscillations; at the same measurement resolution less measured values describe the single oscillation in case of a thicker film as compared to a thin film. In analogy, higher MSE values are considered acceptable for ellipsometry spectra with much structure in the measured data. The MSE value is also expected to be higher when analysis is performed simultaneously on spectra taken at multiple angles of incidence, due to errors accumulation (angle of incidence determination accuracy, beam collimation etc.).

The layer thickness range that can be determined by Ellipsometry matches well with the typical thickness range of selective membrane skin layers (30 - 2000 nm) [2, 24, 25]. However, a crucial requirement for spectroscopic ellipsometry is that the support layer beneath the studied thin film needs to be very well defined and uniform. Typical substrates include polished silicon wafers, glass slides or metallic discs. If the substrate surface features dimensions exceed ~30% of the wavelength of the probing light, pronounced scattering effects occur that may strongly complicate analysis [22]. This requirement is very rarely met in asymmetric or composite membranes where the support pore dimensions are often much larger than this limit.

In addition to light scattering by pores in the support layer, ellipsometry is also complicated by large surface roughness or pronounced thickness variations. Such sample non-idealities result in a partial depolarization of the reflected light, which can significantly increase the errors of the analysis. For instance, if the analyzed sample is characterized by large surface roughness some portion of the probing light will be scattered (multiply reflected) on the surface. That will result in a different polarization state as compared to the light reflected from the sample surface only once. Similarly, if the thin film deposited on the substrate is non-uniform with respect to its thickness, light reflected from such a sample carries different polarization state depending on the lateral position of the light ray reflection. Other physical phenomena responsible for depolarization include incident angle or wavelength variations and are related to the characteristics of the experimental setup. The intensity of reflected light also affects modeling quality, as the polarization state of light is determined from the light intensity. Thus, severe reduction in light intensity upon reflection complicates ellipsometry analysis.

The optical properties of a mix of materials can be approximated using an effective medium approximation (EMA) theory. EMA theories are based on the assumption that the mean optical dispersion of a medium which comprises of two different dielectric substances can be approximated by mixing their dielectric constants or, using the relationship $\varepsilon = n^2$, their refractive indices (n_a and n_b), for instance according to the formula proposed by Bruggeman (eq. 8.3):

$$f_a \cdot \frac{n_a^2 - n_{eff}^2}{n_a^2 + 2 \cdot n_{eff}^2} + (1 - f_a) \cdot \frac{n_b^2 - n_{eff}^2}{n_b^2 + 2 \cdot n_{eff}^2} = 0 \quad (8.3)$$

where fa is the volume fraction of the substance a and n_{eff} is the effective refractive index. Bruggeman approach, therefore, makes the self-consistent choice of the host material where the polarizability of the intruded material is related to the polarizability of the host. In this way the porosity of a material can be represented as a mix of void refractive index (n=1) and refractive index of dense material. The EMA approach can also be used to approximate the concentration of a penetrant in a polymer matrix for instance treating the dissolved substance as a liquid phase homogeneously mixed with host on a molecular level [8, 18]. Complex optical models can be devised in an attempt to account for the effects of thickness non-uniformity, surface roughness, refractive index gradients, and materials mixing.

8.3. Experimental part

8.3.1. Materials

Alpha alumina porous disks were prepared form commercial alumina powders: AKP-15, AKP-30 and AKP-50 (Sumitomo Chemical, Japan) with average particle size of 0.7 µm, 0.3 µm, and 0.2 µm, respectively. Commercial polysulfone (PSU) Udel P-3500 (Amoco, Solvay Advanced Polymers) and cyclopentanone (Sigma Aldrich) were used as received. 3 mm thick glass slides prepared in house were used for the PSU free standing film preparation.

8.3.2. Support preparation

The α-alumina supports in a flat disc geometry were prepared according to the protocol described in detail elsewhere [26]. The procedure involved the preparation of the AKP powder suspension in an acidic solution with the addition of poly(vinyl acetate). A green compact was obtained by filtering the suspension in a mould. After sintering at 1100 °C the obtained disk was cut to the desired dimensions, and one surface was polished mechanically to produce a smooth interface.

8.3.3. Layer deposition

A solution of 10 %wt PSU in cyclopentanone was spin coated on a clean glass slide, followed by annealing for 5 hours at 120 °C under nitrogen flow in order to remove the remaining solvent. The glass slide with film was then immersed in de-

ionised water, causing it to dewet and float on the surface within 1 hour. The free standing film was gently placed on top of an AKP-50 support and dried in a furnace at 100 °C for 1 hour under nitrogen flow. Subsequently, the furnace temperature was increased to 250 °C (PSU T_g =185 °C) for 2 hours to accomplish partial intrusion of the polymer into the surface roughness of the alumina support, ensuring a good adhesion of the film. Samples prepared in this way were then quenched to room temperature by removing them from the furnace, and used for spectroscopic ellipsometry analysis.

8.3.4. Characterization

8.3.4.1. Atomic force microscopy

Atomic Force Microscopy (AFM) imaging was performed with a Dimension 3100 AFM equipped with a hybrid scanner and NanoScope Iva controller (Veeco/Digital Instruments, Santa Barbara, CA, USA) operated in a tapping mode. Commercially available silicon cantilevers (PointProbe® Plus silicon probes, PPP-NCH, Nanosensors, Neuchatel, Switzerland) were used.

8.3.4.2. Spectroscopic ellipsometry

Spectroscopic ellipsometry measurements were performed with two systems, both supplied by J.A. Woollam Co., Inc. A rotating compensator ellipsometer (M-2000X) was used for the UV-VIS range of the spectrum 210-1000 nm. The M-2000X was characterized by fast acquisition times: less than 10 seconds per single incident angle. The second system, a rotating analyzer ellipsometer (VASE), was used to probe the samples in the near infrared, up to about 1700 nm. The combined range of wavelengths available for analysis was 210 - 1700 nm. The spot size of the probing light had a diameter of 2 mm in case of both spectroscopic ellipsometers used. The spectral resolution for the M-2000X and the VASE ellipsometers was 2 nm and 5 nm respectively which was high enough to adequately capture Ψ and Δ oscillations of the polymer deposited sample. For all samples measurements were conducted at multiple angles of incidence, to improve reliability of data interpretation and modeling. Data modeling was performed with a commercial software package (Complete EASE v.4.41) supplied with the M-2000X system.

The thickness and optical constants of the PSU film deposited on glass were determined with the M-2000X, assuming using simple Cauchy dispersions for the glass substrate and the polymer film. Firstly, the pure glass substrate was analyzed, accounting for surface roughness on the nanometer scale. The derived optical constants were kept fixed in the subsequent analysis of the supported PSU layer. Secondly, the thin supported PSU layer was characterized, yielding thickness (1115 nm) and Cauchy optical dispersion function with $n_{632.8nm}$ = 1.625. The dispersion

function was assumed the same after deposition onto the alpha alumina porous support.

8.3.4.3. Mercury porosimetry

Porosity of all the samples was determined with a mercury PoreMaster® porosimeter (Quantachrome).

8.4. Results and discussion

8.4.1. Characterization of the α-alumina disks

8.4.1.1. AFM

The AFM topography images of polished flat disk samples of AKP-15, AKP-30 and AKP-50 are presented in Figure 8.1. In each case the scan area presents a square region of 10 µm × 10 µm. The surfaces of AKP-30 and AKP-50 disks exhibit surface roughness features of a comparable size. In the case of AKP-15 the surface roughness features are much larger and surface morphology is significantly more irregular.

More precise analysis of the topmost roughness layer is performed based on depth line scans over a distance of 10 µm (Figure 8.2) and their corresponding cumulative height distributions (Figure 8.3). In Figure 8.2 the zero value on the Y-axis represents the average depth of the sample features as determined for the whole analyzed area. AKP-30 and AKP-50 types are relatively uniform over the area analyzed, as is indicated by only slightly asymmetric bell-shaped line scan histograms (not shown). In the case of AKP-15 the line scan histogram presents a much wider, though also symmetric shape.

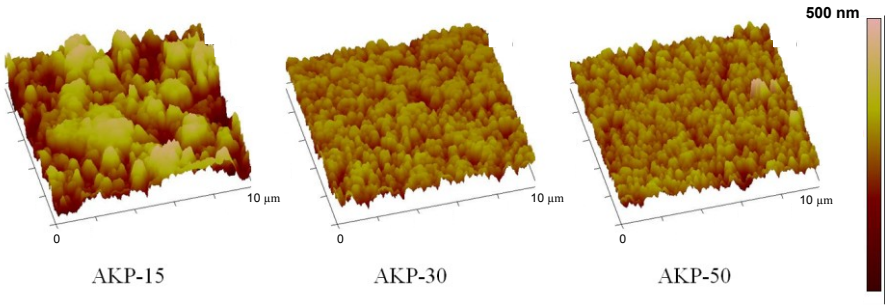

Figure 8.1 AFM topology images for AKP-15, AKP-30 and AKP-50 samples, vertical (out of plane) height scale relates to all three topology maps

Correlation analysis of the AFM images reveals the average sizes of the surface roughness features to be 370 nm, 170 nm and 160 nm for the AKP-15, AKP-30 and AKP-50 respectively.

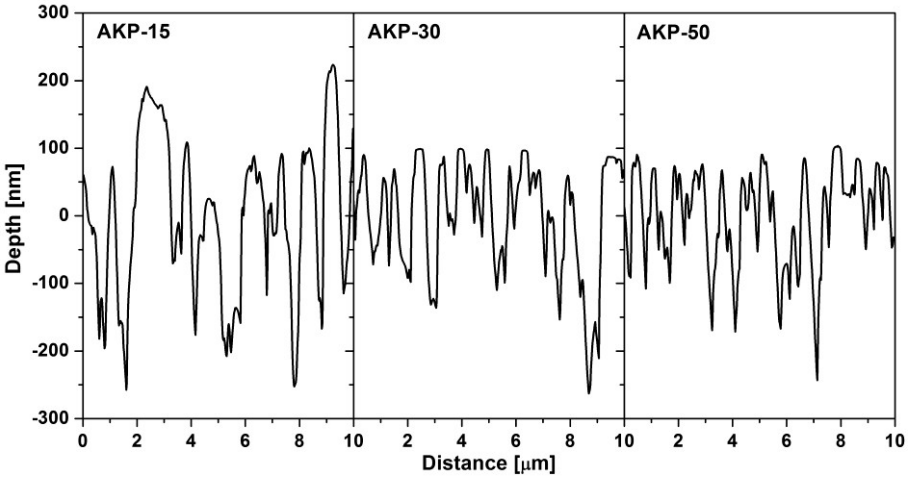

Figure 8.2 Representative AFM line scans over 10 micron distances of the surface

In Figure 8.3 the AKP-30 and AKP-50 profiles nearly completely coincide. The corresponding profiles of the cumulative height distribution show an almost linear increase of the void fraction, going from the uniform bulk of the sample outwards. The depth over which the increase occurs can be quantified by a simple tangent construction as indicated in Figure 8.3. In the case of AKP-15 the range over which the void fraction changes reaches 510 nm which is approximately two times more than in the case of AKP-30 and AKP-50 (240 nm).

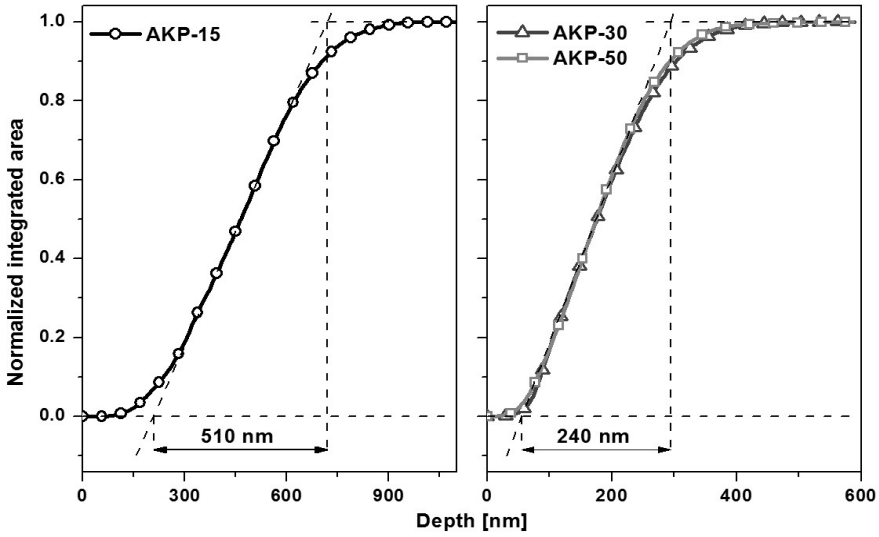

Figure 8.3 AFM cumulative height distribution for AKP-15, AKP-30 and AKP-50; symbols are guides for the eyes

8.4.1.2. Spectroscopic ellipsometry

Figure 8.4 combines the measurements of signal intensity and depolarization of light reflected at 70° angle of incidence as a function of light wavelength, for three support types. In all cases the light intensity decreases for shorter wavelengths. This is probably related to more pronounced scattering as the wavelength approaches the scale of sample surface roughness features. In the case of AKP-15 the reflected signal is much weaker than in the case of AKP-30 and AKP-50 and vanishes completely below about 300 nm. In the visible range depolarization is very low for all measured samples. Only for AKP-15 a sharp decrease in depolarization is observed below 300 nm. This is in a good agreement with the much larger scale of surface irregularities of the AKP-15, and is related to significant scattering at shorter wavelengths.

Table 8.1 shows, for the three sample types, the mean value and standard deviation (*SDev*) of Ψ (at 632.8 nm, 70° angle of incidence) for 10 measured spots across a sample surface, and the instrumental *SDev* in Ψ determination. The instrumental *SDev* is largest for AKP-15. For all samples the instrumental *SDev* is much less than the spot to spot *SDev*, indicating that non-uniformity can be assessed with higher accuracy than the experimental error. The results show that the spot to spot non-uniformity increases strongly with increasing grain size. Apparently, surface polishing of the alumina, supports made with smaller particles, results in much more uniform surface roughness features. In accordance, AKP-50 samples are characterized by the highest uniformity of surface roughness.

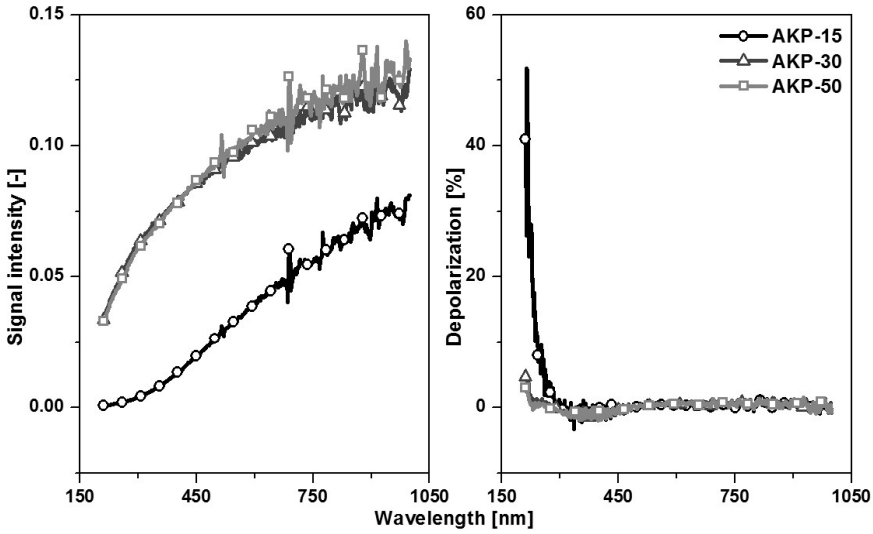

Figure 8.4 Signal intensity and depolarization of light for AKP-15, AKP-30 and AKP-50 disks measured with a 2 mm light spot size at 70° angle of incidence; symbols are guides for the eyes

Table 8.1 Measured mean Psi values at 632.8 nm wavelength together with calculated standard deviation (*SDev*) from 10 different spots on AKP-15, AKP 30 and AKP-50. Instrumental *SDev* in *Ψ* determination and particle grain size used for the preparation of the samples also indicated.

Sample	Mean *Ψ* at 632.8 nm	*SDev* of *Ψ* from 10 spots at 632.8 nm	Instrumental *SDev* of *Ψ* at 632.8 nm	Particle grain size [µm]
AKP-15	28.8	0.8	0.03	0.7
AKP-30	28.5	0.3	0.02	0.3
AKP-50	28.34	0.05	0.02	0.2

For AKP-30 and AKP-50 the sufficient signal intensity, the low depolarization, and uniform surface features indicate that it may be possible to construct an appropriate optical model for interpretation of ellipsometry data.

8.4.2. Spectroscopic ellipsometry model development

8.4.2.1. Uncoated *α*-alumina support

Constructing an appropriate optical model is facilitated by investigating the behavior of the so called pseudo optical transforms <*n*> and <*k*>, especially with respect to dependence on angle of incidence. As defined in eq. 8.4, <*n*> and <*k*> are directly related to the measured *Ψ* and *Δ* values.

$$(< n > + i < k >)^2 = sin\,(\theta)^2 \cdot \left[1 + tan\,(\theta)^2 \cdot \left(\frac{1-\rho}{1+\rho}\right)^2\right] \quad (8.4)$$

In equation 8.4, *θ* stands for the angle of incidence. Pseudo optical transformation of multi-angle spectroscopic data is useful in order to gain some basic information about the sample structure. If the analyzed sample morphology is isotropic and comprises only a single optical interface, for instance in the case of a bare polished substrate, the pseudo optical constants are independent on the angle of incidence and are equivalent to the materials actual optical constants *n* and *k*. If the pseudo optical constants are angle dependent, the sample can be represented more appropriately by an anisotropic or a multilayer structure. This is for instance typical for samples possessing oxide layers, thin films, roughness, or complex anisotropic geometry [27].

The pseudo optical constants for an AKP-30 sample, for angles of incidence 65°, 70° and 75°, are depicted in Figure 8.5. The results are representative also for AKP-15 and AKP-50, and show a significant dependence of the pseudo transforms on angle of incidence. Additionally, the <*k*> values show unphysical negative

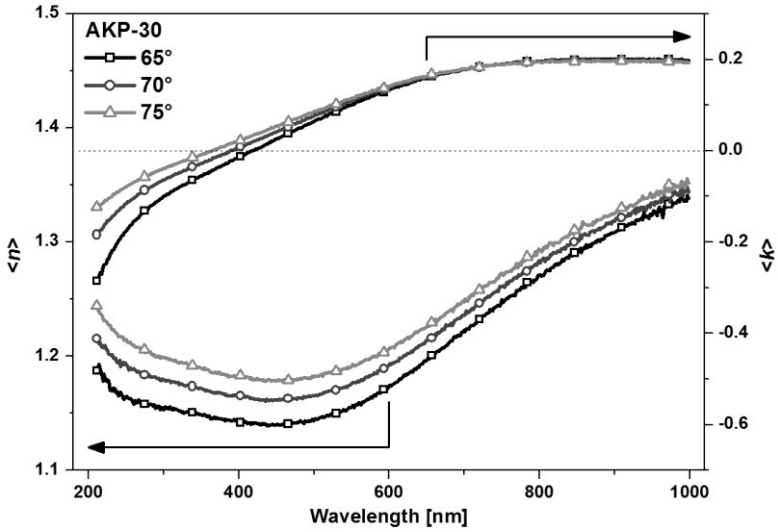

Figure 8.5 Pseudo transforms <*n*> and <*k*> for AKP 30 at angles of incidence of 65°, 70° and 75°; symbols are guides for the eyes

values at wavelengths below about 450 nm. This strongly suggests that the samples do not possess a single isotropic interface structure. An appropriate optical model for such samples should involve a multilayer system or anisotropy.

Based on the conclusions from the AFM and ellipsometry analysis it seems reasonable to treat the surface roughness of the alumina supports as a separate layer

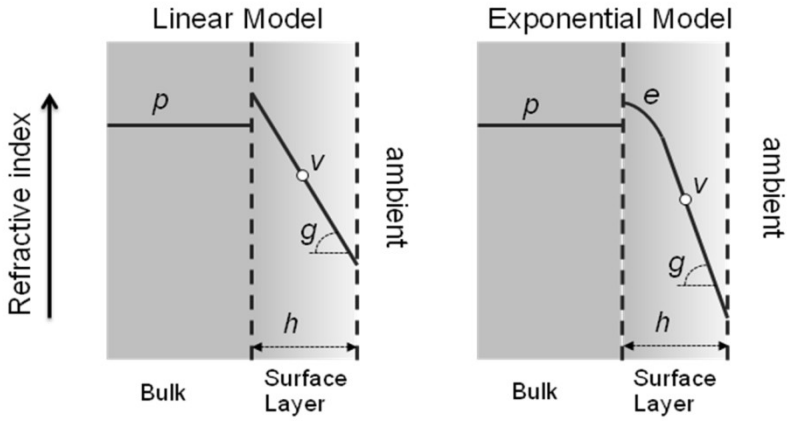

Figure 8.6 Schematic representation of the ellipsometric model for AKP materials

with graded porosity. The corresponding model is schematically presented in Figure 8.6 and involves the use of the Bruggeman EMA for mixing the optical constants of two components. The first component is dense alumina, represented by a fit of the Cauchy equation to optical dispersion data of corundum - Al_2O_3 taken from literature[28]. The calculated parameters are: A = 1.751, $B = 6.32 \cdot 10^{-3}$, $C = 1.0152 \cdot 10^{-5}$ and produce the value of refractive index of n_{Al2O3} = 1.766 at 632.8 nm. The other component is void, representing the porosity of the porous alumina structure, with n_{void} = 1.000 over the whole wavelength range.

The optical model comprises two materials distributed over two distinct optical layers. The bottom layer, Bulk, consists of porous alumina with a constant void fraction p. This void fraction is used as a fitting parameter and the value obtained from the fit is expected to agree with the results of mercury porosimetry measurements (~40%).

The top layer, Surface Layer, consists of porous alumina with decreasing void fraction, going from the interface with the bottom layer towards the outer surface (the interface with the ambient). The thickness of the layer (h) is considered a fitting parameter in the optical model. For each position in the layer, the local void fraction can be transformed into the refractive index using the Bruggeman EMA. For this, the optical model requires an expression for the spatial variation in void fraction. In this study two expressions are proposed. The first expression considers the void fraction to be a linear function of the depth (Linear Model). This expression contains two adjustable fit parameters: the gradient in void fraction g, and the void fraction in the middle of the film v. The second expression considers the refractive index to be an exponential function of the depth (Exponential Model). This expression is expected to be able to account for the curvature of the density profile closer to the support, visible between 250 nm and 400 nm in Figure 8.3. In the Exponential Model, in addition to g and v the exponent e is an adjustable fitting parameter. Importantly, the values of refractive indices corresponding to porosity of the surface layer at the bulk interface are not coupled to those related to the porosity of the bulk support. This is done in order to test whether the model is able to reproduce the index profile in a physically consistent way (i.e. more or less continuous index profile) without introducing any initial restrictions.

The void profiles obtained from the ellipsometry analysis should correspond with the cumulative height distributions from AFM analysis (Figure 8.3). Bruggeman EMA is therefore used to transform the mass density profile obtained from AFM directly into the profile of refractive index. The bulk value of support refractive index is calculated based on the known refractive index and density of dense alpha alumina which are n_{Al2O3} = 1.766 at 632.8 nm and ρ_{Al2O3} = 4.0 g cm^{-3} respectively. The porosity of the samples is taken from mercury porosimetry measurements and indicated in Table 8.2. The AFM reference profile prepared in this way is thus completely independent from the ellipsometric measurements.

Representative fit results for Ψ in the wavelength range 450 - 1000 nm and 5 angles of incidence are shown in Figure 8.7, for both the Linear Model and the Exponential Model. Visual inspection of the spectra suggests a proper fit for both models, as is confirmed by the low MSE (~7) obtained with both models. The same is also true for the Δ parameter that is not shown for the sake of clarity. The fit quality decreases at lower wavelengths, especially for smaller angles of incidence. This is probably an effect of more pronounced scattering.

Table 8.2 Model fitting results for AKP-15, AKP-30 and AKP-50 flat disc samples

Model	Sample	Range [nm]	Thickn. of top layer, *h* [nm]	Mean Void fraction in the top layer, *v* [%]	Gradient in the top layer, *g* [%]	Exp., *e* [-]	Porosity of the support, *p* [%]	Porosity of the support from Hg porosi-metry [%]	Average pore diameter [nm]
Linear	AKP 50	525 – 1700 MSE = 5	198.9 ±0.4	56.0±0.06	71.6±0.1	-	39.7±0.1	41.9	78
	AKP 30	560 – 1700 MSE = 5	212.6±1	49.8±0.1	75.7±0.4	-	33.8±0.1	35.6	74
	AKP 15	1200 – 1700 MSE = 16	307±15	56.2±0.7	23.3±5.5	-	41.5±0.9	42.4	130.6
Exponential	AKP 50	550 – 1700 MSE = 5.2	318.6±3.7	76.1±0.1	104.1±0.3	2.01±0.04	37.0±0.2	41.9	78
	AKP 30	600 – 1700 MSE = 5.2	370.2±2.8	75.7±0.04	119.4±0.4	2.50±0.04	31.0±0.2	35.6	74
	AKP 15	1200 – 1700 MSE = 14.8	296±11	78±11	56±19	13.1±1.8	42.0±0.8	42.4	130.6

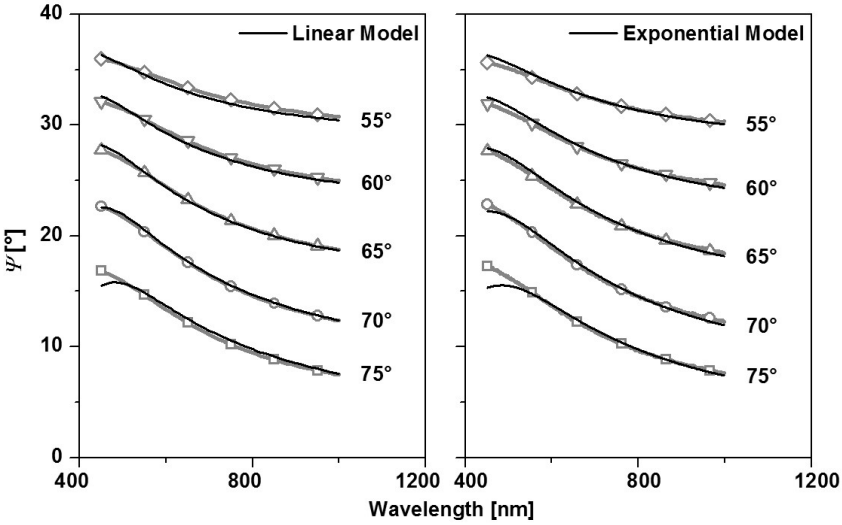

Figure 8.7 Measured and fit generated values of Ψ for AKP-50 sample over the wavelength range 450 nm – 1000 nm for angles of incidence of 55°, 60°, 65°, 70°, 75°. Both Linear and Exponential models are presented. Symbols are guides for the eyes.

To reduce the negative effects of scattering and to concurrently improve reliability of the fit, smaller wavelengths were omitted in the fitting procedure. The lower limit of the wavelength range is determined from a maximum value allowed for the MSE. The criterion in case of AKP-30 and AKP-50 was an MSE lower than an arbitrary value of about 5, for simultaneous fit for all angles of incidence. This value indicates a very good fit quality considering the simultaneous fit to 5 sets of data. Fit results for all investigated materials using both Linear and Exponential models, and the wavelength range used for the fit are collected in Table 8.2. In the case of AKP-15 the wavelength range was confined to the NIR range, due to large experimental uncertainties caused by low signal intensity and scattering effects in the UV and visible range. For AKP-15, even in the IR range the MSE obtained is still high (MSE = 16) and the models are considered poorly applicable.

In Figure 8.8 the generated refractive index profiles for the Linear Model and Exponential Model are compared with the AFM derived refractive index profile, for an AKP-50 support. The refractive index profile predicted by both models is in good agreement with the profile obtained with AFM. For both models the refractive index of Bulk corresponds to porosity (p) comparable with that obtained via Mercury Intrusion. The thickness of the graded layer (Surface Layer) obtained from the optical models (h) and the AFM data are in good agreement. The refractive index at the interface between the two layers is more or less continuous,

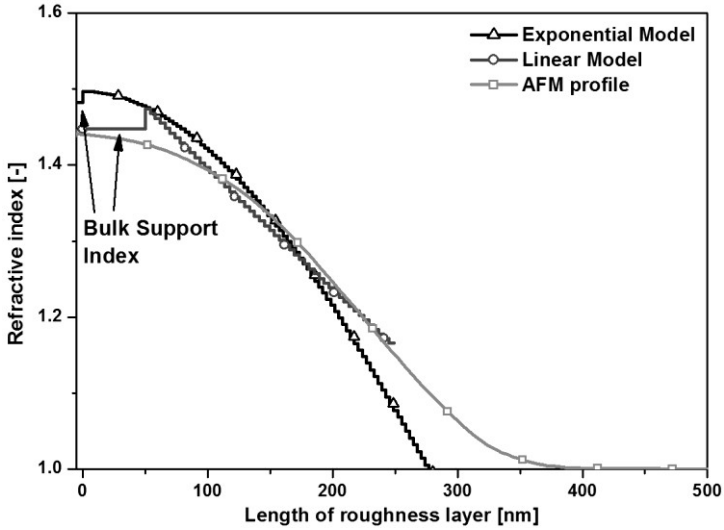

Figure 8.8 Generated refractive index profile compared with the void - alpha alumina profile obtained from the integrated histogram AFM analysis; symbols are guides for the eyes

and the average value (*v*) and slope (*g*)/shape (*e*) of the refractive index is similar to that derived from AFM. It is important to mention that all fit parameters are fitted simultaneously, with no restrictions imposed on their values. The physically realistic values that are obtained indicate that the models are reliable, robust and stable. Comparable conclusions hold for AKP-30.

The thickness of Surface Layer obtained from the Linear Model is smaller as compared to the Exponential Model. It can be rationalized by the consideration that the Linear Model tends to represent better the linear part of the AFM profile, which is located in the middle of Surface Layer. The curvature of the density profile in between the Bulk and the linear part of the AFM profile cannot be captured adequately by the Linear Model. Instead this non-linear region in the density profile is considered part of Bulk, resulting in a lower value for the thickness *h*.

The Exponential Model estimates a slightly larger value for the thickness *h*, and generates a refractive index smaller than 1 at the ambient interface. This model tends to match the shape of the non-linear variation in density close to Bulk, and at the same time tends to match the linear shape in the region closer to sample surface. In this way, the Exponential Model includes this non-linear density variation in Surface Layer, whereas this region is considered part of Bulk in the Linear Model. Consequently, the Exponential Model predicts a larger overall thickness of the Surface Layer as compared to the Linear Model. Because only a single parameter *e* is available, the Exponential model is forced to consider a linear variation of refractive index at the interface with the ambient. This is physically

unrealistic and results in the non-physical value of the refractive index at the ambient interface. Additionally, refractive index overestimation at the Bulk interface is produced by the Exponential Model. Since the MSE values obtained for both models in a similar wavelength range are very close together ($MSE_{LinearModel}$ = 5.0 and $MSE_{ExponentialModel}$ = 5.2) it is difficult to discern which one is more appropriate.

Overall, it can be concluded that the most consistent and robust results are obtained in the case of AKP-30 and AKP-50, for both types of models. The wavelength range of the fit with an MSE of about 5 is the largest in the case of AKP-50.

8.4.2.2. PSU layer deposited on *α*-alumina support – preliminary model

The models can be extended to account for composite membrane geometry: a thin dense film on top of the support with surface roughness. We have selected AKP-50 as support, given conclusions from the AFM and ellipsometry characterization of the three support types investigated, and polysulfone as material for the dense thin film, due to the wide application of this polymer in the membrane science and technology. AKP-50 was chosen over AKP-30 due to its best-fit quality, widest applicable wavelength range, and higher reflected light intensity. For AKP-15 the combination of high MSE, much narrower applicable wavelength range (only NIR), lower intensity (Figure 8.4) and moderate agreement with the AFM profile would make the analysis of a composite sample much more difficult and less relevant for the intended application. The approach is not limited to polysulfone; for other polymers sample preparation, post treatment, and modeling can be similar, provided that the polymer can dewet from a glass slide during immersion in solvent. That is because most typical high *T*g polymers have their refractive indices in the range between ~1.55 – 1.65 which is close to that of the polymer applied in this study (1.625).

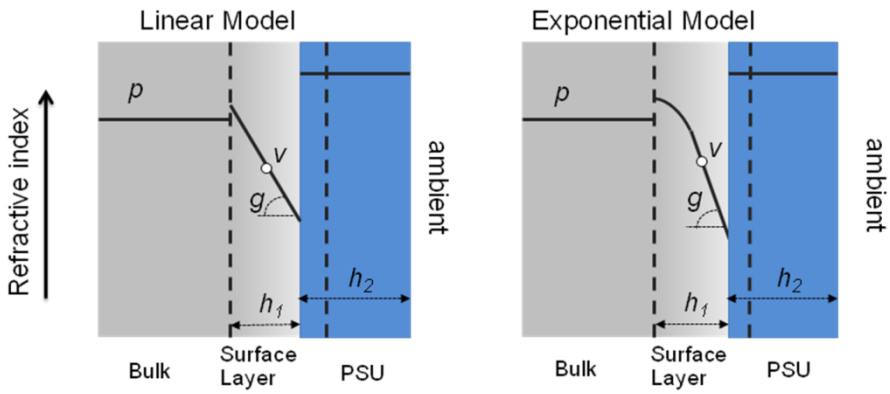

Figure 8.9 Schematic of the model for thin PSU layer deposited on AKP-50

The optical model for the alumina support with thin polymer layer comprises three distinct layers, as shown schematically in Figure 8.9. In this model, referred to as Multilayer Model, essentially the two-component geometry of the AKP-50 support is extended with an additional PSU layer. This layer accommodates a thin region in which the polymer is intruding the porous alumina. This intrusion layer comprises predominantly PSU, a small fraction of dense alumina and presumably a very small fraction of void. The difference in refractive indices of PSU and dense alumina is not very large (n_{PSU} = 1.625 and n_{Al2O3} = 1.766; both with typical Cauchy dispersion and negligible extinction coefficients in the analyzed wavelength range). Assuming an alumina volume fraction of 15% in the intruded region, the index of the intrusion layer can be calculated to be approximately n_{Intr} = 1.646. Considering that the value is very close to the index of pure PSU and that the intrusion layer is estimated to be an order of magnitude thinner than the total thickness of the deposited film, the refractive index of this intrusion region is assumed identical to that of pure PSU. This assumption avoids the introduction of a fourth layer in the optical model, which would significantly complicate data analysis. The optical dispersion of the PSU Cauchy layer is taken from the ellipsometry results for PSU layer deposited on glass. For the AKP-50 support, the Linear Model or Exponential model can be used to describe the variation in void fraction. In case of the Exponential Model the curvature (exponent fit parameter, e) was first determined from bare AKP-50 and then held fixed. Also the void fraction of the bulk alpha alumina substrate (p) is determined from bare AKP-50 and held fixed. These assumptions are considered viable and substantially decrease the amount of fit parameters in the Multilayer Model for the deposited sample.

The remaining fit parameters in the Multilayer Model are the thickness of the PSU layer (comprising the intrusion region) h_2, thickness of the remaining roughness layer h_1, and the average value v and gradient g of the void fraction of the remaining roughness layer. For both models the refractive index profiles are presented in Figure 8.10, together with the profile obtained from AFM for reference. Figure 8.11 shows the fit to Ψ and Δ parameters measured for the coated sample. The model fitting is performed in the wavelength range of 450 – 1000 nm and with angle of incidence of 70°.

The model fitting results are also presented in Table 3. For both models the MSE value is relatively high (Exponential: MSE = 33, Linear: MSE = 35), however, the calculated thickness of the deposited PSU layer agrees excellently with the value obtained for the film before floating from a glass support. The high MSE is probably due to the complexity of the models and limited validity of the assumptions made. In particular, the intrusion layer may in fact comprise PSU, alumina, and remaining void and the assuming identical refractive index for the intrusion region and PSU contentious. Even though, the Exponential Model seems to represent the curved index AFM profile very well and remains consistent with

respect to the index profile of a bare AKP-50 as shown in Figure 8.10a. Based on this model the thickness of the intrusion region is estimated at about 90 nm.

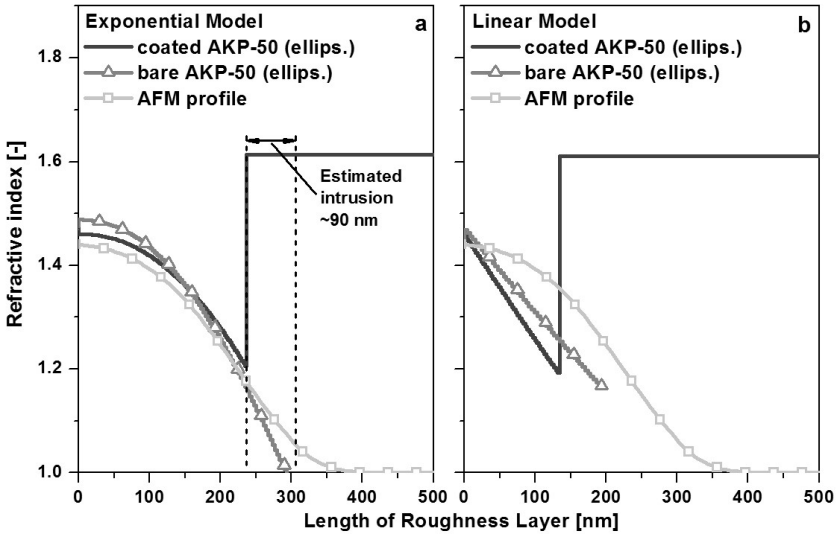

Figure 8.10 Optical index profile for PSU film deposited on AKP-50 compared with bare AKP-50 (obtained previously) and AFM profiles for Exponential and Linear profile based models; symbols are guides for the eyes

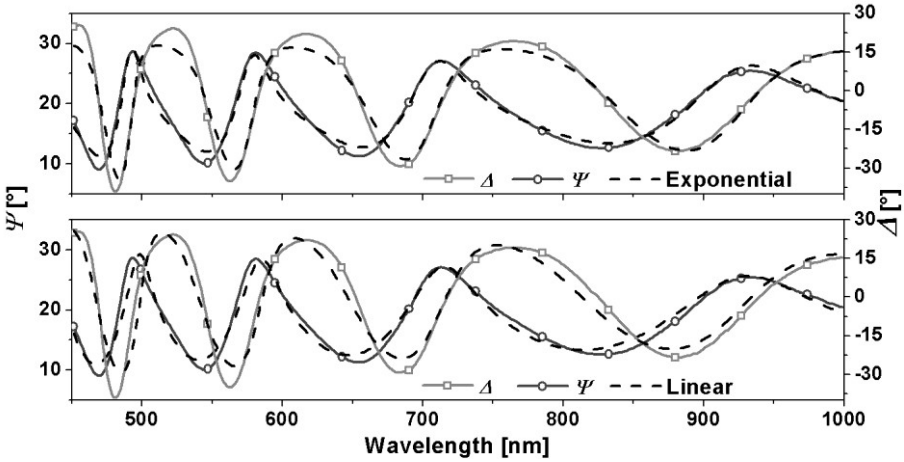

Figure 8.11 Ψ and Δ fit results of the multilayer models for ~1100 nm PSU layer deposited on AKP-50 based on the exponential model

Table 3 Model fitting results for the AKP 50 coated with PSU layer at 70° angle of incidence and wavelength range of 450 – 1000 nm; for the sample coated with PSU layer exponent (e) and bulk porosity (p) were held the same as for the uncoated sample

	Uncoated AKP 50 **MSE Linear = 1.2** **MSE Exponential = 2.7**					**AKP 50 coated with PSU** **MSE Linear = 35** **MSE Exponential = 33**			
Model	**Thickn. of Surface Layer, *h* [nm]**	**Mean Void fraction in Surface Layer, *v* [%]**	**Gradient in the Surface Layer, *g* [%]**	**Exponent, *e* [-]**	**Porosity of the support, *p* [%]**	**Thickness of PSU Layer, h_2 [nm]**	**Thickness of Surface Layer, h_1 [nm]**	**Mean Void fraction in Surface Layer, *v* [%]**	**Gradient in the Surface Layer, *g* [%]**
Linear	193.1±1.8	57.0±0.2	62.9±0.7	-	39.8±0.1	1110.7±1	134±22	55±25	54±11
Exponential	336.6±2	76.5±0.1	104.3±1.1	2.16±0.04	38.0±0.6	1109.3±1	181±49	59±3	63±8

In the case of the Linear Model the refractive index profile shows large deviations from the AFM data and from the modeling results for the bare support. In particular, the slope of the void fraction is too high. Moreover, for the Linear Model the uncertainties in the fitting parameters are relatively large. The oscillating pattern of Ψ with wavelength, related to the PSU layer on top of the sample, is captured much less accurately in comparison to the Exponential Model (Figure 8.11). The reason for the Linear Model to be less appropriate as compared to the Exponential Model is the loss of symmetry in the void profile upon addition of the PSU layer. For a bare support the curvature in void profile at both interfaces is comparable, allowing the Linear Model to capture the linear variation in void fraction in the middle of the layer. When the PSU layer is added, the curvature in the void space at the interface with the ambient is replaced by an intrusion region, which is accommodated in the PSU layer. The Linear Model is in this case forced to mimic the curvature at the interface with Bulk together with the linear profile adjacent to it. In contrast, the Exponential Model inherently attempts to capture the

curvature at the interface with the Bulk. In the case of a bare support, the Exponential model fails to describe the curvature in void fraction at the interface with the ambient, which in the Multilayer Model is replaced by the intrusion region. Consequently, the Exponential Model appears more appropriate for a support with thin polymer film, as compared to the Linear Model.

It has to be emphasized that, despite the high MSE, the Exponential Model is intended primarily to observe changes in thickness and refractive index of the thin polymer layer, under permeation and sorption experiments. Thickness changes are strongly related to the shifts in the oscillating pattern observed both in Ψ and Δ measured data, as shown in Figure 8.11. It is plausible that the sensitivity to thickness changes is sufficient to obtain meaningful thickness variation data (swelling) in realistic membrane application conditions.

8.5. Conclusions

Variable angle spectroscopic ellipsometry is successfully applied to model polished porous alumina flat discs. Two optical models are designed that consider the surface roughness of these supports as distinct layer, with a porosity profile. The first model considers the porosity profile to be linear; the second model assumes an exponential profile. Density profiles generated by both models are physically realistic and correspond well with atomic force microscopy and mercury porosimetry. The models are extended to accommodate a thin polysulfone film placed on top of the alumina support, representative for a composite membrane. The supported polysulfone layer can be appropriately fit using the exponential model. This indicates that the approach can be used to obtain meaningful information on the *in-situ* swelling behavior of thin dense supported membranes.

8.6. Acknowledgments

The authors would like to acknowledge Michel Klein Gunnewiek for the help with atomic force microscopy analysis and Hammad Qureshi for performing the mercury porosimetry measurements.

8.7. References

[1] Bertrand, P., et al., Ultrathin polymer coatings by complexation of polyelectrolytes at interfaces: suitable materials, structure and properties. Macromolecular Rapid Communications, 2000. **21**(7): p. 319-348.

[2] Kawakami, H., M. Mikawa, and S. Nagaoka, Gas Transport Properties of Asymmetric Polyimide Membrane with an Ultrathin Surface Skin Layer. Macromolecules, 1998. **31**(19): p. 6636-6638.

[3] Wessling, M., M. Lidon Lopez, and H. Strathmann, Accelerated plasticization of thin-film composite membranes used in gas separation. Separation and Purification Technology, 2001. **24**(1-2): p. 223-233.

[4] Ram, M.K., et al., CO gas sensing from ultrathin nano-composite conducting polymer film. Sensors and Actuators B: Chemical, 2005. **106**(2): p. 750-757.

[5] Opila, R.L. and J. Eng Jr, Thin films and interfaces in microelectronics: composition and chemistry as function of depth. Progress in Surface Science, 2002. **69**(4-6): p. 125-163.

[6] Kamiya, Y., et al., CO2 Sorption and Dilation of Poly(methyl methacrylate). Macromolecules, 1998. **31**(2): p. 472-478.

[7] Wessling, M., et al., Plasticization of gas separation membranes. Gas Separation & Purification, 1991. **5**(4): p. 222-228.

[8] Simons, K., et al., CO2 sorption and transport behavior of ODPA-based polyetherimide polymer films. Polymer, 2010. **51**(17): p. 3907-3917.

[9] Wormeester, H., et al., CO2 sorption of a ceramic separation membrane. Thin Solid Films, 2004. **455-456**: p. 747-751.

[10] Mattsson, J., et al., Quantifying glass transition behavior in ultrathin free-standing polymer films. Physical Review E, 2000. **62**(4): p. 5187.

[11] Ilton, M., D. Qi, and J.A. Forrest, Using Nanoparticle Embedding to Probe Surface Rheology and the Length Scale of Surface Mobility in Glassy Polymers. Macromolecules, 2009. **42**(18): p. 6851-6854.

[12] Kamiya, Y., K. Mizoguchi, and Y. Naito, A dielectric relaxation study of plasticization of poly(ethyl methacrylate) by carbon dioxide. Journal of Polymer Science Part B: Polymer Physics, 1990. **28**(11): p. 1955-1964.

[13] Mapesa, E.U., et al., Glassy dynamics in nanometer thin layers of polystyrene. European Physical Journal: Special Topics, 2010. **189**(1): p. 173-180.

[14] Stafford, C.M., et al., Combinatorial and high-throughput measurements of the modulus of thin polymer films. Review of Scientific Instruments, 2005. **76**(6).

[15] Soles, C.L., et al., Comparative Specular X-ray Reflectivity, Positron Annihilation Lifetime Spectroscopy, and Incoherent Neutron Scattering Measurements of the Dynamics in Thin Polycarbonate Films. Macromolecules, 2004. **37**(8): p. 2890-2900.

[16] Koga, T. and et al., X-ray Photon Correlation Spectroscopy Study on Dynamics of the Free Surface in Entangled Polystyrene Melt Films. Journal of Physics: Conference Series, 2011. **272**(1): p. 012003.

[17] Benes, N.E., et al., CO2 sorption of a thin silica layer determined by spectroscopic ellipsometry. Aiche Journal, 2001. **47**(5): p. 1212-1218.

[18] Sirard, S.M., P.F. Green, and K.P. Johnston, Spectroscopic Ellipsometry Investigation of the Swelling of Poly(Dimethylsiloxane) Thin Films with High Pressure Carbon Dioxide. The Journal of Physical Chemistry B, 2001. **105**(4): p. 766-772.

[19] Madami, M., et al., In situ Brillouin scattering study of the thickness dependence of magnetic anisotropy in uncovered and Cu-covered Fe/GaAs(100) ultrathin films. Physical Review B, 2004. **69**(14): p. 144408.

[20] Yang, J., et al., Analysis of polystyrene surface properties on thin film bonding under carbon dioxide pressure using nanoparticle embedding technique. Journal of Polymer Science Part B: Polymer Physics, 2009. **47**(16): p. 1535-1542.

[21] Pham, J.Q., K.P. Johnston, and P.F. Green, Retrograde Vitrification in CO2/Polystyrene Thin Films. The Journal of Physical Chemistry B, 2004. **108**(11): p. 3457-3461.

[22] Fujiwara, H. and I. Wiley. Spectroscopic ellipsometry principles and applications. 2007; Available from: http://dx.doi.org/10.1002/9780470060193.

[23] Tompkins, H.G. and E.A. Irene. Handbook of ellipsometry. 2005; Available from: http://www.knovel.com/knovel2/Toc.jsp?BookID=1175.

[24] Dong, G., H. Li, and V. Chen, Plasticization mechanisms and effects of thermal annealing of Matrimid hollow fiber membranes for CO2 removal. Journal of Membrane Science, 2011. **369**(1-2): p. 206-220.

[25] Visser, T., G.H. Koops, and M. Wessling, On the subtle balance between competitive sorption and plasticization effects in asymmetric hollow fiber gas separation membranes. Journal of Membrane Science, 2005. **252**(1-2): p. 265-277.

[26] Nijmeijer, A., Hydrogen-selective silica membranes for use in membrane steam reforming, 1999: Enschede. p. 136.

[27] Nerbo, I.S., et al., Characterization of inclined GaSb nanopillars by Mueller matrix ellipsometry. Journal of Applied Physics, 2010. **108**(1): p. 014307.

[28] Lichtenstein, T., Handbook of Thin Film Materials, Academic Press. 1972.

Chapter 9

n-Hexane induced swelling of thin PDMS films under non-equilibrium nanofiltration permeation conditions, resolved by spectroscopic ellipsometry

This chapter has been adapted from:

Ogieglo W., van der Werf H., Tempelman K., Wormeester H., Wessling M., Nijmeijer A., Benes N.E., Journal of Membrane Science 2013;437(0):313-323.
Copyright 2013 Elsevier

Abstract

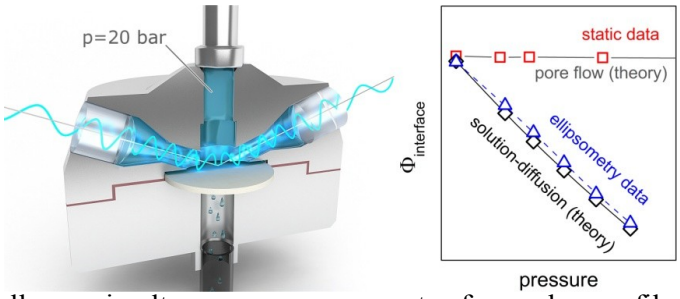

A nondestructive technique is presented for *in-situ* analysis of solvent induced membrane swelling. The technique is based on spectroscopic ellipsometry (SE) and allows simultaneous measurement of membrane film thickness and solvent sorption. The attainable experimental conditions are only limited by the test cell (≤ 200 °C, ≤ 200 bar) and by far exceed those encountered in typical solvent resistant nanofiltration (SRNF) applications. The influence of cross-linker concentration on swelling of thin films and bulk samples of poly(dimethyl siloxane) (PDMS) is resolved and interaction parameters according to Flory-Huggins and Flory-Rehner theories are calculated. It is found that due to confinement on the support for the thin supported films a correction for elastic deformation of the network is necessary. In the pressurized swollen film the thickness and refractive index are found to be independent of pressure in the range of 1 – 100 bar suggesting that the molar volumes of the penetrant in the liquid and sorbed phases are not significantly different. When a pressure difference over the membrane is applied and the solvent is allowed to permeate, a progressing reduction in thickness of the membrane is observed with increasing upstream pressure. The derived concentrations of n-hexane at the interface between thin film and support, at the permeate side, are in excellent agreement with values calculated using the Solution-Diffusion model. This implies that *in-situ* spectroscopic ellipsometry allows quantification of the contribution of Solution-Diffusion to mixed mode transport, for instance occurring simultaneously with Pore-Flow and transport through defects, in composite membranes.

9.1. Introduction

Solvent resistant nanofiltration (SRNF) is a relatively new and growing field [1, 2]. Further advancements in SRNF will benefit from a thorough understanding of the relation between membrane properties, solvent properties, and performance. In particular, solvent sorption and related effects such as membrane swelling are of great consequence for flux and retention behavior [3].

There are several techniques available to measure solvent induced membrane swelling. In general, these techniques determine either the change in geometry of a membrane (swelling), or the extent of solvent uptake of a membrane (sorption). Swelling analysis is commonly done by visually observing changes in the dimensions of a sample (dilation) upon exposure to a solvent. One of the first studies using this approach was aimed at solvent polymer interactions under high pressure [4], and this technique is still used at present [5, 6]. Alternative methods to measure dilation were presented by Tarleton et al., who used a probe to directly measure the lateral swelling of a thin layer [7] and applied this approach to SRNF membranes, and Böhning et al., who used a capacitive distance measurement to investigate the volumetric behavior of glassy polymers under gas pressure [8]. Sorption data can be obtained using several techniques, including the use of a quartz crystal microbalance [6, 9], gravimetric methods [1, 10, 11] or barometric methods [5, 12, 13]. Often a combination of the above methods is used to obtain both the sorption and swelling data. These include interferometric measurements with an optical thickness meter [14, 15], ATR-IR measurements [16-19] and spectroscopic ellipsometry (SE) [9, 20-22]. Of the above techniques, SE has the potential to measure *in-situ* sorption and swelling under true permeation conditions.

In this chapter we investigate the use of SE to quantify the effects of cross-linking and pressure on n-hexane induced swelling of thin poly(dimethyl siloxane) (PDMS) layers. PDMS is chosen as a model system because its thermodynamic behavior is well documented. Furthermore, it is used in a wide variety of application areas, ranging from sealant elastomer to dense membranes for volatile organic component extraction [23]. Several studies have been presented in which PDMS is used for SRNF [10, 24, 25]. Behavior of n-hexane swollen thin supported film of PDMS under permeation and static conditions is analyzed in order to gain insights into the solvent transport behavior through SRNF membranes.

9.2. Theory

9.2.1. Spectroscopic ellipsometry – basic principles

Spectroscopic ellipsometry is a non-invasive and non-destructive technique that can be used to determine the thickness and optical properties of thin supported layers [26, 27]. The technique relies on the measurement of the change in the

polarization state of light of specular reflected light at oblique incidence. This polarization change reflects the different reflctivitities of *p* (in plane) and *s* (out of plane) polarized light. The ratio of *p*- and *s*- reflectivities is commonly expressed in terms of ellipsometric parameters Ψ and Δ:

$$\rho = \frac{r_p}{r_s} = tan(\Psi) \cdot e^{i\Delta} \quad (9.1)$$

The first parameter, Ψ, is related to the amplitude ratio of the *p*- and *s*- waves. The second parameter, Δ, is related to the phase difference between *p*- and *s*- polarized waves upon reflection from a sample. Typically, Ψ and Δ parameters are plotted as a function of wavelength and are named a spectroscopic ellipsometry spectrum. The very high precision of ellipsometric measurements stems from the high accuracy with which polarization angles can be measured. Furthermore, a large number of Ψ and Δ pairs, as a function of both wavelength and incidence angle provides a large number of data points that can be used to determine a few physical parameters in an optical model that reflects the measured sample. Because ellipsometry measures the changes in the state of polarization upon reflection as a ratio of reflectivities, the technique is less sensitive to the absolute intensity of the light [28]. This renders the technique especially suitable for *in-situ* applications, in which the experimental ambient, cell windows or sample features might reduce the overall intensity of the reflected light beam.

The variations in Ψ and Δ parameters that occur during light reflection are described by well-known Fresnell relations [26]. In general, the direct interpretation of the ellipsometric parameters is difficult and an optical model needs to be constructed. Usually, a multilayer optical model is used in which each of the optical layers is described by its thickness, *h*, and a complex refractive index, $N=n+ik$. For transparent layers ($k = 0$) often a Cauchy-type optical dispersion is used given by a formula:

$$n(\lambda) = A + \frac{B}{\lambda^2} + \frac{C}{\lambda^4} \quad (9.2)$$

Here *A*, *B* and *C* are fit parameters. During the fitting procedure the model generated Ψ and Δ are numerically fitted to the measured Ψ and Δ over the entire wavelength spectrum. The fit is considered to be good, meaning that a high confidence in the determined parameters describing a sample is obtained, when the model generated data lies on top of the measured data. Goodness of fit is conveniently expressed as Root Mean Squared Error (RMSE, more commonly depicted as MSE) which expresses the deviation between the measured and model produced data. For a single thin film (<1 μm) on a substrate a good fit is characterized low MSE (~1). For more complex optical models and relatively thick films (1-2 μm). Higher values of MSE (~10-20) are considered acceptable. For further details of spectroscopic ellipsometry the interested reader is referred to one of the textbooks [26, 27, 29].

The dispersion of a mixture of materials with known refractive indices can be approximated using an effective medium approximation (EMA) theory. A commonly used EMA expression for concentrated mixtures was derived by Bruggeman [30]. For a binary mixture of n-hexane and PDMS the Bruggeman expression is:

$$\phi_H^{EMA} \cdot \frac{n_H^2 - n_{SP}^2}{n_H^2 + 2n_{SP}^2} + (1 - \phi_H^{EMA}) \cdot \frac{n_{DP}^2 - n_{SP}^2}{n_{DP}^2 + 2n_{SP}^2} = 0 \quad (9.3)$$

In the formula the ϕ_H^{EMA} is the n-hexane volume fraction, n_H is the n-hexane refractive index, n_{SP} is the refractive index of the swollen polymer and n_{DP} is the refractive index of the dry polymer. For a swollen polymer this expression allows calculation of volume fraction of the solvent from experimentally determined refractive index of the mixture, n_{SP}. If volume additivity in the n-hexane – PDMS system is assumed, the volume fraction of n-hexane can also be calculated from the increase of thickness (dilation) of the swollen film, $\phi_H^{dil.}$:

$$\phi_H^{dil.} = 1 - \frac{h_{DP}}{h_{SP}} \quad (9.4)$$

Here h_{SP}, h_{DP} are the dry and swollen film thicknesses respectively. In equation 9.4 the polymer is assumed to swell only in the direction perpendicular to the substrate due to its confinement on the support.

An important requirement for spectroscopic ellipsometry is that the supporting layer beneath the film of interest provides a well-defined optical interface. This is often easily accomplished for dense substrates, such as silicon wafers or glass slides. However, porous substrates with pore dimension on the order of >30% of probing light wavelength are known to severely hinder the analysis procedure due to unwanted scattering effects [26]. This largely limits the applicability of spectroscopic ellipsometry for asymmetric or composite membranes, where the support pore sizes are often in the strongly scattering region. Additionally, the polymer pore intrusion during membrane preparation process further decreases sharpness of the polymer – support interface. Recently, we have shown that utilization of a well-defined polished α-alumina support together with floating of the polymer layer (instead of dip- or spin-coating) may help to produce a better defined optical interface between the dense skin and the support [31]. Such preparation of the membrane facilitates the spectroscopic ellipsometry analysis of the system.

9.2.2. Optical models

Two different optical models have been used in this work. The first model represents the PDMS film as a layer deposited on a glass slide (Figure 9.1a). The optical dispersion and thickness of the PDMS layer are fitting parameters and the dispersion of the substrate is determined from fitting the data for bare substrate to

Cauchy dispersion. The second model is related to the PDMS film deposited on a porous substrate with a graded roughness layer (Figure 9.1b). In this case the support is represented by a bulk porous α-alumina with certain porosity, p, which is represented as void fraction in dense corundum (α-Al_2O_3) calculated according to EMA with the known optical dispersion of dense α-Al_2O_3 [32]. The graded roughness layer is a surface layer of the substrate which properties are determined by the polishing procedure. It is represented as graded layer with density linearly decreasing from the bulk value at the bulk interface toward the PDMS film. The mean void fraction in the graded roughness layer, v, is higher than p. The gradient in density (or refractive index) is expressed by g and given in percentage difference between the index at the top and bottom of the layer normalized for mean layer index. The graded roughness layer thickness is denoted h_g. All of the parameters: p, v, g and h_g can be fitted to spectrum of a bare α-alumina support. Justification for the use of such representation of the porous α-alumina substrate, supported by detailed characterization by variable angle spectroscopic ellipsometry in combination with mercury porosimetry and atomic force microscopy, has recently been given elsewhere [31]. When the films are swollen in the presence of liquid n-hexane the ambient optical dispersion is taken into account in the modeling.

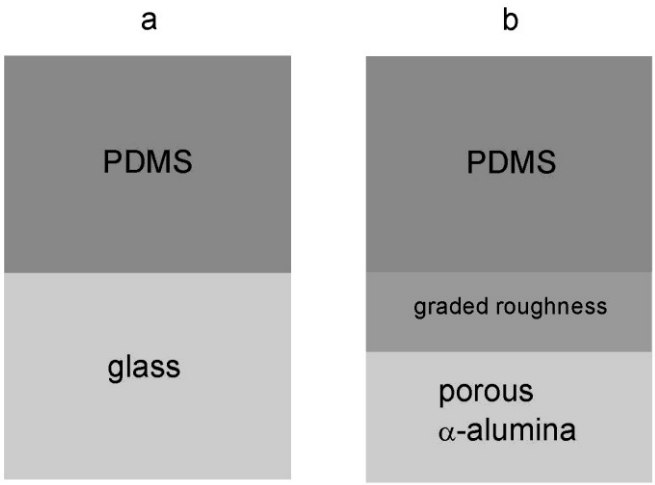

Figure 9.1 Schematics of optical models used to model PDMS thin films deposited on various supports: a) glass slide, b) porous α-alumina

9.2.3. n-Hexane sorption in PDMS

According to the Flory-Huggins theory the equilibrium volume fraction of n-hexane in PDMS, ϕ, is related to the activity of n-hexane (a) according to:

$$ln(a) = ln(\phi) + (1-\phi) + \chi(1-\phi)^2 \quad (9.5)$$

In this equation, χ is the interaction parameter for PDMS and n-hexane. This expression is derived from the change in the free energy resulting from mixing of the polymer and solvent (ΔG_{mix}). It does not take into account elastic contribution to the change in the free energy due to deformation of the polymer network. This elastic contribution can be accounted for by adding an additional term (Ω) on the right hand side of eq. 9.5, yielding the Flory-Rehner expression [33]. The change in elastic free energy depends on the dimensionality of deformation of the film. For a free-standing film expansion is identical in all directions, whereas for a thin film on a substrate swelling can only occur in the direction perpendicular to the substrate. The corresponding expressions for Ω are:

Free-standing film: $$\Omega = \left(1 - \frac{2M_c}{M}\right)\frac{V_H E}{3RT}\left(\frac{1}{\alpha} - \frac{1}{2\alpha^3}\right) \quad (9.6)$$

Thin supported film: $$\Omega = \left(1 - \frac{2M_c}{M}\right)\frac{V_H E}{3RT}\left(\alpha - \frac{1}{2\alpha}\right) \quad (9.7)$$

Here V_H is the molar volume of n-hexane, E is the elastic modulus of PDMS, M_c is the average molecular weight of the PDMS between the crosslinks, and M is the molecular weight of PDMS. The symbol α denotes the swelling factor of the polymer defined as:

$$\alpha \equiv \frac{\delta}{\delta_0} \quad (9.8)$$

The symbols δ and δ_0 denote the dimension of the swollen and dry film, respectively. For a thin supported film α can be simply calculated from thickness change upon swelling:

$$\alpha = \frac{h_{SP}}{h_{DP}} \quad (9.9)$$

Equation 9.9, together with equation 9.4, yields an expression for the volume fraction of the sorbed n-hexane using α:

$$\phi_H^{DIL} = 1 - \frac{1}{\alpha} \quad (9.10)$$

9.2.4. Models describing transport in SRNF membranes

Various models have been proposed for describing transport through SRNF membranes. A distinction can be made between models that consider the selective membrane layer as *non-porous* or *porous*. For non-porous materials transport is

commonly described by the Solution-Diffusion model; for porous materials descriptions the Pore-Flow model is considered more appropriate.

In the Solution-Diffusion model permeation through dense polymeric materials has been described as a combination of two processes: sorption/desorption and diffusion of the components [34]. In this model the entire polymer layer is considered to be at feed pressure and a pressure step occurs at the interface between the polymer layer and its support. For a rubbery polymer, such as PDMS, this is consistent with liquid-like behavior of the polymer. The transport of the solvent occurs down the activity gradient inside the film.

In Pore-Flow models transport is assumed to occur by viscous flow of a fluid through a porous structure. The permeating component forms a fluid inside a solid porous medium and they are considered two separate phases. It is also frequently assumed that for this mode of transport no significant change in swelling occurs. For a pure and incompressible solvent the concentration in the pores is constant, the main driving force in this case is the hydrostatic pressure gradient.

Pore-Flow models can be applied when the free volume elements (pores) of the membrane are relatively large and fixed (they do not fluctuate in position or volume). On the other hand, the Solution-Diffusion model is applicable to fluctuating free volume elements in a dense membrane that appear and disappear as a result of thermal motion of polymer chains. Generally, polymer membranes used in reverse osmosis, gas separation, and pervaporation, with pores smaller than 5 Å, are believed to be best described by Solution-Diffusion model. For ultra- and microfiltration the Pore-Flow model is considered more applicable [35].

For SRNF there is no full consensus which of the two models is most suitable. For transport of a pure solvent both models yield a relation between flux and pressure difference that contains the convoluted properties of the polymer and solvent. In this respect, it will be beneficial to directly monitor the film properties during permeation, rather than derive these from the flux and selectivity. Spectroscopic ellipsometry in principle allows such *in-situ* characterization.

9.3. Experimental part

9.3.1. Materials

PDMS (RTV 615 type) was obtained from GE Bayer Silicones (Germany) as a two-component system, consisting of a vinyl-terminated pre-polymer (RTV A) and a cross-linker containing several hydrosilane groups (RTV B). N-hexane p. a. and toluene p. a. was obtained from Merck (The Netherlands) and was used as received. Glass slides were cut in discs of 39 mm in diameter and 2 mm thickness. The backside was roughened mechanically to minimize back-side reflection in the ellipsometry measurement. The polished porous α-alumina (AKP-30) discs of 39 mm in diameter were purchased from Pervatech (The Netherlands).

9.3.2. Sample preparation

Thin PDMS films deposited on silicon wafers and glass slides were made by spin coating ~15 % (w/w) pre-polymer solutions containing the desired amount of cross-linker. The free-standing, thick PDMS films were prepared from 75% (w/w) PDMS/hexane solution, at room temperature, by mixing the pre-polymer and cross-linker. Samples were transported to a furnace and annealed at 80 °C under nitrogen flow for 16 hours to facilitate cross-linking. After annealing the samples were cooled and washed with n-hexane. The thickness of the prepared PDMS films ranged from about 0.8 to 1.5 μm.

Preparation of α-alumina supported PDMS films were done by a floating technique. First, a thin (~400 nm) polystyrene (PS) layer was deposited on a glass slide by spin-coating from a solution in toluene and subsequently annealed at 120 °C, which is 20 °C above T_g of the polymer, to remove residual solvent and relax post-spin coating stress. Afterwards, PDMS pre-polymer/cross-linker solution was spin coated from n-hexane on top of the PS coated glass substrate and the sample was annealed at 80 °C under nitrogen flow for 16 hours to cross-link the PDMS layer. The cooled sample was immersed in toluene to dissolve the PS layer and enabled the PDMS layer to float freely on the surface of the solvent. The floating film was "fished out" on top of the polished side of the porous α-alumina support and the sample was dried under nitrogen flow at 50 °C for 16 hours.

9.3.3. Measurement of the bulk sample *E* modulus and swelling

The elastic modulus of the bulk PDMS films, E, was determined by performing tensile tests on a Zwiek Z020 apparatus. For the swelling measurements, pre-weighed dry dense PDMS membranes were immersed in pure n-hexane until equilibrium swelling was reached. The swollen membranes were then weighed every 30 seconds for 3 minutes and the original weight increase was extrapolated from those. The dimensional changes of the samples were calculated using the (assumed constant) densities of PDMS and n-hexane. All the measurements were performed at room temperature (24 ± 3 °C).

9.3.4. *In-situ* high pressure spectroscopic ellipsometry

Spectroscopic ellipsometry measurements were conducted with an Alpha-SE® ellipsometer (J. A. Woollam Co. Inc.,). All measurements were done at a fixed angle of incidence (70°) in the wavelength range from 370 to 900 nm. Samples were placed in a home-built stainless steel cell (p_{max} = 200 bar, T_{max} = 200 °C) equipped with temperature and pressure control system depicted in Figure 9.2.

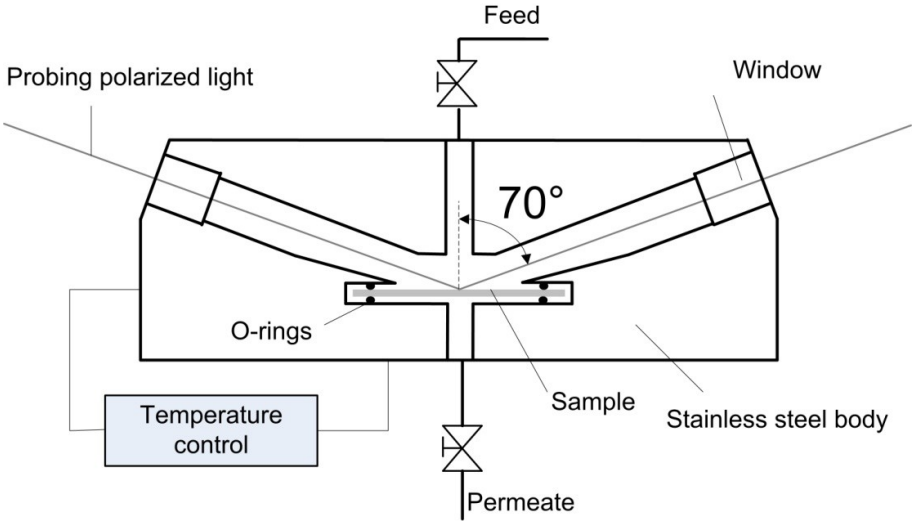

Figure 9.2 Schematic of the permeation cell used in the spectroscopic ellipsometry analysis of n-hexane induced swelling

Accurate pressure and flow determination was assured by a solvent resistant syringe pump (Teledyne ISCO, 500D). Light entered and exited the cell through 1 cm thick quartz windows positioned perpendicular to the light beam. The PDMS samples were exposed to either: vacuum, nitrogen gas with n-hexane vapor or liquid n-hexane. The vapor was introduced into the cell via an n-hexane saturated nitrogen stream in equilibrium with liquid n-hexane at temperature of ~1 °C lower than that of the cell. In this way, the activity of the n-hexane will be significantly lower than one. For measurements involving liquid n-hexane the cell was evacuated before filling with the liquid to guarantee complete filling of the cell. Pressure induced birefringence of the cell windows was taken into account via a high-pressure nitrogen calibration on a 25 nm SiO_2/Si wafer. This provides an appropriate Δ offset parameter that negates the pressure induced birefringence. Static high-pressure liquid n-hexane experiments were performed by pressurizing the sample in conditions of mechanical equilibrium with the same upstream and downstream pressures (no flow). Permeation experiments were performed by supplying the desired pressure on the upstream side of the membrane and allowing the flowing liquid to be collected in a vessel vented into the atmosphere.

The optical dispersion of n-hexane needed for the analysis of the optical spectra was taken from literature [36]. The optical dispersion of crystalline silicon and native oxide were taken from literature and were always fixed in the calculations [37]. The optical dispersion of each glass slide was measured before spin-coating of the PDMS layers and was fitted to the Cauchy dispersion (eq. 9.2). For glass as a substrate (Figure 9.1a) the wavelength range for the fit was 370 – 900 nm. For porous α-alumina (Figure 9.1b) the employed wavelength range was limited to 500

– 900 nm to reduce the influence of light scattering as a result of the roughness of the porous support on the optical measurement, which is especially manifest at shorter wavelengths [31]. All values reported for the refractive index, in this work, have been obtained at 632.8 nm.

Important note: the risks of using the flammable n-hexane liquid in combination with the use of high pressure were extensively assessed. A variety of safety measures were taken, including working in a fume hood, reducing volumes, and using equipment with a pressure rating (calculated and tested by the High Pressure Lab at the University of Twente) at least 1.43x the maximum operating pressure (European Pressure Equipment Directive) equipped with appropriate pressure safety valves and pressure relief valves.

9.4. Results and discussion

9.4.1. Thickness and refractive index of PDMS film as function of temperature

Figure 9.3 shows the influence of temperature on the Ψ oscillations measured for a PDMS film supported on a glass slide at different temperatures. Upon increase of temperature the oscillations in Ψ are seen to move towards longer wavelengths, Figure 9.3a and, at the same time, the oscillations amplitudes increase. Both findings can be explained by an increase of film thickness and a simultaneous decrease of the film refractive index. The results of the fit of the model to the measured data are shown in Figure 9.3b where heating (closed symbols) and cooling (open symbols) data are distinguished.

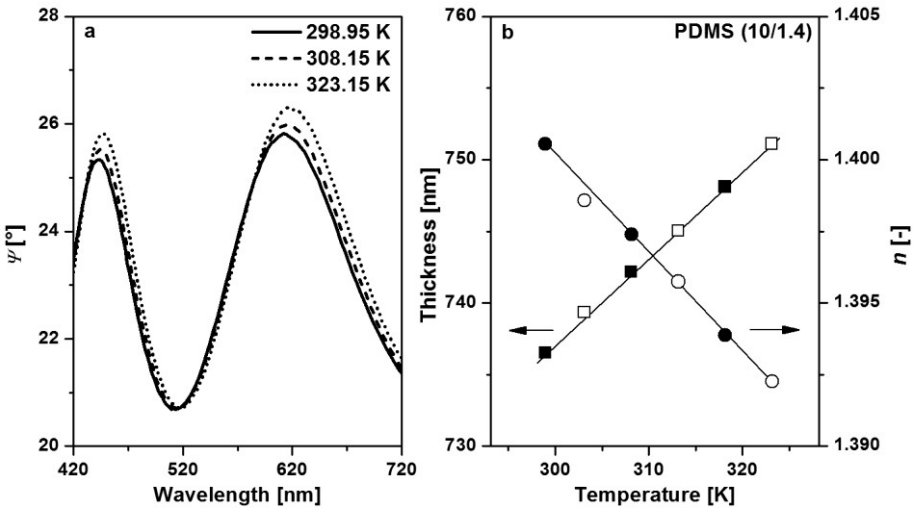

Figure 9.3 a) Ψ spectra for different temperatures and b) the derived values of PDMS film thickness and refractive index. The film was prepared with 10/1.4 pre-polymer/cross-linker ratio

The expansion with temperature is linear with no heating-cooling hysteresis, consistent with rubbery behavior of the studied polymer. The thickness and optical dispersion are considered independent fitting parameters, but they are physically interrelated and comply with the Clausius-Mossotti equation, proving consistency of the obtained results. The ability to accurately resolve small changes of Ψ and Δ, and translate these into the changes of polymer film properties, demonstrates high sensitivity and precision of the technique. The determined thermal expansion coefficient is $8.06 \cdot 10^{-4}$ °C^{-1} which is within 11% of the value of $9.07 \cdot 10^{-4}$ °C^{-1} reported for PDMS in the Polymer Handbook [38].

9.4.2. n-Hexane induced swelling of supported thin PDMS films

During *in-situ* swelling of PDMS films various changes in the ellipsometric spectra occur. To demonstrate this, Figure 9.4 depicts Ψ variations of PDMS films supported on glass (a) and porous α-alumina (b) for dry and wet films.

The symbols depict the measured data; for clarity only every sixth point of the recorded spectra are shown in the figure. Continuous lines represent the model-generated data. The dashed lines represent the, so-called, optical envelopes. These envelopes represent Ψ spectra generated by the optical model, based on *p*- and *s*-reflectivities of bare substrates in the respective ambients. The transparent PDMS film is observed as an oscillatory pattern, with the envelopes as a base, as a result of interference of light in the thin film. In Figure 9.4a it is seen that upon

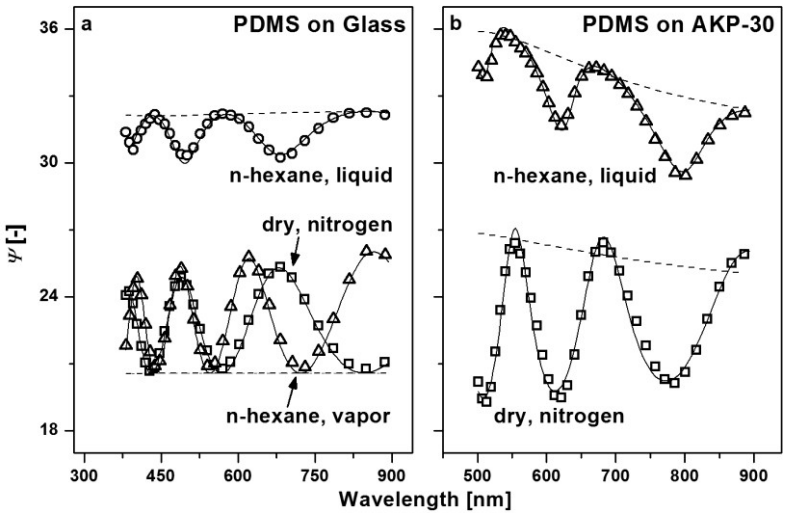

Figure 9.4 Ψ spectra for a glass slide (a) and porous α-alumina (b) supported PDMS film in dry, vapor, and wet conditions; the dotted lines are 'envelopes' generated by the optical model when the thickness of the PDMS layer is set equal to zero

introduction of n-hexane vapor, the periodicity in the oscillations in Ψ significantly reduces. This indicates swelling of the film. When the sample is immersed in liquid n-hexane the oscillations amplitude decrease and the substrate envelope inverts to follow the top maxima of Ψ oscillations instead of the bottom maxima. This behavior is related to changes of the Brewster and critical angles characteristic for the substrate when the vacuum ambient is replaced by liquid n-hexane. Fitting of the data, using the optical model from Figure 9.1a results in thicknesses and refractive indices of the PDMS presented in Table 9.1. Good fits, characterized with MSE values lower than 10 were obtained in all cases.

The data indicate that, as the film swells its refractive index reduces towards and almost reaches the value of pure liquid n-hexane (1.365). The swelling in n-hexane vapor saturated nitrogen flow is lower than in liquid n-hexane due to activity of the penetrant in gaseous state being lower than 1.

Figure 9.4b shows the Ψ oscillations obtained for a PDMS film deposited on porous α-alumina support with a floating technique. Such preparation procedure is found to practically eliminate the undesired polymer pore intrusion into the porosity of the substrate [31]. Upon introduction of n-hexane, changes in the Ψ oscillations and substrate envelopes occur. Unlike for the PDMS film deposited on glass, the envelopes mark the top maxima of Ψ oscillation both before and after introduction of n-hexane. This different behavior is related to the fact that the optical dispersion of the porous α-alumina substrate changes significantly when its pores are filled with liquid solvent. This influences the Brewster and critical angles of the system in a different way as compared to glass supported PDMS. The slight mismatch between the envelope and maxima of Ψ oscillations, especially for the dry sample, is related to the fact that the support representation in the case of porous α-alumina does not comprise only single optical interface (as for glass support). In this case the influence of a graded roughness layer [31] is visible. The envelope represents, in fact, a porous α-alumina/roughness layer and might be regarded as pseudo-envelope. The influence of the graded roughness layer is much less in the case of the swollen sample. The thickness of the roughness layer is small compared the thickness of the swollen film, which in turn is much thicker than the dry film. Consequently, the envelope generated for the swollen sample corresponds

Table 9.1 Fitting results for PDMS film supported on a glass slide with a use of an optical model from Figure 9.1a

	Thickness of PDMS film, h [nm]	Refractive index of PDMS film, n [-]	Swelling factor, α [-]
dry, nitrogen flow	804.3±0.8	1.414±0.0008	-
n-hexane, vapor	1039.9±0.7	1.406±0.0005	1.29
n-hexane, liquid	1700.9±4.5	1.378±0.004	2.11

Table 9.2 Results of ellipsometric data fitting for a dry and n-hexane swollen PDMS film supported on porous *α*-alumina substrate

	Thickn of PDMS film, *h* [nm]	Ref. index of PDMS film, *n* [-]	Thickness of graded roughness layer, h_g [-]	Mean porosity in the roughness layer, *v* [%]	Gradient in refractive index or roughness layer, *g* [%]	Swelling factor of PDMS film, α [-]
Dry, nitrogen flow	1311 ±13	1.420 ±0.005	225±37	50.4±1.3	24.6±2.1	-
n-hexane, liquid	2744 ±6	1.380 ±0.001	240±38	63.2±2.5	44.1±8.5	2.10

better to the maxima of *Ψ* oscillations. Fitting results are shown in Table 9.2. The MSE for the dry sample is 28.8 and for the swollen in n-hexane 10.3. Porosity of the bulk support is determined from a fit for an uncoated sample (46%) and is fixed in the modeling of the coated sample.

9.4.3. Influence of cross-linker content on the swelling of thin supported and bulk PDMS samples

The swelling factor and volume fraction of n-hexane in thin glass supported PDMS as a function of cross-linker content is presented in Figure 9.5.

The volume fraction of n-hexane is calculated from the EMA (equation 9.3) and the thickness change (dilation) upon swelling (equation 9.4). With increasing cross-linker concentration the extent of swelling decreases. In the case of 4.3 wt% cross-linker, the sorption induced increase in thickness of the PDMS film exceeds a factor of 3. For 9.1 wt% cross-linker the change in the thickness is slightly less than 2. At higher cross-linker concentrations both the swelling factor and the volume fraction of n-hexane remain more or less constant, suggesting that all vinyl groups have reacted and the extent of cross-linking cannot be further increased. The volume fraction calculated from the swelling is in a reasonable agreement with the volume fraction obtained with EMA. The discrepancies are probably related to errors in determination of the refractive index of swollen PDMS film, because the accuracy of the measurement decreases when n-hexane is introduced as an ambient. The refractive indices of glass substrate (~1.505), dry and swollen PDMS (~1.415 and ~1.385 respectively), and that of liquid n-hexane (1.365) are all very close. Especially for the EMA approach this means that already slight inaccuracies related to various measurement errors and sample quality have large influence on the calculated penetrant volume fraction. In addition, it might be that due to significant polymer network extension the assumption of its identical refractive

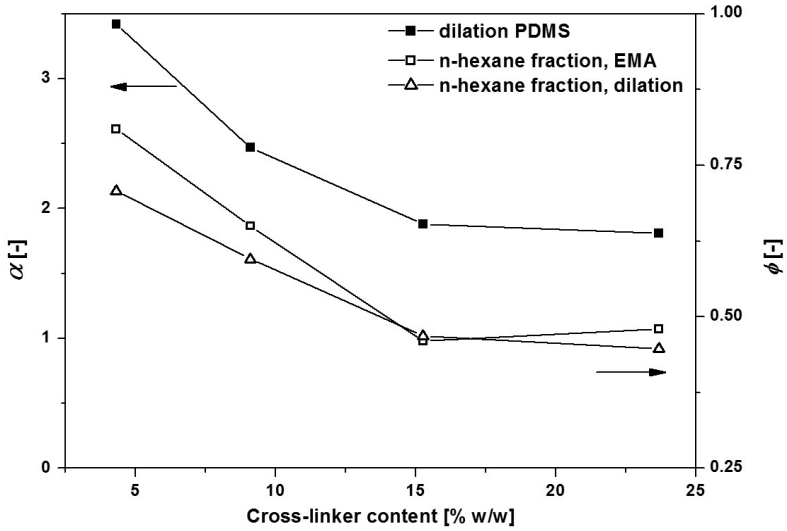

Figure 9.5 Swelling factor and n-hexane volume fraction in thin glass supported PDMS films as a function of cross-linker content

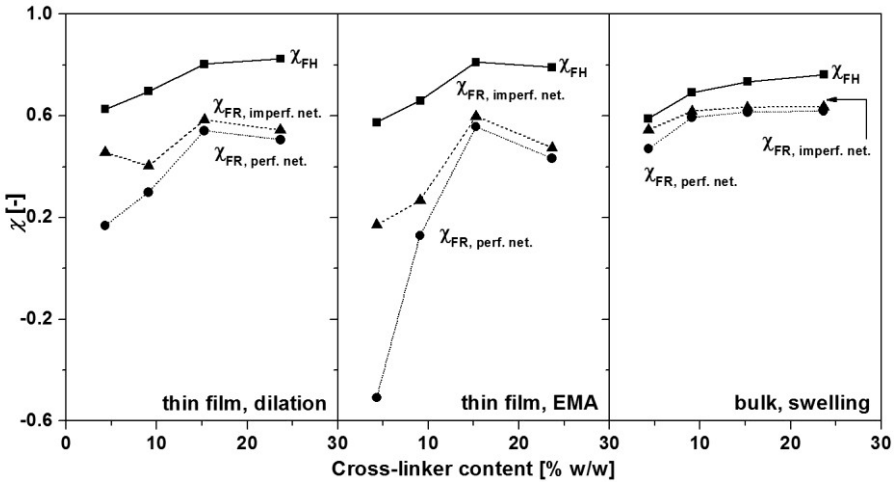

Figure 9.6 χ parameters calculated based on Flory-Huggins and Flory-Rehner theories

index in a dry and swollen state may fail. In that perspective the agreement with swelling calculated volume fractions, equation 9.4, seen in Figure 9.5 is considered acceptable.

The observed decrease in sorption with cross-linker concentration suggests that the

Table 9.3 Elastic modulus of bulk samples, *E*, dimensionality change for bulk and thin film samples, and network parameters as a function of cross-linker concentration

wt. % cross-linker	E [MPa]	$\frac{\delta}{\delta_0}$, bulk	$\frac{\delta}{\delta_0}$, thin	M [g mol^{-1}]	M_c [g mol^{-1}]
4.3	0.7	1.65	3.42	35000	10990
9.1	1.68	1.36	2.47	35000	4570
15.2	2.69	1.3	1.88	35000	2850
23.7	3.71	1.27	1.81	35000	2070

elastic contribution to the change in free energy, due to deformation of the polymer network, is significant. To investigate its implications the polymer-penetrant interaction parameter, χ, calculated according to Flory-Huggins theory, Flory-Rehner theory assuming perfect network and Flory-Rehner theory taking account for the network imperfections is shown in Figure 9.6.

The E modulus measured for bulk samples is assumed to be the same for the thin glass supported films; the corrections for network imperfections, M_c, and network molecular mass, M, are estimated based on literature data [39]. The parameters used to obtain data depicted in Figure 9.6 are collected in Table 9.3.

As expected the dilation for bulk samples, in one single direction, is much lower than that of the thin supported films. The bulk samples are allowed to expand in all directions whereas the thin films can only swell in the direction perpendicular to the substrate. If no correction for the elastic contribution of the network is implemented for the supported thin films the interaction parameter calculated using Flory-Huggins theory is affected by the cross-linker content. It decreases with decreasing cross-linker content in all cases. The values calculated with Flory-Rehner equation with the assumption of perfect network, $\left(1-\frac{2M_c}{M}\right)=1$, are significantly lower than the values calculated by Flory-Huggins theory indicating a strong polymer-penetrant affinity. It seems that, for the two thin film samples with lowest degree of cross-linking, the assumption of a perfect network does not hold anymore. When corrected with appropriate M and M_c parameter values, Table 9.3, χ is found to vary less with the degree of cross-linking. As expected the impact of implementation of elastic contribution and network imperfection corrections is more significant for the thin films, as compared to bulk samples, due to much larger swelling induced deformation of the former.

9.4.4. Swelling of thin PDMS film supported on glass and porous α-alumina in pressurized n-hexane: no-flow conditions (static)

Thin PDMS films can be used for solvent nanofiltration [1, 10, 39, 40]. In such applications the driving force for transport of solvent through the membrane is a

trans-membrane pressure difference. The corresponding mechanical force imposed on the thin PDMS film may affect the extent of solvent induced swelling. Studies have been presented in literature in which mechanical force is applied to a solvent swollen polymer, while the solvent is allowed to flow out of the polymer at ambient pressure [1, 7]. In contrast, we study the swelling of PDMS films in a pressurized solvent. Swelling of bulk polymer samples in highly pressurized solvent has been previously studied to gain insights on polymer-solvent interactions [4]. To the best of our knowledge swelling of thin PDMS films in a pressurized liquid has not yet been reported.

In Figure 9.7 the thickness of an n-hexane swollen PDMS film, supported on a glass slide, is depicted as a function of pressure. The numerical fit accuracy for the fitted thickness is smaller than ~5 nm. When the dry PDMS film (645.2 nm) is brought in contact with liquid n-hexane the thickness increases to 1741.7 nm, corresponding to $\alpha = 2.7$ (Figure 9.7b) Variation of the hydrostatic pressure applied to the solvent in the range 1 – 100 bar does not significantly affect the thickness of the swollen film. This is also confirmed in the raw data behavior shown in Figure 9.7a. No significant change in Ψ oscillations amplitude, envelope position or oscillations position is observed upon pressure increase. The negligible effect of pressure on the extent of swelling and the fraction of sorbed n-hexane suggests that the molar volume of n-hexane, V_H, does not change upon sorption in PDMS, and hence the change in partial molar free energy due to pressurization, $V_H \Delta p$, is

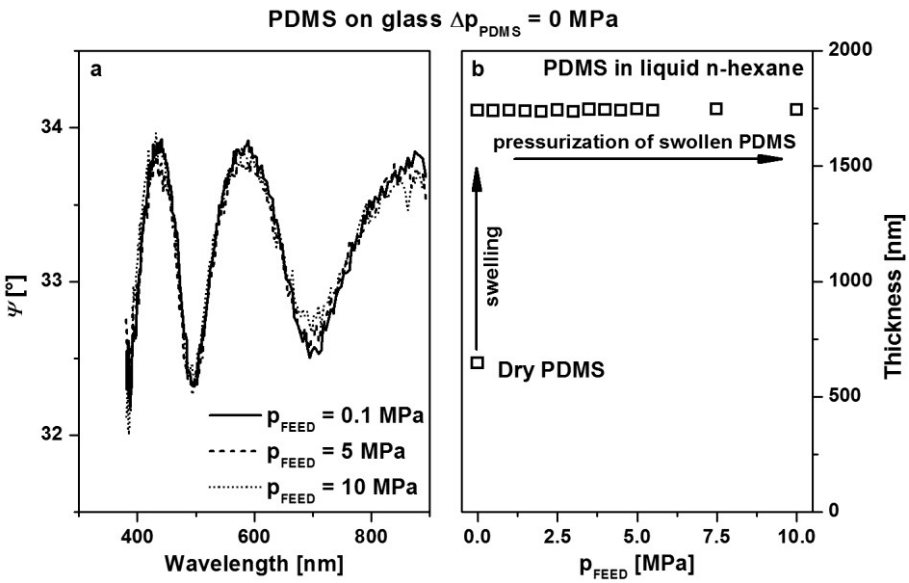

Figure 9.7 Ψ spectra and thickness evolution of a thin PDMS film supported on glass substrate in pressurized liquid n-hexane

similar for the pure and sorbed n-hexane. To rationalize the finding one can write the equilibrium equation for the n-hexane in the liquid and in the PDMS phases assuming the same pressure in both phases, p:

$$RT \cdot ln\left(a_H^{liq}\right) + V_H^{liq} \cdot (p - p_{sat}^0) = RT \cdot ln(a_H^{PDMS}) + V_H^{PDMS} \cdot (p - p_{sat}^0) \quad (9.11)$$

As the term a_H^{PDMS} the activity given by eq. 9.5 can be used with added term including the elastic deformation for the thin film, eq. 9.7. For pure n-hexane the eq. 9.11 reduces to:

$$V_H^{liq} \cdot (p - p_{sat}^0) = RT \cdot ln(a_H^{PDMS}) + V_H^{PDMS} \cdot (p - p_{sat}^0) \quad (9.12)$$

which suggests that, if a_H^{PDMS} is independent of $p, V_H^{liq} = V_H^{PDMS} = V_H$. The finding allows to significantly simplify some of the relevant membrane transport equations, presented for instance in the work of Wijmans [41], thereby reducing complexity in analysis of some membrane systems.

To resolve the behavior of the membrane thin selective layer under permeation a porous substrate is essential. Since the porosity of a substrate is known to complicate ellipsometry analysis [31], it has to be confirmed that the behavior under pressure of the complex sample consisting of a thin PDMS film deposited on porous substrate is the same as the behavior of the relatively simple sample (PDMS film deposited on glass). The results of pressurization of n-hexane swollen PDMS film on porous α-alumina substrate are shown in Figure 9.8.

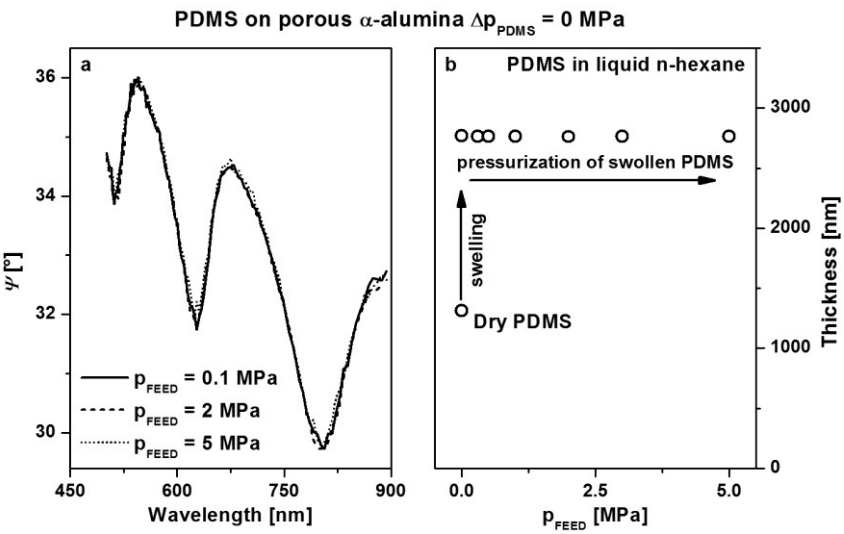

Figure 9.8 *Ψ* spectra and thickness evolution of a thin PDMS film supported on porous *α*-alumina substrate in pressurized liquid n-hexane

Both the raw data (Figure 9.8a) and the modeling results (Figure 9.8a) indicate that, when pressurized in liquid n-hexane, the PDMS deposited on the porous support shows the same behavior as the film deposited on glass substrate. No significant changes in thickness are observed up to 50 bar. This suggests that the sample prepared with the floating technique can be used to successfully represent the swelling behavior of a composite asymmetric membrane in solvent nanofiltration.

9.4.5. Swelling of thin PDMS film supported on porous α-alumina in pressurized n-hexane: permeation

Results of thickness behavior of a thin PDMS film deposited on porous α-alumina support during solvent permeation are shown in Figure 9.9. The data in the figure indicate that, upon increase of the feed pressure, significant changes in the Ψ spectra occur. The oscillations shift towards shorter wavelengths, indicating a decrease in thickness of the swollen PDMS layer at higher pressures. The corresponding thickness is presented in Figure 9.9b in which on the x-axis the pressure drop over the PDMS film is presented. This pressure drop is calculated from a resistance in series model [42]; the resistance of the porous support is obtained from the solvent flux through a bare support. The contribution of the support is significant, for instance, at the maximum feed pressure of 30 bar the pressure drop over the thin swollen PDMS film is calculated to be Δp_{PDMS} =11.4 bar. The large contribution of the support originates from its limited pore size, moderate porosity, and hydrophilic characteristics. In addition, the thin PDMS films obtained with the floating technique have significant defects, such as pinholes, allowing for viscous transport, parallel to the transport through the actual PDMS matrix. Although these defects obstruct use of the thin films as high performance SRNF membranes, they do not constrain characterization of the evolution of film thickness with pressure.

Figure 9.9b indicates a progressing reduction in thickness of the swollen thin PDMS layer when the pressure difference is increased. The thickness decrease suggests a reduction in the fraction of n-hexane in the PDMS. A similar reduction in concentration with pressure has been observed by Rosenbaum and Cotton (see figure 2 in their publication [43]), which has been considered convincing evidence for the applicability of the solution diffusion model [35].

The thickness evolution obtained from ellipsometry can be confronted quantitatively with predictions of the solution-diffusion model. Assuming a linear concentration of n-hexane in the film, and a constant molar volume of n-hexane (*vide supra*), the volume fraction of n-hexane at the interface with the porous support, ϕ_H^{int}, can be directly calculated from the thickness of the film. For the solution diffusion model, the fraction can be calculated from the presumed jump in pressure at the interface between support and the PDMS film, assuming

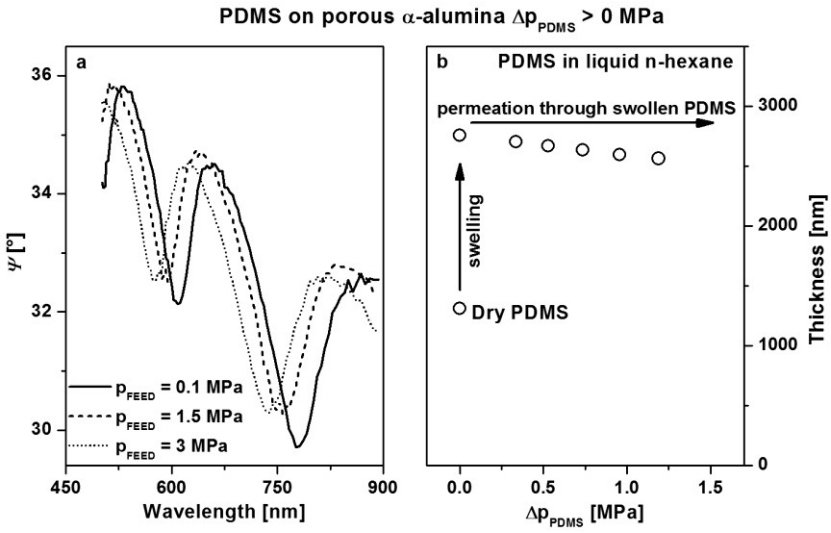

Figure 9.9 *Ψ* spectra and thickness evolution of a thin PDMS film supported on porous *α*-alumina substrate during permeation of high pressure liquid n-hexane; in b) on *x*-axis the pressure difference over thin PDMS film is shown, as calculated from resistances-in-series model [42]

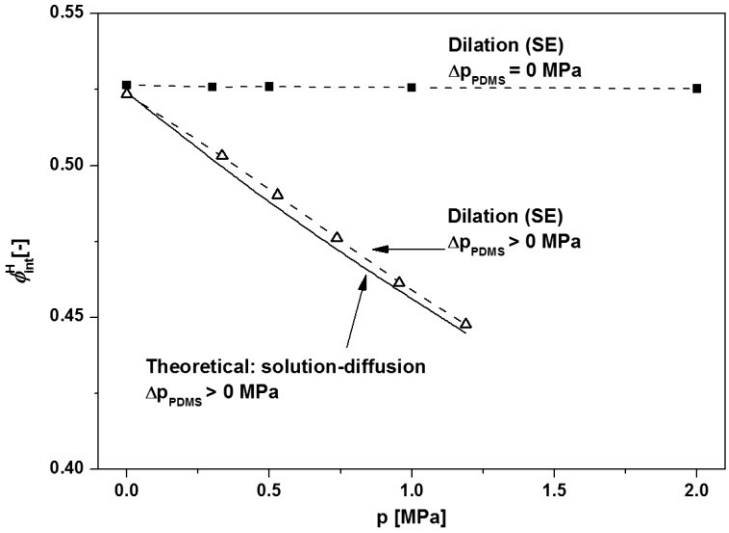

Figure 9.10 n-Hexane volume fraction dissolved in swollen PDMS at the interface with porous support, calculated based on solution-diffusion theory and from ellipsometry data

thermodynamic equilibrium at this interface:

$$ln(\phi_H^{int}) + (1 - \phi_H^{int}) + \chi(1 - \phi_H^{int})^2 + \left(\frac{V_H E}{3RT}\right)\left(\alpha - \frac{1}{2\alpha}\right) = \frac{V_H}{RT}\Delta p_{PDMS} \quad (9.13)$$

The χ parameter is calculated from ellipsometry data using eq. 9.13 for the conditions of Δp_{PDMS} = 0, using an appropriate value of E based on Table 9.3. The obtained χ=0.438 and the value of E are kept fixed for further calculations and a perfect polymer network is assumed. The value of the concentration of n-hexane dissolved in PDMS at feed interface is kept equal to the value of ϕ_H^{int} obtained at Δp_{PDMS} = 0. The results of the calculations are presented in Figure 9.10 as a function of feed pressure.

The n-hexane volume fraction from the static experiment (i.e., no pressure drop, taken from Figure 9.8) is depicted as well. For this dataset the pressure on the *x*-axis denotes the hydrostatic pressure exerted on the swollen PDMS film with zero flow through the membrane. There is excellent agreement between the experimental data obtained using spectroscopic ellipsometry and the Solution-Diffusion model. This indicates that our method allows quantification of the contribution of Solution-Diffusion to mixed mode transport through composite membranes, for instance where some imperfections may exist in the selective membrane layer.

9.5. Conclusions

In-situ, high-pressure spectroscopic ellipsometry has been used to study solvent induced swelling of a thin film composite membrane. The system used involves a thin (~1 μm), cross-linked poly(dimethyl siloxane) (PDMS) film deposited on non-porous (glass) or porous (polished α-alumina) supports. The influence of cross-linker concentration on swelling of the thin film and bulk samples is investigated and interaction parameters according to Flory-Huggins and Flory-Rehner theories are calculated. The importance of including the elastic contribution to the change of Gibbs free energy of the system is stressed and is related to significant degree of polymer network deformation in swollen polymer. When exposed to elevated pressure of the solvent the swelling of the thin PDMS layer is found to be independent of pressure in the range of 1 – 100 bar. This finding suggests that the molar volumes of the penetrant in the liquid and sorbed phases are not significantly different. When the solvent is allowed to permeate through a membrane upon applied pressure difference, a progressing compaction of the membrane is observed with increasing upstream pressure. The observed compaction is in excellent agreement with predictions from the Solution-Diffusion model, indicating that *in-situ* spectroscopic ellipsometry can be used to quantify the contribution of Solution-Diffusion to mixed mode transport of n-hexane.

9.6. Acknowledgments

The Netherlands Organization for Scientific Research (NWO) is acknowledged for financial support (VIDI STW 07055).

MW acknowledges support through the Alexander von Humboldt Foundation.

9.7. References

[1] Vankelecom, I.F.J., et al., Physico-chemical interpretation of the SRNF transport mechanism for solvents through dense silicone membranes. Journal of Membrane Science, 2004. **231**(1–2): p. 99-108.

[2] Sereewatthanawut, I., A.T. Boam, and A.G. Livingston, Polymeric Membrane Nanofiltration and Its Application to Separations in the Chemical Industries. Macromolecular Symposia, 2008. **264**(1): p. 184-188.

[3] Van der Bruggen, B., M. Mänttäri, and M. Nyström, Drawbacks of applying nanofiltration and how to avoid them: A review. Separation and Purification Technology, 2008. **63**(2): p. 251-263.

[4] Ham, J.S., M.C. Bolen, and J.K. Hughes, The use of high pressure to study polymer—solvent interaction. Journal of Polymer Science, 1962. **57**(165): p. 25-40.

[5] Wessling, M., et al., Plasticization of gas separation membranes. Gas Separation & Purification, 1991. **5**(4): p. 222-228.

[6] Piccinini, E., M. Giacinti Baschetti, and G.C. Sarti, Use of an automated spring balance for the simultaneous measurement of sorption and swelling in polymeric films. Journal of Membrane Science, 2004. **234**(1–2): p. 95-100.

[7] Tarleton, E.S., et al., New experimental measurements of solvent induced swelling in nanofiltration membranes. Journal of Membrane Science, 2005. **261**(1–2): p. 129-135.

[8] Böhning, M. and J. Springer, Sorptive dilation and relaxational processes in glassy polymer/gas systems--I. Poly(sulfone) and poly(ether sulfone). Polymer, 1998. **39**(21): p. 5183-5195.

[9] Rouessac, V., et al., Three characterization techniques coupled with adsorption for studying the nanoporosity of supported films and membranes. Microporous and Mesoporous Materials, 2008. **111**(1–3): p. 417-428.

[10] Stafie, N., D.F. Stamatialis, and M. Wessling, Insight into the transport of hexane–solute systems through tailor-made composite membranes. Journal of Membrane Science, 2004. **228**(1): p. 103-116.

[11] Ho, W.S.W.S., K. K., Membrane Handbook1992, New York: Van Nostrand.

[12] Bondar, V.I., B.D. Freeman, and I. Pinnau, Gas sorption and characterization of poly(ether-b-amide) segmented block copolymers. Journal of Polymer Science Part B: Polymer Physics, 1999. **37**(17): p. 2463-2475.

[13] Merkel, T.C., et al., Gas sorption, diffusion, and permeation in poly(dimethylsiloxane). Journal of Polymer Science Part B: Polymer Physics, 2000. **38**(3): p. 415-434.

[14] Stamatialis, D.F., et al., Optical vs. direct sorption and swelling measurements for the study of stiff-chain polymer-penetrant interactions. Journal of Membrane Science, 1997. **130**(1-2): p. 75-83.

[15] Stamatialis, D.F., M. Sanopoulou, and J.H. Petropoulos, Phenomenology and mechanisms of unidimensional stress-dependent micromolecular transport in a stiff-chain polymer. III. Effect of modification of the polymer. Journal of Polymer Science Part B: Polymer Physics, 1997. **35**(16): p. 2593-2607.

[16] Flichy, N.M.B., et al., An ATR-IR study of poly (dimethylsiloxane) under high-pressure carbon dioxide: Simultaneous measurement of sorption and swelling. Journal of Physical Chemistry B, 2002. **106**(4): p. 754-759.

[17] Brantley, N.H., S.G. Kazarian, and C.A. Eckert, In situ FTIR measurement of carbon dioxide sorption into poly(ethylene terephthalate) at elevated pressures. Journal of Applied Polymer Science, 2000. **77**(4): p. 764-775.

[18] Guadagno, T. and S.G. Kazarian, High-Pressure CO2-Expanded Solvents: Simultaneous Measurement of CO2 Sorption and Swelling of Liquid Polymers with in-Situ Near-IR Spectroscopy. The Journal of Physical Chemistry B, 2004. **108**(37): p. 13995-13999.

[19] Pereira, A.M.M., Characterization of polymeric membranes for non-aqueous separations, 2007, Eindhoven University of Technology.

[20] Sirard, S.M., P.F. Green, and K.P. Johnston, Spectroscopic Ellipsometry Investigation of the Swelling of Poly(Dimethylsiloxane) Thin Films with High Pressure Carbon Dioxide. The Journal of Physical Chemistry B, 2001. **105**(4): p. 766-772.

[21] Spaeth, K., G. Kraus, and G. Gauglitz, In-situ characterization of thin polymer films for applications in chemical sensing of volatile organic compounds by spectroscopic ellipsometry. Fresenius' Journal of Analytical Chemistry, 1997. **357**(3): p. 292-296.

[22] Elbs, H. and G. Krausch, Ellipsometric determination of Flory-Huggins interaction parameters in solution. Polymer, 2004. **45**(23): p. 7935-7942.

[23] Blume, I., J.G. Wijmans, and R.W. Baker, The separation of dissolved organics from water by pervaporation. Journal of Membrane Science, 1990. **49**(3): p. 253-286.

[24] Robinson, J.P., et al., Influence of Cross-Linking and Process Parameters on the Separation Performance of Poly(dimethylsiloxane) Nanofiltration Membranes. Industrial & Engineering Chemistry Research, 2005. **44**(9): p. 3238-3248.

[25] Tarleton, E.S., J.P. Robinson, and M. Salman, Solvent-induced swelling of membranes — Measurements and influence in nanofiltration. Journal of Membrane Science, 2006. **280**(1–2): p. 442-451.

[26] Fujiwara, H. and I. Wiley, Spectroscopic ellipsometry principles and applications, 2007, John Wiley & Sons: Chichester, England; Hoboken, NJ.

[27] Tompkins, H.G. and E.A. Irene, Handbook of ellipsometry, 2005, William Andrew Pub. ; Springer: Norwich, NY; Heidelberg, Germany.

[28] Woollam, J.A., et al. Overview of variable angle spectroscopic ellipsometry (VASE), part I: basic theory and typical applications. 1999.

[29] Azzam, R.M.A. and N.M. Bashara, Ellipsometry and polarized light1977, Amsterdam; New York; New York: North-Holland Pub. Co. ; Sole distributors for the U.S.A. and Canada, Elsevier North-Holland.

[30] Bruggeman, D., The calculation of various physical constants of heterogeneous substances. I. The dielectric constants and conductivities of mixtures composed of isotropic substances. Annalen der Physik, 1935. **24**(7).

[31] Ogieglo, W., et al., Spectroscopic Ellipsometry analysis of a thin film composite membrane consisting of polysulfone on a porous α-alumina support. ACS Applied Materials & Interfaces, 2012.

[32] Lichtenstein, T., Handbook of Thin Film Materials, Academic Press. 1972.

[33] Flory, P.J., Principles of Polymer Chemistry1953: Cornell University Press, Ithaca, New York.

[34] Yampolskii, Y.P., I. Freeman, B. D., Materials Science of Membranes for Gas and Vapor Separation2006: John Wiley & Sons.

[35] Wijmans, J.G. and R.W. Baker, The solution-diffusion model: a review. Journal of Membrane Science, 1995. **107**(1-2): p. 1-21.

[36] Stokes, R., Dielectric constants and molar polarizations of cycloalkanes, benzene, n-hexane, and carbon tetrachloride in the range 278 to 343 K. The Journal of Chemical Thermodynamics, 1973. **5**(3): p. 379-385.

[37] Herzinger, C.M., et al., Ellipsometric determination of optical constants for silicon and thermally grown silicon dioxide via a multi-sample, multi-wavelength, multi-angle investigation. Journal of Applied Physics, 1998. **83**(6): p. 3323-3336.

[38] Mark, J.E., Polymer Data Handbook1999: Oxford University Press, Inc.

[39] Stafie, N., D. Stamatialis, and M. Wessling, Effect of PDMS cross-linking degree on the permeation performance of PAN/PDMS composite nanofiltration membranes. Separation and Purification Technology, 2005. **45**(3): p. 220-231.

[40] Dobrak-Van Berlo, A., I.F.J. Vankelecom, and B. Van der Bruggen, Parameters determining transport mechanisms through unfilled and silicalite filled PDMS-based membranes and dense PI membranes in solvent resistant nanofiltration: Comparison with pervaporation. Journal of Membrane Science, 2011.

[41] Wijmans, J., The role of permeant molar volume in the solution-diffusion model transport equations. Journal of Membrane Science, 2004. **237**(1): p. 39-50.

[42] Peng, F., J. Liu, and J. Li, Analysis of the gas transport performance through PDMS/PS composite membranes using the resistances-in-series model. Journal of Membrane Science, 2003. **222**(1): p. 225-234.

[43] Polzer, F., et al., Synthesis and analysis of zwitterionic spherical polyelectrolyte brushes in aqueous solution. Macromolecules, 2011. **44**(6): p. 1654.

Chapter 10

Effects of time, temperature, and pressure in the vicinity of the glass transition of a swollen polymer

This chapter is in preparation for publication, authored by:

Ogieglo W., Upadhyaya L., Nijmeijer A., Wessling M., Benes N.E.

Abstract

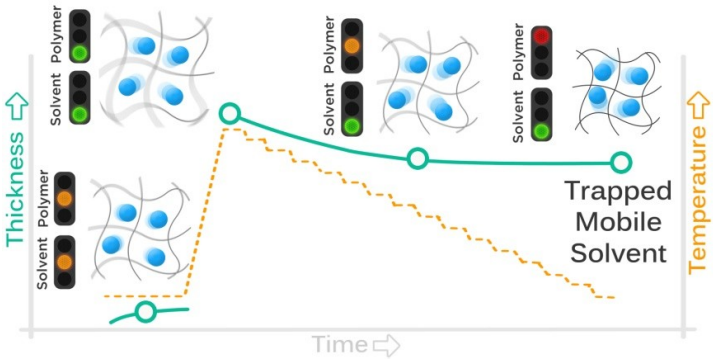

In-situ spectroscopic ellipsometry is used for the dynamic study of thermally perturbed thin polystyrene films, swollen with n-octane or n-decane. The thermal evolution of the swollen films reveals pronounced changes both in equilibrium and kinetic properties. Upon vitrification, a kinetically arrested swollen matrix is observed. This phenomenon is related to the excess energy term in the chemical potential of the solvent, associated with the non-equilibrium status of the swollen polymer matrix. The swollen polystyrene – n-decane system shows no measurable compression when exposed to hydrostatic pressures up to 50 bar, neither above or below the glass transition temperature. A slight compression is observed for a glassy, non-swollen polystyrene film in pressurized water, corresponding to partial relaxation of excess free volume. The results are of importance, for instance, in membrane technology, where penetrant-swollen glassy polymer layers can be operated under high pressures to provide for molecular separation.

10.1 Introduction

Solvent resistant nanofiltration (SRNF) has gained a considerable attention in the recent years due to its large potential in the chemical, the pharmaceutical, and the food industry [1, 2]. As compared to traditional technologies, SRNF may offer significant advantages in terms of energy efficiency, ecological benevolence, process design and intensification, and scalability [3]. However, controversies remain with respect to a suitable description of mass transport through SRNF membranes.

In most cases, SRNF membranes consist of a thin organic polymer film that has favorable interactions with a penetrant that is intended to permeate. Generally, mass transport through SRNF membranes is described by one of two models. In the first model, transport occurs by diffusion of molecules that are dissolved in the polymer material. The diffusion of permeating species is considered to occur on the timescale of the individual motions of the polymeric chains that form constantly fluctuation small (~0.5 nm) pores. This model is referred to as the Solution Diffusion Model and requires an activity gradient within the material. The model has been shown successful for describing mass transport in the case of reverse osmosis, gas separation, or pervaporation [4, 5]. In nanofiltration extensive swelling of the thin membrane can occur, often exceeding 100% [6, 7]. Such extensive swelling implies a significant increase in polymer chain separation, allowing for the existence of a connected open structure of 'pores' with ~ 1 nm size [8]. In the second model, molecules are envisioned to permeate through this connected open structure by viscous transport. This model is referred to as the Pore Flow Model and it requires a hydrostatic pressure gradient within the membrane material. Combination and extensions of these two distinct models have also been proposed to describe transport in SRNF membranes.

The lack of consensus with respect to the transport description is largely related to the fact that, at a moderate level of swelling and practically applicable pressure differences (<30 bar), both models predict a linear proportionality between flux and applied pressure difference. At higher pressures, a concave relation between the flux and the pressure difference is predicted by both models [8-13]. For the Solution Diffusion model the concave shape is related to the non-linear relation between solvent volume fraction and hydrostatic pressure. In the Pore Flow Model the higher pressure differences are thought to cause compaction of the film, negatively affecting the flux. Based on transport measurements alone it is virtually impossible to determine which model is physically accurate. Therefore, other more direct, methods to measure properties of the membrane selective layer under relevant pressure have been proposed [6, 7, 14-16]. Using *in-situ* spectroscopic ellipsometry (SE) it has been shown that, in the case of n-hexane permeating through a thin rubber poly(dimethyl siloxane) (PDMS) membrane, the film dilation complies very well with predictions from the Solution Diffusion model. No change

in dilation of the swollen film was observed upon isostatic pressurization of the solvent, in which it was immersed. This indicates that for this solvent-polymer system the molar volume of the solvent remains equal upon sorption, and there is no compaction of free volume of the swollen polymer. Changes in dilation due to pressure difference over the film have been proven directly related to the thermodynamic description of the system, according to the well-known Flory-Rehner theory. The results indicate that the swollen PDMS can be considered as a true equilibrium liquid that is well above its glass transition.

When a polymer undergoes a transition from a liquid to glass state, the chain relaxation times change by many orders of magnitude [17]. As a consequence, the system is not able to densify towards thermodynamic equilibrium at an appreciable time-scale and a certain excess of fractional free volume (EFFV) remains entrapped. The densification of the kinetically arrested glassy structure is very slow, with a timescale strongly dependent on the difference between the experimental temperature and the glass transition temperature, T_g. This slow densification is referred to as physical aging. When a polymer is swollen with a solvent, the T_g of the mixture is brought down significantly. This is mainly due to a severe plasticization of the polymer network [18-24].

In the present work we extend the study of pressurization of swollen films to a glass-forming polymer, above and below its glass transition. Above the glass transition, the effects of pressure on swelling of the polymer can be expected to be analogous to that of PDMS. Aim is to establish if the swelling behavior is distinct below the glass transition, where the swollen polymer can no longer be considered equilibrium liquid.

10.2. Experimental part

10.2.1. Materials

Polystyrene (PS) supplied by Sigma Aldrich with a molecular weight of 280 kg/mol was used in the study. Solutions of about 3 or 10 wt% in toluene (Merck) were used to spin coat the thin films in a 100 – 1500 nm thickness range. This range corresponds to the thicknesses used in membrane applications. The ultra thin region (<100 nm) is omitted, to avoid complications related to nano-confinement effects. These effects are known to alter the glass transition temperature [25] or physical aging [26] of the glassy films.

As substrates, either silicon wafers with native oxide or glass slides were used. The silicon wafers were used in the temperature-resolved measurements at atmospheric pressure to assure very high optical contrast between the film and the substrate, whereas the more robust glass slides were used for the high pressure measurements. The silicon substrates were 2 by 2 cm square pieces of a 0.5 mm thick wafer. The glass substrates were approximately 2 mm thick round discs, 39

mm in diameter. The backside of each glass substrate was mechanically roughened, to avoid light reflection from the bottom interface. All PS films were annealed after spin coating for at least 2 hours under nitrogen flow at 120 °C to remove the residual solvent and relax post-preparation stresses. For swelling experiments n-octane or n-decane (Merck) were used without further purification.

10.2.2. Ambient pressure ellipsometry measurements

Glass transition temperature of polymer films swollen with n-octane and n-decane was determined by spectroscopic ellipsometry using a commercial device M-2000X (by J.A. Woollam, Co., Inc.). Swelling was done in a custom-built, temperature-controlled glass cell with windows perpendicular to incident light beam at an angle of 70°. The employed wavelength range was 370 – 1000 nm. In this range the PS was considered optically transparent and its optical dispersion was modeled using a simplified Cauchy relation:

$$n(\lambda) = A + \frac{B}{\lambda^2} \qquad (10.1)$$

where, A and B were adjustable parameters describing the wavelength, λ, dependence of the refractive index, n. The optical dispersions of silicon wafers, with native oxide of about 2 nm, were taken from literature [27]. The refractive indices of the solvents were determined from spectroscopic ellipsometry spectra for solvent - silicon wafers, at the relevant experimental temperatures. The obtained data were in a very good agreement ($\Delta n \sim 0.001$) with the measurements done on a simple laboratory refractometer (Carl Zeiss).

The dried and annealed PS films were placed in the experimental cell and exposed to the solvent (about 60 ml) at 21 °C. After thermal equilibration the temperature was raised to 42 °C within about 20 minutes, and stabilized for 95 minutes. Subsequently, a stepwise temperature decrease followed, in steps of 2 °C within 15 minutes and 95 minutes of equilibration per step. During the scan, the film properties were recorded with spectroscopic ellipsometry, every 30 seconds. A small temperature induced window birefringence was corrected for in the optical model, by including an appropriate fitting parameter.

10.2.3. High pressure ellipsometry measurements

A custom-built stainless-steel test cell with 1 cm thick windows was used for the high-pressure swelling experiments. The cell was coupled with a commercial spectroscopic ellipsometer Alpha-SE (J.A. Woollam Co., Inc.), recording full spectra between 390 and 900 nm every 30 seconds. The cell was equipped with temperature stabilization system able to operate between 10 °C and 60 °C. The pressure was accurately adjusted and stabilized with a use of a solvent resistant syringe pump (Teledyne ISCO, 500D). The solvent was introduced into the measurement cell, after evacuating the system with a mechanical vacuum pump.

No pressure differences were allowed to exist between various locations in the cell. Further details of the experimental setup can be found in literature [28].

Polystyrene films supported on glass slides were used for the high pressure experiments. The optical dispersion of the glass slides were always determined on bare supports (fitted to Cauchy equation, eq. 10.1) and fixed for the measurements of thin film samples. After sample equilibration with solvent at 45 °C (above the glass transition of the mixture), at 1 bar, the pressure was raised stepwise up to 50 bar with a continuous recording of the sample properties. For the experiments below the glass transition temperature the sample was first swollen till equilibrium at 40 °C and then the temperature was reduced to the desired value (12 °C) within 3 hours. Afterwards the pressure was raised stepwise up to 50 bar. The experiments with water instead of the organic solvent were carried out in a similar fashion.

10.3. Results and discussion

10.3.1. T_g of swollen polystyrene films

Figure 10.1a shows the thermal evolution of the thickness of a polystyrene film swollen by n-octane, in the range 40 °C down to 10 °C. Initially, down to about 30 °C, the thickness follows changes in temperature in a linear fashion. This temperature range corresponds to a liquid state of the polymer. For temperatures below ~28 °C, per temperature step only very small changes in thickness are observed. The slope change is similar to what is typically observed for temperature induced dilation of dry polymers, in a temperature range covering the glass transition temperature. In the presented experiment the glass transition of polystyrene-n-octane system is reduced from 100.0 °C for pure PS, to around 28 °C for the swollen system. In the case of PS swollen with n-decane, Figure 10.1b, the glass transition occurs at about 36 °C.

The curvature change is accompanied with a significant change in the dynamics of the system which can be investigated by quantification of the thickness versus time slope (inset in Figure 10.1a). In the rubbery state the polymer chain mobility is very high and, consequently, the penetrant diffusion coefficient is large. As a result, upon every change of temperature, the system equilibrates almost instantaneously and the slope of thickness versus time after temperature stabilization is close to zero. This slope is related to the so-called secondary polymer relaxations. Above the *T*g these relaxations are fast, as compared to the timescale of the experiment. In the vicinity of the glass transition temperature, the secondary relaxations become more significant. This indicates that relaxation of the swollen polymer occurs on a similar timescale as the experiment. As the temperature is reduced further, the slope of the curve, during stabilization, becomes close to zero again. This indicates that the secondary relaxations occur on a time-scale that is much longer than that of the experiment. Below the T_g the system

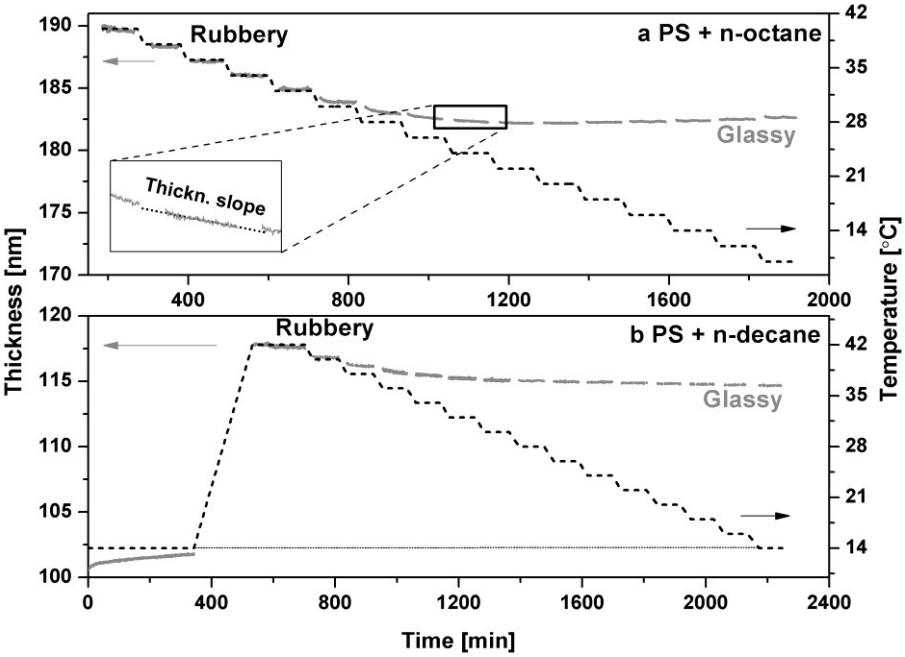

Figure 10.1 a) Thermal evolution of the n-octane swollen PS film thickness, plotted together with the temperature profile; b) Thermal evolution of the n-decane swollen polystyrene film thickness, plotted together with the temperature profile; data at 0 – 350 min represents swelling of a dry film at 14 °C, before the temperature was increased to 42 °C. The thickness variations observed during the actual short temperature steps are removed due to ellipsometry modeling artifacts arising from temperature gradients in, for instance, the cell windows and the liquid solvent.

becomes glassy and the diffusion coefficient of the penetrant drops a few orders of magnitude [24, 29, 30]. However, the drop of the solvent diffusion coefficient alone does not explain the virtually complete arrest of the swollen structure. The solvent diffusion in the glassy polymer is slow, but it still allows significant changes in swelling at the employed timescales. This is apparent from the initial swelling of the dry polymer with n-decane, during the first ~ 350 minutes of the experiment. During this period the initially dry polymer swells about 1% at 14 °C. At the end of the experiment, at the same temperature, changes of less than 0.01% are observed.

The explanation for this behavior is that below the glass transition the polymer chain mobility is very low, and the matrix is unable to relax to equilibrium state. This creates an additional contribution to the chemical potential of the solvent, as introduced by Vrentas et. al. [31]. In effect, the solvent loss is opposed by an energy barrier. This contribution can be expressed in terms of the polymer compression modulus, K, [32, 33]:

$$\mu_{glass} = V_S \cdot K \cdot log\,(\frac{1-\phi_S}{\phi_g}) \qquad (10.2)$$

where V_S is the solvent molar volume, ϕ_S is the solvent volume fraction in the mixture (1- ϕ_S is the polymer volume fraction), and ϕ_g is the polymer volume fraction at glass transition. For the decreasing ϕ_S, the excess contribution becomes greater. The result is a non-equilibrium glassy polymer, swollen by a quasi-equilibrium excess of mobile solvent. Such a system cannot be described with equilibrium thermodynamics, such as the Flory – Huggins theory [34].

In Figure 10.2 the swelling factor ($h_{swollen}/h_{dry}$), the refractive index, and the secondary relations are plotted against the temperature. The data are derived from Figure 10.1. The values of swelling and refractive index represent average of the respective values, over 95 minute stabilization period following a temperature step. The secondary relaxations are expressed by the slope of thickness versus time, normalized with respect to the thickness of the dry film. The glass transition temperature is quantified from the intersection of linear regions above and below curvature change. For n-octane and n-decane swollen PS the values are 27.2 °C and 35.4 °C, respectively. A clear transition is also observed in the behavior of refractive index (Figure 10.2b) and corresponds to the same temperatures as the ones obtained from the dilation curvatures. The refractive index of the swollen system increases with decreasing temperature, signifying a reduction of penetrant volume fraction with reducing temperature. This is because the indices of n-octane (~1.39) and n-decane (~1.40) are lower than that of dry polystyrene (~1.59). The refractive index of a mixture lies in between the values of its constituents. It is seen that the refractive index below the transition does not follow the equilibrium line that can be extrapolated from the liquid state, i.e., the dotted line in Figure 10.2b. The observed values of the refractive indices are lower, indicating that solvent volume fraction is larger than that of a hypothetical equilibrium swollen polymer. This further signifies an excess of solvent in the swollen system.

The dynamics of the system, Figure 10.2c, show a minimum value (fastest dynamics) almost exactly at the quantified glass transition. This is consistent with the observation of a viscoelastic regime, where dynamics of the system coincide with the experimental timescale. In the liquid and deeply in glassy state, secondary relaxations are not significant at the time-scale of the experiment. The analysis of the dynamics of the system confirms that the complete arrest of the structure occurs already only about 6 °C below glass transitions. In the range approximately from T_g to T_g - 6 °C the polymer behaves similarly to dry glassy polymers during the physical aging process, with progressing reduction of thickness in time.

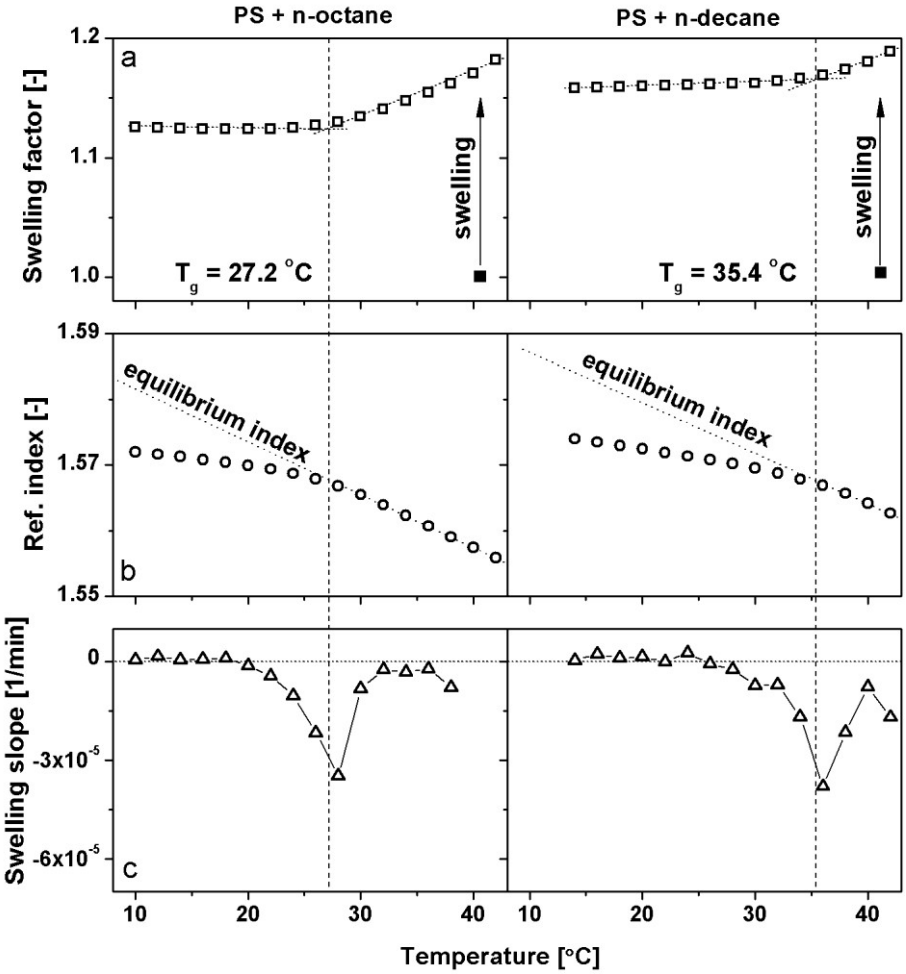

Figure 10.2 Swelling factor ($h_{swollen}/h_{dry}$) (a), refractive index (b), and swelling slope (c) for polystyrene swollen with n-octane (left column) and n-decane (right column), extracted from Figure 10.1a and b, respectively, and plotted against temperature. The glass transition temperature is quantified based on the slope change in the thickness plot (a).

10.3.2. Isostatic pressurization of swollen films above and below the T_g

The impact of pressure on the properties of an n-decane swollen polystyrene film above and below the T_g is depicted in Figure 10.3 and Figure 10.4, respectively. The choice for n-decane over n-octane allows experiments at a higher degree of undercooling, as the T_g of n-decane solvent is highest; the lowest achievable temperature of our set-up is about 12 °C.

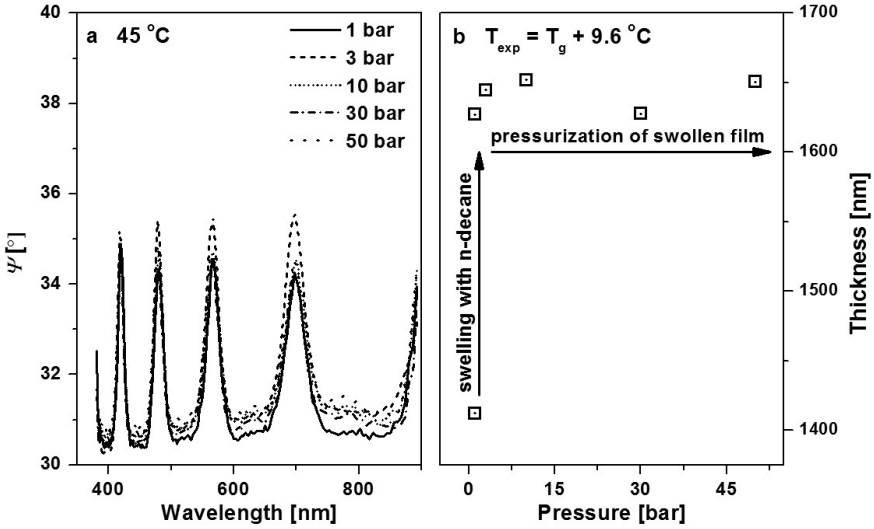

Figure 10.3 Raw ellipsometric data (Ψ) (a) and the resulting film thickness (b) as a function of the applied hydrostatic pressure of the n-decane above the glass transition temperature of the system

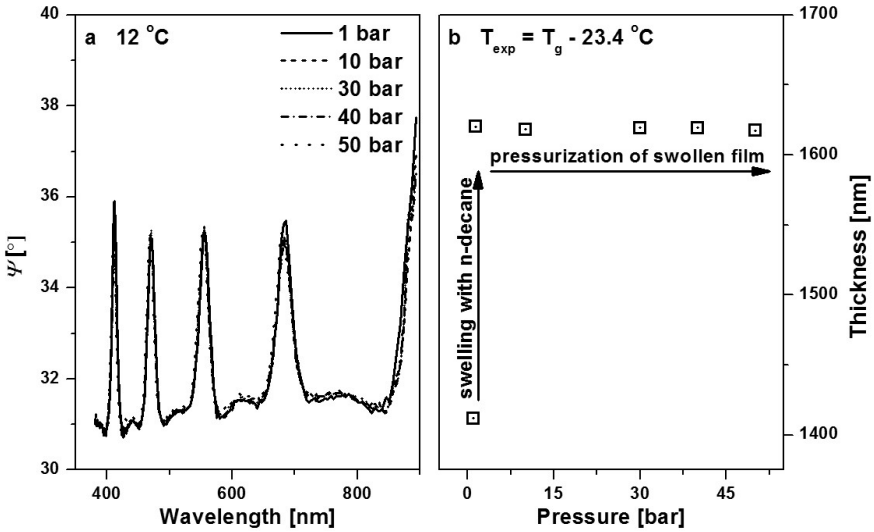

Figure 10.4 Raw ellipsometric data (Ψ) (a) and the resulting film thickness (b) as a function of the applied hydrostatic pressure of the n-decane below the glass transition temperature of the system

At ambient pressure and 9.6 °C above its T_g, the swollen film has a thickness of 1640 nm, which corresponds to ~16% swelling as compared to the initial dry thickness of 1412 nm. An isothermal increase in pressure, up to 50 bar, does not

induce any systematic change in film thickness, Figure 10.3b, or refractive index (not shown). The thickness data do show some scatter. The raw ellipsometric data, Figure 10.3a, show no significant shifts in the oscillatory patterns, either to the left or right. This confirms that the thickness is not affected by the pressure. The thickness scatter is probably related to the slight temperature fluctuations in the system. Such fluctuations affect thermal stresses in the optical windows of the cell, inducing errors in modeling. Another explanation could be incomplete wetting of the roughened bottom interface of the glass slides, which is consistent with the slight fluctuations of the Ψ envelopes (baselines between the upward peaks) in Figure 10.3a.

The presented results are in agreement with the swelling behavior under pressure shown previously in poly(dimethyl siloxane) (PDMS) swollen with n-hexane [28], under isostatic conditions. The insensitivity of the thickness of the swollen film to hydrostatic pressure suggests the change in molar free energy of the solvent, due to pressurization, is similar for the liquid and the sorbed phase. This requires that the term $V_S\Delta p$ is equal for these phases, implying that the molar volume of the solvent is unchanged upon sorption. In other words, the penetrant-polymer mixture behaves as an ideal incompressible liquid.

Figure 10.4 shows the pressure effect on the fresh sample of swollen polystyrene which was first equilibrated with n-decane at 45 °C (~16.2% swelling) and then brought down in temperature to 12 °C, which is 23.4 °C below its glass transition temperature. At 12 °C the polymer swelling at ambient pressure has reduced to ~14.7%. This high degree of swelling is again associated with an excess amount of mobile solvent, as has been discussed elaborately above. Isostatic pressurization of solvent and immersed film, up to 50 bar, does not result in changes in raw ellipsometry spectra or film thickness (Figure 10.4). These observations indicate that the mobile solvent is not expelled from the swollen matrix at increased pressure. The difference in activity of the sorbed and pure solvent due to the pressure change, related to the term $V_S\Delta p$, is small, at least in comparison to the excess term associated with the non-equilibrium status of the polymer. In addition, the excess term is also not significantly impacted by the increase in pressure, as this would have been manifested by a decrease in thickness. The physical interpretation can be given as follows. The change in pressure does not induce a significant difference between the activities of the sorbed and pure solvent. Consequently, there is no tendency for the solvent to be removed from the swollen system. The degree of swelling of the polymer matrix is also not affected, indicating that there is, besides the volume taken up by the solvent, no compressible unfilled excess free volume within the swollen system.

The main conclusion is that isostatic pressurization does not necessarily cause compaction of a swollen polymer film, above and below the T_g.

10.3.3. Water pressurization of a non-swollen film

In a dry glassy system, with unrelaxed EFFV, isostatic pressurization may lead to irreversible compaction. This is demonstrated by isostatic pressurization of water, with a PS film submersed in it, to 100 bar at at 35 °C. Before and after contact with the water, the thickness of the PS film is within experimental error. This indicates that there is almost no penetration of water into the PS film. This is expected, because of the very high hydrophobicity of PS. The impact of isostatic pressure on the dry film thickness and refractive index is shown in Figure 10.5. A slight, but well measurable, thickness decrease of about 0.26% is observed. Concurrently, the refractive index shows a corresponding slight increase. After release of the pressure from 100 bar to 1 bar no significant changes in the thickness and refractive index have been observed, indicating that the compaction upon pressurization is irreversible.

The results indicate that irreversible compaction by relaxation of EFFV can occur. However, the effect (0.26% at 100 bar) is very small as compared to the total EFFV in the polymer, which in this case is about 2.4%. This corresponds to an order of magnitude smaller compaction of polystyrene at 100 bar hydrostatic pressure than thermodynamically possible (assuming total relaxation of EFFV). Similar results were obtained in the compression experiments conducted on dry PMMA films, [35], and indicated that the compression of the glassy matrix is possible, but requires very high pressures (hundreds of bars, much higher than in typical SRNF applications) for the effects to be significant.

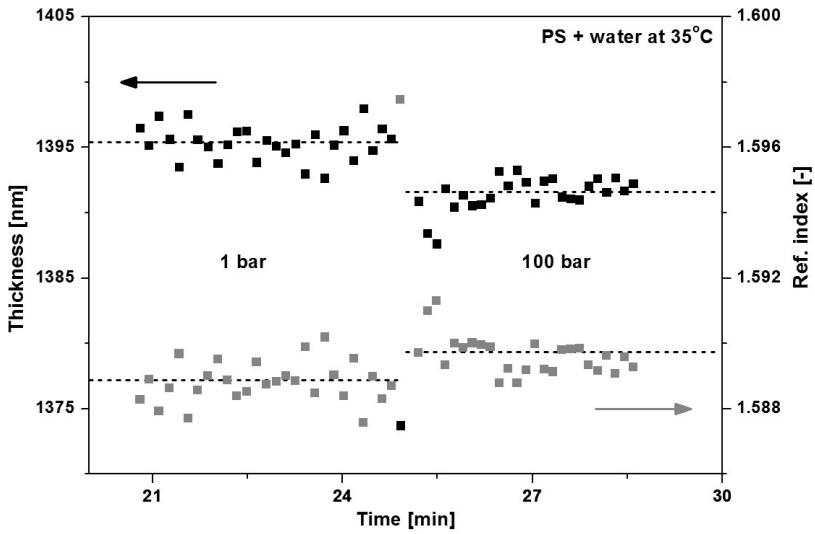

Figure 10.5 Water pressurization of polystyrene thin film on a glass support in the range from 1 to 100 bar

10.4. Conclusions

The dynamic behavior of a swollen glassy polymer – penetrant system in the vicinity of glass transition of the system has been studied with *in-situ* spectroscopic ellipsometry. It has been shown that pronounced changes in both equilibrium and kinetic properties occur as a result of vitrification. Above glass transition temperature both polymer chains and penetrant mobility are large and the system is in thermal equilibrium. Upon reducing the temperature, the solvent concentration in the swollen matrix reduces. This causes a reduction in polymer matrix and penetrant mobility. In a region very close to the glass transition dynamics of the system are manifested as a distinct thickness changes occurring on the timescale of the experiment. Below glass transition very little further swelling reduction is observed, which is related to the emergence of compression energy barrier. This produces a glassy, solvent-oversaturated system in which the penetrant mobility remains relatively large. Pressurization of the swollen system both above and below its glass transition, results in no significant changes in thickness in both cases and rules out the possibility of compaction. An irreversible compaction, in a sense of reduction of non-equilibrium excess free volume in the system is show to be possible in a dry polymer (pressurized with a non-solvent, water) and its effect is relatively small.

10.5. References

[1] Vandezande, P., L.E. Gevers, and I.F. Vankelecom, *Solvent resistant nanofiltration: separating on a molecular level.* Chemical Society Reviews, 2008. **37**(2): p. 365-405.

[2] Sereewatthanawut, I., A.T. Boam, and A.G. Livingston, *Polymeric Membrane Nanofiltration and Its Application to Separations in the Chemical Industries.* Macromolecular Symposia, 2008. **264**(1): p. 184-188.

[3] Nasso, M. and A.G. Livingston, *Solvent nanofiltration in organic processes: A rapid and scalable purification technology.* Chimica Oggi, 2008. **26**(5).

[4] Wijmans, J., *The role of permeant molar volume in the solution-diffusion model transport equations.* Journal of Membrane Science, 2004. **237**(1): p. 39-50.

[5] Wijmans, J.G. and R.W. Baker, *The solution-diffusion model: a review.* Journal of Membrane Science, 1995. **107**(1-2): p. 1-21.

[6] Tarleton, E.S., J.P. Robinson, and M. Salman, *Solvent-induced swelling of membranes — Measurements and influence in nanofiltration.* Journal of Membrane Science, 2006. **280**(1–2): p. 442-451.

[7] Tarleton, E.S., et al., *New experimental measurements of solvent induced swelling in nanofiltration membranes.* Journal of Membrane Science, 2005. **261**(1–2): p. 129-135.

[8] Vankelecom, I.F.J., et al., *Physico-chemical interpretation of the SRNF transport mechanism for solvents through dense silicone membranes.* Journal of Membrane Science, 2004. **231**(1–2): p. 99-108.

[9] Gibbins, E., et al., *Observations on solvent flux and solute rejection across solvent resistant nanofiltration membranes.* Desalination, 2002. **147**(1–3): p. 307-313.

[10] Paul, D.R. and O.M. Ebra-Lima, *Pressure-induced diffusion of organic liquids through highly swollen polymer membranes.* Journal of Applied Polymer Science, 1970. **14**(9): p. 2201-2224.

[11] Machado, D.o.R., D. Hasson, and R. Semiat, *Effect of solvent properties on permeate flow through nanofiltration membranes. Part I: investigation of parameters affecting solvent flux.* Journal of Membrane Science, 1999. **163**(1): p. 93-102.

[12] Paul, D., M. Garcin, and W. Garmon, *Solute diffusion through swollen polymer membranes.* Journal of Applied Polymer Science, 1976. **20**(3): p. 609-625.

[13] Paul, D. and J. Paciotti, *Driving force for hydraulic and pervaporative transport in homogeneous membranes.* Journal of Polymer Science: Polymer Physics Edition, 1975. **13**(6): p. 1201-1214.

[14] Ham, J.S., M.C. Bolen, and J.K. Hughes, *The use of high pressure to study polymer—solvent interaction.* Journal of Polymer Science, 1962. **57**(165): p. 25-40.

[15] Piccinini, E., M. Giacinti Baschetti, and G.C. Sarti, *Use of an automated spring balance for the simultaneous measurement of sorption and swelling in polymeric films.* Journal of Membrane Science, 2004. **234**(1–2): p. 95-100.

[16] Rouessac, V., et al., *Three characterization techniques coupled with adsorption for studying the nanoporosity of supported films and membranes.* Microporous and Mesoporous Materials, 2008. **111**(1–3): p. 417-428.

[17] Gibbs, J.H. and E.A. DiMarzio, *Nature of the Glass Transition and the Glassy State.* The Journal of Chemical Physics, 1958. **28**(3): p. 373-383.

[18] Zhang, Z. and Y.P. Handa, *An in situ study of plasticization of polymers by high-pressure gases.* Journal of Polymer Science Part B: Polymer Physics, 1998. **36**(6): p. 977-982.

[19] Zhang, Z. and Y.P. Handa. *In-situ measurements of the plasticization of polymers by gases using a high-pressure DSC*. 1997.

[20] Condo, P.D. and K.P. Johnston, *In situ measurement of the glass transition temperature of polymers with compressed fluid diluents.* Journal of Polymer Science Part B: Polymer Physics, 1994. **32**(3): p. 523-533.

[21] O'Neill, M.L. and Y.P. Handa. *Plasticization of polystyrene by high pressure gases: A calorimetric study*. 1994.

[22] Sanders, E.S., S.M. Jordan, and R. Subramanian, *Penetrant-plasticized permeation in polymethylmethacrylate.* Journal of Membrane Science, 1992. **74**(1-2): p. 29-36.

[23] Wessling, M., et al., *Plasticization of gas separation membranes.* Gas Separation & Purification, 1991. **5**(4): p. 222-228.

[24] Ogieglo, W., et al., *Temperature-induced transition of the diffusion mechanism of n-hexane in ultra-thin polystyrene films, resolved by in-situ Spectroscopic Ellipsometry.* Polymer, 2013. **54**(1): p. 341-348.

[25] Keddie, J.L., R.A.L. Jones, and R.A. Cory, *Interface and surface effects on the glass-transition temperature in thin polymer films.* Faraday Discussions, 1994. **98**: p. 219-230.

[26] Huang, Y. and D.R. Paul, *Physical aging of thin glassy polymer films monitored by gas permeability.* Polymer, 2004. **45**(25): p. 8377-8393.

[27] Herzinger, C.M., et al., *Ellipsometric determination of optical constants for silicon and thermally grown silicon dioxide via a multi-sample, multi-wavelength, multi-angle investigation.* Journal of Applied Physics, 1998. **83**(6): p. 3323-3336.

[28] Ogieglo, W., et al., *n-Hexane induced swelling of thin PDMS films under non-equilibrium nanofiltration permeation conditions, resolved by spectroscopic ellipsometry.* Journal of Membrane Science, 2013. **437**(0): p. 313-323.

[29] Wang, B.-G., T. Yamaguchi, and S.-I. Nakao, *Solvent diffusion in amorphous glassy polymers.* Journal of Polymer Science Part B: Polymer Physics, 2000. **38**(6): p. 846-856.

[30] Artsis, M., et al., *Diffusion of organic diluents into ethyl cellulose.* European Polymer Journal, 1972. **8**(4): p. 613-626.

[31] Vrentas, J.S. and C.M. Vrentas, *Sorption in glassy polymers.* Macromolecules, 1991. **24**(9): p. 2404-2412.

[32] Leibler, L. and K. Sekimoto, *On the sorption of gases and liquids in glassy polymers.* Macromolecules, 1993. **26**(25): p. 6937-6939.

[33] Richardson, H., M. Sferrazza, and J.L. Keddie, *Influence of the glass transition on solvent loss from spin-cast glassy polymer thin films.* The European Physical Journal E: Soft Matter and Biological Physics, 2003. **12**(0): p. 87-91.

[34] Flory, P.J., *Principles of Polymer Chemistry*1953: Cornell University Press, Ithaca, New York.

[35] Kleideiter, G., M.D. Lechner, and W. Knoll, *Pressure dependence of thickness and refractive index of thin PMMA-films investigated by surface plasmon and optical waveguide spectroscopy.* Macromolecular Chemistry and Physics, 1999. **200**(5): p. 1028-1033.

Chapter 11

Outlook

11.1. Introduction

There remain many interesting research questions regarding fundamentals of physics of thin polymer films interacting with penetrants, that have been unexplored in this work, or have only been partially addressed. This chapter provides a brief outline of possible new research topics and directions, as is schematically depicted in Figure 11.1. Examples are presented for entirely new venues, follow-up studies based on the insights generated in this thesis, and potentially attractive combinations of *in-situ* ellipsometry with other complementary techniques. The studies described in this chapter focus mostly on model systems. Extending such studies to practically applied materials, for instance in membrane technology, might open even larger unexplored areas. Most of the content of this chapter is supported by a significant amount of preliminary results and observations.

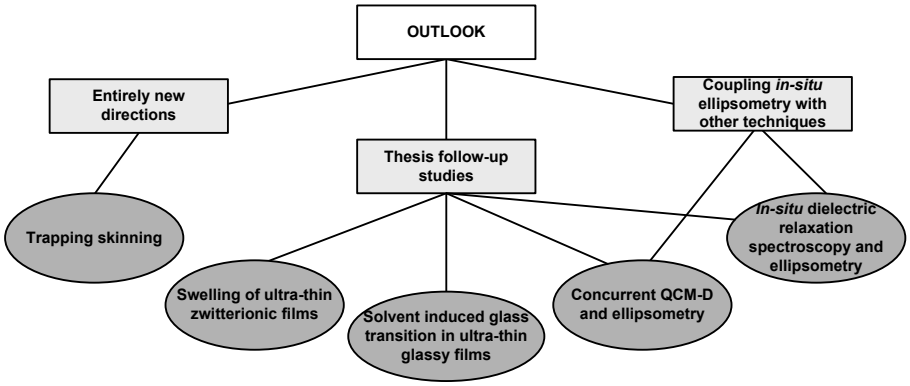

Figure 11.1 Scheme of the Outlook chapter with division into 3 interesting research directions

11.2. Trapping skinning

Although several research groups have investigated drying processes in thin and ultra thin supported glassy films with *in-situ* spectroscopic ellipsometry [1-4] (this subject is reviewed as part of Chapter 1 of this Thesis), there are a number of questions which remain unaddressed. In particular, the solvent evaporation from a glassy polymer film was reported to reveal a phenomenon called trapping skinning [5-8]. This phenomenon is a manifestation of anomalous solvent diffusion out of the drying polymer and is somewhat similar to the progress of the penetrant wave in Case II diffusion (Chapters 2 and 3), but occurring in the opposite direction. Counter intuitively, it has been observed that application of more vigorous drying conditions (faster drying gas flow, higher temperature of drying) resulted in larger solvent retention as compared when less intense drying was employed, Figure 11.2.

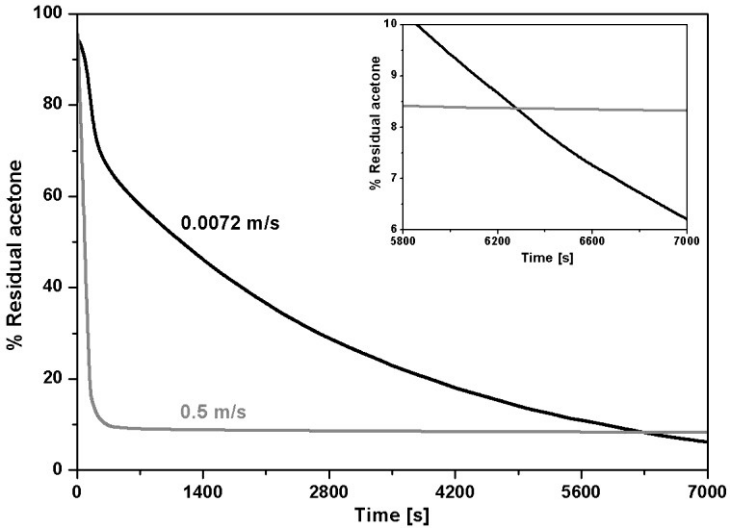

Figure 11.2 Residual acetone content in the thin PMMA coating at low gas velocity (0.0072 m/s) and high gas velocity (0.50 m/s). The crossover of the two curves indicates trapping skinning. With permission [8].

This phenomenon occurs only in glassy polymers, or more precisely, in polymers which dry glass transition lies above drying temperature. As can be seen from Figure 11.2, the higher drying gas velocity results in much faster initial drying (large drop within the first 100 – 200 s), but in the longer timescales the residual solvent content is higher, as compared with the lower drying gas velocity. It is easy to see a practical consequence of such behavior: if the aim is to obtain a polymer films with a low final residual solvent content, the gas velocity should not be too high. The explanation of this phenomenon is relatively well accepted and is shown schematically in Figure 11.3.

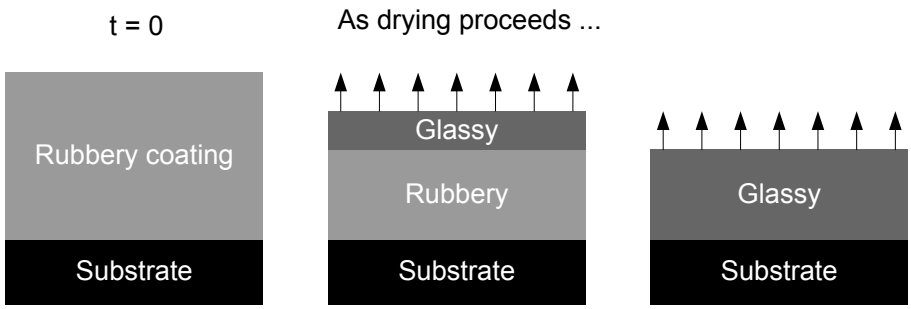

Figure 11.3 Explanation of the trapping skinning phenomenon; see text for details of the process. With permission from [5]. Copyright 2001 American Chemical Society

When the polymer solution starts to dry, initially it still behaves as a liquid. When more solvent evaporates from the film the polymer concentration increases, in particular close to the outer surface of the film. The concentration of polymer at this interface is dictated by rate of evaporation and the rate at which solvent is supplied from the film to the interfacial region. For a sufficiently large rate of solvent evaporation the glass transition occurs in the outer region of the film. In this glassy skin the solvent diffusion coefficient is several orders of magnitude lower than in the remaining rubbery inner part. This creates a barrier for the solvent removal from the rest of the film and gives rise to the name of the phenomenon: trapping skinning. As a result the overall concentration of solvent in the film remains relatively high. When the solvent evaporation rate is lower the formation of a trapping skin is less pronounced allowing a sustained removal of solvent. This leads to a lower residual solvent content in the film after long drying times.

The residual solvent content in thin glassy polymers at the end of drying was studied as a function of polymer film thickness (down to about 15 nm) by Richardson et al. [1, 2]. However, to date there are no studies focusing on the details of the glassy skin development in the very early stages of solvent evaporation for technologically important thickness region (below ~150 nm). This is partly because for such studies very high temporal resolution, as well as very high precision and accuracy are required. The recent progress of *in-situ* spectroscopic ellipsometry instrumentation may allow such studies. In the following, several illustrative preliminary results are presented for the model system: polystyrene – n-heptane.

To be able to gain information on the refractive index changes with distinction of the skin and inner parts of the film, a Two-layer skin model is proposed, Figure 11.4. In this optical model, instead of the usual uniform index distribution, the film thickness is divided into two parts: the outer skin layer, which always represents the first 20% of the total film thickness, and the remaining 80% of the film constituting the inner part. This ratio is arbitrary and is chosen so that the skin layer

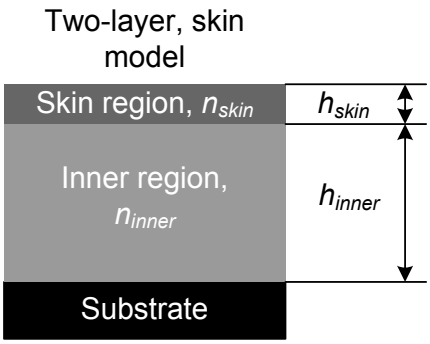

Figure 11.4 Two-layer, skin model used in trapping skinning investigations

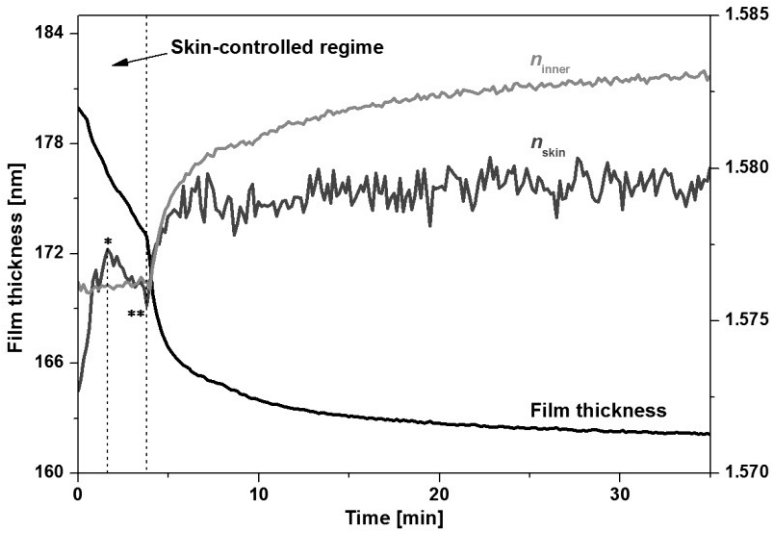

Figure 11.5 Film thickness and refractive indices of the skin and inner layers of the polystyrene film during drying from n-heptane

is of about 30-40 nm for a 160 nm dry film thickness. This is necessary to be able to independently fit refractive indices in the top and bottom parts of the film with reasonable accuracy, thereby generating spacial optical density distribution data.

However, such treatment may lead to some inconsistencies, especially because it can well be expected that the skin layer could be much thinner than 30-40 nm.

Figure 11.5 shows the dynamic thickness variation during drying of about 160 nm (dry thickness) polystyrene film together with refractive index data obtained by the Two-layer skin model. Before the drying experiment the film was completely swollen with n-heptane and thermally equilibrated slightly above room temperature. The swollen system was rubbery, which was confirmed by the observation of Case II diffusion during swelling, as thoroughly discussed in Chapters 2 and 3 of this Thesis. The thickness variation is somewhat surprising, because before the exponential-like period of solvent removal (after ~3.8 minutes), at first a linear decrease is observed. This general feature has not been seen in the literature before, but is found to be reproducible for at least 5 measurements done for different dry thicknesses and drying gas flows. The interpretation of such behavior is aided by the information gained from the refractive index dynamics. It suggests that indeed a glassy skin is being formed at the very beginning of drying, in the "Skin-controlled regime", that slows down diffusion of the solvent from beneath the skin. In this Skin-controlled regime the refractive index of the bottom of the film (n_{inner}) stays approximately the same – indicating the trapping of the solvent, and the changes of the index occur mainly in the top, skin layer (n_{skin}). In particular the very sharp index increase within the first 1.7 minutes indicates

drastic solvent removal predominantly at the top of the film. The index of this skin region rises above the one from the bottom part around 1.7 minute, indicated with *, as expected if the skin possessed a lower concentration of the solvent.

It is surprising, that after the initial linear regime the drying process accelerates when it enters the exponential regime, indicated with **. It could be possibly explained by realizing that the skin formation, that occurs earlier, leads to a very steep concentration gradient: inner film part is still very significantly swollen with the solvent, whereas the skin remains practically dry. This situation is quite unstable and when the concentration gradient reaches a certain threshold value the solvent from the inner part is forced to diffuse towards the skin. This could explain the n_{skin} drop between 1.7 and 3.8 minutes, approximately between * and **. This forced swelling of the skin weakens its trapping ability and allows more rapid removal of the solvent – onset of the faster exponential-like period at 3.8 minutes, **. Afterwards, it is apparent that a gradient in the refractive index is developed, with n_{skin} being lower than n_{inner}. This suggests that in this already quite dry film the inner part is significantly denser than the outer part (where the dense skin was previously formed).

It may be speculated that this inversion of the density gradient can be related to the different non-equilibrium status in the two parts. For instance, in the initial stages of drying the inner part was plasticized much more than the outer part, as it possessed more solvent. The inner part could, therefore, relax towards the denser, closer to equilibrium state by a process of physical aging. The outer part was effectively frozen in, or quenched rapidly during skin formation and its status is much further from equilibrium (less dense).

Although definitely not fully consistent yet, and limited by the assumptions of the used optical model, these results show an example of an unprecedented richness of information that can be gained when advanced optical modeling is utilized. Moreover, the results may be used to probe and tailor the morphology of the dried films with potential practical consequences. For instance, the graded index profiles suggest that the density of the as dried film is highly non uniform. This could lead to different rates of, for instance, physical aging of the formed film, depending on the position along its normal. This can have interesting consequences for the microscale morphology, and in turn for barrier or membrane properties of such prepared layers, with a possibility of some fine tuning by choosing different drying conditions. In any case, there remains significant room for exploration, particularly for more practical or promising, quickly aging membrane polymers like PPO or PTMSP.

11.3. Swelling of ultra-thin zwitterionic films

Chapters 6 and 7 dealt with electrolyte swelling of zwitterionic co-polymer films based on n-butyl acrylate and sulfobetaine. This material is known to possess

interesting anti-fouling properties that can be possibly utilized in membrane surface modification. Chapter 6 described the advanced optical modeling of the relatively thick (~250 – 800 nm) films during swelling with a particular focus on the observation of emerging and vanishing optical anisotropy within the films. This optical anisotropy was explained in terms of the swelling-induced partial orientation of the zwitterionic polymer side-chains related to the formation of charge-based cross-links. The last figure of that chapter, repeated here as Figure 11.6, presented the dynamic results obtained with a tri-layer anisotropic model that allowed tracking changes in the optical anisotropy of the layer, Δn, as a function of the distance from the substrate. Interestingly, it was found that the largest optical anisotropy existed closest to the substrate. This could be interpreted as a severe perturbation of the polymer chain arrangement by the proximity of the substrate onto which the polymer was physically (possibly also ionically) immobilized.

This pronounced nano-confinement effect was only touched upon in Chapter 6 but deserves more detailed investigation. The reason is that the interplay of enthalpic and entropic effects (charge repulsion/attraction and chain stretching) in zwitterionic films has been suggested to be responsible for the hindrance in protein adsorption, relevant in turn for anti-fouling. The perturbation of the chain morphology in such films caused by the substrate proximity may have important consequences in membrane technology where the utilization of one or another substrate is usually unavoidable.

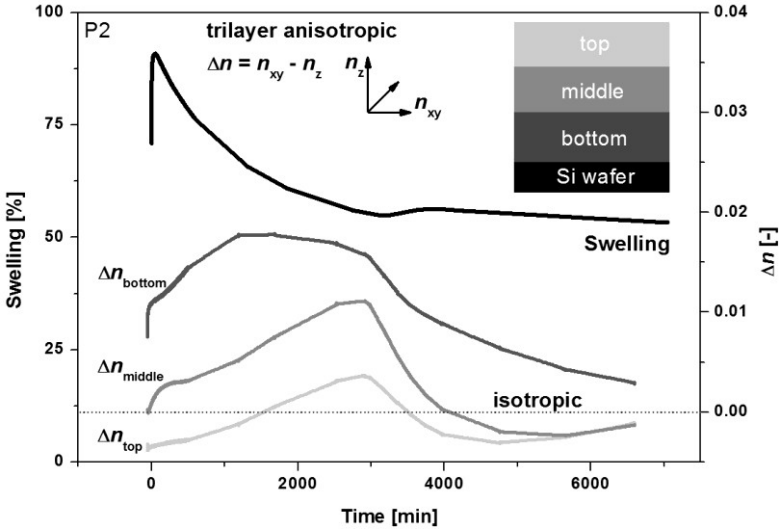

Figure 11.6 Tri-layer anisotropic optical model for the swelling of a ~400 nm zwitterionic film, see Chapter 6. With this model the optical anisotropy, Δn, as a function of the distance from the substrate is studied. The results indicate largest anisotropy in the region closest to the supporting silicon wafer (bottom layer).

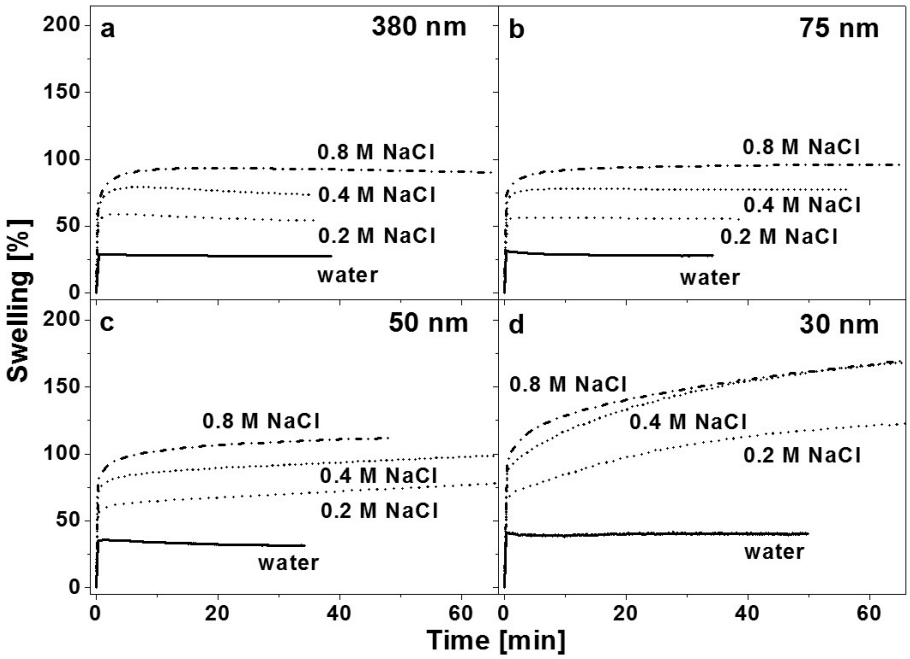

Figure 11.7 Swelling of zwitterionic films in pure water, 0.2, 0.4 and 0.8 M NaCl for various dry film thicknesses

A range of interesting preliminary results on this subject is available. Figure 11.7 shows swelling of the same zwitterionic films in pure water, 0.2, 0.4 and 0.8 M NaCl as a function of dry film thickness. It can be seen that down to 75 nm dry film thickness all swelling curves are quite similar. However, for films thinner than 75 nm already significant deviations from the bulk behavior are found. These deviations are related both to the "equilibrium" swelling of the films as well as the dynamic response. In particular, the thinnest films (30 nm) seem to swell much more and show much slower secondary dynamics (processes following the initial fast Fickian response). The behavior of the thinnest films is presented in Figure 11.8 over much larger timescales (~17 hours) and is indeed drastically different than the bulk. To our knowledge these are one the most pronounced deviations from bulk behavior ever observed in non-covalently attached (spin-coated) films.

For the highest concentrations of NaCl (0.8 and 1 M) the swelling reaches above 200% indicating an almost brush-like stretch of the polymer films. Such a configuration may result in different nature of zwitterionic interactions within the polymer as compared with bulk, which is swollen up to 100% at most. In addition, whereas the thickness relaxation in bulk starts within the first 1-2 hours of swelling, in the case of the 30 nm films much later (0.8 M) or no relaxation (0.2 and 1 M) is found. The explanation might be related to the substrate itself, in

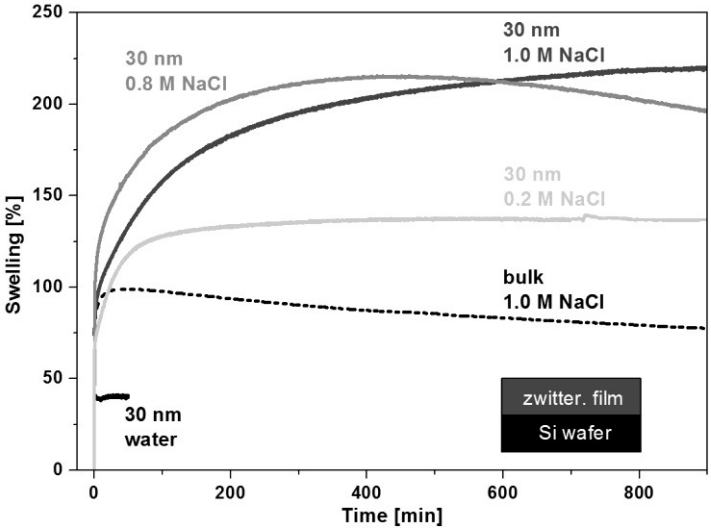

Figure 11.8 Swelling for 30 nm films in various molar concentrations of $NaCl_{aq}$. The dashed line shows swelling of bulk films (~380 nm) in 1 M NaCl.

particular, to its charge and electrostatic screening depth penetrating the film and the electrolyte solution. Impact of changing the solution pH may need to be investigated as well. Overall, more work is required to better understand these phenomena, as well as to study their ultimate consequences for a modified membrane operation.

11.4. Solvent induced glass transition in ultra-thin glassy films

In Chapter 10 of the Thesis, effects of time, temperature and pressure in the vicinity of glass transition induced by the solvent are investigated. This has been done for a single thickness (above 100 nm) of polystyrene. By analyzing the response of the swollen polymer to the gradual decrease of temperature from rubbery to glassy states a region where a curvature change, or a kink, in swollen thickness occurred. In this region also the dynamics of the swollen polymer were possible to be observed on the same timescale as the timescale of the experiment, itself exposing the viscoelastic region. The peak of the dynamic response seemed to coincide with the curvature change characteristic for the glass transition.

These measurements were done for relatively thick polystyrene films: in the thickness region where nano-confinement effects (dependence of system properties on thickness alone [1, 3, 9-13]) are not dominating and the more or less bulk response is visible. Given, however, the substantial experimental evidence from literature pointing to significant changes in glass transition and physical aging characteristics of thinner films, as discussed in the introduction of Chapter 3, it

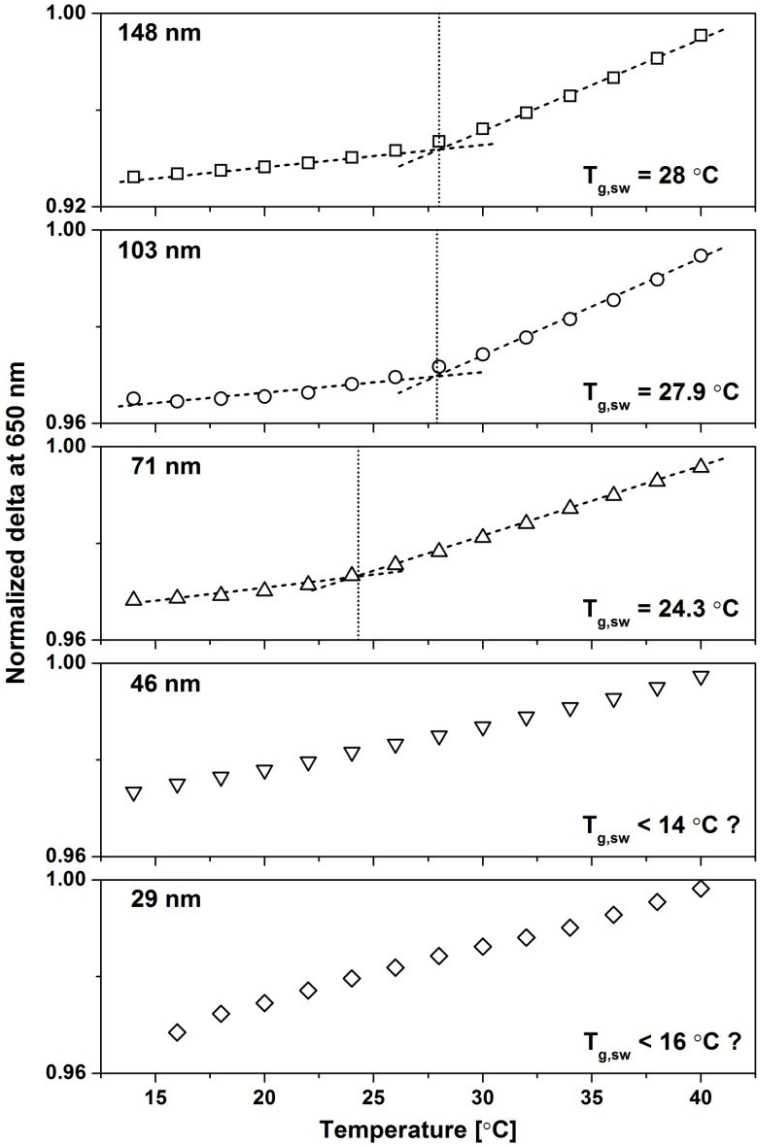

Figure 11.9 Normalized delta parameter changes at 650 nm for polystyrene films with variable dry thickness swollen with n-octane at 42 °C and subjected to stepwise temperature decrease. Down to thickness of about 71 nm the curvature change, interpreted as T_g in swollen system, is distinct and shifts towards lower temperatures. Below 71 nm the curvature change point no longer visible.

seems very interesting to examine thinner films as well. In polystyrene films on silicon wafer, in general, reductions of the apparent glass transition temperature are

reported with reduction of film thickness below about 100 nm (sometimes below 50 nm). Results of Chapter 3 suggested, that at the outer film interface a region of about 14 nm exists that swells very fast in the solvent, arguably possessing much greater chain dynamics than the rest of the film. It could be, therefore, expected that with decreasing film thickness this region may play an increasing role in dictating the overall dynamic response of the films. This could manifest itself in the curvature change shifts.

Figure 11.9 shows the preliminary results of experiments where the glass transition in polystyrene – n-octane system is investigated as a function of dry film thickness. The experiments were conducted in exactly the same way as the ones presented in Chapter 10. The films were first exposed to solvent at 42 °C and equilibrated to define starting point in the rubbery region of the system. Afterwards, the stepwise temperature decrease protocol (2 °C steps lasting 15 minutes, and 85 minutes of constant temperature) was started and ellipsometric parameters were recorded continuously. As can be seen from the figure, the curvature changes in the normalized delta parameter are quite distinct above 71 nm films. The glass transition temperature associated with the kink is the same for 148 and 100 nm films, corresponding to bulk-like behavior, but drops at 71 nm by a few degrees. Below 71 nm the kink is not possible to be observed in the probed temperature range. This could indicate that the glass transition temperature shifted outside of this range and could be probably found below about 14 °C. This would indicate indeed a pronounced nano-confinement effect with deviation from bulk value of $T_{g,sw}$ of at least 14 °C starting below about 50 nm of dry thickness. Because penetrant diffusion coefficients are known to severely depend on the degree of matrix plasticization, these drops of the apparent glass transition related to thickness variation alone may have pronounced consequences for the permeability of thin film membranes. More experiments in a broader temperature range should clarify this phenomenon and the analysis of the dynamics of the system (slope of thickness or delta parameter versus time) may possibly lead to further interesting insights.

11.5. Concurrent QCM-D and ellipsometry

As discussed in Chapter 1 of the Thesis ellipsometry can be successfully complemented with other *in-situ* techniques. In particular, the concurrent ellipsometry and QCM-D experiments yield interesting complementary information. This is because ellipsometry is highly compatible with typical QCM-D samples comprising a non-transparent layer of metal electrode, usually gold, on top of a quartz crystal. This compatibility is a big advantage as it avoids problems with assessing whether samples of the same material but dedicated for different techniques behave equivalently due to preparation differences. Currently, both techniques allow for very high temporal resolutions on the order of a few seconds

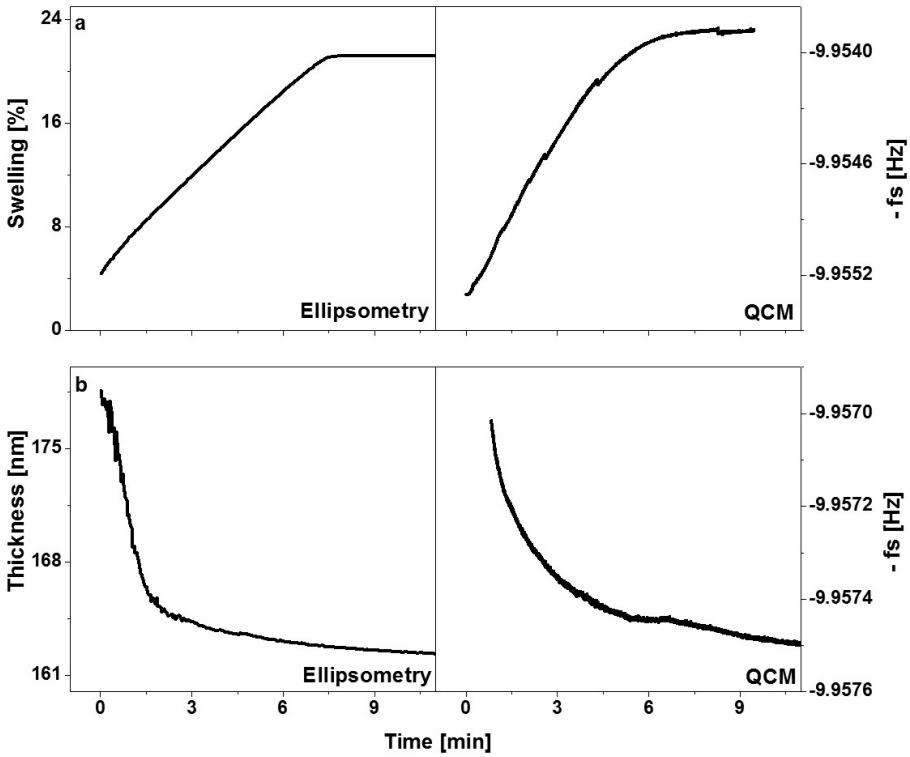

Figure 11.10 Ellipsometry and QCM experimental data for swelling (a) and drying (b) processes in the case of thin polystyrene films and n-hexane penetrant. The data was collected non-concurrently: ellipsometry and QCM were done on separate samples

per full scan and work in fluid environments. Figure 11.10 shows two examples of the experimental ellipsometry and QCM data collected for the same processes: Case II diffusion of n-hexane into polystyrene (a) and subsequent drying of the swollen layer (b). The data in the figure were collected non-concurrently and on different samples.

As can be seen in Figure 11.10 for both experiments the thickness evolution (ellipsometry) and frequency shifts (QCM), corresponding to changes in mass of the films, are in agreement with each other and show the same trends. The complementarity here is based on the fact that ellipsometry is sensitive to the film thickness and refractive index. Actual changes in mass are not possible to be determined directly and require application of effective medium approximation (EMA) models with many assumptions about volume additivity and molar volumes (or densities) of the components in a mixture. On the other hand QCM response is much more directly related to sample mass changes because these changes influence the resonant frequency of the oscillating quartz crystal to which sample is

attached. By combining the two techniques in a concurrent way it would be possible, for instance, to deduce whether the response of the sample regarding its optical density and thickness corresponds exactly to its mass changes. This may be an interesting question particularly in the research related to glassy polymers which are known to possess unrelaxed excess free volume (voids) within the structure. The voids within the polymer are present below glass transition temperature and effectively reduce the polymer matrix refractive index below its equilibrium value. When a plasticizing penetrant dissolves in the glassy network, partial or complete relaxation of the excess free volume may occur and the polymer matrix index of the resulting plasticized network is difficult to determine. This in turn hinders the precise determination of the penetrant mass uptake with an EMA. All these issues may be significantly improved when the more direct mass sorption data obtained by the QCM is considered. In this case there is no need to know the optical properties of the matrix. The combination of the two techniques can be particularly useful also in drying studies, Figure 11.10b, because the structural polymer relaxation, thickness decrease, during drying is related to solvent loss and physical aging occurring simultaneously. Ellipsometry alone cannot resolve these two processes [3]. Separation of the effects of solvent loss and physical aging can be obtained, when ellipsometry is combined with the QCM. This is because QCM is only measuring the former process and is non-sensitive to the latter.

The usefulness of ellipsometry-QCM combination can be further expanded when dissipation mode QCM (QCM-D) is used. In this technique the dissipation of the resonant energy of the crystal is measured, from which the changes in viscoelastic properties of the analyzed layers can be obtained. This information may be particularly useful in studies of dynamic glass transitions induced by penetrants. It is known that during glass transition the mechanical properties of the polymer change drastically, for instance the Young's modulus drops by a few orders of magnitude. In the vicinity of the transition itself the polymer may display viscoelastic behavior characterized with pronounced changes in energy dissipation. These phenomena, though widely studied in dry polymers, have been rarely investigated in polymer – penetrant systems.

11.6. *In-situ* dielectric relaxation spectroscopy and ellipsometry

Dielectric relaxation spectroscopy (DRS) measures the dielectric properties of a medium as a function of frequency of the external electric field. From the dielectric spectrum the dynamics of the molecules can be determined [14-18]. The property determined in this method is the complex dielectric permittivity, ε''. Its real part carries information about energy storage, whereas the imaginary part describes energy dissipation. The peak in the dissipation corresponds to a particular type of molecular movement. In polymers these relaxations can be related to cooperative motions at glass transition or movements of smaller fragments like side chains. Depending on experimental temperature certain relaxations are active and others

deactivate. Thus a temperature scan can easily reveal a region where glass transition occurs. The dielectric relaxation spectrum will also change if a small molecule species is dissolved in the polymer. For example plasticization of the polymer matrix may enhance the mobility of the chains and contribute to an effective reduction of glass transition temperature.

The possibility to observe effects of penetrants on the relaxational phenomena in very thin films on the order of a few nanometers makes DRS highly complementary to ellipsometry. However, there are little studies that address such topics [19], and almost none for thin and ultra-thin films relevant in membrane applications.

Complementation of ellipsometry by DRS could be particularly useful in studies where the polymer – penetrant mixture is close to its glass transition. This is because, as seen in Chapters 2, 5 and 10 of this Thesis, the dynamic behavior of swollen polymers close to glass transition may be significantly different than the behavior of dry polymeric films. For example, it would be very interesting to investigate the details of chain relaxation occurring during secondary relaxations of the CO_2-plasticized polystyrene films just below and at penetrant induced glass transition, Chapter 5. Another interesting study would focus on the change in dynamic relaxation of the arrested swollen polymer matrix during temperature reduction below the glass transition, Chapter 10. Such studies would have important consequences for the transport properties of plasticized membranes, operating close to glass transition of the separating material, both for gaseous (gas separation) and liquid penetrants (aqueous nanofiltration and solvent resistant nanofiltration).

11.6. References

[1] Richardson, H., et al., *Thickness dependence of structural relaxation in spin-cast, glassy polymer thin films.* Physical Review E - Statistical, Nonlinear, and Soft Matter Physics, 2004. **70**(5 1): p. 051805-1-051805-8.

[2] Richardson, H., M. Sferrazza, and J.L. Keddie, *Influence of the glass transition on solvent loss from spin-cast glassy polymer thin films.* The European Physical Journal E: Soft Matter and Biological Physics, 2003. **12**(0): p. 87-91.

[3] López García, Í., J.L. Keddie, and M. Sferrazza, *Probing the early stages of solvent evaporation and relaxation in solvent-cast polymer thin films by spectroscopic ellipsometry.* Surface and Interface Analysis, 2011. **43**(11): p. 1448-1452.

[4] Atarashi, H., et al., *Uptake of water in as-spun poly (methyl methacrylate) thin films.* RSC Adv., 2013. **3**(11): p. 3516-3519.

[5] Hadj Romdhane, I., et al., *Drying of Glassy Polymer Films.* Industrial & Engineering Chemistry Research, 2001. **40**(14): p. 3065-3075.

[6] Vinjamur, M. and R.A. Cairncross, *Non-Fickian nonisothermal model for drying of polymer coatings.* AIChE Journal, 2002. **48**(11): p. 2444-2458.

[7] Vinjamur, M. and R.A. Cairncross, *Guidelines for dryer design based on results from non-Fickian model.* Journal of Applied Polymer Science, 2003. **87**(3): p. 477-486.

[8] Vinjamur, M. and R.A. Cairncross, *Experimental investigations of trapping skinning.* Journal of Applied Polymer Science, 2002. **83**(10): p. 2269-2273.

[9] Keddie, J.L., R.A.L. Jones, and R.A. Cory, *Interface and surface effects on the glass-transition temperature in thin polymer films.* Faraday Discussions, 1994. **98**: p. 219-230.

[10] Rowe, B.W., B.D. Freeman, and D.R. Paul, *Physical aging of ultrathin glassy polymer films tracked by gas permeability.* Polymer, 2009. **50**(23): p. 5565-5575.

[11] Horn, N.R. and D.R. Paul, *Carbon Dioxide Sorption and Plasticization of Thin Glassy Polymer Films Tracked by Optical Methods.* Macromolecules, 2012.

[12] Pham, J.Q., K.P. Johnston, and P.F. Green, *Retrograde Vitrification in CO2/Polystyrene Thin Films.* The Journal of Physical Chemistry B, 2004. **108**(11): p. 3457-3461.

[13] Pham, J.Q., et al., *Pressure, Temperature, and Thickness Dependence of CO_{2}-Induced Devitrification of Polymer Films.* Physical Review Letters, 2003. **91**(17): p. 175503.

[14] van den Berg, O., et al., *Dielectric and Fluorescent Probes To Investigate Glass Transition, Melt, and Crystallization in Polyolefins.* Macromolecules, 2004. **37**(7): p. 2460-2470.

[15] Wübbenhorst, M., C.A. Murray, and J.R. Dutcher, *Dielectric relaxations in ultrathin isotactic PMMA films and PS-PMMA-PS trilayer films.* The European Physical Journal E: Soft Matter and Biological Physics, 2003. **12**(0): p. 109-112.

[16] Wubbenhorst, M., et al. *Dielectric relaxations in ultra-thin films of PMMA: assessing the length scale of cooperativity in the dynamic glass transition*. in *Electrets, 2002. ISE 11. Proceedings. 11th International Symposium on*. 2002.

[17] van Turnhout, J. and M. Wübbenhorst, *Analysis of complex dielectric spectra. II: Evaluation of the activation energy landscape by differential sampling.* Journal of Non-Crystalline Solids, 2002. **305**(1-3): p. 50-58.

[18] Wübbenhorst, M. and J. van Turnhout, *Analysis of complex dielectric spectra. I. One-dimensional derivative techniques and three-dimensional modelling.* Journal of Non-Crystalline Solids, 2002. **305**(1-3): p. 40-49.

[19] Kamiya, Y., K. Mizoguchi, and Y. Naito, *A dielectric relaxation study of plasticization of poly(ethyl methacrylate) by carbon dioxide.* Journal of Polymer Science Part B: Polymer Physics, 1990. **28**(11): p. 1955-1964.

Thesis summary

The properties of a thin polymer film can be significantly affected by the presence of a penetrant. It is also known that the behavior of ultra-thin polymer films (<100 nm) may deviate from the bulk behavior. This sole impact of film thickness reduction is often referred to as a nano-confinement effect. Superposition of the penetrant and the nano-confinement can have potential implications for many technological applications, such as protective and functional coatings, sensors, microelectronics, surface modification and membrane separations. *In-situ* ellipsometry is a powerful technique for the characterization a films in contact with penetrants, due to its high precision and non-invasive character. This thesis explores the applicability of the technique to study fundamentals of various physical phenomena occurring in thin and ultra-thin polymer films in the presence of interacting penetrants.

The introductory **chapter 1** reviews the work done with *in-situ* ellipsometry in the field of polymer films interacting with various penetrants. The chapter addresses a variety of topics, covering instrumental aspects of *in-situ* studies, approaches to data analysis and optical models, reported precision and repeatability, the polymer-penetrant systems that have been studied, the kind of information that has been extracted, and other *in-situ* techniques that have been combined with ellipsometry. Various examples are presented to illustrate different practical approaches, the consequences of the optical properties of the ambient, and the various ways that have been employed to bring polymer films in contact with a penetrant, ranging from simple *ex-situ*-like configurations (i.e. drying studies) to complex high pressure cells. The versatility of *in-situ* ellipsometry is demonstrated by examples of the distinctive phenomena studied, such as film dilation, penetrant diffusion mechanisms, film degradation, electrochemical processes, and the broad variety of polymer penetrant systems studied (glassy and rubbery polymers, multilayer stacks, etc.). An outlook is given on possible future trends.

Chapter 2 describes a study on a transition in the diffusion mechanism of liquid n-hexane in thin PS films. It is shown that in a very narrow temperature range around room temperature, from 16 - 28 °C, the process changes characteristics from simultaneously occurring Fickian diffusion and polymer relaxation to purely relaxation limited Case II diffusion. The transition is shown to influence the kinetics of the process dramatically with the timescales of the processes changing from several hours at 16 °C to a few minutes at 28 °C. Ellipsometry is shown to be well capable of tracking the progress of a sharp penetrant wave accompanying the Case II process with a very high spectral resolution. Important aspects of appropriate dynamic optical modeling are addressed. In particular, the utilization of

the simplest, uniform optical model is shown to be inadequate and a more complex, two-layer model is required to resolve the process.

In **Chapter 3** the detailed optical modeling approach of the Case II diffusion, developed in **Chapter 2**, is applied to probe superimposed effects of nano-confinement and penetrant in ultra thin PS films. It is shown that a region of about 14±3 nm exists in the outer surface of these glassy films that is swollen almost instantaneously upon contact with the penetrant. After this interfacial region is swollen, a much slower front diffusion follows. The diffusion temperature and physical aging are shown not to influence the instantaneously swelling region but do influence the subsequent front progression dynamics in the remaining volume of the films. These findings may have significant implications for the areas where small molecule penetrants diffuse through ultra thin glassy polymer layers, i.e. membrane separations.

The very high precision of *in-situ* spectroscopic ellipsometry is utilized in **Chapter 4** to develop a procedure to accurately determine penetrant volume fraction in thin swollen glassy polymer films. The method is based on a Bruggeman Effective Medium Approximation and takes account for the relaxation of non-equilibrium Excess Fractional Free Volume (EFFV) of a glassy polymer upon sorption above glass transition temperature of the polymer – penetrant mixture. The newly developed method is compared to those not taking account for the EFFV relaxation but frequently applied in literature. The errors in penetrant volume fractions obtained when relaxation of EFFV is not accounted for are shown to be especially large for membrane-related high EFFV polymers, such as poly[1-(trimethylsilyl)-1-propyne] (PTMSP).

Chapter 5 focuses on the sorption and relaxation processes that occur in the vicinity of penetrant induced glass transition, P_g. It is shown for the first time, that although P_g is phenomenologically similar to thermally induced glass transition, T_g, significant differences in the dynamic behavior exist. These differences are related to the much more pronounced polymer matrix deformation by the sorbing penetrant around P_g that seems to activate complex long term chain relaxation processes. The dilation curvature alteration cannot always be straightforwardly treated as an indication of glass transition, as done in the case of the T_g. Such a slope change in the case of the P_g, is a complex consequence of mutually influencing sorption and relaxation phenomena, and is very much affected by the sample conditioning history. These findings are anticipated to contribute to better understanding of the complex plasticization phenomena in ultra-thin membranes.

Chapter 6 and **chapter 7** describe dynamic *in-situ* spectroscopic ellipsometry studies on thin films of zwitterionic polymers based on sulfobetaine methacrylate and n-butylacrylate. These materials represent an interesting class of polymers with a large potential in reduction of biofouling in ultrafiltration membranes. The **chapter 6** focuses on the characterization of the overshoot dynamic swelling

response in the material upon exposure to 1 M NaCl solution. Emerging and vanishing optical anisotropy within the polymer films is reported. This is rationalized via the orientations of the polymer backbone and zwitterionic chains as a result of swelling and relaxation in the presence of the screening electrolyte. The **chapter 7** explores the effects of different salts and their concentration on the swelling the same polymer. An antipolyelectrolyte effect is found, as indicated by increased swelling of the films in response to increasing salt concentrations. The work provides meaningful insights on the behavior of zwitterionic copolymer films for applications such as membrane filtration with different salts and ionic strengths.

In membrane technology often composite membranes consisting of a porous substrate and a thin separating film are employed. Application of ellipsometry to such systems has been severely limited by the size of the substrate roughness and porosity. These surface features resulted in unwanted probing light scattering effects. In **chapter 8** appropriate optical models that allow *in-situ* ellipsometry analysis of composite membranes are developed. The models consider the surface roughness of the support as a distinct, graded density layer and are shown to be applicable to composite membranes with relatively thick, ~ 1 μm, separating layers.

The optical models developed in **chapter 8** are utilized for the non-equilibrium, high pressure permeation investigation of thin PDMS membranes in **chapter 9**. The newly developed high pressure *in-situ* ellipsometry chamber is shown to be capable of investigating the membrane behavior in conditions by far exceeding the ones found in nanofiltration. It is found that the confinement of the films to the substrate implies the necessity of elastic deformation network correction. In the pressurized swollen film the thickness and refractive index are found to be independent of pressure in the range of 1 – 100 bar suggesting that the molar volumes of the penetrant in the liquid and sorbed phases are not significantly different. When a pressure difference over the membrane is applied and the solvent is allowed to permeate, a progressing reduction in thickness of the membrane is observed with increasing upstream pressure. The derived concentrations of n-hexane at the interface between thin film and support, at the permeate side, are in excellent agreement with values calculated using the Solution-Diffusion model. This implies that in-situ spectroscopic ellipsometry allows quantification of the contribution of Solution-Diffusion to mixed mode transport through composite membranes.

Chapter 10 extends the application of variable temperature and pressure ellipsometry to supported glassy films. In this chapter the effect of time, temperature, and pressure in the vicinity of the solvent induced glass transition are studied. Dynamic temperature scans reveal the pronounced changes in both equilibrium and kinetic properties of the system upon vitrification. The phenomenon of kinetically arrested swollen matrix is observed and explained in

terms of the significant changes in the penetrant diffusion coefficient and the simultaneous emergence of the glass compression energetic barrier below the glass transition of the polymer – penetrant mixture. The PS – n-decane system shows no measurable compression, in a sense of the free volume reduction, when exposed to hydrostatic pressures up to 50 bar neither above or below its glass transition temperature. A small, but well resolvable, compression is shown to occur in dry polystyrene and is correlated to the partial relaxation of the excess fractional free volume. The results are of importance for membrane technology, where swollen glassy selective layers are operated under high pressures to provide for molecular transport by solution-diffusion.

Chapter 11 provides an outlook of the remaining interesting research questions that could be pursued. The examples are divided into several categories, highlighting the entirely new directions, follow-up studies and attempts couple *in-situ* ellipsometry with other techniques. Most of the content of this chapter is supported by a significant amount of preliminary results and observations.

Samenvatting

De eigenschappen van een dunne polymeerlaag kunnen sterk worden beïnvloed door de aanwezigheid van een penetrant. Het is ook bekend dat het gedrag van ultradunne polymeerlagen (< 100 nm) kan afwijken van het bulkgedrag. Veranderingen die uitsluitend ten gevolge van een verandering in de dikte van een polymeerlaag optreden worden het nano-insluitingseffect genoemd. Effecten geïnduceerd door aanwezigheid van een penetrant en nano-insluiting kunnen gevolgen hebben in veel technologische toepassingen, zoals in beschermende en functionele coatings, sensoren, micro-elektronica, oppervlaktemodificatie, en membraanscheidingen. *In situ* ellipsometrie is vanwege haar hoge precisie en niet-invasieve karakter een krachtige techniek voor de karakterisering van lagen die worden blootgesteld aan een penetrant. Deze scriptie verkent de toepasbaarheid van deze techniek voor het bestuderen van grondbeginselen van diverse fysische fenomenen die optreden in dunne en ultradunne polymeerlagen in de aanwezigheid van een penetrant.

Het introducerende **hoofdstuk 1** geeft een overzicht van onderzoek dat gedaan is met *in situ* ellipsometry aan polymeerlagen in wisselwerking met diverse penetranten. In dit hoofdstuk worden verscheidene onderwerpen behandeld, waaronder de technische aspecten van *in situ* onderzoeken, verschillende benaderingen voor data-analyse en optische modellen, de beschreven precisie en herhaalbaarheid, de polymeer-penetrantsystemen die zijn bestudeerd, de soorten informatie die af te leiden zijn, en andere *in situ* technieken die zijn gecombineerd met ellipsometrie. Uiteenlopende voorbeelden worden besproken ter verduidelijking van de verschillende praktische methoden, de gevolgen van de optische eigenschappen van de aangebrachte omgeving en de verschillende benaderingen die zijn toegepast om polymeerlagen in contact te brengen met een penetrant, die uiteenlopen van simpele *ex situ* opstellingen (in bijvoorbeeld droogstudies) tot complexe hogedrukcellen. De brede toepasbaarheid van *in situ* ellipsometrie wordt toegelicht aan de hand van karakteristieke fenomenen die zijn bestudeerd, zoals dilatatie van lagen, penetrant-diffusiemechanismen, degradatie van lagen, elektrochemische processen, en de zwelling van een brede verscheidenheid van polymeer-penetrantsystemen (glasachtige en rubberachtige polymeren, meerlaagsstapelingen, etc.). Een aantal mogelijke toekomstige *in situ* ellipsometrie studies wordt voorgesteld.

Hoofdstuk 2 beschrijft een onderzoek naar een overgang in het diffusiemechanisme van vloeibaar n-hexaan in dunne polystyreenlagen. Het is aangetoond dat de eigenschappen van het diffusiemechanisme veranderden van tegelijkertijd optredende Fickse diffusie en polymeerrelaxatie naar het puur relaxatie gelimiteerde Type II diffusie in een betrekkelijk nauw temperatuursbereik

rond kamertemperatuur van 16 – 28 graden Celsius . Deze overgang beïnvloedt de kinetiek van het proces drastisch, waarbij de tijdschaal waarin het fenomeen optreedt verandert van meerdere uren op 16 graden Celsius naar enkele minuten op 28 graden Celsius. Het is aangetoond dat ellipsometrie zeer geschikt is om de voortgang van een scherp penetrantfront dat het Type II proces vergezelt, te volgen met een zeer hoge spectrale resolutie. Het belang van een fysisch realistisch optisch model wordt aangestipt. In het bijzonder wordt aangetoond dat het gebruik van het simpelste, uniforme optische model niet voldoende is en dat een complexer twee-lagenmodel benodigd is om de zwelling te kunnen verklaren.

In **hoofdstuk 3** wordt de gedetailleerde aanpak van het optisch modelleren van Type II diffusie die is ontwikkeld in **hoofdstuk 3** toegepast om de gestapelde effecten van nano-insluiting en van het penetrant in ultradunne polystyreenlagen te meten. Hier wordt aangetoond dat in de buitenste laag van deze glasachtige lagen zich een domein van 14±3 nanometer bevindt dat nagenoeg instantaan zwelt wanneer het in contact komt met het penetrant. Nadat dit grenslaagdomein gezwollen is volgt een veel langzamere frontdiffusie. Er is aangetoond dat de temperatuur waarbij de diffusie optreedt en de fysische veroudering geen invloed hebben op het instantaan gezwollen gebied, maar dat ze de dynamica van de daaropvolgende frontdiffussie in de rest van het volume van deze lagen wel beïnvloedt. Deze resultaten kunnen aanmerkelijke gevolgen hebben in toepassingen waar kleine moleculaire penetranten diffunderen door ultradunne glasachtige polymeerlagen, bijvoorbeeld in membraanscheidingen.

De zeer hoge precisie van *in-situ* spectroscopische ellipsometrie wordt toegepast in **hoofdstuk 4** om een procedure te ontwikkelen waarmee de volumefractie penetrant in een dunne gezwollen polymeerlaag nauwkeurig kan worden bepaald. Deze methode is gebaseerd op de effectieve medium aanpak van Bruggeman en houdt rekening met penetrant geïnduceerde volledige relaxatie van de overmaat vrij volume die behoort bij de niet-evenwicht status van het oorspronkelijke droge glasachtig polymeer. De nieuw ontwikkelde methode wordt vergeleken met andere methoden die in de literatuur toegepast worden, maar die de vrij-volumerelaxatie buiten beschouwing laten. De fouten in de penetrantvolumefracties die worden verkregen wanneer vrij volume wordt genegeerd zijn met name groot voor membraanachtige hoge vrij-volume polymeren zoals poly[1-(trimethylsilyl)-1-propyn] (PTMSP).

Hoofdstuk 5 richt zich op de sorptie- en relaxatieprocessen die optreden in de nabijheid van een door penetrant geïnduceerde glasovergang, P_g. Hier wordt voor de eerste keer aangetoond dat hoewel P_g fenomenologisch vergelijkbaar is met de door temperatuur geïnduceerde glasovergang T_g, er aanmerkelijke veranderingen optreden in het dynamisch gedrag. Deze veranderingen zijn geassocieerd met de veel uitgesprokener vervorming van de polymeermatrix door het absorberende penetrant rond P_g die complete lange-termijn ketenrelaxatieprocessen lijkt te

activeren. De verandering in de helling van de dilatatiecurve kan niet altijd eenvoudig worden beschouwd als een indicatie voor een glasovergang, zoals wordt gedaan in het geval van de T_g. Een dergelijke verandering in de helling in het geval van P_g is een complex gevolg van sorptie- en relaxatiefenomenen die elkaar wederzijds beïnvloeden en wordt sterk beïnvloed door de conditioneringscondities van het polymeer. Het wordt verwacht dat deze bevindingen bijdragen aan een beter begrip van het complexe plastificeren van ultradunne membranen.

In **hoofdstuk 6** en **hoofdstuk 7** worden de studies naar dunne lagen van zwitterionische polymeren gebaseerd op sulfobetaïnemethacrylaat en n-butylacrylaat door middel van dynamische *in-situ* spectroscopische ellipsometrie beschreven. Deze materialen belichamen een interessant type polymeren met een groot potentieel in het verminderen van biovervuiling op ultrafiltratiemembranen. **Hoofdstuk 6** richt zich op de karakterisering van de dynamisch-overschrijdende zwellingsreactie in het materiaal wanneer het wordt blootgesteld aan een 1 M NaCl-oplossing. Opkomende en verdwijnende optische anisotropie in de polymeerlagen wordt beschreven. Dit gedrag wordt aannemelijk gemaakt door de oriëntatie van de polymeerhoofdketen en zwitterionische ketens ten gevolge van zwelling en relaxatie in de aanwezigheid van een afschermend elektrolyt. **Hoofdstuk 7** verkent de effecten van verschillende zouten en hun concentraties op het zwellen van eenzelfde polymeer. Een antipolyelektrolyt effect is waargenomen, zoals te zien is aan de toegenomen zwelling van de lagen in reactie op toenemende zoutconcentraties. Deze studie biedt nuttig inzicht in het gedrag van zwitterionische copolymeren films in toepassingen als membraanfiltratie met verschillende zouten en ionische sterkten.

In membraantechnologie worden vaak composietmembranen toegepast die bestaan uit een poreuze drager en een dunne scheidende laag. Het gebruik van ellipsometrie voor het bestuderen van dit soort systemen is sterk beperkt door de porositeit en de mate van de ruwheid van het substraat. Deze oppervlaktekenmerken resulteren in ongewenste verstrooiing van de lichtbundel. In **hoofdstuk 8** worden optische modellen ontwikkeld die geschikt zijn voor de *in situ* analyse van composietmembranen door middel van ellipsometrie. Deze modellen beschouwen de oppervlakteruwheid van de drager als een afzonderlijke, gegradeerde dichtheidslaag; er wordt gedemonstreerd dat deze modellen toepasbaar zijn voor composietmembranen met een relatief dikke, ~1 μm, scheidende laag.

De optische modellen die zijn ontwikkeld in **hoofdstuk 8** zijn in **hoofdstuk 9** gebruikt voor het onderzoeken van hoge druk gedreven permeatie van n-hexaan door dunne PDMS membranen. Een nieuw ontwikkelde hogedrukellipsometriecel voor *in situ* metingen wordt gedemonstreerd die het mogelijk maakt om het membraangedrag te onderzoeken bij condities die overeenkomen met die van nanofiltratieprocessen. In de afwezigheid van een drukgradient over de membraanlaag zijn de dikte en de brekingsindex van de gezwollen laag

onafhankelijk van de hydrostatische druk, in het bereik van 1 tot 100 bar. Dit wijst er op dat de molaire volumes van het penetrant in de vloeibare en geabsorbeerde fase niet beduidend verschillend zijn. Wanneer een drukverschil over het membraan wordt aangelegd, en de penetrant kan permeëren, neemt de dikte van het membraan af met het toenemende drukverschil. Uit de dikteverandering kan de concentratie van n-hexaan op het grensvlak tussen de dunne laag en de drager aan de permeaatzijde worden bepaald. De verkregen waarden komen uitstekend overeen met de waarden die worden berekend via het Oplossing-Diffusiemodel. Dit impliceert dat *in situ* spectroscopische ellipsometrie het mogelijk maakt om de bijdrage van het Oplossings-Diffusiemodel aan het totale transport door composietmembranen te kwantificeren.

Hoofdstuk 10 breidt de toepassing van variërende temperatuur- en drukellipsometrie uit naar gedragen glasachtige lagen. In dit hoofdstuk worden de effecten van tijd, temperatuur en druk in de nabijheid van de door oplosmiddel geïnduceerde glasovergang bestudeerd. Dynamische temperatuurscans onthullen de uitgesproken veranderingen in zowel evenwicht als kinetische eigenschappen van het systeem onder verglazing. Een kinetische immobilisatie van een gezwollen matrix wordt hier waargenomen en wordt uitgelegd aan de hand van de sterke veranderingen in de penetrantdiffusiecoëfficient en de gelijktijdige opkomst van de energetische barrière voor compressie onder de glasovergang van het polymeer-penetrantmengsel. Het polystyreen-n-decaansysteem vertoont geen meetbare compressie in termen van reductie in vrij volume wanneer het wordt blootgesteld aan hydrostatische drukken tot 50 bar, noch boven noch onder de glasovergangstemperatuur. Een kleine, maar goed verklaarbare, compressie is waargenomen in droog polystyreen; deze is gecorreleerd aan de partiële relaxatie van het overmaat vrije volume. De resultaten zijn belangrijk in de membraantechnologie, waar gezwollen glasachtige selectieve lagen worden toegepast onder hoge druk om te zorgen voor moleculair transport door oplossing-diffusietype transport.

Hoofdstuk 11 geeft een vooruitzicht op de overgebleven interessante onderzoeksvragen die kunnen worden geformuleerd. De voorbeelden zijn verdeeld in diverse categorieën, waarin de compleet nieuwe richtingen, vervolgstudies en pogingen om *in situ* ellipsometrie te koppelen met andere technieken worden benadrukt. Het merendeel van de inhoud van dit hoofdstuk wordt onderbouwd door een uitgebreide hoeveelheid preliminaire resultaten en observaties.

Streszczenie

Droga Rodzino, drodzy Przyjaciele i Znajomi,

Gdy zabrałem się do przygotowania streszczenia niniejszej pracy doktorskiej w języku polskim szybko doszedłem do wniosku, że napisanie go w formie dosłownego tłumaczenia tekstu angielskiego na polski mija się z celem. Wnioski te nasunęły się wraz z pojawieniem się tego typu „kwiatków”:

„...metoda ta jest oparta na wprowadzonym przez Bruggemana przybliżeniu efektywnego medium (ang. EMA) i bierze pod uwagę relaksację nadmiarowej wolnej objętości, uwięzionej w suchym polimerze szklistym, w czasie sorpcji penetrantu wywołującej w spuchniętym materiale dewitrifikację...”

A zatem nie tędy droga.

Pozwólcie, że przybliżę Wam temat mojej pracy w sposób bardziej przystępny.

Polimery

W wielu nowoczesnych technologiach wykorzystywane są bardzo cienkie warstwy polimerowe. Polimerowe, to znaczy składające się z materiałów posiadających bardzo długie łańcuchowe cząsteczki zbudowane z powtarzających się identycznych chemicznie segmentów (merów). Typowe przykłady polimerów to polistyren (każdy zna styropian, czyli spieniony polistyren) lub wychodzące z obiegu plastikowe torebki na zakupy (polietylen). Chemiczne struktury styrenu (meru) i poli-styrenu (poli-meru) znajdują się poniżej:

Styren **Polistyren (fragment złożony z 7 merów)**

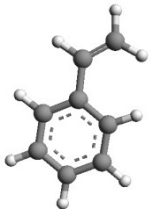

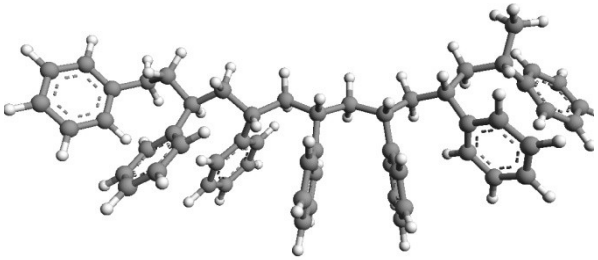

Ciecz *Ciecz lub ciało stałe w zależności od długości łańcucha*

Jak widać, cząsteczka polistyrenu to długi łańcuch, który może być zbudowany nawet z tysięcy merów. Łańcuchowa budowa nadaje tym materiałom właściwości

mechaniczne odpowiednie do zastosowań (pod warunkiem użycia odpowiednio długich łańcuchów). Zatem można z polimerów produkować części samochodów, opakowania, obudowy sprzętu AGD i wiele innych użytecznych rzeczy.

Z polimerów, można także uformować bardzo cienkie warstwy – dużo cieńsze niż np. folie opakowaniowe.

Cienkie warstwy polimerowe

Cienkie warstwy polimerowe stosowane w przemyśle pełnią przeróżne role np. warstw ochronnych lub funkcyjnych (tzn. spełniające jakąś konkretną funkcję typu uniemożliwienie „przyklejania się" kropli wody do powierzchni), warstw wykrywających pewne gazy w atmosferze (czujniki trujących związków organicznych), warstw używanych w nowoczesnych urządzeniach elektronicznych (wyświetlacze w niektórych smartfonach) oraz warstw będących membranami. Na badaniu tych ostatnich skupiona jest w dużej mierze niniejsza praca doktorska. Ale o membranach za chwilę.

Jak cienkie są takie warstwy?

Mogą być bardzo cienkie: ultra-cienkie, to znaczy w granicach ok. 100 nanometrów, czyli $100 \cdot 10^{-9}$ m. Żeby uzmysłowić sobię skalę, o której mowa, wystarczy wyobrazić sobie tysiąckrotne zmniejszenie skali pomiędzy przekątną wyświetlacza typowego smartfona (ok. 100 milimetrów), a typową średnicą ludzkiego włosa (ok. 100 mikrometrów), a następnie zastosować takie samo tysiąckrotne zmniejszenie w stosunku do ludzkiego włosa, aby otrzymać skalę wielkości typowej ultra-cienkiej warstwy polimerowej (100 nanometrów).

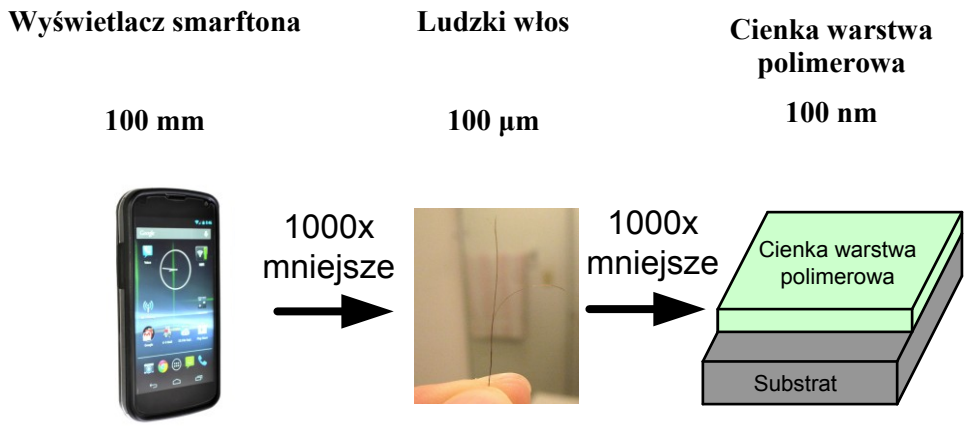

Membrany

Dlaczego zależy nam na stosowaniu takich cienkich warstw? Żeby to zrozumieć, przyjrzyjmy się procesom membranowym. W takich procesach chodzi nam o rozdzielenie mieszaniny na jej poszczególne składniki. W zasadzie membrany działają na podobnej zasadzie co kuchenne sitko.

Filtracja makaronu z wody

Filtracja na poziomie molekularnym

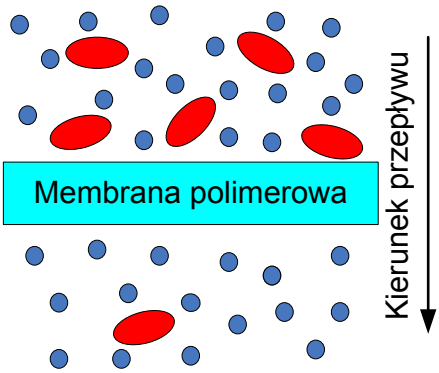

Rozdziela ono, filtruje, makaron od wody (lewa strona powyższego diagramu). W membranach, zwłaszcza bazujących na ultra-cienkich warstwach polimerowych, chodzi o filtrację mieszaniny na poziomie molekularnym (prawa strona diagramu).

Zagadnienia tego typu występują w wielu gałęziach przemysłu chemicznego np. przy produkcji leków (gdzie chcemy uzyskać lek składający się z jak najczystszej substancji czynnej – niezanieczyszczonej innymi składnikami mieszaniny reakcyjnej) lub przy odsalaniu wody przy produkcji wody pitnej z wody morskiej. W pierwszym przypadku chodzi o odfiltrowanie na poziomie molekularnym cząsteczek leku od np. rozpuszczalnika, natomiast w drugim o rozdzielenie cząsteczek soli od cząsteczek wody. Funkcję filtracyjną spełnia w tym przypadku właśnie odpowiednio cienka warstwa polimerowa – membrana, która ma właściwość selektywnego przepuszczania jednego ze składników mieszaniny natomiast zatrzymywania drugiego. Ponieważ szybkość przepływu składnika rośnie wraz ze zmniejszeniem grubości membrany, aby uzyskać wydajny proces (duży przepływ) potrzebne są jak najcieńsze membrany. Oczywiście grubość membran nie może być zbyt niska, gdyż ucierpiałaby ich stabilność mechaniczna i nawet małe defekty, nieselektywne dziury lub pęknięcia, wpłynęłyby negatywnie na jej zdolności filtracyjne. Innymi słowy, gdyby oczka sita były większe niż wielkość makaronu, byłoby ono nieefektywne.

Używanie membran zamiast innych metod separacyjnych ma wymierne korzyści ekonomiczne. Membrany są znane z tego, że do działania potrzebują znacznie

mniejszej ilości energii niż bardziej tradycyjne technologie, takie jak destylacja (znana z przemysłu naftowego) lub krystalizacja (znana z przemysłu farmaceutycznego).

Elipsometria

Jedną z najbardziej interesujących technik eksperymentalnych nadających się do badania interakcji cienkich warstw polimerowych i filtrowanych mieszanin jest elipsometria spektroskopowa. Jest to technika bazująca na pomiarze zmian w polaryzacji światła podczas jego odbicia od badanej próbki. Polaryzacja światła ma związek z kierunkiem oscylacji fali elektromagnetycznej (np. wektora pola elektrycznego (*E)*) względem kierunku propagacji. Ludzkie oko nie potrafi określić polaryzacji światła widzialnego, w przeciwieństwie do oczu niektórych owadów, dlatego zagadnienie to jest nieco trudne do intuicyjnego uchwycenia. Dla przykładu motyle z rodzaju *Heliconius* rozpoznają i używają polaryzacji światła w celach rozrodczych. Na poniższej ilustracji, lewe skrzydła motyli ukazane są tak jak można je zobaczyć gołym okiem, prawe strony widziane są przez filtry polaryzacyjne przepuszczające tylko odpowiednio spolaryzowane (ukierunkowane w płaszczyźnie prostopadłej do kierunku padania) światło.

Polaryzacja światła odbitego od skrzydeł motyli z rodzaju *Heliconius*, źródło: Alison Sweeney et al., Nature, May 1, 2003

W laboratorium nie używamy motyli, bo nie wykazują one zainteresowania membranami. Do określenia polaryzacji światła wykorzystywane są urządzenia optyczne, które zostały wynalezione już ok. 200 lat temu i są ciągle udoskonalane. Poniższy schemat wyjaśnia zasadę działania elipsometrii.

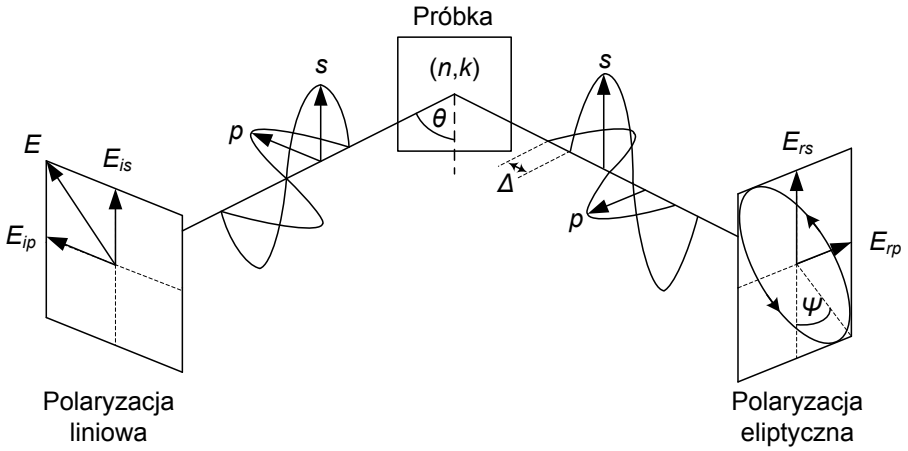

Źródło: Hiroyuki Fujiwara „Spectroscopic ellipsometry: principles and applications"

W elipsometrii kierujemy strumień światła liniowo spolaryzowanego (lewa strona schematu), które po odbiciu pod kątem θ zmienia się w światło eliptycznie spolaryzowane (prawa strona). Z nazwy tego kształtu pochodzi nazwa techniki. Mierząc stopień zmiany kształtu, czyli parametry powstałej elipsy nazywane psi (Ψ) i delta (Δ), możemy określić właściwości badanej próbki. Na przykład możemy zbadać, jak gruba jest badana warstwa oraz jakie właściwości optyczne ona posiada. Jedną z najbardziej użytecznych właściwości optycznych jest współczynnik załamania światła (n), który może być użyty do określenia np. jakie zmiany strukturalne zachodzą w badanej cienkiej warstwie lub jaka ilość filtrowanej mieszaniny przenikła do jej wnętrza.

Nowoczesne urządzenia badawcze są w stanie bardzo dokładnie określić interesujące nas parametry elipsometryczne. W pracy tej wykorzystane zostały odpowiednio zmodyfikowane urządzenia amerykańskiej firmy J. A. Woollam Co. Inc., których zdjęcia znajdują się poniżej.

Elipsometr Alpha-SE

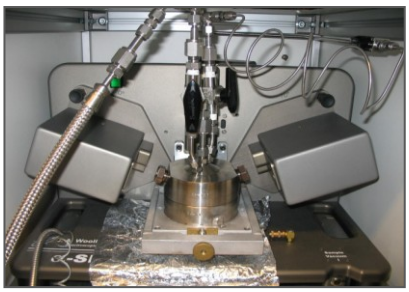

Elipsometr M-2000X

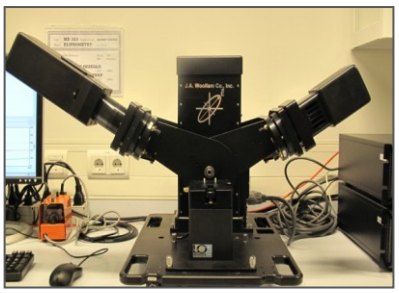

Oba te urządzenia posiadają źródła światła (lampy żarowe lub łukowe) oraz przyrządy optyczne (takie jak polaryzatory, kompensatory oraz spektrografy) do określania polaryzacji po odbiciu od badanej próbki.

Temat pracy doktorskiej

Praca, którą trzymacie w rękach, jest owocem czterech lat badań nad cienkimi warstwami polimerowymi i membranami będącymi w kontakcie z filtrowanymi mieszaninami przy użyciu elipsometrii. Badania te mają za zadanie eksplorację zastosowania tej techniki do lepszego zrozumienia interakcji między materiałem polimerowym a filtrowanym medium po to, aby móc w bardziej efektywny sposób projektować nowe procesy membranowe.

Streszczenie dla Weroniki

Weroniczko, pamiętaj, że możesz sobie dowolnie wybrać karierę jak dorośniesz.

Żadnej presji...

Acknowledgments

It has been a great and inspiring journey. In fact, in many ways it surpassed my expectations and showed me how wonderfully unpredictable certain things are. I feel that I grew professionally and personally on so many levels and learnt so many new skills in the last four years. Along the way there were people, to whom I would like to express my sincere gratitude.

I would like to thank **Prof. Dr.-Ing. Matthias Wessling** for being my Promotor and mentor. I appreciate your support, supervision and great scientific input. You were always a source of inspiration, with a unique ability to think a few steps ahead, as well as to take a few steps back and see things from a broader perspective. I think many would agree that your charisma and communication skills are unmatched, and I have learnt much from you in that respect. Thank you also for initiating the yearly Winterschools in Austria, which were amazing social/scientific events and helped nucleating nice collaborations.

Dr. Ir. Nieck E. Benes, Nieck, you are the person I have learnt the most from. I am grateful for your trust in me, limitless support, great scientific discussions, but also for teaching me skeptical thinking. You possess a very valuable combination of scientific enthusiasm anchored to evidence-based reality. I especially appreciate the huge amount of freedom in directing the flow of my PhD, with a gentle push in the right direction from time to time. Sorry for always bringing complicated curved lines instead of some linearly distributed points, but on the other hand it was great fun figuring out what was hiding behind them. Thanks also for the many social events, including the bike trip that almost killed me. Only now I realize that the Dutch must really be born for biking. However, it seems to somehow conflict with the habit of insisting to stop at every possible Burger King along the way of each business trip. I never figured out this mystery.

I am grateful to **Dr. Ir. Herbert Wormeester** for bringing to our research the insightful contributions from the physicist's perspective. It was always a great pleasure to discuss with you and see your enthusiastic responsiveness, encouragement and persistence to go deeper into the subject. Thank you also for being a part of my doctoral committee.

I would like to thank **Prof. Dr. Guido Mul**, **Prof. Dr. Nico van der Vegt**, **Dr. rer. nat. Klaus-Jochen Eichhorn** and **Prof. Julius Vancso** for agreeing to review my thesis and take part in the doctoral committee. I am thankful to **Prof. Dr. Ir. Guus Rijnders** for chairing the defense session.

To my paranymphs, **Dr. Szymon Dutczak** and **Dr. Katarzyna Matras-Postolek**, I am thankful for taking a special place in my defense ceremony. Both of you turned out to be great friends, but also played a major role in my professional career. **Szymon**, in conspiracy with my yet-to-be wife Joanna, opened my perspective on the University of Twente. On the other hand, **Kasia** did the same at an earlier stage, sharing information on the possibility to do Master studies in Steinfurt. I sincerely appreciate your advice and friendship!

Being a part of the stimulating environment of the Membrane Science and Technology (MST) Group was a great pleasure, largely because of the efforts of its head, **Prof. Dr. Ir. Kitty Nijmeijer**. Kitty, thank you for creating this very pleasant atmosphere for research

and collaboration, as well as for the scientific input in parts of this thesis. My kind words go also to the other staff members of the MST and to the members of the European Membrane Institute (EMI), **Prof. Dr. Ir. Erik Roesink**, **Dr. Ing. Zandrie Borneman, Dr. Ir. Antoine Kemperman**, **Dr. Wiebe de Vos**, **Erik Rolevink**, **Herman Teunis**, **Harmen Zwijnenberg**, **John Heeks** and **Greet Kamminga**. In particular, I will always remember the extremely positive attitude of all of you for helping people out. **Greet**, thank you for all your help and eagerness in solving all sort of formal issues – which many times turned out to be as complex as the science. Just to mention the struggle to properly fill in tax declaration forms of Polish people living in Germany, working in the Netherlands, who, to make matters worse, decided to marry in the meantime ;) However, with you, Greet, nobody felt left alone!

I would like to thank my bachelor and master students, **Kristianne**, **Lakshmeesha** and **Denys**, for your enthusiasm and passion for learning. The work of all of you had a big impact on the shape of the thesis. You were all extraordinary students and I wish you great success in your future personal and professional paths.

To my office mates over the years, **Katja**, **Enver**, **Irdham**, **Marlon**, **Yusuf**, **Joris** and **Harmen** – thanks for all the serious and less serious (sometimes quite abstract) discussions, and for the joyful atmosphere. Some of you were also stubborn enough to constantly remind me that I had not biked to work as promised :) Thanks for that.

I am thankful to the remaining current and former members of the MST: **Krzysiek T.**, thanks for sharing the passion of discussing car stuff, though we had major disagreements (I still think VW is terrible in all respects), **Beata**, thanks for helpfulness and teaching Dutch people polish curse words, **Jeroen**, thanks for the computer games discussions and learning to correctly pronounce the polish curse words, **Olga**, thanks for being Olga (I don't think I should elaborate on that!) – I hope you will never change, **Enver**, thanks for your humor and friendliness, **Erik V.**, thanks for being indestructible, **Sinem**, thanks for your smile and sorry for finally forgetting to organize the promised house warming party, **Can**, thanks for being a one of a kind social "glue" keeping people together, **Karina**, thanks for being one of the most determined and ambitious women I have ever met, **Joanna C.**, thanks for all the scientific collaborations, friendliness and talking a bit too fast during presentations, **Salman**, thanks for your crazy partying skills, **Charu**, thanks for your endlessly positive attitude, **Hans**, thanks for helping me out in the very beginning, **Roberto**, **Shazia**, **Christina**, **Zeljka**, **Harro**, **Jordi**, **Timon, Jigar, Al-Hadidi, Ikenna, Sander R., Anne-Corine** and others, thanks for sharing the nice moments with me.

I am grateful to the members of the Soft Matter and Fluidics (SFI) Group: **Prof. Dr. Rob Lammertink**, head of the SFI, for scientific and non-scientific discussions as well as for companionship during determination of the slip velocity of skies on the alpine snow, **Damon**, thanks for your dancing and acting skills and your disarming friendliness, **Yali**, thanks for your smile and friendly hand-waving gestures, **Amy**, **Elif**, **Vic**, **Sander, Anne, Khalid**, **Joeri** and **Ineke**, it was a pleasure to discuss and laugh together.

To the members of the Inorganic Membranes (IM) Group, with whom I have worked in close collaboration, **Prof. Dr. Ir. Arian Nijmeijer**, head of the IM, thanks for many scientific and humorous discussions, **Emiel** and **Michiel**, thanks for sharing the passion for ellipsometry and other cool stuff, as well as for designing thought experiments proving a

quantum nature of our supervisor. Thanks also for the help in dealing with capricious nature of the lab equipment (which was actually mostly our own fault, but poor machines can't defend themselves, … at least yet, because some already have moving arms…), **Frank**, thanks for lots of help with building setups, ordering necessary equipment and taking the duties of our soccer team leader. I also appreciate the presence and nice atmosphere created be **Prof. Dr. Henny Bouwmeester**, **Dr. Louis Winnubst**, **Dr. ing. Mieke**, **Cindy**, **Susanne**, **Hammad**, **Wei**, **Martin**, **Tan**, **Bas** and others.

I would also like to thank the people from RWTH Aachen, with whom I had a great time during Winterschools and other events, especially **Stefanie Kriescher**, **John Wong** and **John Linkhorst**.

To the polish mafia from Steinfurt: **Szymon**, in addition to being my paranympf, I am grateful for your help, especially during the initial, child-in-the-fog, phase of my work in Twente. I admire your modesty and kindness and I enjoyed endless conversations about the automotive industries. I also enjoyed our habit of buying new cars once every week (unfortunately, using imaginary money). **Danusia**, I admire your optimism, compassion, and Photoshop skills. I am also grateful for being a close friend to me and my wife, but also for designing a great cover for my thesis. Unfortunately, that particular project could not be accepted ;) **Dawidek** is extremely lucky to have both of you as his parents. The same can be said about **Kubuś**, son of **Kasia** and **Grzegorz**. Particularly, you guys made our stay in Steinfurt a great time, and we will always remember the many times when we laughed at intentional or unintentional jokes, **Grzegorz**, you certainly were, and continue to be, an "ideal person" ;) Thanks also to **Asia M.** for your extraordinary sense of humor and great skills in picking as colorful outfits as possible, **Arturas**, for your scientific and physical strength, **Gosia**, for being our social glue, **Ania** and **Jagoda**, for sharing the difficult first few months abroad, **Krzysiek G.**, **Michał** i **Ewelina**, and all the others that relished the peaceful (some would say boring, but they know nothing!) atmosphere of Steinfurt.

"It was a good habit to complain about Steinfurt…"

Szczególne podziękowania chciałbym przekazać w kierunku moich rodziców, **Doroty** i **Piotra**. Dziękuję Wam za miłość, pomoc i to, że mogłem mieć w Was oparcie przez cały ten czas. Dziękuję Ci **Kinga**, za bycie cudowną siostrą, z której jestem niesamowicie dumny. Dziękuję babci **Teresie** i dziadkowi **Tadeuszowi**, za nieustanne wsparcie i życzliwość. Dziękuję serdecznie także babci **Romanie**, **Dagmarze** i **Leszkowi** z dziećmi. Jestem również ogromnie wdzięczny najbliższej rodzinie mojej żony, **Dorocie** i **Marianowi**, braciom **Piotrowi** i **Pawłowi** z żonami, za obecność i trzymanie za mnie kciukuów.

Jestem szczęściarzem, że mogłem mieć Was wszystkich obok siebie w ciągu tych kilku lat oraz liczyć na Wasze wsparcie, pomoc i życzliwość, gdy tyle się w moim życiu zmieniało. Dziękuję!

Moja **Asieńko**, Pysiaczko, kocham Cię najbardziej na świecie! Dziękuję Ci za bycie wspaniałą, kochającą i nieustannie wspierającą żoną, z którą każdy dzień jest pełen radości i szczęścia. Wiem, że poradzimy sobie razem ze wszystkim co przyniesie życie. Ten doktorat dedykuję Tobie i naszej **Weronice**.

Curriculum Vitae

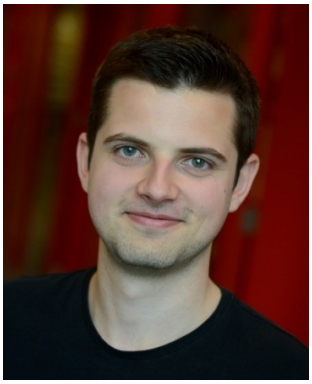

Wojciech Ogieglo was born on the 25th of November 1985 in Oświęcim, near Cracow, in the southern Poland. He attended a class with extended mathematics and physics at Stanislaw Konarski high school in Oświęcim, where he obtained the High School Diploma in 2004. In the same year, he started combined B.Sc. and M.Sc. studies in the field of Chemical Technology at the Cracow University of Technology. In 2008 Wojciech continued his studies at Münster University of Applied Sciences, division in Steinfurt, Germany, in a framework of the SOCRATES-ERASMUS student exchange program. In 2009 he obtained a double M.Sc. Diploma, with the highest grade, from the Cracow University of Technology and Münster University of Applied Sciences. His Master Thesis was entitled: "Investigation of interactions between ultraviolet laser beam and polymer matrices with a use of Total Organic Carbon and Laser Ablation ICP-MS". The Master Thesis research was performed in the Instrumental Analysis Laboratory under the supervision of Prof. Dr. Martin Kreyenschmidt. Prof. dr hab. inż. Jan Pielichowski was the supervisor of the Master Thesis from the Cracow University of Technology. Since July 2010 Wojciech has been married to Joanna Ogieglo.

Starting from January 2010 Wojciech has been working at the University of Twente in Enschede, The Netherlands, as a PhD student in the Membrane Science and Technology group headed by Prof. Dr. Ir. Kitty Nijmeijer. His doctoral Thesis has been supervised by Prof. Dr.-Ing. Matthias Wessling from RWTH Aachen University in Germany and Dr. Ir. Nieck E. Benes from the Inorganic Membranes group at the University of Twente. The research of Wojciech was presented as oral and poster presentations at numerous international conferences and workshops, including the International Congress of Membranes and Membrane Processes (ICOM2011) in Amsterdam, The Netherlands, 7th Ellipsometry Workshop in 2012 in Leipzig, Germany, and Euromembrane Conference in 2012 in London, UK. He has been awarded best oral presentation prizes at the Euromembrane Conference in the UK and at the 7th Ellipsometry Workshop in Germany (Paul Drude Medal). He has also qualified as a finalist of the LANXESS Talent Award at the DWI/RWTH Summerschool in Aachen, Germany.

Wojciech's teaching experience includes supervision of Bachelor students during practical laboratory courses at Münster University of Applied Sciences and at the University of Twente. He supervised one final Bachelor assignment and two final Master assignments at the University of Twente.

Wojciech holds the "Registered Polymer Scientist" certificate for completing the RPK–A, –B, –C, and –D&E courses organized by the National Dutch Graduate School of Polymer Science & Technology in Eindhoven, The Netherlands. He is a member of the European Membrane Society (EMS).

List of publications (as of February 2014):

1. Ogieglo, W., H. van der Werf, K. Tempelman, H. Wormeester, M. Wessling, A. Nijmeijer, and N.E. Benes, *n-Hexane induced swelling of thin PDMS films under non-equilibrium nanofiltration permeation conditions, resolved by spectroscopic ellipsometry.* Journal of Membrane Science, 2013. **437**(0): p. 313-323.

2. Ogieglo, W., H. Wormeester, M. Wessling, and N.E. Benes, *Temperature-induced transition of the diffusion mechanism of n-hexane in ultra-thin polystyrene films, resolved by in-situ Spectroscopic Ellipsometry.* Polymer, 2013. **54**(1): p. 341-348.

3. Ogieglo, W., H. Wormeester, M. Wessling, and N.E. Benes, *Probing the surface swelling in ultra-thin supported polystyrene films during Case II diffusion of n-hexane.* Macromolecular Chemistry and Physics, 2013. **214**(21): p. 2480-2488

4. Ogieglo, W., J. de Grooth, H. Wormeester, M. Wessling, K. Nijmeijer, and N.E. Benes, *Relaxation induced optical anisotropy during dynamic overshoot swelling of zwitterionic polymer films.* Thin Solid Films, 2013. **545**(0): p. 320-326

5. Scorticati, D., A. Illiberi, G.R.B.E. Römer, T. Bor, W. Ogieglo, M. Klein Gunnewiek, A. Lenkferink, C. Otto, J.Z.P. Skolski, F. Grob, D.F. de Lange, and A.J. Huis in 't Veld. *Optical and electrical properties of SnO_2 thin films after ultra-short pulsed laser annealing*. Proc. SPIE 8826, Laser Material Processing for Solar Energy Devices II, 2013.

6. Ogieglo, W., H. Wormeester, M. Wessling, and N.E. Benes, *Spectroscopic ellipsometry analysis of a thin film composite membrane consisting of polysulfone on a porous α-alumina support.* ACS Applied Materials & Interfaces, 2012. **4**(2): p. 935-943.

7. Karabudak, E., Kas, R., Ogieglo, W., Rafieian, D., Schlautmann, S., Lammertink, R.G.H., Gardeniers, H.J.G.E. and Mul, G., *Disposable attenuated total reflection-infrared crystals from silicon wafer: a versatile approach to surface infrared spectroscopy.* Analytical Chemistry, 2012. **85**(1): p. 33-38.

8. Visan, A., Rafieian, D., Ogieglo, W., Lammertink, R.G.H. *Modeling intrinsic kinetics in immobilized photocatalytic microreactors*. Applied Catalysis B, 2014. **150-151**: p. 93-100.

9. Ogieglo, W., Wormeester, H., Wessling, M., Benes, N.E. *Effective medium approximations for penetrant sorption in glassy polymers accounting for excess free volume*, Polymer, *accepted*

10. Kezia, K., Lee, J., Ogieglo, W., Hill, A., Benes, N.E., Kentish S. *The transport of hydronium and hydroxide ions through reverse osmosis membranes*, Journal of Membrane Science, *accepted*

Work submitted or in preparation:

11. de Grooth, J., Ogieglo, W., de Vos, W., Gironès, M., Nijmeijer, K., Benes, N.E. *Swelling Dynamics of Zwitterionic Copolymers: The Effects of Concentration and Type of Anion and Cation*

12. Ogieglo, W., Wormeester, H., Eichhorn, K-J., Wessling, W., Benes, N.E. *In-situ ellipsometry studies of thin swollen polymer films, a review*

13. Ogieglo, W., Wessling, M., Benes, N.E. *Polymer relaxations in thin films in the vicinity of penetrant or temperature induced glass transition*

14. Ogieglo, W., Upadhyaya, L., Nijmeijer, A., Wessling, M., Benes, N.E. *Effects of time, temperature, and pressure in the vicinity of the glass transition of a swollen polymer*

Selected conference oral presentations:

04.2013 – Dutch Ellipsometry Workshop, Enschede, The Netherlands

09.2012 – Euromembrane Conference London, UK (**best presentation prize**)

03.2012 – 7th Workshop Ellipsometry, Leipzig, Germany (**best presentation prize** – Paul Drude medal)

03.2012 – Dutch Polymer Days, Lunteren, The Netherlands

09.2011 – MESA+ Institute Workshop, Enschede, The Netherlands

07.2011 – ICOM 2011 (International Congress on Membranes and Membrane Processes), Amsterdam, The Netherlands

ISBN: 978-90-365-3631-8